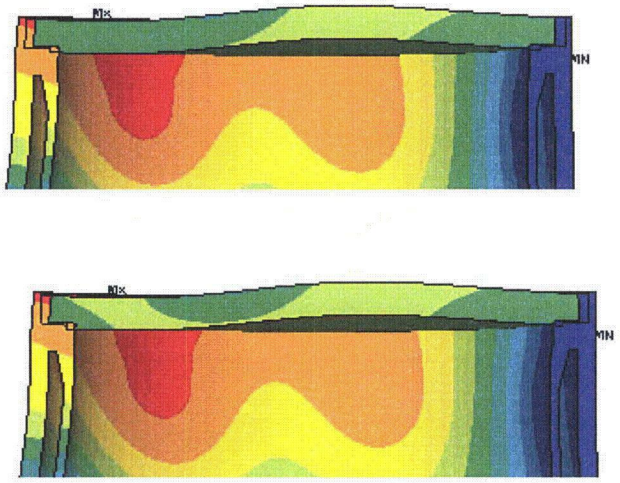

Figure B.2.13.2-2
Deformation Plot Near Lid–Flange Interface for 59 and 90 kips Preload

Appendix B.2.13.3
MP197TAD TO Lead Slump and Containment Boundary Buckling Analysis

TABLE OF CONTENTS

B.2.13.3.1 Introduction B.2.13.3-1
B.2.13.3.2 Finite Element Model B.2.13.3-2
B.2.13.3.3 Material Properties B.2.13.3-5
B.2.13.3.4 Loading and Boundary Conditions B.2.13.3-5
B.2.13.3.5 FEA Results B.2.13.3-6
B.2.13.3.6 Conclusions B.2.13.3-7
B.2.13.3.7 References B.2.13.3-7

LIST OF FIGURES

Figure B.2.13.3- 1 Schematic for End Drop on Lid End B.2.13.3-8
Figure B.2.13.3- 2 Schematic for End Drop on Bottom End B.2.13.3-9
Figure B.2.13.3- 3 Boundary Condition & Loads for End Drop on Lid End with 25 psig External Pressure B.2.13.3-10
Figure B.2.13.3- 4 Nodes Selected for Time-History Post Processing B.2.13.3-11
Figure B.2.13.3- 5 Displacement vs. G-Load Curve for End Drop on Lid End with 30 psig Internal Pressure B.2.13.3-12
Figure B.2.13.3- 6 Displacement vs. G-Load Curve for End Drop on Lid End with 25 psig External Pressure B.2.13.3-13
Figure B.2.13.3- 7 Displacement Plot at 125g (End Drop on Lid End with 25 psig External Pressure) B.2.13.3-14
Figure B.2.13.3- 8 Lead Slump at 65g (End Drop on Lid End with 25psig External Pressure) B.2.13.3-15

Appendix B.2.13.3
MP197TAD TO Lead Slump and Containment Boundary Buckling Analysis

NOTE: References in this appendix are shown as [1], [2], etc., and refer to the reference list in Section B.2.13.3.7.

B.2.13.3.1 Introduction

The purpose of this analysis is to determine the amount of lead slump that occurs in the NUHOMS®-MP197TAD Transportation Overpack (TO) containment boundary and to determine the containment buckling loads due to hypothetical accident condition (HAC) end drop incidents. The load cases considered in this calculation are 30 ft End Drop on Lid End and 30 ft End Drop on Bottom End.

During a hypothetical accident condition end drop, permanent deformation of the lead gamma shield may occur. The lead gamma shield is supported by friction between the lead and cask shells, in addition to bearing at the end of the lead column. The lead to cask shells friction model used friction factor 0.25.

A nonlinear finite element analysis is performed in order to quantify the amount of lead slump generated during the end drop event. The 3-dimensional half symmetric ANSYS [1] finite element model, used in HAC events evaluations, is employed for this purpose. The results of the finite element analysis provide both stresses and displacements generated during the end drop event. The displacement results are used in this section to determine the maximum size of the axial gap that develops between the lead gamma shield column and the structural shell of the cask. The effect of this cavity size on the shielding ability of the transport package is evaluated in Chapter B.5.

The calculations of end drop events, discussed in this section, serve also the determination of buckling loads of the inner containment shell of the NUHOMS®-MP197TAD Transportation Overpack. The conservative estimation of buckling loads is based on the examination of the shell deformation development at its weakest location. In this calculation, the minimum acceptable buckling load is assumed equal to 150% of the HAC g-load 65g.

B.2.13.3.2 Finite Element Model

Geometry

The schematic of structural components of 3D model of the MP197TAD Transportation Overpack is presented in the following figure.

The Finite Element Model represents MP197TAD TO assembly by means of eight structural components: outer shell, inner shell, lid, top flange, bottom flange, bottom plate, ram closure plate and gamma shield. The neutron shield assembly structure is not modeled but its mass is accounted for as a surface mass load.

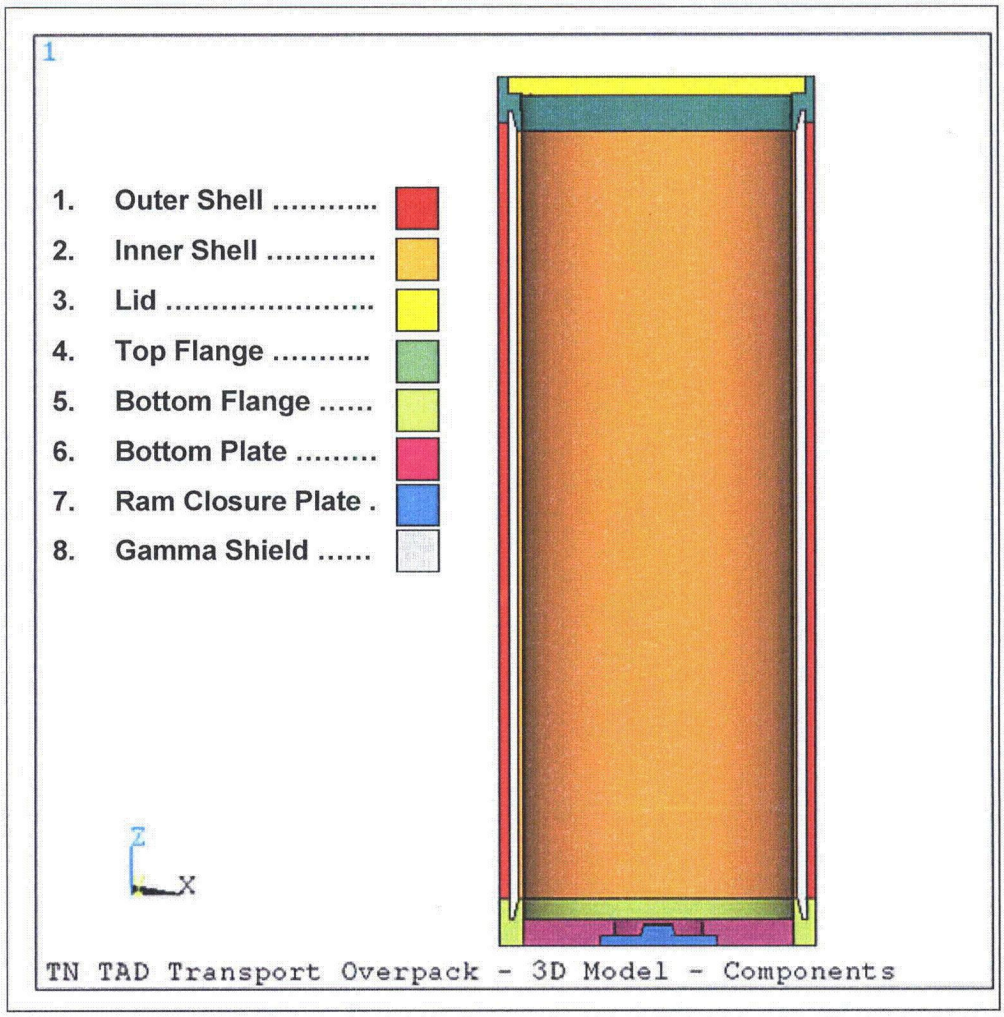

Schematic of the MP197TAD TO - 3D FEA Model.

ANSYS Elements

The following table lists ANSYS element types used to represent in analyses structural components of cask design.

ANSYS Elements Specifications

COMPONENT	MATERIAL TYPE NUMBER	ELEMENT TYPE NUMBER	ANSYS MODEL ELEMENTS
Outer Shell.	1	1	SOLID45
Inner Shell	2	2	SOLID45
Lid	3	3	SOLID45
Top Flange	4	4	SOLID45
Bottom Flange	5	5	SOLID45
Bottom Plate	6	6	SOLID45
RAM Closure Plate	7	7	SOLID45
Gamma Shield	8	8	SOLID45
Lid Bolts (Radial Shear Interaction)	9	391	COMBIN39
Lid (Tangential Shear Interaction)	9	392	COMBIN39
Lid (Axial Interaction)	9	393	COMBIN39
RAM Closure Bolts (Radial Shear Interaction)	10	394	COMBIN39
RAM Closure Bolts (Tangential Shear Interaction)	10	395	COMBIN39
RAM Closure Bolts (Axial Interaction)	10	396	COMBIN39
Neutron Shield	14	14	SURF154
Canister Lifting Device Spacer (Item 67 & 69)	20 & 21	20 & 21	SURF154

The following table shows specifications of the contact model between material components done by means of surface contact elements (elements CONTA173, TARGE170).

ANSYS Elements Specifications –Contact elements

INTERFACE DESCRIPTION	CONTACT ELEMENT DETAILS [1]			
	Target Element.	Contact Element.	Element Real Constants	Material Type Number
Lid and Top Flange (Top Radial Interface)	1101	101	101	11
Lid and Top Flange (Plate Contact Interface)	1102	102	102	11
Lid and Top Flange (Bottom Radial Interface)	1103	103	103	11
RAM Closure Plate and Bottom Plate - Radial Interface	1111	111	111	12
RAM Closure Plate and Bottom Plate - Plate Contact Interface	1112	112	112	12
Outer Shell and Gamma Shield (Radial) Interface	1201	201	201	13
Top Flange and Gamma Shield (Top Contact Surface)	1202	202	202	13
Top Flange and Gamma Shield (Conical Surface)	1203	203	203	13
Inner Shell and Gamma Shield (Radial) Interface	1204	204	204	13
Bottom Flange and Gamma Shield (Conical Surface)	1205	205	205	13
Bottom Flange and Gamma Shield (Bottom Contact Surface)	1206	206	206	13
Notes: (1) The model uses contact element CONTA173 & TARGE170				

Methodology

An ANSYS elastic-plastic buckling analysis with large displacement option was performed to calculate buckling loads. The 200g drop load is applied in each analysis. This 200g drop load is ramped in small increments by many load sub-steps. The ANSYS solution was set to stop and exit at any load sub-step that fails to result in a converged solution. When the imposed sub-step load reaches the buckling instability load, ANSYS will be unable to produce a converged solution.

For the end drop on bottom end buckling analysis, the ANSYS calculation was converging adequately till final 200g load. For end drop on lid end cases the calculation failed to converge at about 145g load.

To get a conservative value of g-load, a time-history postprocessing is done for selected nodes to plot the radial deformation against g-loads for end drop on lid end buckling analyses. The g-load where the slope of radial deformation changes significantly is conservatively assumed to be the buckling load.

Lead slump values are calculated at 65g.

B.2.13.3.3 Material Properties

Properties of NUHOMS®-MP197TAD TO materials are taken at 350 °F for both hot and cold environment cases, which is conservative. The transportation overpack material properties used for the analysis are the same as used in the elastic-plastic accident analysis of the Appendix B.2.13.1 "NUHOMS®-MP197TAD TO Body Structural Analysis."

B.2.13.3.4 Loading and Boundary Conditions

DSC Weight

DSC impact is applied to the cask model based on the assumption of DSC weight of 106.0 kips. This is the bounding weight for the DSC weight. The DSC weight is imposed as a pressure load distributed uniformly at the area of DSC contact with lid (end drop on lid end) or bottom plate (end drop on bottom end). The DSC load for end drop on lid end and end drop on bottom end are illustrated in Figure B.2.13.3-1 and B.2.13.3-2 respectively. The DSC load pressure for these loads is denoted by P_I.

Impact Limiter Weight

Loads applied to the cask model are based on the assumption that the front impact limiter mass is 16,000 lbs and the rear impact limiter mass is 16,000 lbs. These values of impact limiter weights envelop the limiter weights calculated in Chapter B.2.

In the end drop on bottom end calculations the full weight of front limiter is imposed as a uniform axial pressure load acting on the effective area of contact of the front impact limiter with cask body.

In the end drop on lid end calculations, the full weight of rear impact limiter is imposed as a uniform axial pressure load acting on the effective area of the contact of the rear impact limiter with cask body.

The pressure loads due to impact limiter weight for end drop on lid end and end drop on bottom end cases are illustrated in Figure B.2.13.3-1 (end drop on lid end) and Figure B.2.13.3-2 (end drop on bottom end). The pressure for these loads is denoted P_L.

Boundary Conditions

There are two boundary conditions imposed on the cask model. The first one is symmetry boundary condition on the cutting plane. The cask is assumed to fall on a rigid surface and accordingly contact elements (CONTA178) are used to model the interface between cask surface and rigid surface of impact plane, with nodes representing rigid surface being constrained in axial direction. A total of 4 load cases are analyzed.

Load Cases

Set No.	Drop Orientation	Pressure Application
1	End Drop on Lid End	Internal Pressure (30psi)
2	End Drop on Lid End	External Pressure (25psi)
3	End Drop on Bottom End	Internal Pressure (30psi)
4	End Drop on Bottom End	External Pressure (25psi)

Loadings and boundary conditions on 3D Finite Element Model for end drop on lid end with 25 psig external pressure is shown on Figure B.2.13.3-3.

B.2.13.3.5 FEA Results

Buckling Load

The last converged solution in case of end drop on lid end with internal pressure and external pressure is 145g and 140g, respectively. To get a more conservative value of g-load, a time-history postprocessing is done for preselected nodes to plot the radial deformation against g-loads.

The location of selected nodes is shown in Figure B.2.13.3-4. The radial displacement plots for selected nodes in end drop on lid end cases are taken (Figures B.2.13.3-5 and B.2.13.3-6). As can be seen from the figures, there is significant shift in the slope of displacement curves at about 125g. Hence, 125g load has been conservatively taken as the buckling load. The displacement plots at 125g for lid end drop with 25 psig external pressure is shown in Figure B.2.13.3-7.

Lead Slump

Since the hypothetical accident condition g-load is 65g, the lead slump is calculated at 65g.

The following table summarizes the lead slump values for various load cases. The maximum lead slump is 0.465 in. and occurs during end drop on lid end case with 25 psig external pressure. The corresponding plot is shown on Figure B.2.13.3-8.

Summary of Lead Slump at 65g

Lead Slump at 65g (inches)		
Load Case	**Internal Pressure (30 psig)**	**External Pressure (25 psig)**
End Drop on Lid End	0.435	0.465
End Drop on Bottom End	0.422	0.453

B.2.13.3.6 Conclusions

The above table shows that the maximum longitudinal gap, caused by lead slump, is 0.465 inches, and occurs during accident condition of end drop on lid end. The effect of the gap on the shielding ability of the NUHOMS®-MP197TAD TO is analyzed in Chapter B.5.

The containment shell buckling load is 125g. That gives the acceptable safety ratio of 1.92 over the 65g HAC g-load.

B.2.13.3.7 References

1. ANSYS Computer Code and User's Manual, Release 10A1

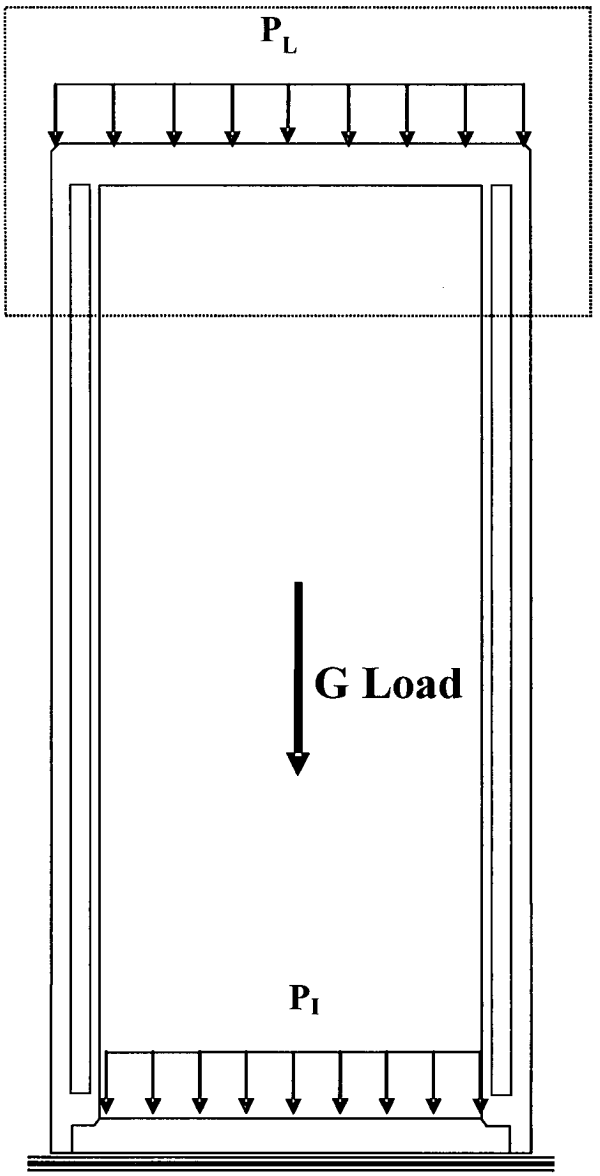

Figure B.2.13.3- 1
Schematic for End Drop on Lid End

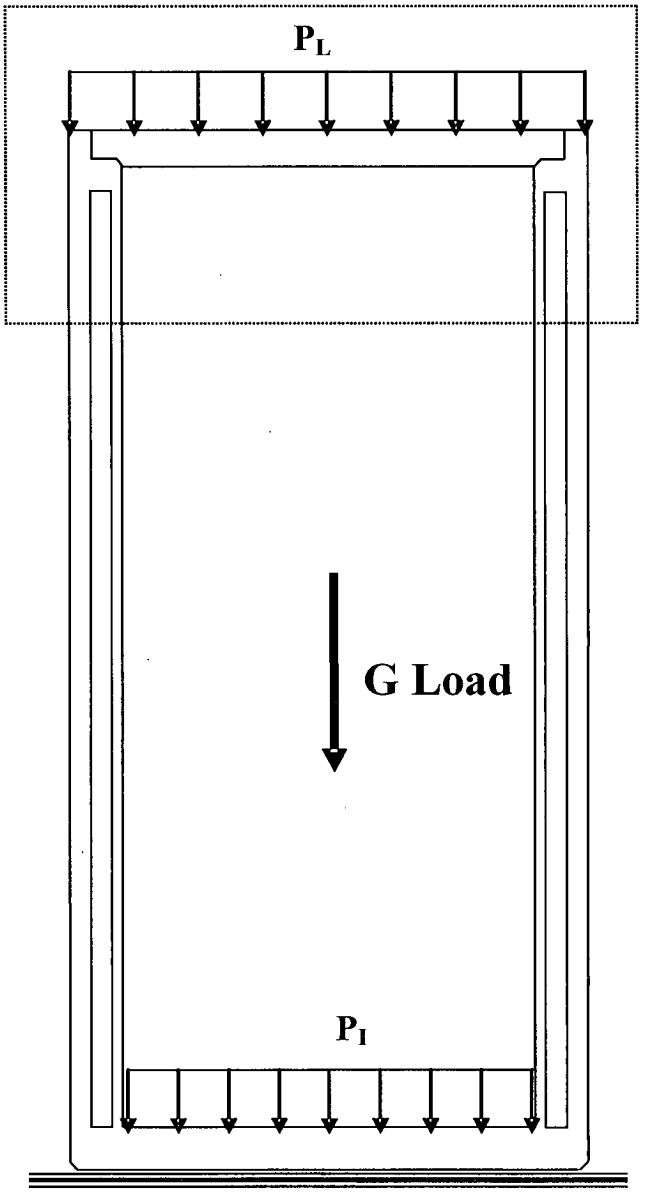

Figure B.2.13.3- 2
Schematic for End Drop on Bottom End

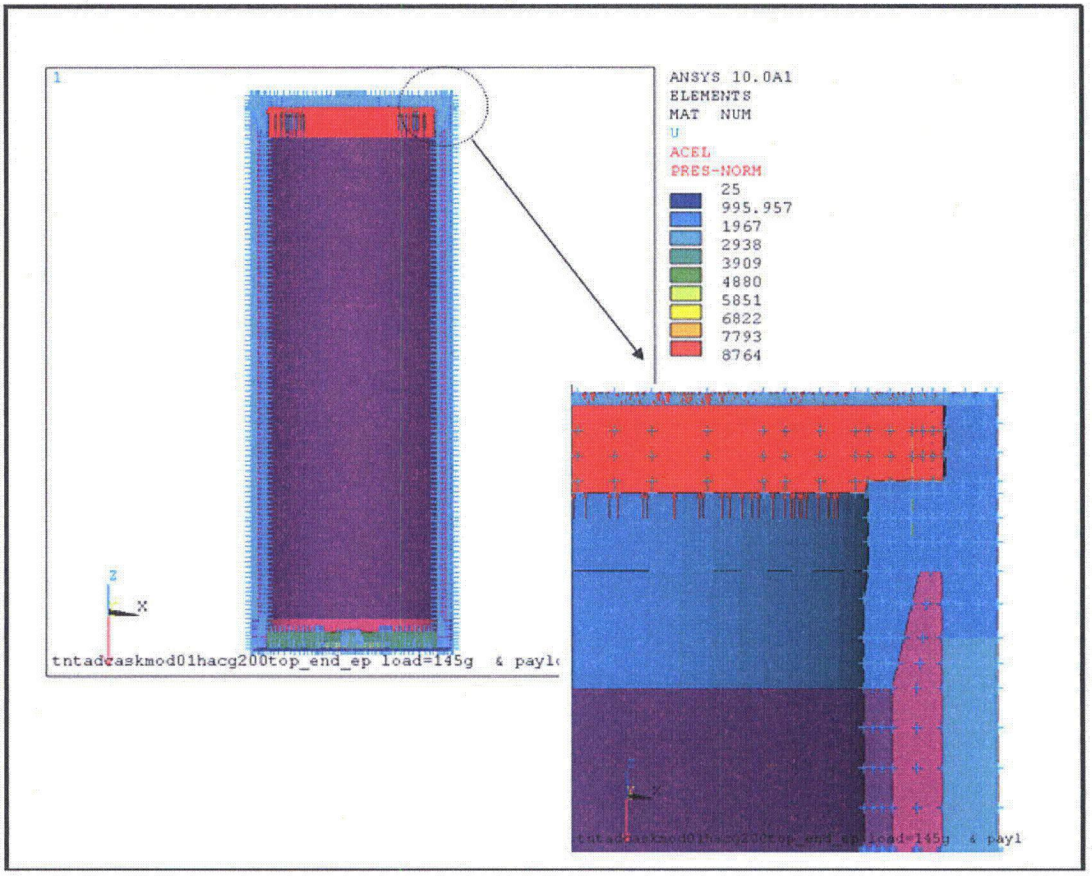

Figure B.2.13.3- 3
Boundary Condition & Loads for End Drop on Lid End with 25 psig External Pressure

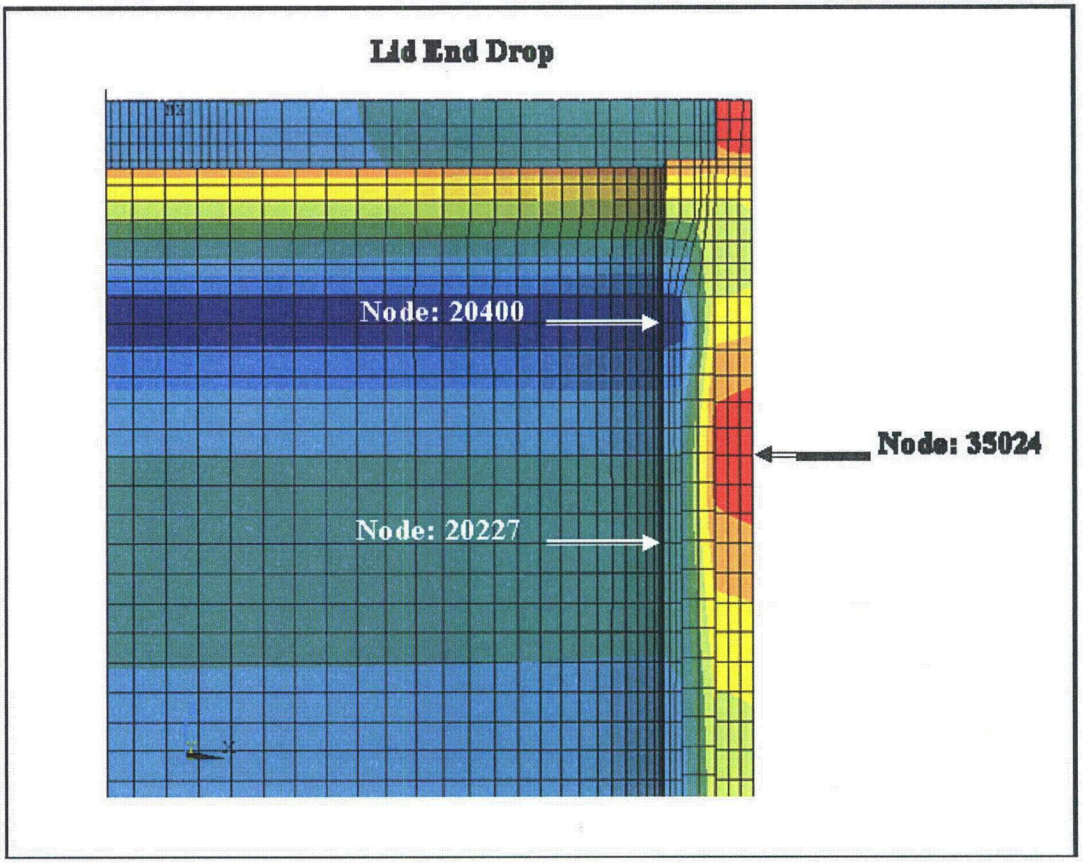

Figure B.2.13.3- 4
Nodes Selected for Time-History Post Processing

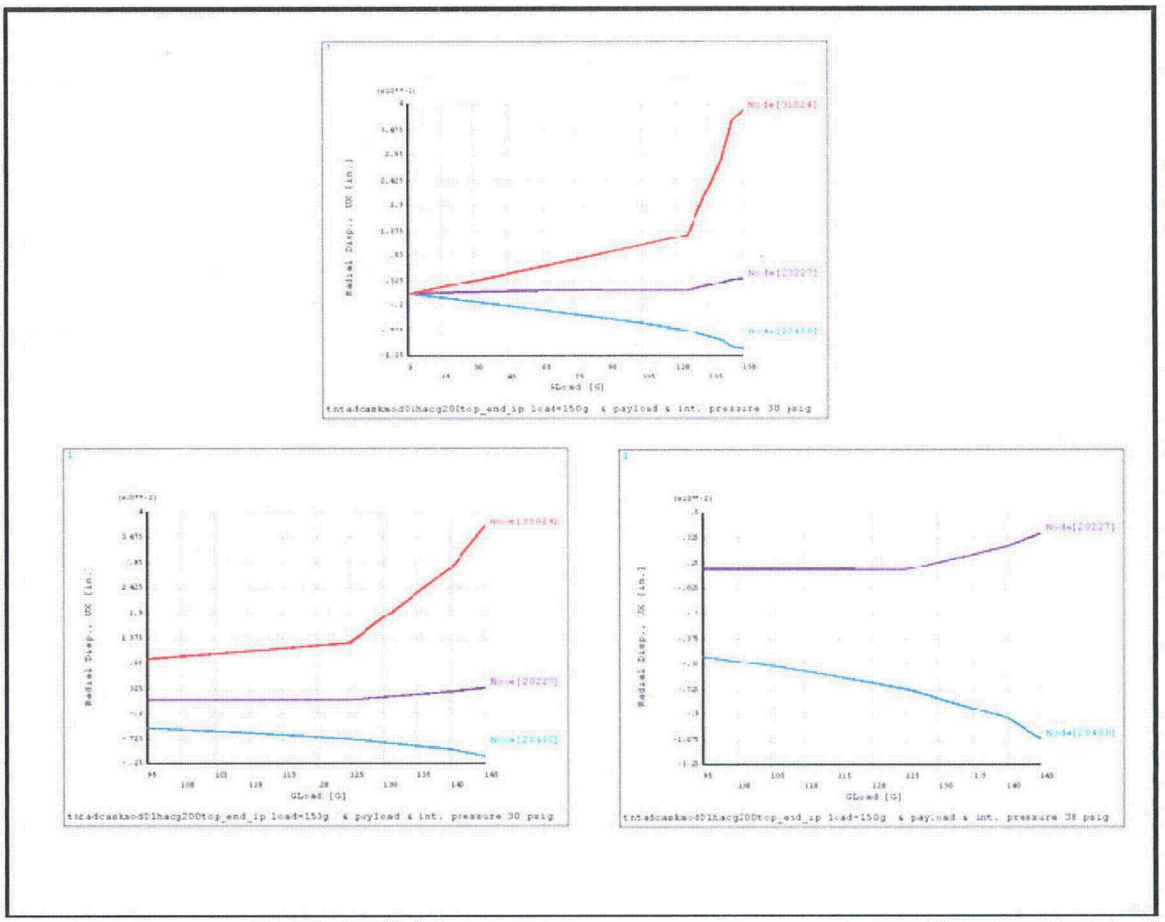

Figure B.2.13.3- 5
Displacement vs. G-Load Curve for End Drop on Lid End with 30 psig Internal Pressure (Enlarged View is Shown in the Bottom Plots)

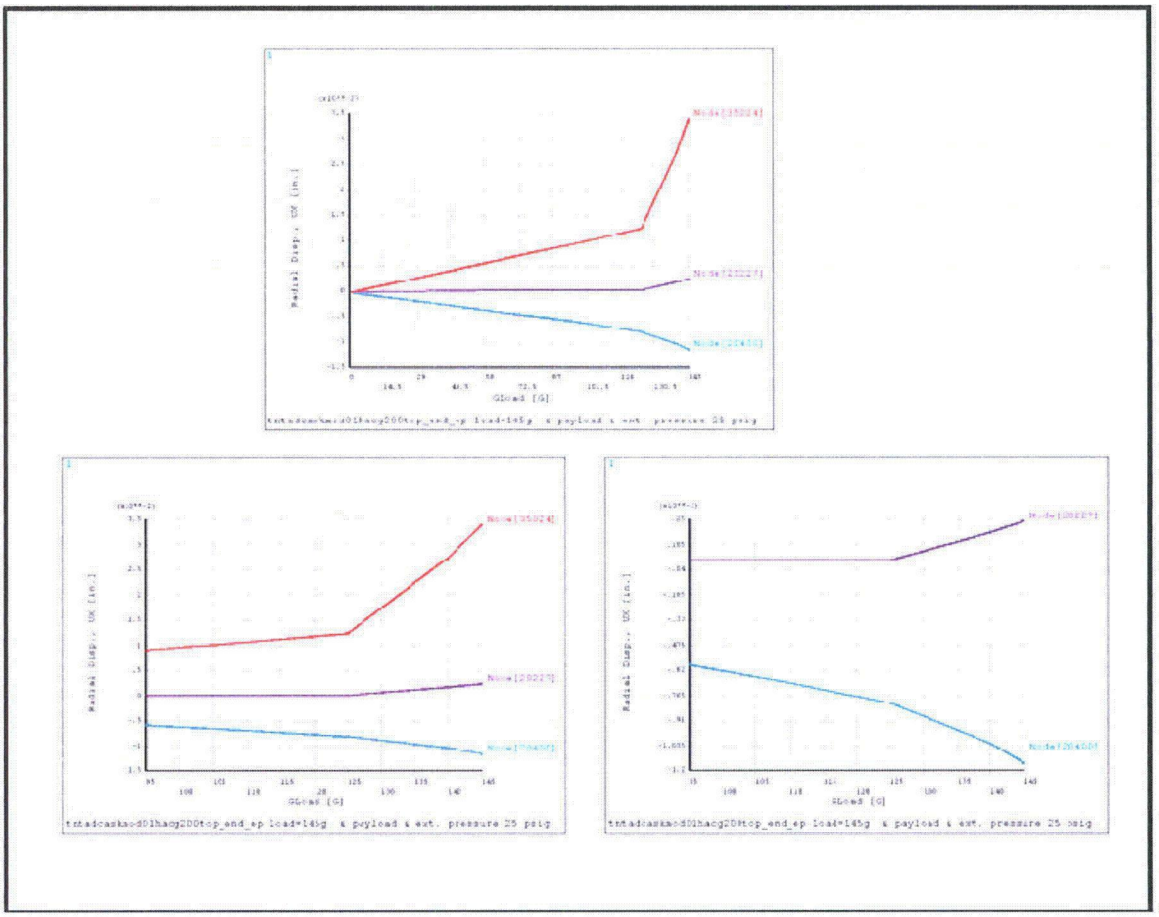

Figure B.2.13.3- 6
Displacement vs. G-Load Curve for End Drop on Lid End with 25 psig External Pressure (Enlarged View is Shown in the Bottom Plots)

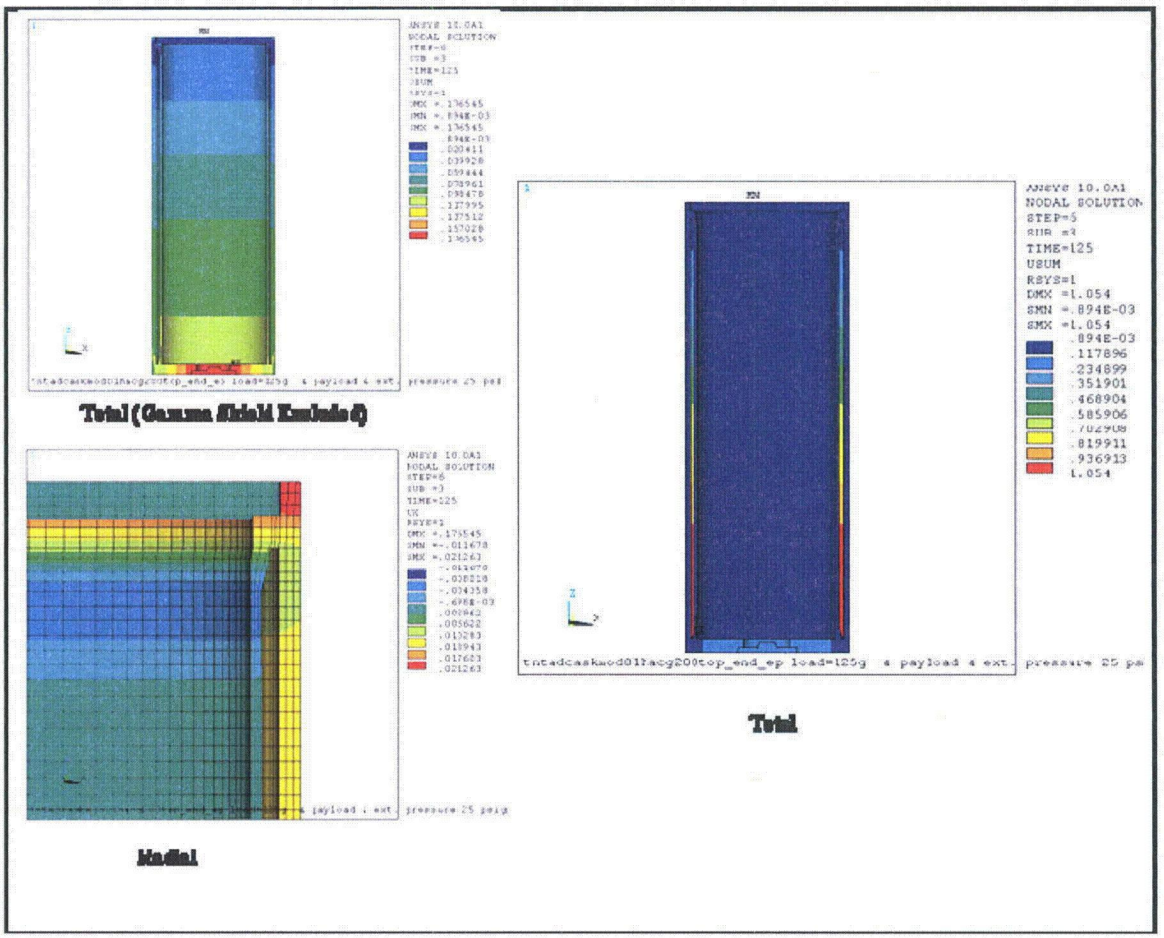

Figure B.2.13.3- 7
Displacement Plot at 125g (End Drop on Lid End with 25 psig External Pressure)

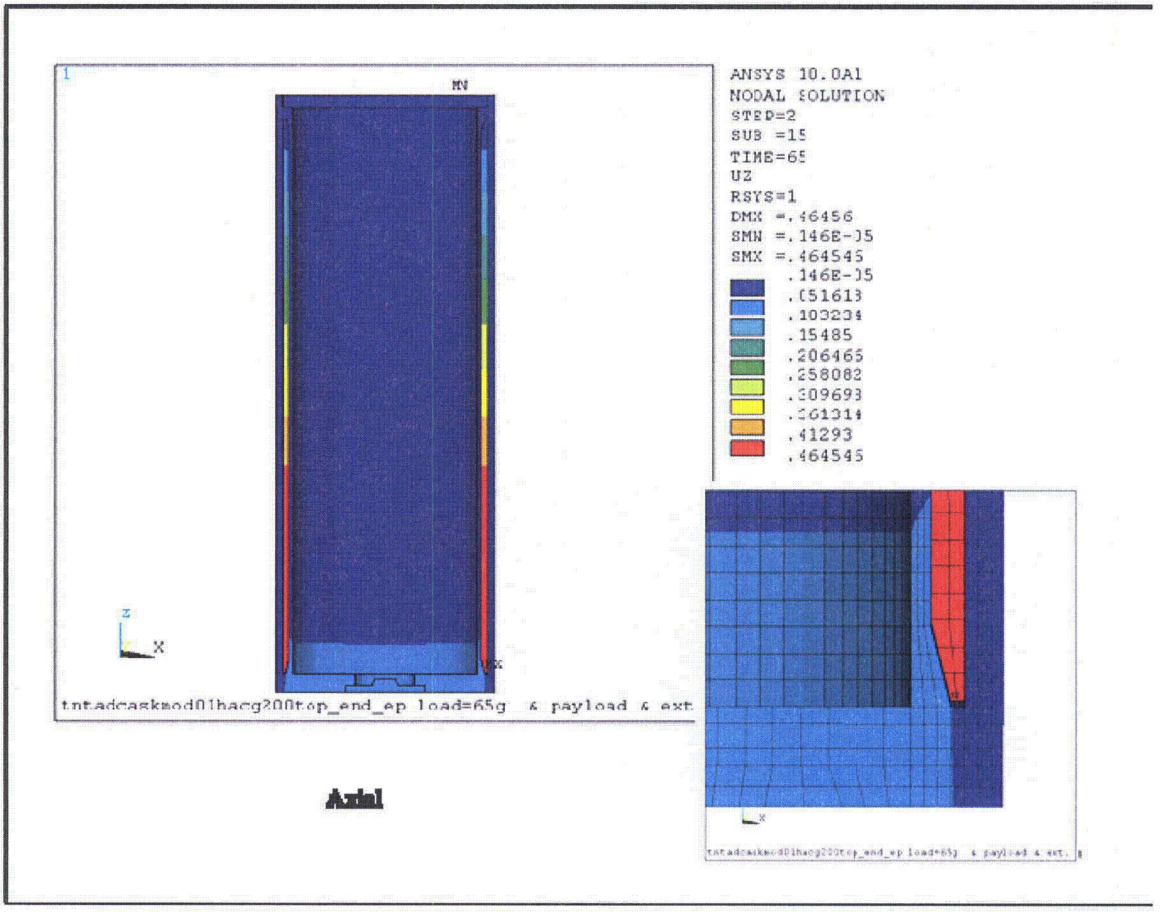

Figure B.2.13.3- 8
Lead Slump at 65g (End Drop on Lid End with 25 psig External Pressure)

Appendix B.2.13.4
MP197TAD TO Structural Analysis of the Neutron Shield Shell

CONTENTS

B.2.13.4.1 Introduction B.2.13.4-1
B.2.13.4.2 Description B.2.13.4-1
B.2.13.4.3 Materials Properties and Stress Criteria B.2.13.4-1
B.2.13.4.4 Finite Element Model Description B.2.13.4-1
B.2.13.4.5 Applied Loads B.2.13.4-2
B.2.13.4.6 Analysis Results B.2.13.4-3
B.2.13.4.7 References B.2.13.4-5

LIST OF TABLES

Table B.2.13.4-1 MP197TAD TO Non-Containment Structure/Weld Allowable Stress B.2.13.4-6
Table B.2.13.4-2 Maximum Stress Summary–Neutron Shield Shell Structure B.2.13.4-7

LIST OF FIGURES

Figure B.2.13.4-1 Cask Shield Shell and Connection to Cask Body B.2.13.4-8
Figure B.2.13.4-2 Finite Element ANSYS Mesh for the Neutron Shield Shell B.2.13.4-9
Figure B.2.13.4-3 MP197TAD TO Cask and Neutron Shield Shell Loads and Boundary Conditions (side drop) B.2.13.4-10
Figure B.2.13.4-4 MP197TAD TO Cask and Neutron Shield Shell Loads and Boundary Conditions (end drop) B.2.13.4-10
Figure B.2.13.4-5 Normal Condition Side Drop 20 g Stress Intensity–Neutron Shield Shell .. B.2.13.4-11
Figure B.2.13.4-6 Normal Condition Side Drop 20 g Maximum Displacement–Neutron Shield Shell B.2.13.4-12
Figure B.2.13.4-7 Normal Condition Side Drop 20 g Stress Intensity–Shield Plate B.2.13.4-13
Figure B.2.13.4-8 Normal Condition End Drop 35 g Stress Intensity–Neutron Shield Shell .. B.2.13.4-14
Figure B.2.13.4-9 Normal Condition End Drop 35 g Maximum Displacement–Neutron Shield Shell B.2.13.4-15
Figure B.2.13.4-10 Normal Condition End Drop 35 g Stress Intensity–Shield Plate B.2.13.4-16
Figure B.2.13.4-11 Accident Condition Side Drop 65 g Stress Intensity–Neutron Shield Shell B.2.13.4-17
Figure B.2.13.4-12 Accident Condition Side Drop 65 g Maximum Displacement–Neutron Shield Shell B.2.13.4-18
Figure B.2.13.4-13 Accident Condition Side Drop 65 g Stress Intensity–Shield Plate B.2.13.4-19
Figure B.2.13.4-14 Accident Condition End Drop 55 g Stress Intensity–Neutron Shield Shell B.2.13.4-20
Figure B.2.13.4-15 Accident Condition End Drop 55 g Maximum Displacement–Neutron Shield Shell B.2.13.4-21
Figure B.2.13.4-16 Accident Condition End Drop 55 g Stress Intensity–Shield Plate B.2.13.4-22

Appendix B.2.13.4
MP197TAD TO Structural Analysis of the Neutron Shield Shell

NOTE: References in this appendix are shown as [1], [2], etc., and refer to the reference list in Section B.2.13.4.7.

B.2.13.4.1 Introduction

This section presents the structural analysis of the neutron shield shell of the MP197TAD TO package. The neutron shield shell consists of a cylindrical shell section and closure plates at each end which connect the shell to the cask body. The shell is evaluated for normal condition of transport (NCT) and hypothetical accident condition (HAC) using ANSYS [3] for both side and end drop events. These stresses are compared to the allowable stress limits in Chapter B.2 to assure that the design criteria are met.

B.2.13.4.2 Description

The neutron shield shell is constructed from SA-240, Type 304 and is welded to the cask outer shell. The cylindrical shell section is 0.375 in. thick and the closure plates are 0.50 inch thick. Pertinent dimensions are shown in Figure B.2.13.4-1 and Drawings in Chapter B.1.

B.2.13.4.3 Materials Properties and Stress Criteria

The neutron shield shell cylindrical section and closure plates are SA-240 Type 304. Material properties and allowable stresses for normal (NCT) and accident (HAC) drop analyses are based on 300°F which bound -40°F, -20°F, and 100°F ambient conditions. The material properties are taken from the ASME Code [2] at a temperature of 300 °F and are listed below.

MP197TAD TO Non-Containment Structure Material Properties

Temp (°F)	E (10^3 ksi)	S_m (ksi)	S_y (ksi)	S_u (ksi)	α_{AVG} x 10^{-6} (in/in/°F)	ρ (lb/in.^{3})
300	27.0	20.0	22.4	66.2	9.2	0.284

The stress criteria are in according to ASME Code Section III, Subsection NF and Appendix F [1] and are listed in Table B.2.13.4-1.

B.2.13.4.4 Finite Element Model Description

ANSYS Model

The geometry used in the ANSYS [3] finite element analysis of the neutron shield shell is shown in Figure B.2.13.4-1 (0.3125" shell thickness is used instead of 0.375").

Cask and neutron shield shells were modeled using ANSYS SOLID45 (8 nodes having 3 translational DOF) elements. Welds were simulated using couplings (all translational degrees of

freedom) at the interface of cask to top and bottom plates of the neutron shield structure and at the interface of the neutron shield shell to the top and bottom plates as pinned connections (see Figure B.2.13.4-3).

CONTACT52 elements were used at the interface of the resin and neutron shield shell, the top/bottom plates and between the resin and cask shell. This CONTACT52 gap element can introduce non linearity in the analysis depending whether they are open or closed. Additionally COMBIN14 weak spring (10 lbs/in stiffness) elements were modeled along with CONTACT52 interface, which is useful for preventing rigid body motion that could occur in the analysis.

Boundary Conditions

Symmetric boundary conditions were applied at the cut face of the model. For the end drop simulation, all bottom surface nodes of the casks were constrained in vertical direction, whereas for the side drop, cask nodes on the neutron shield diameter, above top end plate and below bottom end plates, were constrained up to 30° in the hoop direction. Figures B.2.13.4-2, B.2.13.4-3, and B.2.13.4-4 show the overall finite element ANSYS model, and boundary conditions for both side and end drop.

Vyal B Resin Density Calculation

The Vyal B resin density (0.0650 lb/in^3) is adjusted to account for (aluminum boxes, bearing blocks, tie bars and other components) that are not captured in the finite element model.

Weight of Vyal B resin = 16,222 lbs
Weight of aluminum, bearing blocks and tie rods (combined) = 3,479 lbs
Density = (16,622+3,479)*0.0650/16,222 = 0.0786046 lb/in^3, conservatively used 0.0787 lb/in^3 in the analysis.

Young's modulus of 5.0E+05 psi is assumed for Vyal B resin material.

B.2.13.4.5 Applied Loads

The neutron shield shell structure is analyzed for both side and end drops to bound all the possible maximum stress cases resulting from normal and accident events. For side drops acceleration due to gravity, g-loads were applied on the model in the hoop direction and for end drops, g-loads were applied in the axial direction.

The ANSYS 1g accelerations, indicating direction of side drop load, are:

- Side drop acel, -1, 0, 0

For 20g, and 65g, loading, the ANSYS acceleration values are 20, and 65 times the above values.

The ANSYS 1g accelerations, indicating direction of end drop load, are:

- End drop acel, 0, 1, 0

For 35g, and 55g, loading, the ANSYS acceleration values are 35, and 55 times the above values.

An internal pressure of 25psig is applied on all the inner walls of the neutron shield structure, outer wall of the Cask shell and also at the interfaces of the partial penetration welds in the ANSYS model.

Load Cases Analyzed

Loading	Service Level	Service Level	Load	Analysis Method
Side Drop		NCT	20g	Finite Element Elastic Analysis
End Drop		NCT	35g	Finite Element Elastic Analysis
Side Drop	HAC		65g	Finite Element Elastic Analysis
End Drop	HAC		55g	Finite Element Elastic Analysis

B.2.13.4.6 Analysis Results

A. Normal Condition Side and End Drops

The resulting stress intensity distribution and displacements on the neutron shield shell for side and end drop are shown in Figures B.2.13.4-5 through B.2.13.4-10. It is seen that the maximum nodal stress intensity in the structure is 21.91 ksi (Figure B.2.13.4-5) for 20g side drop and 11.51 ksi (Figure B.2.13.4-8) for 35g end drop. All the normal condition stresses are below the allowable stress values. See Table B.2.13.4-2 for stress comparison.

B. Accident Condition Side and End Drop

Accident condition side and end drop stress intensity and displacement plots are shown in Figures B.2.13.4-11 through B.2.13.4-16. It is seen that the maximum nodal stress intensity in the structure is 73.15 ksi (Figure B.2.13.4-11) and 18.95 ksi (Figure B.2.13.4-14) for 65g side drop and 55g end drops respectively. All the accident condition stresses are below the allowable stress values. See Table B.2.13.4-2 for stress comparison.

C. Weld Stress Calculations

All welds in ANSYS were represented by couplings as pin connections. For partial penetration fillet welds, stresses are calculated as:

$F_w = F_{\text{resultant}} / (L_{\text{tributary}})\ (T_{\text{weld}})$,

where,

$F_{\text{resultant}}$ = maximum resultant nodal force = $(F_x^2 + F_y^2 + F_z^2)^{1/2}$

$L_{tributary}$ = minimum tributary length associated with the nodes = $\pi R / (n - 1)$, where $R = 39.50$ (cask radius) and n is the maximum nodes used at weld interface locations (29 number of nodes used in the ANSYS model)

T_{weld} = appropriate weld throat or base metal dimension: The effective throat thickness is taken as 0.4375" (7/16") for welds at the cask to neutron shield shell top and bottom end plates, where as welds throat thickness at the interface of neutron shield shell to top and bottom end plates is 0.3125 (5/16").

The weld stress results are listed in Table B.2.13.4-2.

D. Summary of Results

The critical stresses are summarized in Table B.2.13.4-2. Based on the results of the structural analysis, it is concluded that the neutron shield shell structure is adequate for the specified loads to use with NUHOMS® MP197TAD TO Package.

B.2.13.4.7 References

1. ASME Boiler and Pressure Vessel Code, Section III, Division 1, Subsection NF and Appendices, 2004 edition.
2. ASME Boiler and Pressure Vessel Code, Section II, Part D, 2004 edition.
3. ANSYS Computer Code and Users Manual, Release 10.0.

Table B.2.13.4-1
MP197TAD TO Non-Containment Structure/Weld Allowable Stress

Stress Category	Structure Allowable Stresses	
	Normal Conditions	**Accident Conditions**
Primary Membrane General P_m Local P_L	S_m 1.5 S_m	Lesser of 2.4S_m or 0.7 S_u (1) Lesser of 3.6S_m or S_u (1)
Primary Membrane + Bending (P_m or P_L) + P_b	1.5 S_m	Lesser of 3.6S_m or S_u (1)
Range of Primary + Secondary (P_m or P_L) + P_b +Q	3.0 S_m	Not applicable
Bearing Stress	S_y	Not applicable
Average Shear Stress	0.6 S_m	0.42 S_u
Fatigue	Not Applicable	Not Applicable
Weld Allowable		
NCT	Full Penetration	Same as base metal
	Partial Grove/Fillet	Tension - 0.3 x S_u Shear – 0.4 x S_y
HAC	Full Penetration	Same as base metal
	Partial Grove/Fillet	Normal condition allowables are increased by a factor: Smaller of 2 or 1.167S_u/S_y if S_u > 1.2S_y, or 1.4 if $S_u \leq 1.2S_y$

Note:

1. Classification and stress limits are as defined in ASME Code, Section III, and Subsection NF. When evaluating the results from the nonlinear elastic plastic analysis for the accident conditions, the general primary membrane stress intensity, Pm, shall not exceed greater of 0.7 S_u or S_y + 1/3 (S_u - S_y) and the maximum primary stress intensity at any location (P_L or P_L + P_b) shall not exceed 0.9 S_u. These limits are in accordance with Appendix F of Section III of the Code [1].

Table B.2.13.4-2
Maximum Stress Summary–Neutron Shield Shell Structure

Drop Orientation	Stress Category	Location	Maximum Stress (ksi)[2]	Allowable Stress (ksi)
20g Side Drop Elastic Analysis Normal Condition of Transport	P_m[1]	Neutron shield Shell	9.66	20.0
	$P_m + P_b$[1]		10.04	30.0
	P_m[1]	Bottom Plate	7.40	20.0
	$P_m + P_b$[1]		17.39	30.0
	P_m[1]	Top Plate	7.46	20.0
	$P_m + P_b$[1]		17.37	30.0
	Partial penetration Groove Welds[2]	Cask and top plate weld	3.40	8.96
		Cask and bottom plate weld	3.23	8.96
		Shield shell and top plate weld	2.82	8.96
		Shield shell and bottom plate weld	2.83	8.96
35g End Drop Elastic Analysis Normal Condition of Transport	P_m[1]	Neutron shield Shell	10.58	20.0
	$P_m + P_b$[1]		11.08	30.0
	P_m[1]	Bottom Plate	6.04	20.0
	$P_m + P_b$[1]		11.66	30.0
	P_m[1]	Top Plate	5.55	20.0
	$P_m + P_b$[1]		10.41	30.0
	Partial penetration Groove Welds[2]	Cask and top plate weld	1.63	8.96
		Cask and bottom plate weld	1.06	8.96
		Shield shell and top plate weld	1.03	8.96
		Shield shell and bottom plate weld	2.90	8.96
65g Side Drop Elastic Analysis Hypothetical Accident Condition	P_m[1]	Neutron shield Shell	21.63	46.3
	$P_m + P_b$[1]		22.67	66.2
	P_m[1]	Bottom Plate	24.83	46.3
	$P_m + P_b$[1]		58.16	66.2
	P_m[1]	Top Plate	24.99	46.3
	$P_m + P_b$[1]		58.15	66.2
	Partial penetration Groove Welds[2]	Cask and top plate weld	10.64	17.92
		Cask and bottom plate weld	10.11	17.92
		Shield shell and top plate weld	9.38	17.92
		Shield shell and bottom plate weld	9.39	17.92
55g End Drop Elastic Analysis Hypothetical Accident Condition	P_m[1]	Neutron shield Shell	14.57	46.3
	$P_m + P_b$[1]		15.39	66.2
	P_m[1]	Bottom Plate	9.33	46.3
	$P_m + P_b$[1]		17.47	66.2
	P_m[1]	Top Plate	9.76	46.3
	$P_m + P_b$[1]		17.23	66.2
	Partial penetration Groove Welds	Cask and top plate weld	2.57	17.92
		Cask and bottom plate weld	1.52	17.92
		Shield shell and top plate weld	2.02	17.92
		Shield shell and bottom plate weld	3.54	17.92

Notes:
[1] Stresses are linearized for Pm and Pm+ Pb values between the inner and outer nodes of the shield shell, top/bottom plate components.
[2] To account for difference in weight of 3/8" thick shell modeled as 5/16" thick shell (see assumption 9) the stresses are multiplied by a scale factor of 1.032 which is the ratio of the (weight of the resin + weight of the 3/8" thick shell) and (weight of the resin + weight of the 5/16" thick shell).

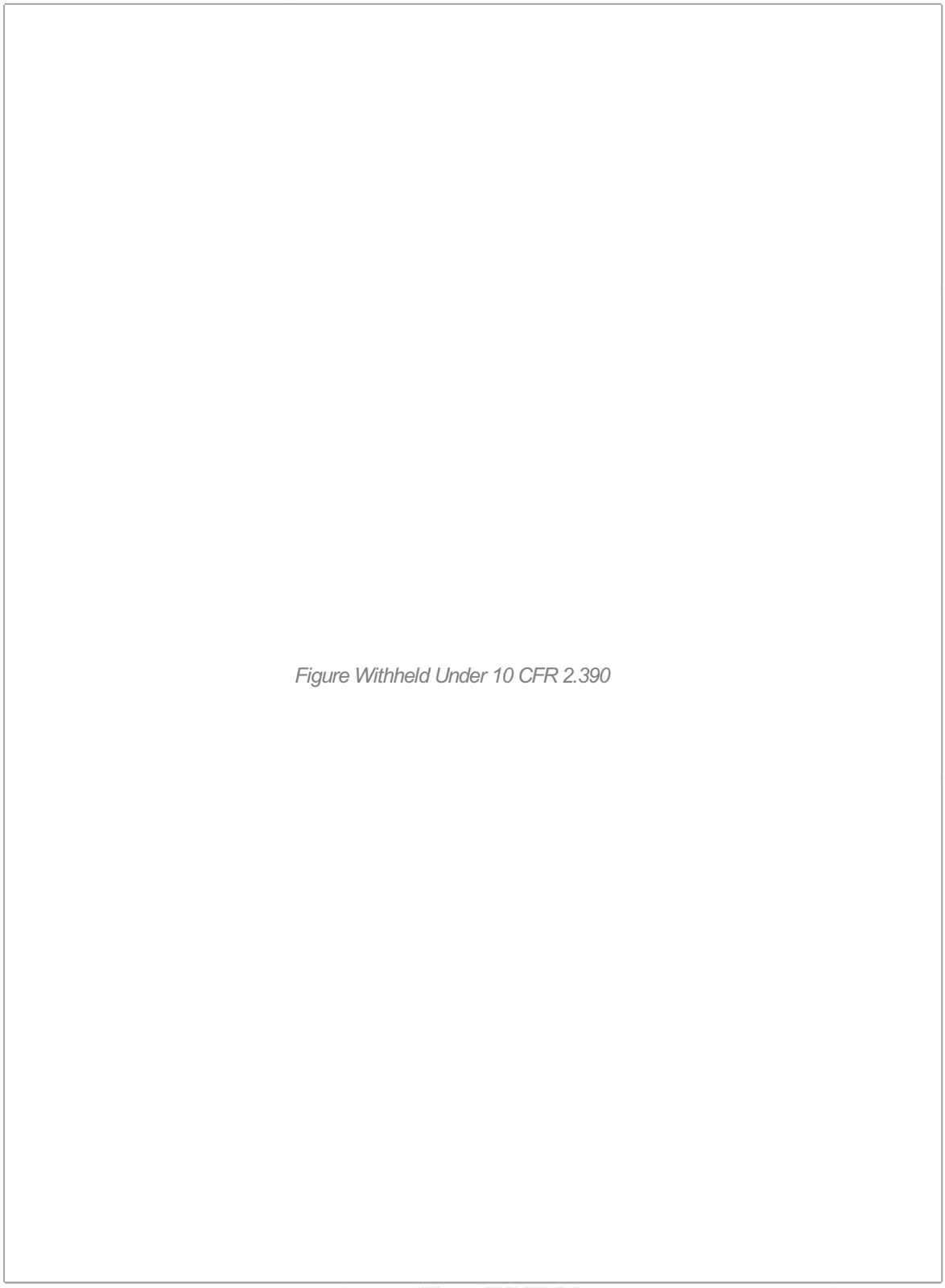

Figure B.2.13.4-1
Cask Shield Shell and Connection to Cask Body

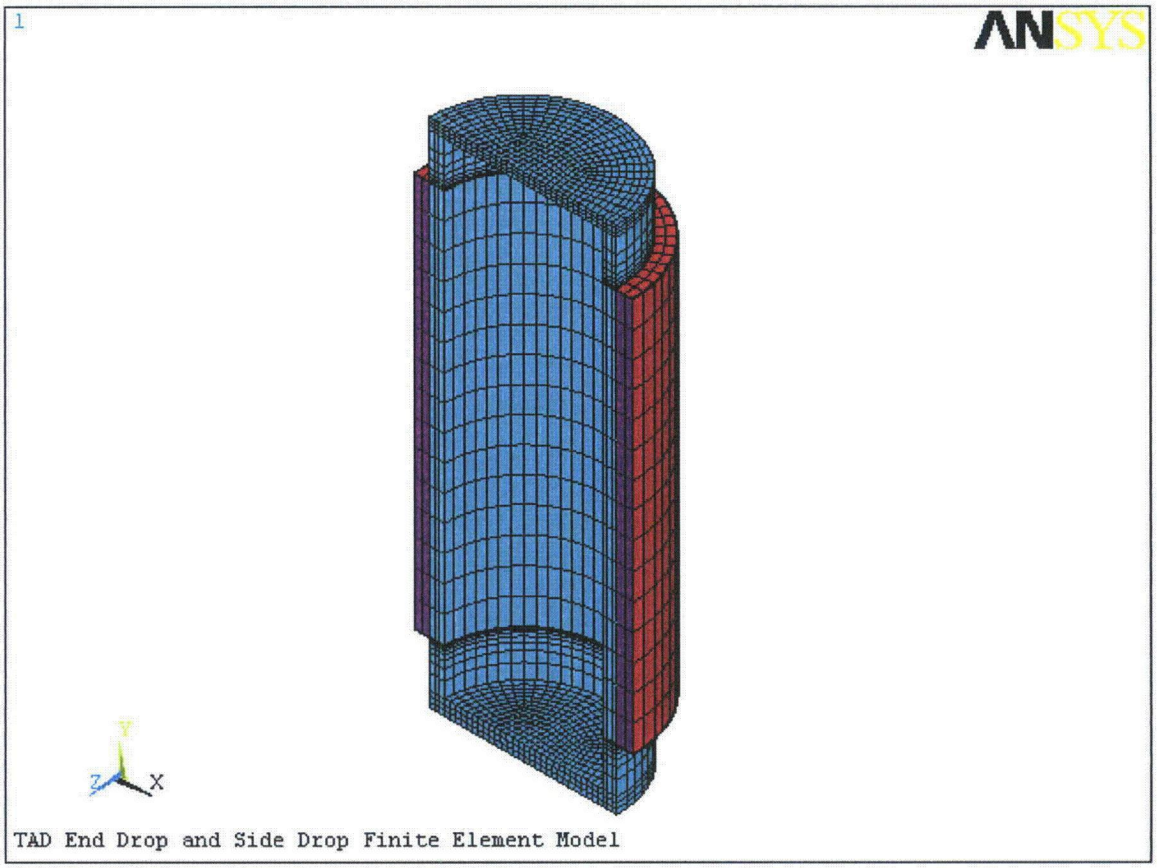

Figure B.2.13.4-2
Finite Element ANSYS Mesh for the Neutron Shield Shell

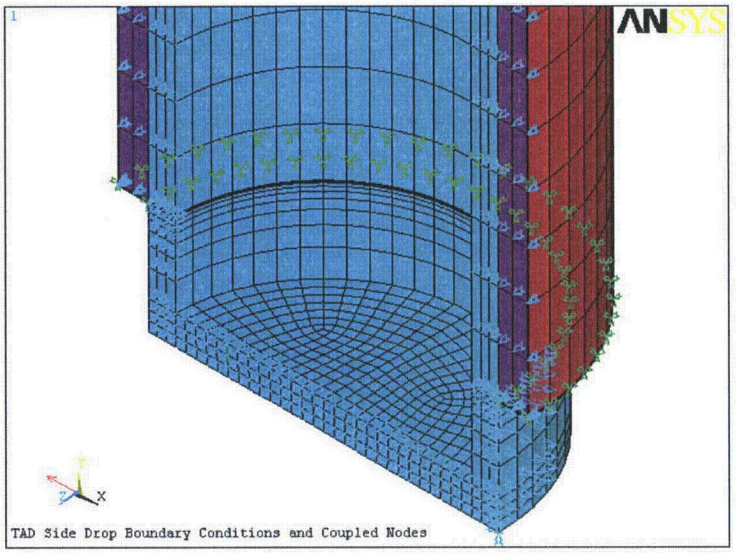

Figure B.2.13.4-3
MP197TAD TO Cask and Neutron Shield Shell Loads and Boundary Conditions (Side Drop)

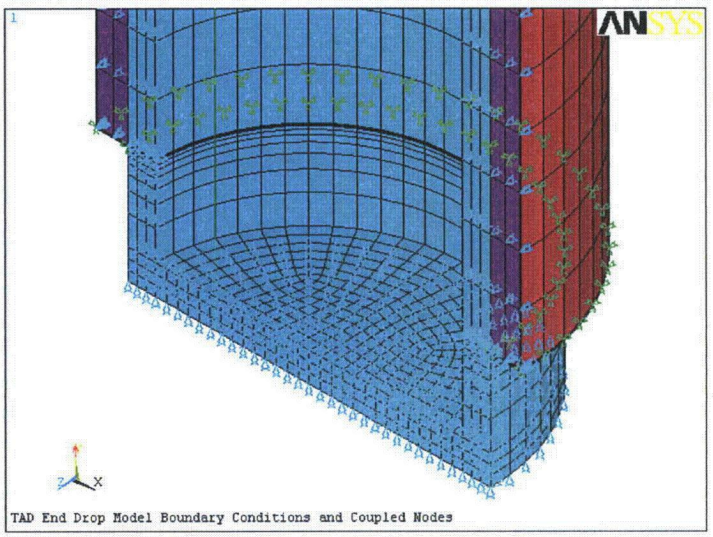

Figure B.2.13.4-4
MP197TAD TO Cask and Neutron Shield Shell Loads and Boundary Conditions (End Drop)

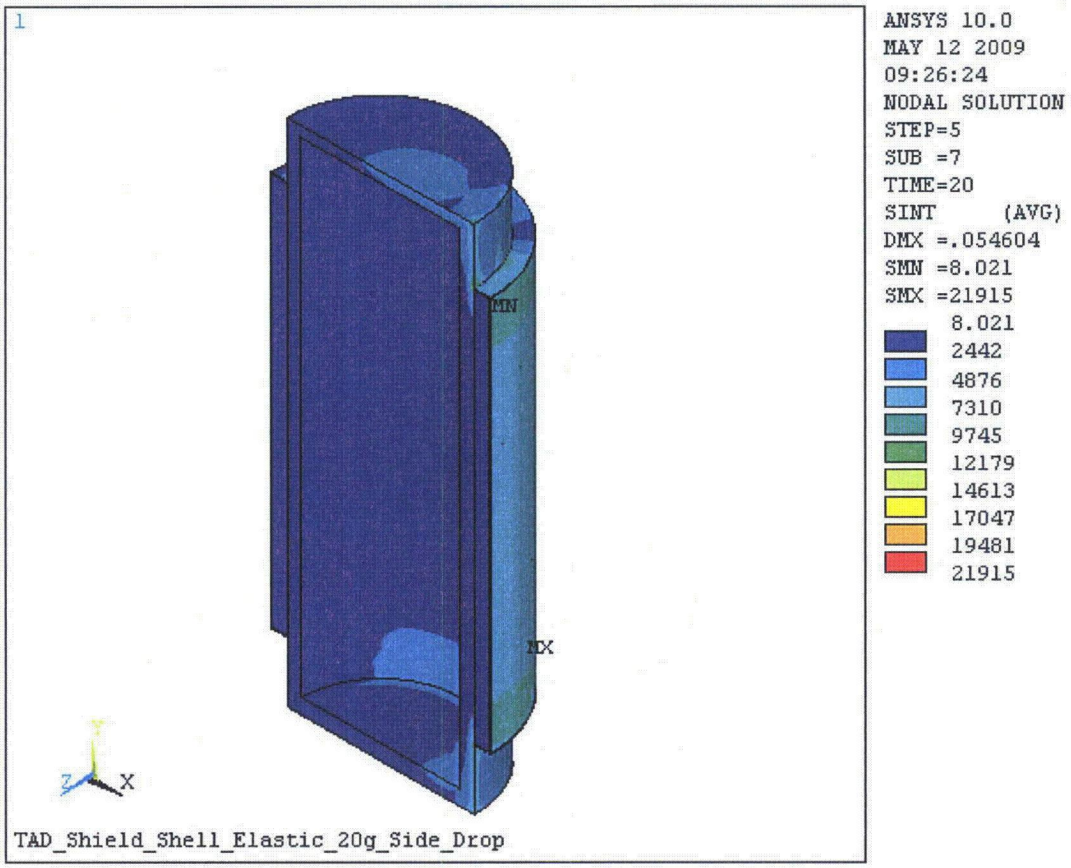

Figure B.2.13.4-5
Normal Condition Side Drop 20 g Stress Intensity–Neutron Shield Shell

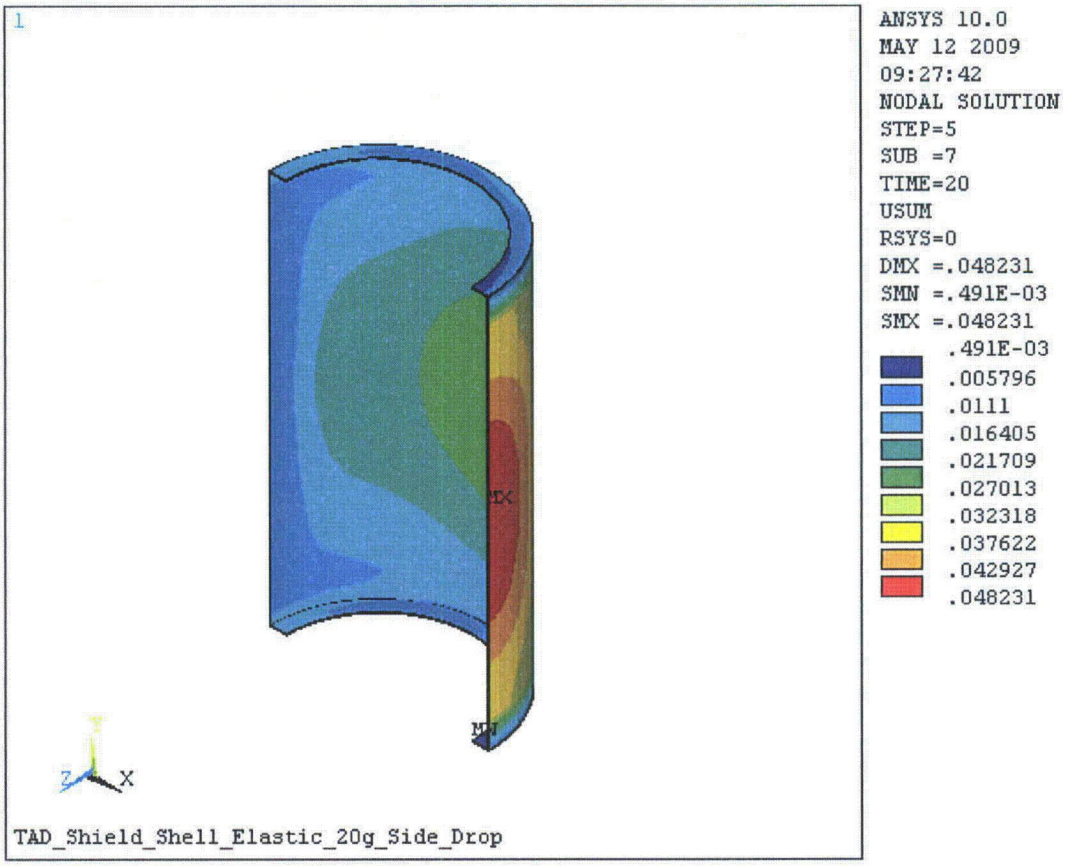

Figure B.2.13.4-6
Normal Condition Side Drop 20 g Maximum Displacement–Neutron Shield Shell

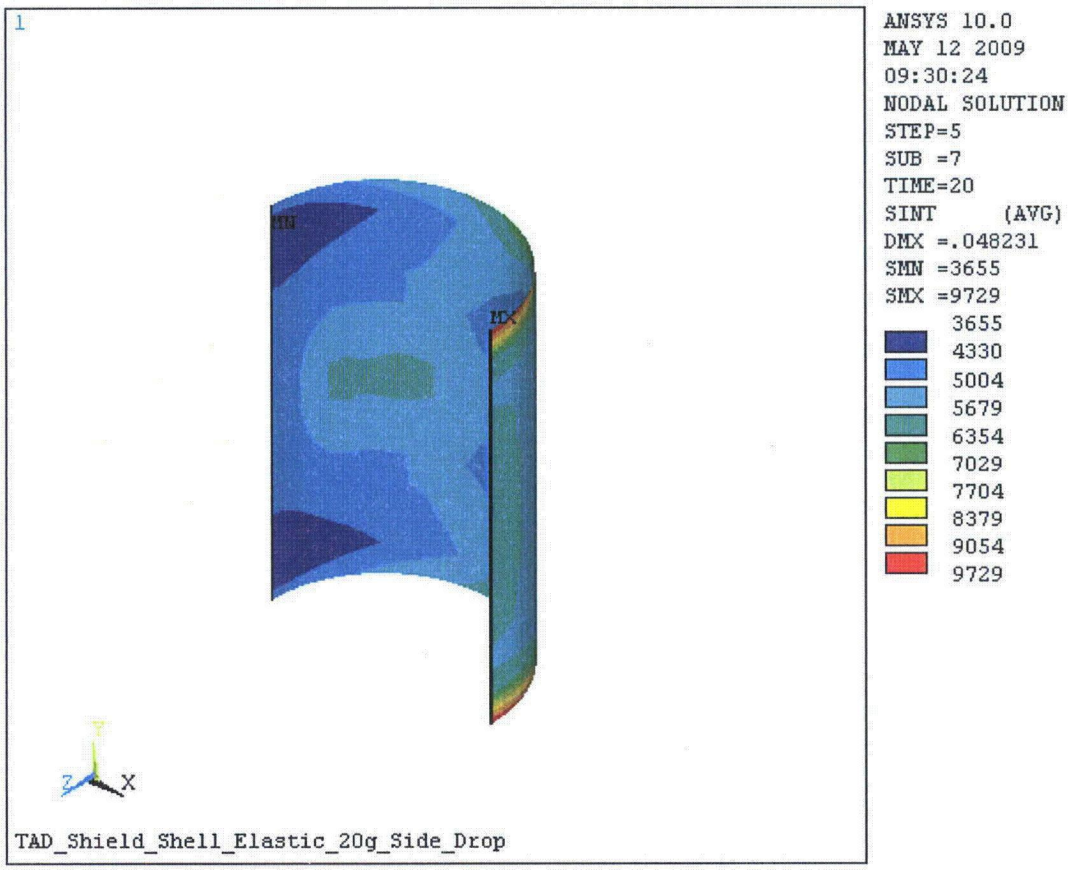

Figure B.2.13.4-7
Normal Condition Side Drop 20 g Stress Intensity–Shield Plate

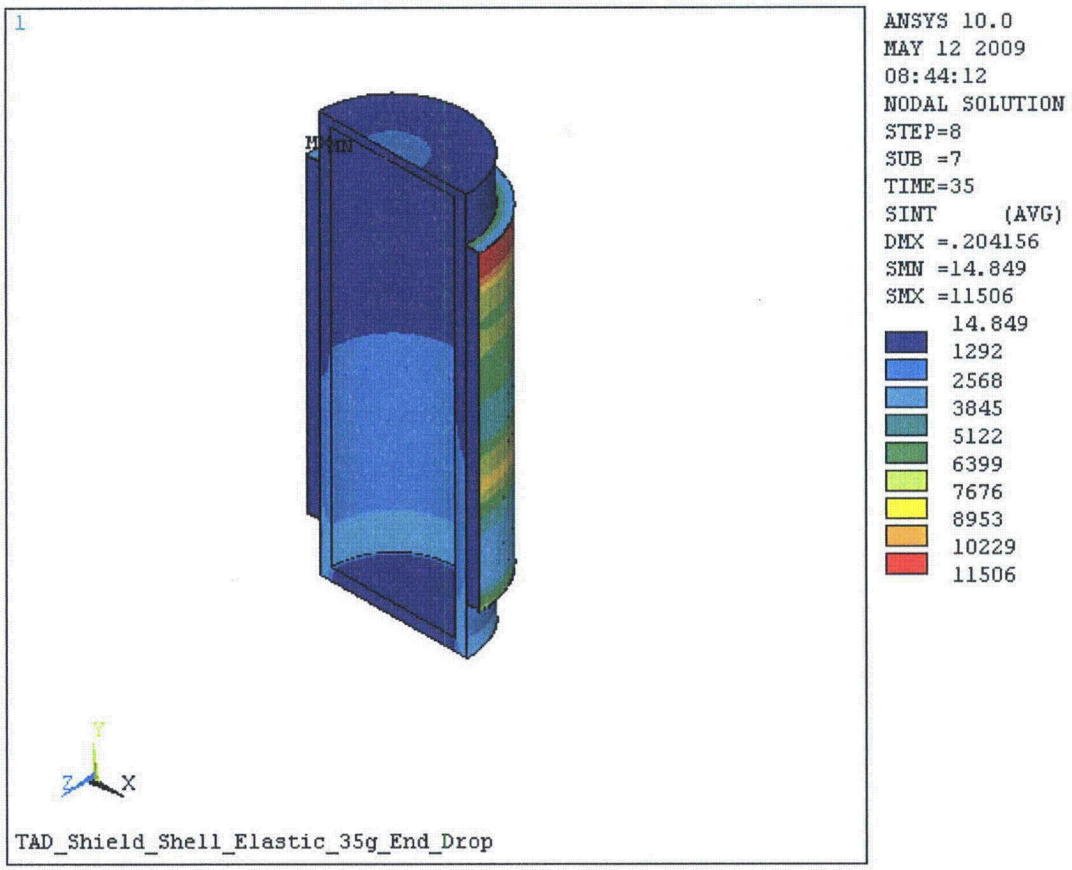

Figure B.2.13.4-8
Normal Condition End Drop 35 g Stress Intensity–Neutron Shield Shell

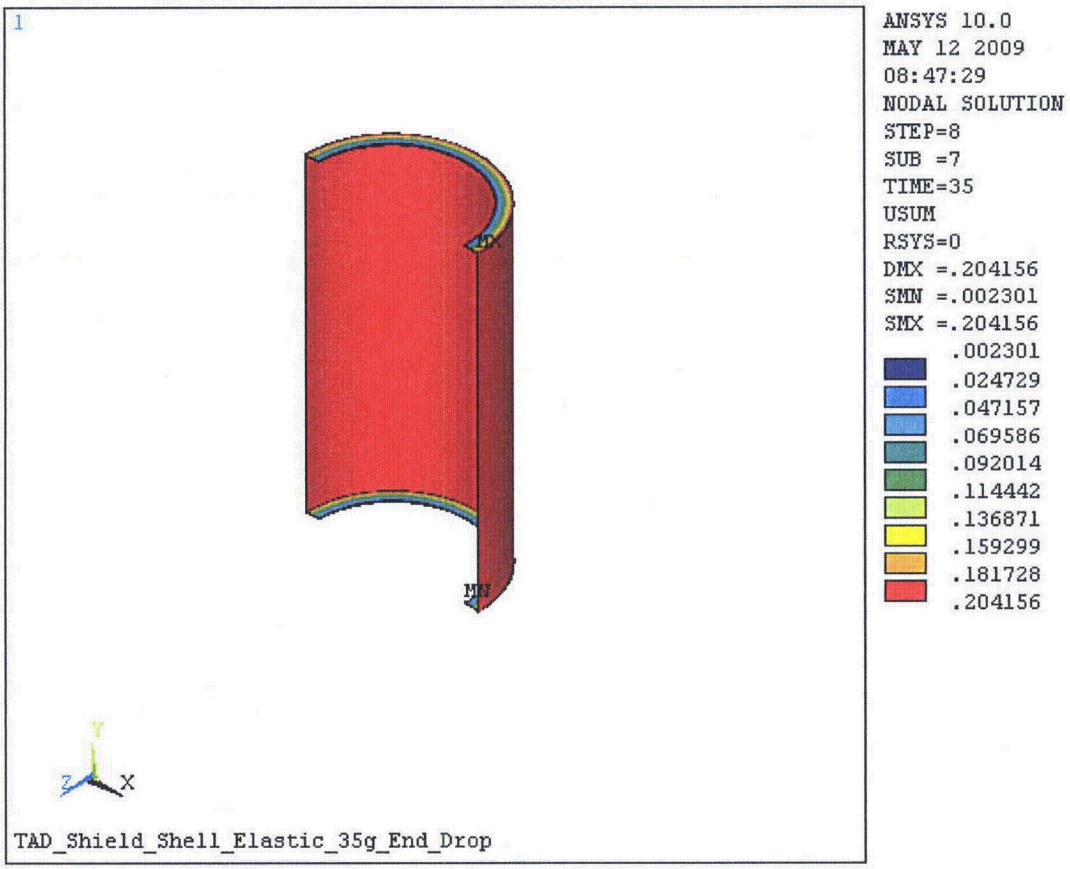

Figure B.2.13.4-9
Normal Condition End Drop 35 g Maximum Displacement–Neutron Shield Shell

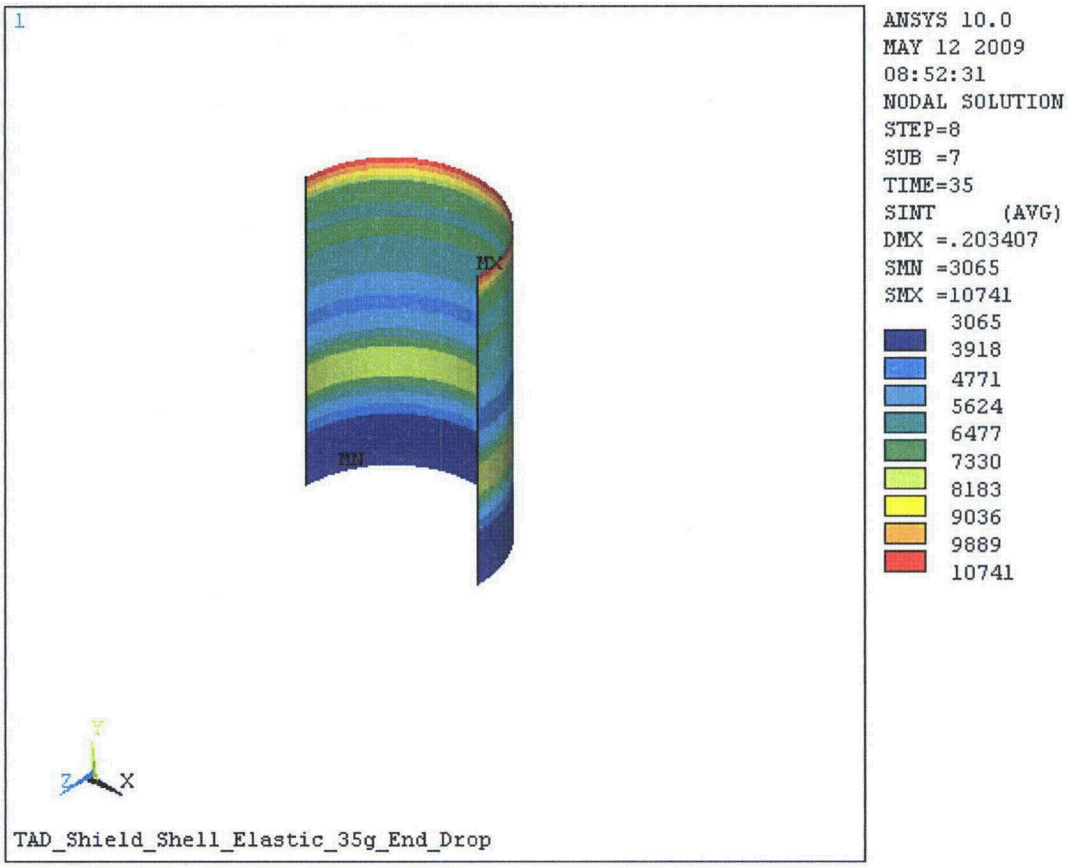

Figure B.2.13.4-10
Normal Condition End Drop 35 g Stress Intensity–Shield Plate

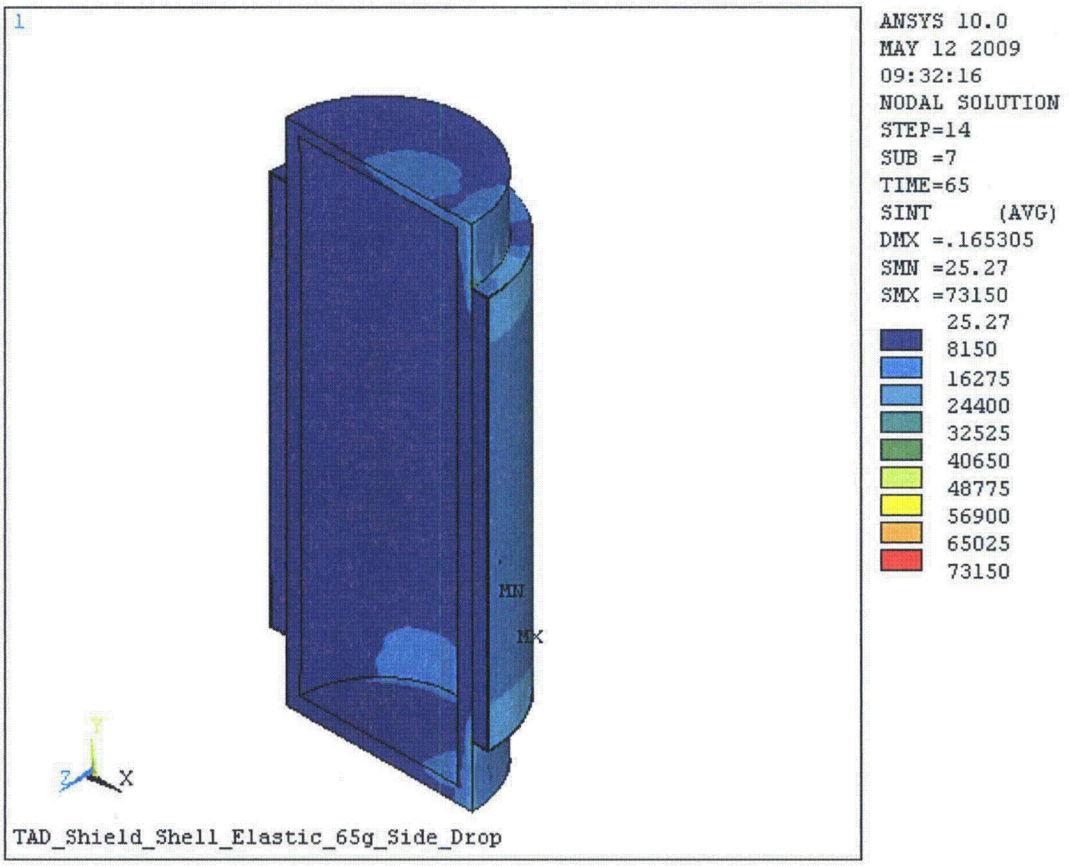

Figure B.2.13.4-11
Accident Condition Side Drop 65 g Stress Intensity–Neutron Shield Shell

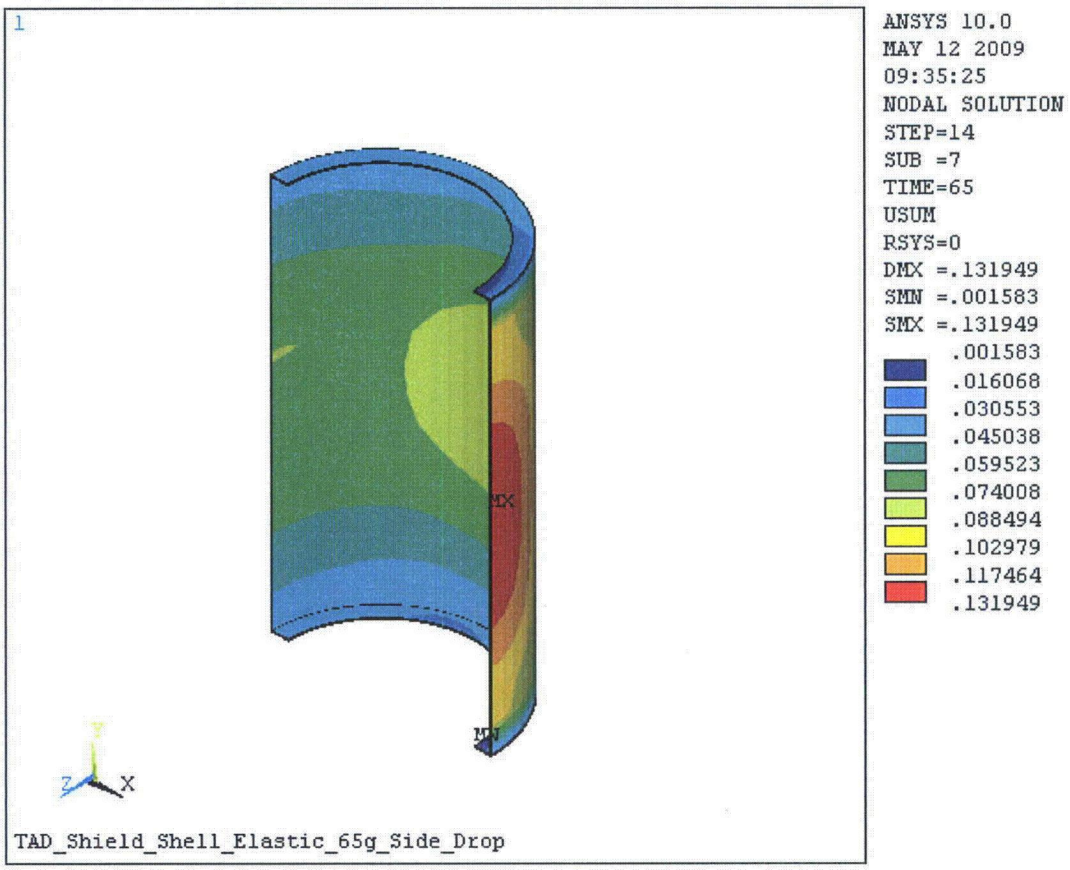

Figure B.2.13.4-12
Accident Condition Side Drop 65 g Maximum Displacement–Neutron Shield Shell

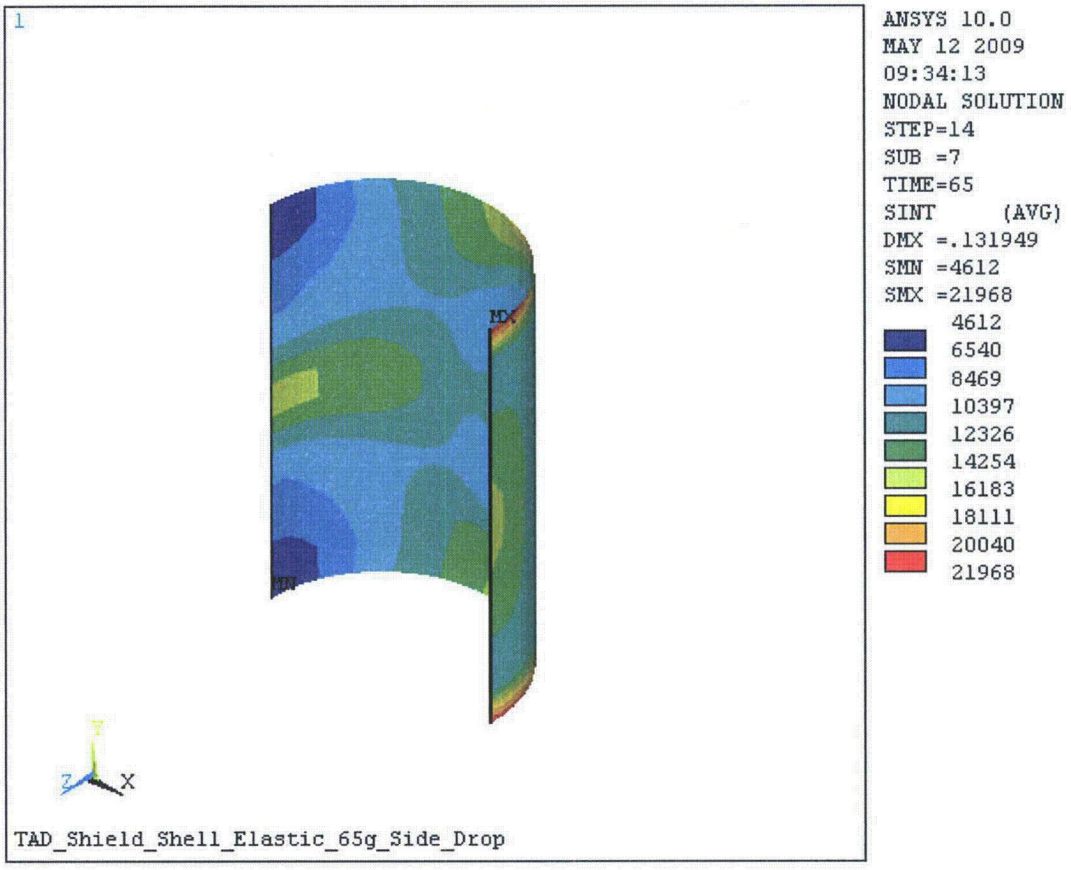

Figure B.2.13.4-13
Accident Condition Side Drop 65 g Stress Intensity– Shield Plate

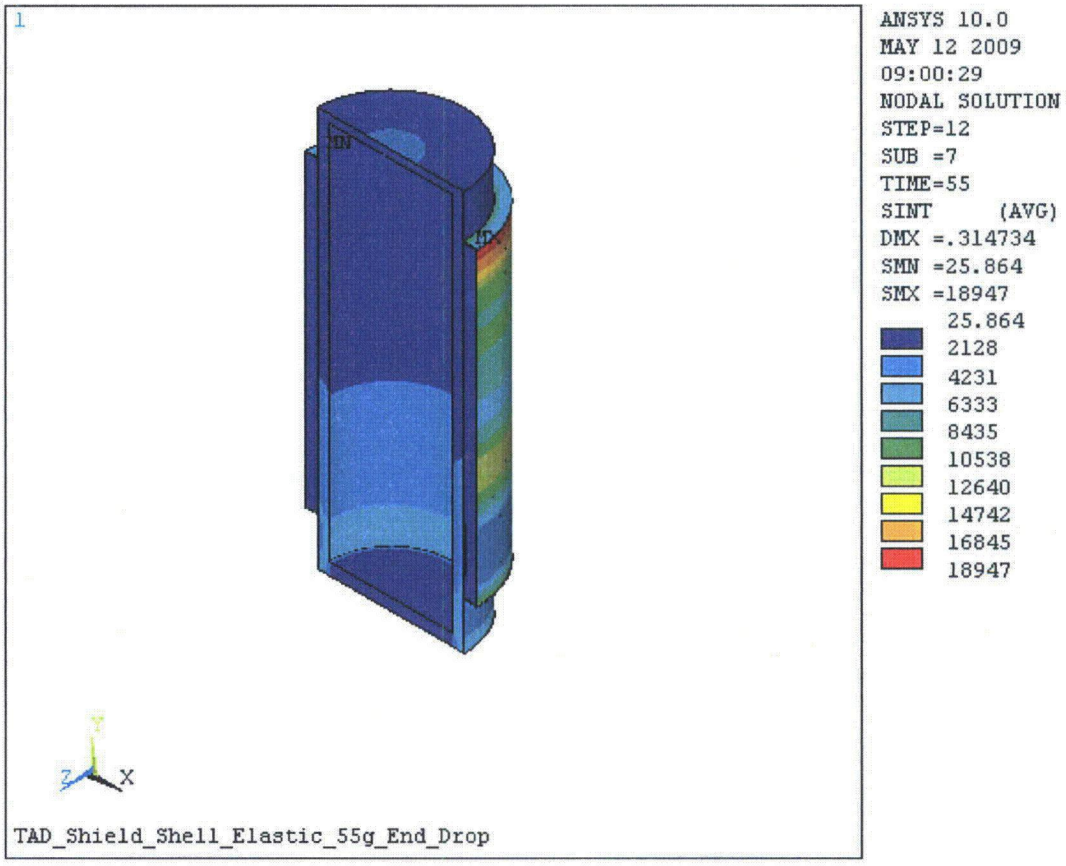

Figure B.2.13.4-14
Accident Condition End Drop 55 g Stress Intensity–Neutron Shield Shell

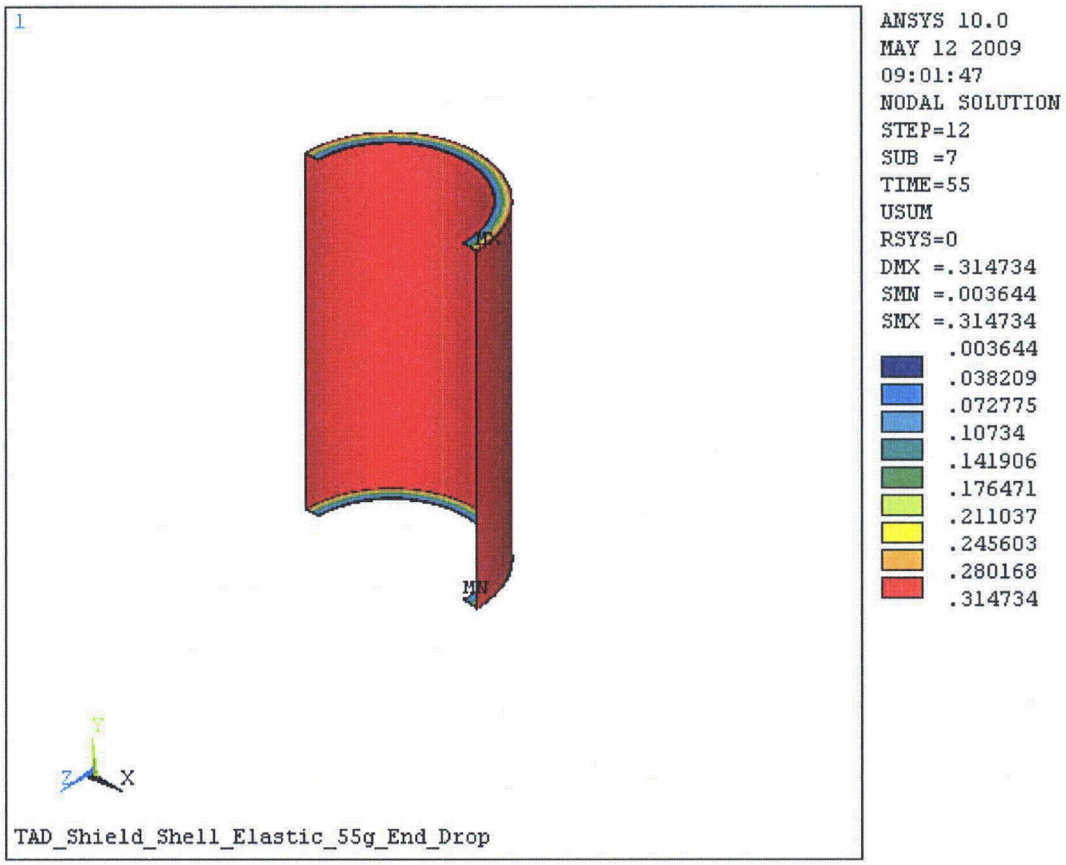

Figure B.2.13.4-15
Accident Condition End Drop 55 g Maximum Displacement–Neutron Shield Shell

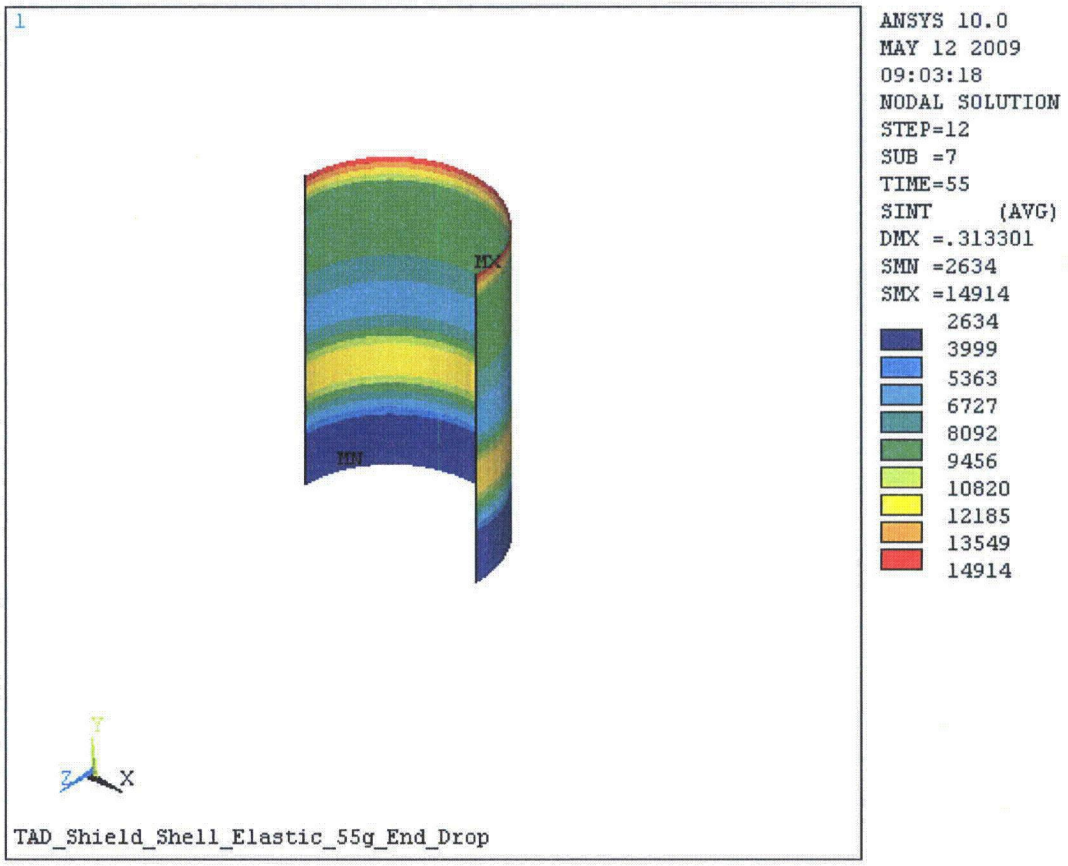

Figure B.2.13.4-16
Accident Condition End Drop 55 g Stress Intensity– Shield Plate

Appendix B.2.13.5
MP197TAD TO Lifting and Tie-Down Devices Structural Evaluation

CONTENTS

B.2.13.5.1 Purpose B.2.13.5-1
B.2.13.5.1.1 Lifting Devices B.2.13.5-1
B.2.13.5.1.2 Tie-Down Devices B.2.13.5-1
B.2.13.5.2 Trunnions Analysis B.2.13.5-2
B.2.13.5.2.1 Trunnions B.2.13.5-2
B.2.13.5.2.2 Shear Key Bearing Block Assembly B.2.13.5-8
B.2.13.5.3 Results B.2.13.5-12
B.2.13.5.3.1 Trunnions B.2.13.5-12
B.2.13.5.3.2 Shear key assembly B.2.13.5-13
B.2.13.5.4 Conclusions B.2.13.5-13
B.2.13.5.4.1 Trunnion assembly B.2.13.5-13
B.2.13.5.4.2 Shear key assembly B.2.13.5-13
B.2.13.5.5 References B.2.13.5-14

LIST OF TABLES

Table B.2.13.5-1 Steel Structural Properties at 350°F (ksi) B.2.13.5-15
Table B.2.13.5-2 Bolt Parameters B.2.13.5-16
Table B.2.13.5-3 Design Parameters B.2.13.5-17
Table B.2.13.5-4 Trunnion Stress Calculation B.2.13.5-18
Table B.2.13.5-5 TO Outer Shell Stresses Calculations (At Trunnion Attachment Block) B.2.13.5-19
Table B.2.13.5-6 Summary of Lifting Stresses - Trunnions (ksi) B.2.13.5-20
Table B.2.13.5-7 Summary of Longitudinal Stresses - Shear Key Assembly (ksi) B.2.13.5-21

LIST OF FIGURES

Figure B.2.13.5-1 Trunnion Section B.2.13.5-22
Figure B.2.13.5-2 Trunnion Stress Sections B.2.13.5-23
Figure B.2.13.5-3 Trunnion Flange B.2.13.5-24
Figure B.2.13.5-4 Shear Key Bearing Area B.2.13.5-25
Figure B.2.13.5-5 Bearing Block Bending Length B.2.13.5-26
Figure B.2.13.5-6 Bearing Block and Pad Plate Weld Bending Length B.2.13.5-27

Appendix B.2.13.5
MP197TAD TO Lifting and Tie-Down Devices Structural Evaluation

NOTE: References in this appendix are shown as [1], [2], etc., and refer to the reference list in Section B.2.13.5.5.

B.2.13.5.1 Purpose

B.2.13.5.1.1 Lifting Devices

The NUHOMS® - MP197TAD TO is lifted by the upper two removable trunnions. The trunnion attachment blocks are welded to the cask structural shell and as such are considered a structural part of the package. The removable trunnions are evaluated to meet the requirements of 10CFR71.45 [4] and are designed and fabricated based on ANSI N14.6 [5].

10CFR71.45 (a) requires that a minimum factor of safety of three and five are needed against material yields and ultimate strengths, respectively, for all lifting attachments which are a structural part of the MP197TAD TO for any lifting condition.

In addition, the package must be designed such that "failure of any lifting device under excessive load would not impair the ability of the package to meet the requirements" of 10CFR71 [4].

Section B.2.13.5.2 provides the analysis of the trunnions which are the only components used to lift the cask. One set of double shoulder (non single failure proof) trunnions will be provided for the NUHOMS® - MP197TAD TO lifting. Appendix B.2.13.1 provides an analysis of the global stresses in the cask walls due to the effects of the lifting loads on the trunnions. The global stress intensities from the ANSYS run at the stress reporting locations of the containment vessel and outer shell are presented in Table B.2.13.1-7.

The stress analysis of the front trunnion, flange and flange bolts are provided in the following sections. Maximum stress intensities for 3g and 5g lifting loads are presented in Table B.2.13.5-6. These stresses are less than the allowable stresses of the material (see Table B.2.13.5-1 for yield and ultimate stresses). The local stress intensities in the cask walls due to the 3 g lifting loads are calculated below and presented in Table B.2.13.5-5. These stresses are also less than the allowable stresses of the outer shell material. Therefore, the requirements of 10CFR71.45 (a) are met.

B.2.13.5.1.2 Tie-Down Devices

10CFR71.45 (b) (1) requires that a system of tie-down devices that is a structural part of the package must be capable of withstanding, without generating stress in any material of the package in excess of its yield strength, a static force applied to the center of gravity of the package having a horizontal component along the direction in which the vehicle travels of 10 times the weight of the package with its contents.

The shear key bearing block and pad plate are parts of the cask structure designed to resist the 10 g longitudinal transportation load. The bearing block is a welded structure. The

36" × 35.084" × 1.5" pad plate is used to spread the longitudinal shear load over a large area of the cask structural shell to which it is welded, thus preventing the cask outer shell to be subjected to any bending moment resulting from the longitudinal load.

B.2.13.5.2 Trunnions Analysis

B.2.13.5.2.1 Trunnions

Lifting Load

The NUHOMS® - MP197TAD TO is lifted vertically by its upper two removable trunnions using the fuel building crane. The weight of the cask used for trunnion structural evaluation is 255,000 lbs, this weight bounds the weight specified in Chapter B.2, Section B.2.1.3. During vertical lifting the impact limiters are not attached to the cask.

The maximum weight of the cask is W_L = 255,000 lb for the vertical lift, distributed evenly between the two upper trunnions. Using a dynamic load factor of 1.1 and a lifting load of 3 g, the vertical design load (yield) for one trunnion is:

$$F_V = W_L \times DLF \times \frac{a_V}{N_{tr}} = 255{,}000 \times 1.1 \times \frac{3}{2} = 420{,}750 \text{ lb}.$$

A section of a trunnion is shown on Figure B.2.13.5-1.

Trunnion Stresses

The stresses in various sections of the trunnion are shown in Figure B.2.13.5-2. The material properties are shown in Table B.2.13.5-1. The design parameters are shown in Tables B.2.13.5-2 and B.2.13.5-3. The stress calculations and results are shown in Table B.2.13.5-4.

Trunnion Bolt Evaluation

Load Due to Trunnion Moment

The trunnions are attached to the cask using 12 1 ¼"-7UNC bolts. The bolts are in tension because of the moment on the trunnion flange. The shear load is supported by the tight-fitting trunnion flange shoulder and a recess in the trunnion attachment block welded to the cask body. The radial clearance between the screw heads and shanks and trunnion flange holes is large enough so that the shear load is supported by the trunnion flange shoulder-to-block recess interface by bearing and not by the bolts.

The bending length is equal to:

$$L_1 + L_2 + Th_{flange} - Th_{tool} = 2.75 + 3.25 + 3.00 - 1.0 = 8.00 \text{ in.}$$

Therefore, the bending moment M_{D_D} is equal to F_V × (bending length), which is equal to:

$$M_{D\_D} = 420{,}750 \times 8.00 = 3{,}366{,}000 \text{ in.lb.}$$

According to [6], case 3, for bolt patterns symmetrical about the vertical axis and flange rotating about the bottom bolt, the maximum bolt force F_m due to the bending moment M_{D_D} is:

$$F_m = \frac{4}{3 \times D_{bolt}/2 \times N_b} M_{D\_D} = \frac{8 \times 3{,}366{,}000}{3 \times 12.5 \times 12} = 59{,}840 \text{ lb}.$$

Thermal Load

From [9], Table 4.4, the bolt force due to differential thermal expansion is calculated as follows:

$$F_{th} = 0.25 \times \pi \times D_b^2 \times E_b \times (\alpha_t \times \Delta T_t - \alpha_b \times \Delta T_b).$$

Where $\Delta T_t \approx \Delta T_b$ = Temperature Change = 350 – 70 =280°F.

Therefore,

$$F_{th} = 0.25 \times \pi \times 1.25^2 \times 26{,}700{,}000 \times 280 \times 10^{-6} \times (8.8 - 7.0) = 16{,}514 \text{lb}.$$

Bolt Stresses

For a lifting load of 3 g, the total bolt force is equal to:

$F_{max} = F_{th} + F_m = 16{,}514$ lb + 59,840 lb = 76,354 lb.

The maximum tensile stress σ_{max} in a bolt is:

$$\sigma_{max} = \frac{F_{max}}{S_{bolt}} = \frac{76{,}354}{0.969} = 78{,}800 \text{ psi}.$$

For a lifting load of 5 g, the total bolt force is equal to:

$F_{max} = F_{th} + (5/3) \times F_m = 16{,}514$ lb + (5/3) x 59,840 lb = 116,247 lb.

The maximum tensile stress σ_{max} in a bolt is:

$$\sigma_{max} = \frac{F_{max}}{S_{bolt}} = \frac{116{,}247}{0.969} = 119{,}970 \text{ psi}.$$

Minimum Engagement Length

The minimum engagement length L_e for the bolt and flange is (see Ref. [3], page 1490):

$$L_e = \frac{2 \times S_{bolt}}{3.1416 \times K_{n\max} \times \left[\frac{1}{2} + .57735 \times n \times (E_{s,\min} - K_{n\max})\right]}.$$

$$L_e = \frac{2 \times 0.969}{3.1416 \times 1.1230 \times \left[\frac{1}{2} + .57735 \times 7 \times (1.1439 - 1.1230)\right]}.$$

$$L_e = 0.940 \text{ in}.$$

According to [3], page 1490:

$$J = \frac{A_s \times S_{ue}}{A_n \times S_{ui}}.$$

S_{ue} is the tensile strength of external thread material, equal to 165 ksi, and S_{ui} is the tensile strength of internal thread material, equal to 65.1 ksi.

A_s is the shear area of external threads:

$$A_s = 3.1416 \times n \times L_e \times K_{n\max} \times \left[\frac{1}{2n} + 0.57735 \times (E_{s\min} - K_{n\max})\right].$$

A_n is the shear area of internal threads:

$$A_n = 3.1416 \times n \times L_e \times D_{s\min} \times \left[\frac{1}{2n} + 0.57735 \times (D_{s\min} - E_{n\max})\right].$$

Therefore:

$$A_s = 3.1416 \times 7 \times 0.940 \times 1.1230 \times \left[\frac{1}{2 \times 7} + 0.57735 \times (1.1439 - 1.1230)\right].$$

$$A_s = 1.938 \text{ in}^2.$$

$$A_n = 3.1416 \times 7 \times 0.940 \times 1.2232 \times \left[\frac{1}{2 \times 7} + 0.57735 \times (1.2232 - 1.1716)\right].$$

$$A_n = 2.559 \text{ in}^2.$$

So:

$$J = \frac{1.938 \times 165}{2.559 \times 65.1} = 1.919.$$

Therefore, the minimum required engagement length $Q = J \times L_e = 1.919 \times 0.940 = 1.804$ in.

Threaded inserts 1185-20CN-1875 are used. Their maximum length is 1.875 in., and they are used with bolts of maximum threaded length = 3.42 in. (total bolt shank length) -3.00 in. (trunnion flange thickness) + 2.00 in. (counter bore depth) = 2.42 in. Bolts are cut to fit as necessary, to engage 1.875 in. helicoil.

Therefore, the minimum threaded length is equal to 1.875 in., which is greater than the minimum required engagement length Q.

Trunnion Flange Stresses

The trunnion flange is shown in Figure B.2.13.5-3.

Stresses at section AA:
Length $L_{f1} = 0.5 \times (D_{bolt} - D_{flange}) = 6.25 - 4.5 = 1.75$ in.

Length $L_{f2} = 0.5 \times [D_{bolt} \times \cos(30°) - D_{flange}] = 6.25 \times \cos(30°) - 4.5 = 0.913$ in.

Flange length: $L = \sqrt{\left(D_{\max}^2 - D_{flange}^2\right)} = 2 \times \sqrt{\left(8.125^2 - 4.5^2\right)} = 13.53 \text{ in}.$

Flange thickness at AA: $Th_{flange} = 3.00$ in.

Maximum bolt load due to 3 g is F_m.

It is conservatively assumed that the two bolts on either side of the vertical axis support the same load F_m.

Bending moment at AA:

$$M = F_m \times L_{f1} + 2 \times F_m \times L_{f2} = 59{,}840 \times (1.75 + 2 \times 0.913) = 213{,}988 \text{ in.lb}.$$

The modulus of section at AA is equal to:

$$Z = \frac{L \times Th_{flange}^2}{6} = \frac{13.53 \times 3.00^2}{6} = 20.295 \text{ in}^3.$$

The bending stress is equal to:

$$\frac{M}{Z} = \frac{213{,}988}{20.295} = 10{,}543 \text{ psi}.$$

The shear stress is equal to:

$$\frac{3 \times F_m}{L \times Th_{flange}} = \frac{3 \times 59{,}840}{13.53 \times 3.00} = 4{,}423 \text{ psi}.$$

The maximum stress intensity is equal to:

$$\sqrt{10{,}543^2 + 4 \times 4{,}423^2} = 13{,}763 \text{ psi}.$$

Trunnion Attachment Block and Cask Shell Weld

There is a 1.75" groove weld on the outer circumference of the attachment block and the transportation overpack shell (Ø D_{w_ext} = 18.32 in). On the inside of the attachment block, there is a 1.25" groove weld (Ø D_{w_int} = 9.04 in). The weld is subjected to a bending moment.

The outer radius of the transportation overpack is 39.5 in. The minimum height of the block is 3.5 in., the maximum height of the block at a distance 9.16 in. from its centerline is:

$$H_{\max} = \sqrt{39.5^2} - \sqrt{39.5^2 - 9.16^2} + 3.5 = 4.58 \text{ in}.$$

The average height H_{avg} is therefore 0.5 × (4.58 + 3.50) = 4.04 in.

The bending length is equal to:

$$L_1 + L_2 - Th_{tool} + H_{avg} + Th_{flange} - 0.5 = 11.54 \text{ in.}$$

Therefore, the weld bending moment is equal to F_V × (bending length), which is equal to:

$$M_w = 420{,}750 \times 11.54 = 4{,}855{,}455 \text{ in.lb.}$$

The footprint of the weld is conservatively assumed to be circular for calculating moment of inertia of weld metal.

The weld moment of inertia is:

$$I_{weld} = \frac{\pi}{64}\left[\left(D_{w\_ext} + 2 \times Th_{w\_ext}\right)^4 - D_{w\_ext}^4 + \left(D_{w\_int} + 2 \times Th_{w\_int}\right)^4 - D_{w\_int}^4\right]$$

$$I_{weld} = \frac{\pi}{64}\left[\left(18.32 + 2 \times 1.75\right)^4 - 18.32^4 + \left(9.04 + 2 \times 1.25\right)^4 - 9.04^4\right].$$

$$I_{weld} = 6{,}141 \text{ in}^4.$$

The bending stress σ_b is:

$$\sigma_b = \frac{M_w \times 0.5 \times \left(D_{w\_ext} + 2Th_{w\_ext}\right)}{I_{weld}} = \frac{4{,}855{,}455 \times 0.5 \times \left(18.32 + 2 \times 1.75\right)}{6{,}141}.$$

$$\sigma_b = 8{,}626 \text{ psi}.$$

Bolt Torque

The bolt torque is calculated so that the preload bolt tensile stress is equal to the maximum applied stress σ_{max} (78,800 psi), and there is lubrication on the threads.

That stress is induced by F_{max} = 76,354 lb.

The maximum torque required for this preload is $Q = K \times D_b \times F_{max}$.

$Q = 0.135 \times 1.25 \times 76{,}354 = 12{,}885$ in.lb = 1,074 ft.lb.

Local Stresses in Cask Outer Shell at Trunnion Attachment Block

Local stresses are calculated using the methodology [7] assuming a rectangular attachment of circumferential side length $2 \times c_1$ and longitudinal side length $2 \times c_2$.

The trunnion shear loads in the longitudinal and circumferential directions are respectively $V_L = F_V$ = 420,750 lb and V_C = 0 lb.

The external overturning moments supported by the intersection in the longitudinal and circumferential directions with respect to the shell are respectively $M_L = M_W$ = 4,855,455 in.lb and M_C = 0 in.lb.

The thickness of the outer shell is Th_{os} = 2.50 in. The cylinder mean radius is:

$$R_m = R_{weld} - 0.5 \times Th_{os} = 38.25 \text{ in.}$$

The block circumferential side length is equal to $2 \times c_1$ = 18.32 in. Its equivalent longitudinal length $2 \times c_2$ is calculated based on its foot-print length L since the block shape is not fully rectangular:

$$L = \pi \times 9.16 + 12 \times 2 + 18.32 = 4 \times (c_1 + c_2) = 71.1 \text{ in.}$$

Therefore:

$$c_2 = \frac{71.1}{4} - c_1 = 17.77 - 9.16 = 8.61 \text{ in.}$$

The geometric parameters are:

$$\gamma = \frac{R_m}{Th_{os}} = \frac{38.25}{2.5} = 15.3, \ \beta_1 = \frac{c_1}{R_m} = \frac{9.16}{38.25} = 0.24 \text{ and } \beta_2 = \frac{c_2}{R_m} = \frac{8.61}{38.25} = 0.23.$$

Since the values of β_1 and β_2 are close it is assumed that the attachment is square and a conservative value of $\beta = 0.23$ is used.

The above quantities are used in spreadsheet in Table B.2.13.5-5 to calculate the stresses in the outer shell of the cask.

The maximum stress intensity is 35,253 psi.

Bearing Stress in Pocket Trunnion

The maximum weight of cask is 255,000 lb. (without impact limiters),

Using a dynamic load factor of 1.1 and a bearing load of 1.5 g, the load for each pocket trunnion is:

$$F = \frac{255{,}000 \times 1.1 \times 1.5}{2} = 210{,}375 \text{ lb}.$$

Assuming bearing on 45° arc, the bearing area:

$$A = 2 \times 3.25 \times \sin(45°) \times (4.00 - 0.50) = 16.087 \text{ in}^2.$$

Therefore, Bearing Stress, $\sigma = \frac{210{,}375}{16.087} = 13{,}077 \text{ psi}.$

This bearing stress is less than the allowable (S_y = 21.6 ksi).

B.2.13.5.2.2 Shear Key Bearing Block Assembly

Horizontal load

The NUHOMS® - MP197TAD TO is blocked in translation by its shear pin key. The weight of the package used in the analysis is 283,000 lbs. This weight bounds the weight of package specified in Chapter B.2, Section B.2.1.3.

The maximum weight of the cask is W_H = 283,000 lb for horizontal loads, concentrated on the shear key (10 g).

Bearing Stress Between the Shear Key and the Bearing Block

Using a dynamic load factor of 1.1, the horizontal design load (yield) is:

$$F_H = W_H \times DLF \times a_L = 283{,}000 \times 1.1 \times 10 = 3{,}113{,}000 \text{ lb}.$$

The bearing stress due to the 10 g longitudinal transportation load is calculated assuming the load is applied uniformly to one face of the bearing block.

The bearing area is divided in two areas (see Figure B.2.13.5-4): a trapezoidal area A_1, of average width $(L_1+L_2)/2$ and height Y, and an area A_2, which is a segment of solid circle. The bearing area is the sum of A_1 and A_2.

$$A_1 = \frac{L_1 + L_2}{2} \times Y .$$

L_1 is the width of the top of the shear key (including its chamfer):

$$L_1 = W_{sk} - 2 \times H_c \times \tan(\alpha_c) = 22.25 - 2 \times 5 \times \tan(12.5°) = 20.03 \text{ in.}$$

L_2 is the width of the shear key at the lowest lateral point of contact with the bearing block:

$$L_2 = L_1 + 2\left[H_{bb} - Th_p - g - \left(\sqrt{R_{weld}^2 + \frac{L_1^2}{4}} - R_{weld} \right) \right] \times \sin(\alpha_c).$$

$$L_2 = 20.03 + 2\left[6.875 - 0.375 - 0.5 - \left(\sqrt{39.5^2 + \frac{20.03^2}{4}} - 39.5 \right) \right] \times \sin(12.5°).$$

$$L_2 = 22.09 \text{ in} .$$

Y is the distance between the planes L_1 and L_2:

$$Y = \sqrt{(R_{weld} + H_{bb} - g)^2 - \left(\frac{L_2}{2}\right)^2} - (R_{weld} + Th_p)$$

$$Y = \sqrt{(39.5 + 6.875 - 0.5)^2 - \left(\frac{22.09}{2}\right)^2} - (39.5 + 0.375)$$

$$Y = 4.65 \text{ in} .$$

$$A_1 = \frac{L_1 + L_2}{2} \times Y = \frac{20.03 + 22.09}{2} \times 4.65 = 97.92 \text{ in}^2$$

According to [8], Table 1:

$$A_2 = \frac{1}{2}(R_{weld} + H_{bb} - g)^2 \times [2\alpha - \sin(2\alpha)]$$

$$\alpha = \sin^{-1}\left[\frac{L_2}{2 \times (R_{weld} + H_{bb} - g)} \right] = \sin^{-1}\left[\frac{22.09}{2 \times (39.5 + 6.875 - 0.5)} \right]$$

$$\alpha = 0.243 \text{ rad} .$$

$$A_2 = \frac{1}{2}(39.5 + 6.875 - 0.5)^2 \times [2 \times 0.243 - \sin(2 \times 0.243)]$$

$$A_2 = 19.90 \text{ in}^2$$

Therefore, A = 97.92 + 19.90 = 117.82 in^2.

The bearing stress is equal to:

$$\frac{F_H}{A} = \frac{3{,}113{,}000}{117.82} = 26{,}422 \text{ psi}$$

Stresses in the Bearing Block

The maximum bending length at the horizontal section A–A on the bearing block for the longitudinal load is e' = x – Th_{pp} (see Figure B.2.13.5-5):

$$e' = \frac{H_{bb} - g + Th_p}{2} - Th_{pp} = \frac{6.875 - 0.5 + 0.375}{2} - 1.5 = 1.875 \text{ in}$$

Therefore, the maximum bending length at the horizontal section A–A on the bearing block for the longitudinal load is:

$$F_H \times e' = 3{,}113{,}000 \times 1.875 = 5{,}836{,}900 \text{ in.lb}$$

The moment of inertia is:

$$I_{yy} = \frac{bd^3}{12} - \frac{(b - 2 \times Th_{bb}) \times (d - 2 \times Th_{bb})^3}{12} = \frac{26.81 \times 12.06^3}{12} - \frac{20.81 \times 6.06^3}{12}$$

$$I_{yy} = 3{,}533 \text{ in}^4$$

The bending stress is:

$$\frac{5{,}836{,}900 \times d/2}{I_{yy}} = \frac{5{,}836{,}900 \times 12.06/2}{3{,}533} = 9{,}962 \text{ psi}$$

The shear stress is:

$$\frac{F_H}{b \times d - (b - 2 \times Th_{bb}) \times (d - 2 \times Th_{bb})} = \frac{3{,}113{,}000}{26.81 \times 12.06 - 20.81 \times 6.06} = 15{,}784 \text{ psi}$$

The maximum stress intensity is:

$$\sqrt{9{,}962^2 + 4 \times 15{,}784^2} = 33{,}103 \text{ psi}$$

Weld Between the Bearing Block and the Pad Plate

The bearing block is welded to the 1.5"-thick pad plate with a full penetration weld and a ½" outside cover fillet weld f_w (see Figure B.2.13.5-6). The welds are loaded in bending, resulting from the offset e (see Figure B.2.13.5-6) of the 10 g longitudinal point to the center of the pad plate (the ½"outside cover fillet weld (f_w) is conservatively neglected for the calculation of the bending length of the applied moment).

The bending moment is applied at the middle of the bearing block bearing area, therefore at a distance x from the outer shell:

$$x = \frac{H_{bb} - (g + Th_p)}{2} + Th_p = \frac{H_{bb} - g + Th_p}{2}$$

The bending length is equal to $e = x - 0.5 \times Th_{pp}$.

$$e = \frac{H_{bb} - g + Th_p}{2} - \frac{Th_{pp}}{2} = \frac{6.875 - 0.5 + 0.375 - 1.5}{2} = 2.625 \text{ in}$$

The bending moment M is therefore $F_H \times e = 3{,}113{,}000 \times 2.625 = 8{,}171{,}630$ in.lb.

The section modulus of the weld is computed by treating the weld as a line per unit thickness t_{eff} [2]:

$$S_w = \left(bd + \frac{d^2}{3} \right) \times t_{eff}$$

$$t_{eff} = Th_{pp} + \frac{\sqrt{2}}{2} f_w = 1.5 + \frac{\sqrt{2}}{2} 0.5 = 1.85 \text{ in}$$

$$S_w = \left(26.81 \times 12.06 + \frac{12.06^2}{3} \right) \times 1.85 = 687.85 \text{ in}^3$$

The bending stress is equal to:

$$\frac{M}{S_w} = \frac{8{,}171{,}630}{687.85} = 11{,}880 \text{ psi}.$$

Weld Between the Pad Plate and the Outer Shell

The shear key pad plate is welded to the cask structure all around with a 1" partial penetration groove weld (g_w) and a 5/8" fillet weld (f_{wp}). The shear area in the base metal of the structural shell is:

$$b_{pp} \times d_{pp} - (b_{pp} - 2 \times g_w) \times (d_{pp} - 2 \times g_w) + 2 \times (b_{pp} + d_{pp}) \times f_{wp}$$

$$36 \times 35.084 - (36 - 2 \times 1.25) \times (35.084 - 2 \times 1.25) + 2 \times (36 + 35.084) \times 0.75 = 278.0 \text{ in}^2$$

The weld shear stress at the junction of the weld material and the cask structural shell is:

$$\frac{F_H}{278.0} = \frac{3{,}113{,}000}{278.0} = 11{,}198 \text{ psi}$$

B.2.13.5.3 Results

The margin of safety will be calculated as follows:

$$\text{Margin} = \frac{\text{Allowable stress}}{\text{Calculated stress}} - 1$$

B.2.13.5.3.1 Trunnions

The stresses calculated for a load of 3 g are summarized in Table B.2.13.5-6 and compared with allowable values (S_y). The stresses for a load of 5 g are also indicated in Table B.2.13.5-6 (simple 5/3 ratio of the values calculated for 3 g) and compared with the allowable values (S_u).

The maximum local shell stress intensity at trunnion block and transportation overpack shell intersection is 35.3 ksi (Table B.2.13.5-5). This discontinuity stress is classified as secondary stress as per 2004 ASME Boiler and Pressure Vessel Code, Section III, Subsection NB, Para NB-3213.9. The allowable for secondary stress is $3S_m$ (NB-3222.2).

Margin of Safety = [3 S_m/S.I] -1.0 = [3 x 19.3/35.3] -1.0 = 0.64

The recommended bolt torque for the trunnion bolts is 1,074 ft.lb.

The minimum engagement length is 1.804 in. Threaded inserts 1185-20CN-1875 are used. The minimum threaded length is equal to 1.875 in, which is greater than the minimum required engagement length.

Since the margins of safety for the trunnions are less than those for the transportation overpack structural shell, their failure under excessive load would not impair the ability of the package to meet the requirements of [4].

B.2.13.5.3.2 Shear key assembly

The stresses calculated for a longitudinal load of 10 g are summarized in Table B.2.13.5-7 and compared with allowable values.

B.2.13.5.4 Conclusions

All of the stresses calculated above are less than the allowable stresses.

B.2.13.5.4.1 Trunnion assembly

Based on the above calculations, the design meets the requirements of 10CFR71.

B.2.13.5.4.2 Shear key assembly

Based on the above calculations, the design meets the requirements of 10CFR71.

B.2.13.5.5 References

1. NOT USED.

2. "Pressure Vessel Design Handbook," Henry Bednar, 1981.

3. Machinery Handbook, 26th Edition, Industrial Press, 2000.

4. 10CFR Part 71, "Packaging and Transportation of Radioactive Materials."

5. ANSI N14.6, "Special Lifting Devices for Shipping Containers Weighing 10,000 Pounds or More," 1993.

6. Machine Design, August 17, 1967, "Eccentrically Loaded Joints," Richard T. Burger.

7. "Local Stresses in Spherical and Cylindrical Shells Due to External Loading," Welding Research Council (WRC), Bulletin 107 by Wichman, Hopper and Mershon.

8. "Formulas for Stress and Strain," Roark, 4th Edition.

9. NUREG/CR-6007 "Stress Analysis of Closure Bolts for Shipping Casks", By Mok, Fischer, and Hsu, Lawrence Livermore National Laboratory, 1992.

10. ASME Code Section II, Part D, 2004 Edition.

Table B.2.13.5-1
Steel Structural Properties at 350°F (ksi)

Part	**Material**	S_y	S_u	**E**
Trunnions	SA–182 FXM-19	42.0	92.7	N/A
Trunnions attachment blocks	SA–182 F304	21.6	65.1	26,700
Outer shell	SA–240 Type 304	21.6	65.1	N/A
Trunnion bolts	SA–540 Gr. B23 Cl. 1	139.1	165.0	N/A
Shear key bearing block	SA–182 F6NM	83.7	114.4	N/A
Pad plate	SA–240 Type 304	21.6	65.1	N/A

Note: Material properties are taken from ASME Code [10]. Material properties and allowable stresses are based on 350 °F which bound -40 °F, -20 °F, and 100 °F ambient conditions.

Table B.2.13.5-2
Bolt Parameters

D_b	Bolt nominal diameter (in)	1.25
S_{bolt}	Bolt stress area (in^2)	0.969
n	Number of threads per inch	7
$K_{n\,max}$	Maximum minor diameter of internal threads (in)	1.1230
$E_{s\,min}$	Minimum pitch diameter of external threads (in)	1.1439
$D_{s\,min}$	Minimum major diameter of external threads (in)	1.2232
$E_{n\,max}$	Maximum pitch diameter of internal threads (in)	1.1716

Table B.2.13.5-3
Design Parameters

N_{tr}	Number of trunnions	2
a_V	Vertical acceleration (g)	3
a_L	Longitudinal acceleration (g)	10
Th_{os}	Outer shell thickness (in)	2.50
N_b	Number of bolts per trunnion	12
K	Nut factor	0.135
D_{bolt}	Bolt circle diameter (in)	12.5
R_{weld}	Radius of outer shell at attachment block (in)	39.5
Th_{tool}	Thickness of lifting tool (in)	1.00
L_{ef}	Length of extremity flange (in)	0.50
D_{ext1}	Minimum trunnion shoulder diameter (in)	6.75
L_1	Outer trunnion shoulder length (in)	2.75
D_{ext2}	Maximum shoulder diameter (in)	8.75
L_2	Inner shoulder length (in)	3.25
D_{max}	Maximum trunnion diameter (in)	16.25
D_{flange}	Diameter of trunnion flange (in)	9.00
Th_{flange}	Thickness of flange at closure bolt circle (in)	3.00
H_{max}	Maximum height of attachment block (in)	4.58
$Th_{w\ ext}$	Thickness of external weld of attachment block (in)	1.75
$Th_{w\ int}$	Thickness of internal weld of attachment block (in)	1.25
$D_{w\ int}$	Inner weld diameter (in)	9.04
$D_{w\ ext}$	Outer weld diameter (in)	18.32
W_{sk}	Shear key width (in)	22.25
H_c	Height of shear key chamfer (in)	5.00
α_c	Angle of shear key chamfer	12.5°
H_{bb}	Height of bearing block (in)	6.875
g	Thickness of bearing block closure plate groove (in)	0.50
Th_p	Thickness of protection plate (in)	0.375
Th_{pp}	Thickness of pad plate (in)	1.50
b	Width of the base of the bearing block (in)	26.81
d	Longitudinal dimension of the bearing block (in)	12.06
Th_{bb}	Thickness of bearing block wall (in)	3.00
b_{pp}	Longitudinal dimension of pad plate (in)	36.00
d_{pp}	Lateral dimension of pad plate (in)	35.084
α_t	Coefficient of thermal expansion of trunnions at 350°F (in/in/°F)	8.8×10^{-6}
α_b	Coefficient of thermal expansion of trunnion bolts at 350°F (in/in/°F)	7.0×10^{-6}

Table B.2.13.5-4 Trunnion Stress Calculation

Section	A–A	C–C
Stress area (in^2)	$S_{AA} = \frac{\pi}{4} D_{ext1}^2 =$ $\frac{\pi}{4} 6.75^2 = 35.78$	$S_{CC} = \frac{\pi}{4} \times D_{ext2}^2 =$ $\frac{\pi}{4} \times 8.75^2 = 60.13$
Moment of inertia (in^4)	$I_{AA} = \frac{\pi}{64} D_{ext1}^4 =$ $\frac{\pi}{64} 6.75^4 = 101.90$	$I_{CC} = \frac{\pi}{64} \times D_{ext2}^4 =$ $\frac{\pi}{64} \times 8.75^4 = 287.74$
Bending distance (in)	$L_1 - Th_{tool}$ $= 2.75 - 1$ $= 1.75 = L_{AA}$	$L_1+L_2-Th_{tool}$ $= 2.75 + 3.25 - 1$ $= 5.0 = L_{CC}$
Bending moment (in.lb)	$M_{AA} = F_V \times L_{AA}$ $= 420{,}750 \times 1.75$ $= 736{,}313$	$M_{CC} = F_V \times L_{CC}$ $= 420{,}750 \times 5.0$ $= 2{,}103{,}750$
Shear stress (ksi)	$\frac{F_V}{S_{AA}} = \frac{420{,}750}{35.78}$ $= 11.76$	$\frac{F_V}{S_{CC}} = \frac{420{,}750}{60.13}$ $= 7.00$
Bending stress (ksi)	$\frac{M_{AA}}{I_{AA}} \times \frac{D_{ext1}}{2}$ $= \frac{736{,}313}{101.90} \times \frac{6.75}{2}$ $= 24.39$	$\frac{M_{CC}}{I_{CC}} \times \frac{D_{ext2}}{2}$ $= \frac{2{,}103{,}750}{287.74} \times \frac{8.75}{2}$ $= 31.99$
Max. stress intensity (ksi)	$\sqrt{24.4^2 + 4 \times 11.8^2}$ $= 33.9$	$\sqrt{32.0^2 + 4 \times 7.0^2}$ $= 34.9$

Table B.2.13.5-5 TO Outer Shell Stresses Calculations (At Trunnion Attachment Block)

From fig.	Read curves for:	Mult.	Abs. stress values		Au	Al	Bu	Bl	Cu	Cl	Du	Dl
3C & 4C		0	0	0	0	0	0	0	0	0	0	0
1C & 2C-1		0	0	0	0	0	0	0	0	0	0	0
3A		0	0						0	0	0	0
1A		0	0						0	0	0	0
3B	1.80	5,772	10,389		-10,389	-10,389	10,389	10,389				
1B or **1B-1**	0.036	529,837	19,074		-19,074	19,074	19,074	-19,074				
	Σ(phi - circumferential stresses)				**-29,463**	**8,685**	**29,463**	**-8,685**	**0**	**0**	**0**	**0**
3C & 4C		0	0	0	0	0	0	0	0	0	0	0
1C-1 & 2C		0	0	0	0	0	0	0	0	0	0	0
4A		0	0						0	0	0	0
2A		0	0						0	0	0	0
4B	0.60	5,772	3,463		-3,463	-3,463	3,463	3,463				
2B or **2B-1**	0.06	529,837	31,790		-31,790	31,790	31,790	-31,790				
	Σ(X - longitudinal stresses)				**-35,253**	**28,327**	**35,253**	**-28,327**	**0**	**0**	**0**	**0**
Shear stress due to torsion, M_T			0		0	0	0	0	0	0	0	0
Shear stress due to load, V_C			0		0	0	0	0				
Shear stress due to load V_L			4,884						4,884	4,884	-4,884	-4,884
Σ(shear stresses τ)					0	0	0	0	4,884	4,884	-4,884	-4,884
Stress intensities					**35,253**	**28,327**	**35,253**	**28,327**	**9,769**	**9,769**	**9,769**	**9,769**

Table B.2.13.5-6
Summary of Lifting Stresses - Trunnions (ksi)

	Calculated (3 g)	Allowable (S_y)	Margin	Calculated (5 g)	Allowable (S_u)	Margin
Stress intensity in section A-A	33.9	42.0	0.24	56.5	92.7	0.64
Stress intensity in section C-C	34.9		0.20	58.2		0.59
Bolt tensile stress	78.8	139.1	0.78	120.0	165.0	0.37
Stress intensity in trunnion flange	13.8	42.0	2.04	23.0	92.7	3.03
Trunnion block and TO shell weld bending stress	8.6	21.6	1.51	14.3	65.1	3.55

Table B.2.13.5-7
Summary of Longitudinal Stresses - Shear Key Assembly (ksi)

		Calculated (10 g)	**Allowable (S_y or $0.6 \times S_y$)**	**Margin**
Bearing block	Bearing stress	26.4	83.7	2.17
	Bending stress	10.0	83.7	7.37
	Shear stress	15.8	50.2	2.18
	Maximum stress intensity	33.1	83.7	1.53
	Bending stress in the weld with pad plate	11.9	21.6	0.82
Weld between pad plate and TO outer shell	Shear stress in base metal	11.2	13.0	0.16

Figure B.2.13.5-1
Trunnion Section

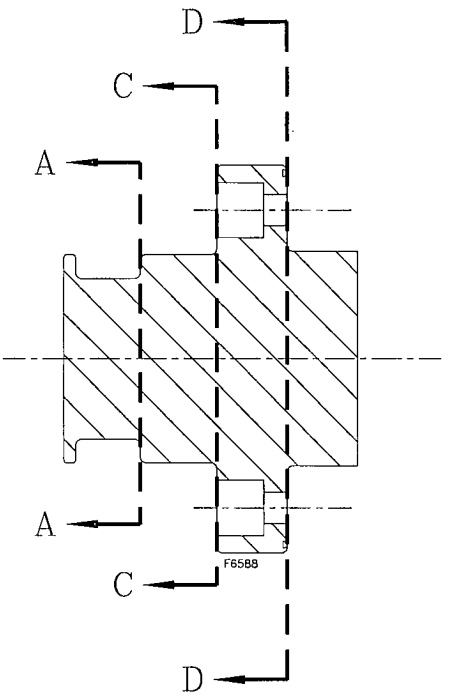

Figure B.2.13.5-2
Trunnion Stress Sections

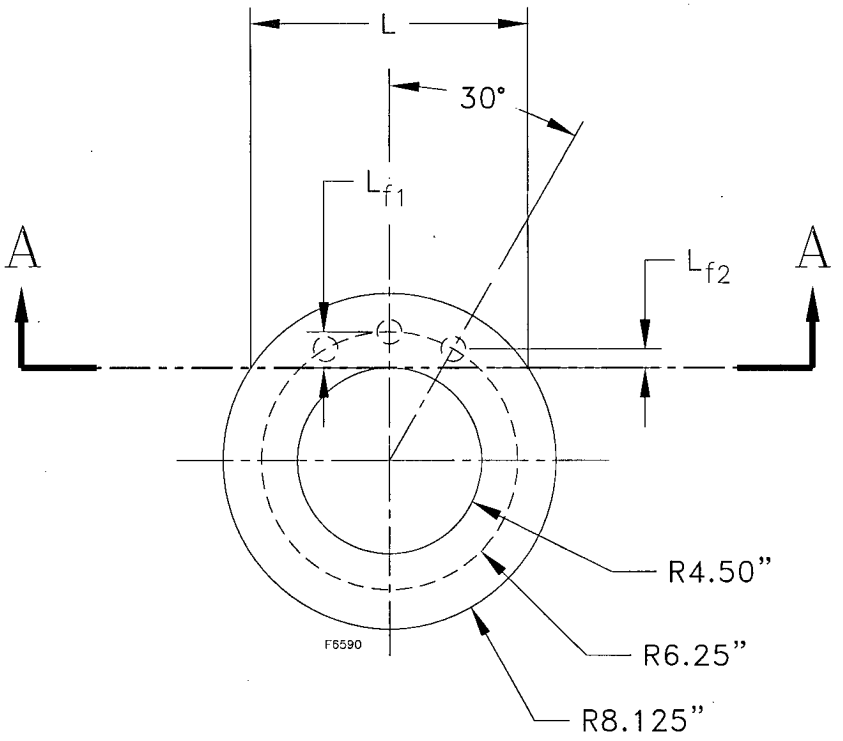

Figure B.2.13.5-3
Trunnion Flange

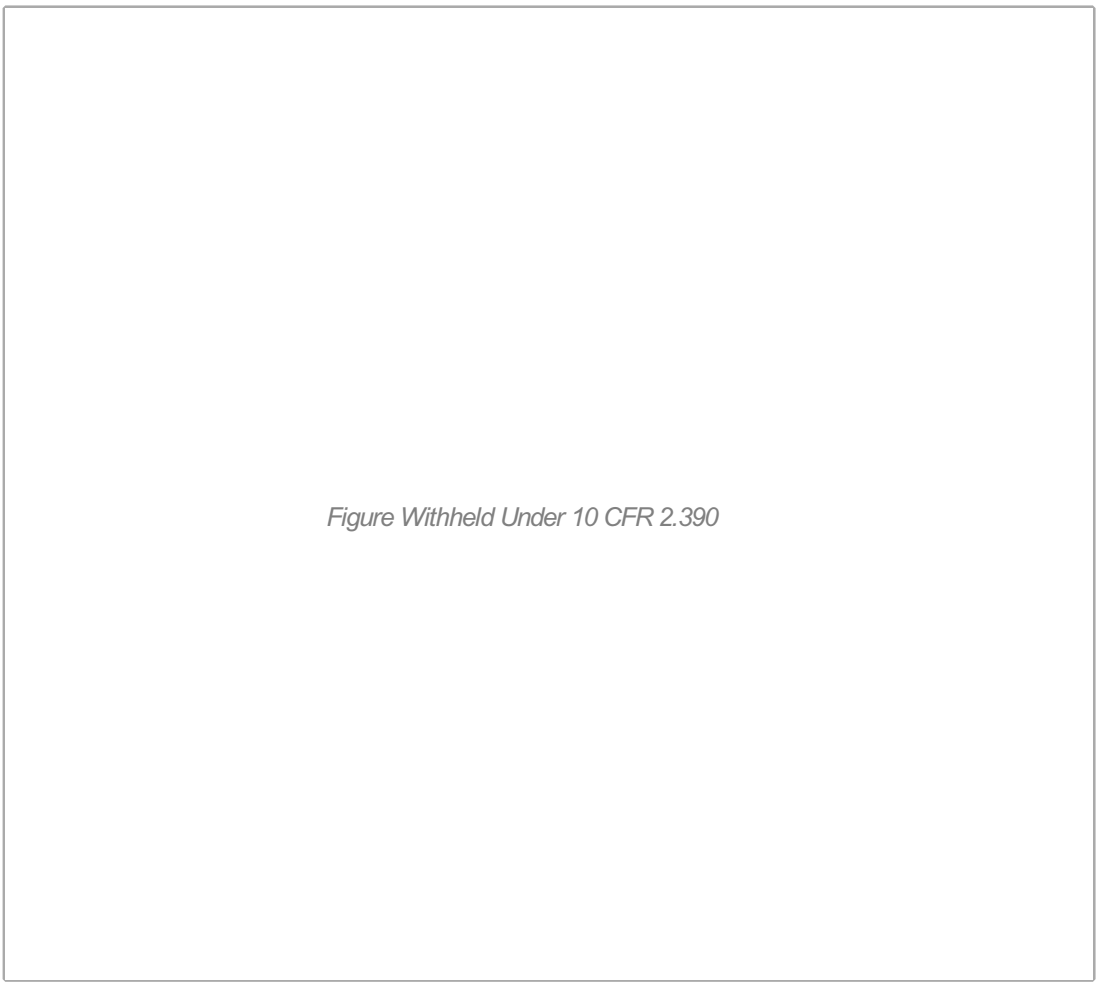

Figure B.2.13.5-4
Shear Key Bearing Area

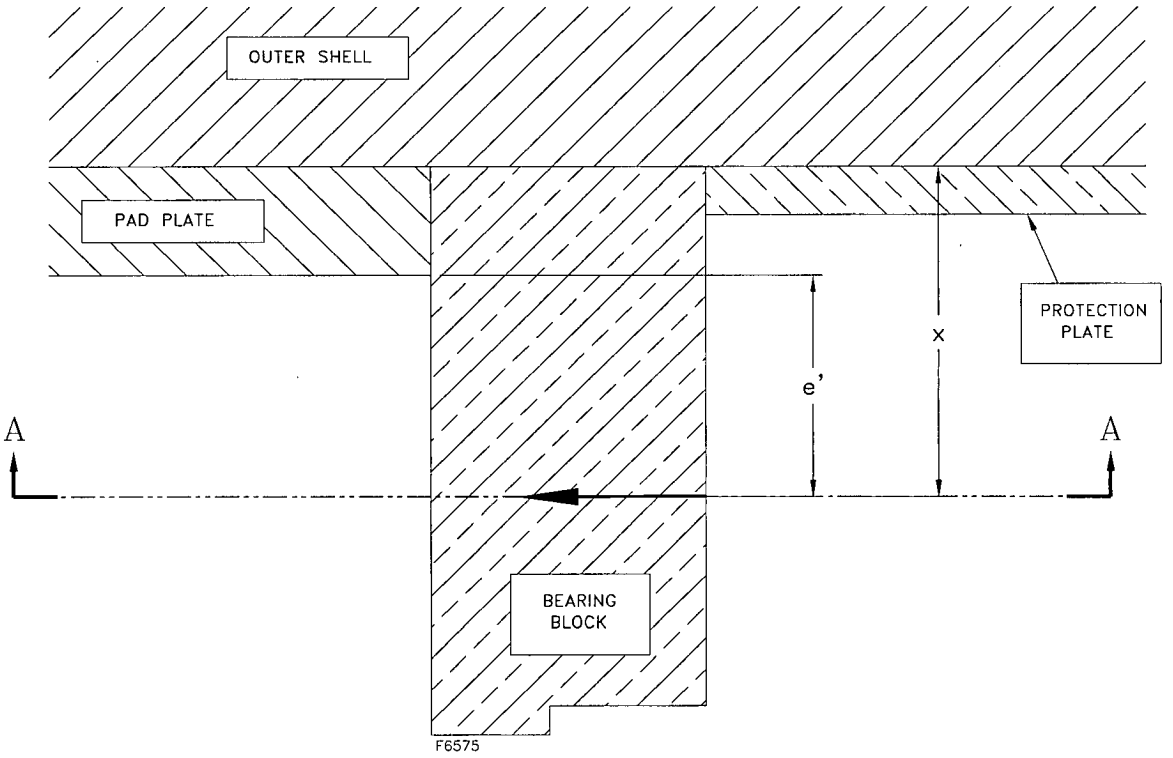

Figure B.2.13.5-5
Bearing Block Bending Length

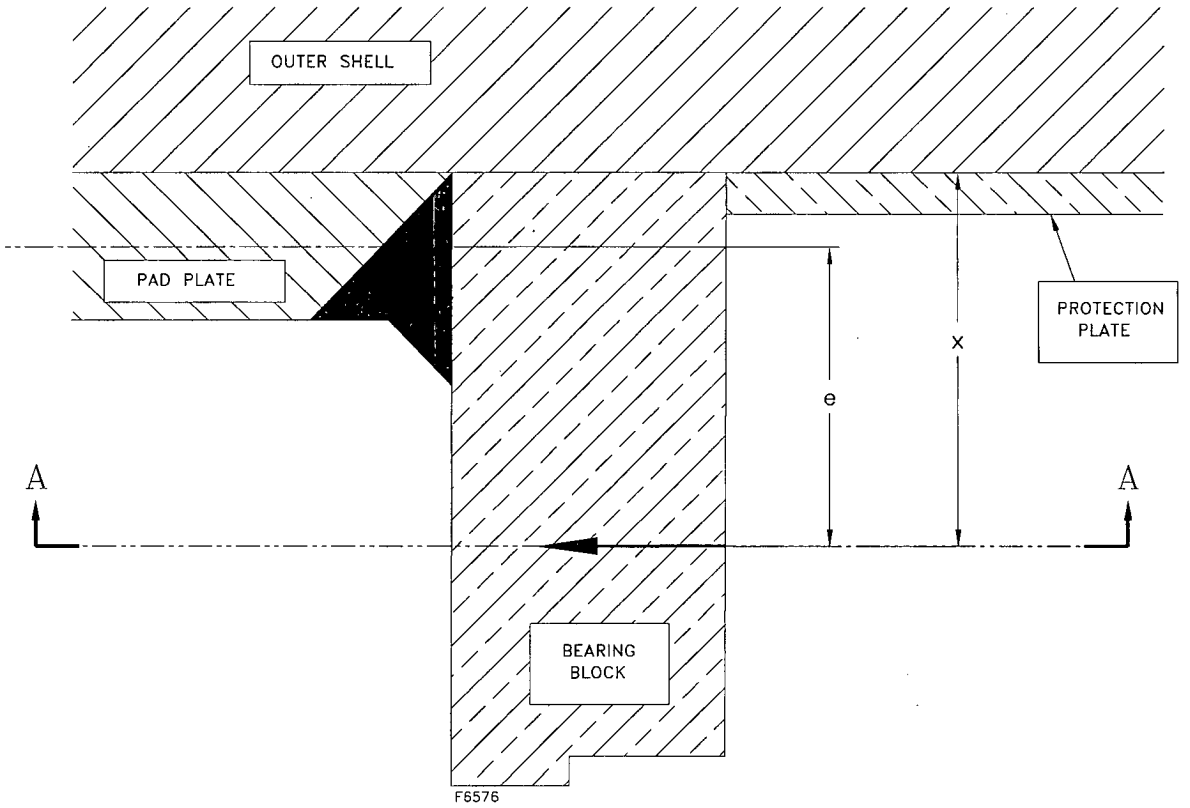

Figure B.2.13.5-6
Bearing Block and Pad Plate Weld Bending Length

Appendix B.2.13.6
MP197TAD TO Containment Boundary Fatigue Evaluation

CONTENTS

B.2.13.6.1 Purpose B.2.13.6-1
B.2.13.6.2 Assumptions B.2.13.6-1
B.2.13.6.3 Calculations B.2.13.6-2
B.2.13.6.3.1 Bolt Preload B.2.13.6-2
B.2.13.6.3.2 Leak test B.2.13.6-2
B.2.13.6.3.3 Pressure Fluctuations B.2.13.6-2
B.2.13.6.3.4 Temperature Fluctuations B.2.13.6-3
B.2.13.6.3.5 Vibration B.2.13.6-3
B.2.13.6.3.6 Shock B.2.13.6-3
B.2.13.6.3.7 1-foot Normal Condition Drop B.2.13.6-3
B.2.13.6.3.8 Transport Cask Fatigue Evaluation–Usage Factor Calculation B.2.13.6-4
B.2.13.6.4 Conclusions B.2.13.6-4
B.2.13.6.5 References B.2.13.6-5

LIST OF TABLES

Table B.2.13.6-1 Damage Factor Calculation B.2.13.6-6

Appendix B.2.13.6
MP197TAD TO Containment Boundary Fatigue Evaluation

NOTE: References in this appendix are shown as [1], [2], etc., and refer to the reference list in Section B.2.13.6.5.

B.2.13.6.1 Purpose

The purpose of the fatigue analysis is to show that the containment vessel stresses are within acceptable NCT fatigue limits. This is done by determining the fatigue usage factor for each NCT event for the containment boundary at locations on the containment vessel with the highest stresses. The cumulative fatigue damage or usage factor for all of the events is conservatively determined by adding the fatigue usage factors for the individual events for the containment boundary, assuming these maximum stress intensities occur at the same location.

The sum of the individual usage factors is checked to make certain that for a given number of round-trip shipments of the NUHOMS® - MP197TAD TO, the total fatigue damage factor for the containment boundary is less than one.

The number of round-trip shipments considered for the containment boundary is 1,000.

B.2.13.6.2 Assumptions

The fatigue analysis is based on the procedure described in Regulatory Guide 7.6 [4] and ASME Section III Appendices [3]. When determining the stress cycles, consideration is given to the superposition of individual loads which can occur together and produce a total stress intensity range greater than the stress intensity range of individual loads. Also, the maximum stress intensities for all individual loads are conservatively combined simultaneously. The sequence of events assumed for the fatigue evaluation is given below.

1. Operating bolt preload
2. Leak test
3. Pressure fluctuations
4. Temperature fluctuations
5. Vibration
6. Shock
7. 1 foot drop.

The maximum stresses in the NUHOMS® - MP197TAD TO containment boundary for each individual load case are taken from Appendix B.2.13.1.

The NUHOMS® - MP197TAD TO is only loaded for one of the two legs of a round trip shipment.

The bolt torque is applied twice every round trip.

The pressure cycle occurs twice every round trip.

In the case of normal conditions thermal loads, the maximum stress intensities occur in the -40°F cold environment load case. Consequently, it is assumed that the temperature cycle occurs twice per round–trip shipment and therefore the number of temperature cycles is twice the number of round–trip shipments.

It is conservatively assumed that the transportation overpack is dropped once per round trip shipment.

Each round trip shipment is assumed to average 3,000 miles each way.

B.2.13.6.3 Calculations

B.2.13.6.3.1 Bolt Preload

The number of preload cycles is two times the number of round-trip shipments.

The bolt preload specified to ensure a leak tight seal produces significant stresses in the lid. Therefore, this loading is conservatively included in the fatigue evaluation. The maximum stress intensity due to bolt preload is 9.9 ksi in the transportation overpack containment boundary (see Table B.2.13.1-1).

B.2.13.6.3.2 Leak test

The proof test is 1.5 × 30 psig (The MNOP is 12.8 psig; 30 psig is conservatively used for design) = 45 psig.

The maximum stress intensity due to a normal condition pressure load of 30 psig is 2.4 ksi in the containment boundary (Table B.2.13.1-2). Therefore, the maximum stress intensity due to the test pressure load is 1.5 × 2.4 ksi = 3.6 ksi in the containment boundary.

B.2.13.6.3.3 Pressure Fluctuations

It is assumed that the pressure cycle occurs twice per round-trip shipment.

The maximum stress intensity due to a pressure load of 30 psig is 2.4 ksi in the containment boundary (Table B.2.13.1-2).

B.2.13.6.3.4 Temperature Fluctuations

The maximum stress intensity in the containment boundary due to normal condition thermal loads occurs in the -40°F cold environment load case, and is 15.3 ksi (Table B.2.13.1-6).

B.2.13.6.3.5 Vibration

Since vibration accelerations are higher on a truck than on a rail car, the truck vibration loads are considered bounding. According to [1], the peak vibration load at the bed of a truck is 0.3 g longitudinal, 0.3 g transverse, and 0.6 g vertical. The maximum stress intensity generated by truck vibration is computed by extrapolating from the maximum stress intensity obtained in the railcar vibration load case.

According to [2], the peak vibration load on a railcar is 0.19 g longitudinal, 0.19 g transverse, and 0.42 g vertical. Therefore the truck vibration load is conservatively roughly 150% of the railcar vibration load.

The maximum stress intensity in the TO containment boundary due to railcar vibration calculated in Table B.2.13.1-13 is 1.2 ksi (outer shell is not containment boundary). Therefore, the maximum stress intensity in the containment boundary (including the lid) due to truck vibration would be roughly 1.8 ksi.

For the number of round trip shipments considered in this analysis, the number of truck vibration cycles would be very large.

B.2.13.6.3.6 Shock

The NUHOMS®-MP197TAD TO may be shipped either by truck or by railcar. ANSI N14.23 [1] specifies a peak shock loading of 2.3 g longitudinal, 1.6 g lateral, 3.5 g vertical up, and 2.0 g vertical down for truck transport, while NUREG 766510 [2] specifies a peak shock loading of 4.7 g in all directions for rail car transport. Consequently, only the inertial loading caused by a railcar shock is considered, since it is bounding.

Each round trip shipments averages 3,000 miles each way. NUREG 766510 [2] reports that there are roughly 9 shock cycles per 100 miles of rail car transport. The maximum stress intensities are found when the contents of the TO load the containment boundary, which happens during only half of a round-trip shipment. Therefore the number of cycles is:

$$3{,}000 \text{ miles} \times 1{,}000 \text{ shipments} \times 0.09 \text{ shocks / mile} = 270{,}000 \text{ cycles.}$$

The maximum stress intensity range due to railcar shock is equal to 24.8 + 1.7 = 26.5 ksi in the containment boundary (Tables B.2.13.1-9 and B.2.13.1-11).

B.2.13.6.3.7 1-foot Normal Condition Drop

The maximum stress intensity due to normal condition impact loads occurs in the 1 foot side drop load case, and is equal to 27.8 ksi in the containment boundary (Table B.2.13.1-16).

B.2.13.6.3.8 Transport Cask Fatigue Evaluation-Usage Factor Calculation

The damage factors listed in Table B.2.13.6-1 are computed based on the stresses and cyclic histories described above, and the fatigue curve shown in Figure I-9.2.1 of [3].

Since the model used for stress analysis of the TO includes detailed meshing of corners and bolt holes, the fatigue strength reduction factor (KF) which accounts for stress concentrations, is already accounted for in the stresses reported above. However, for conservatism, a stress concentration factor of 2 is used to obtain peak stresses. It may also be stated that the highest stresses, regardless of their location in the containment boundary, are conservatively used to calculate the damage factors.

The NUHOMS®-MP197TAD TO containment boundary is constructed from SA-240 Type 304N, SA-182 Type F304N, SA-240 Type 304 and SA-182 Type F304. The modulus of elasticity of these materials is 26.4×10^6 psi at 400°F. Fatigue curve is based on a modulus of elasticity of 28.3×10^6 psi.

Consequently, $K_E = 28.3 \times 10^6 / 26.4 \times 10^6 = 1.072$ [3].

Here n is the number of cycles, N is taken from Figure I-9.2.1 of [3], and S_a is defined in the following way:

If one cycle goes from 0 to +S.I., then $Sa = (1/2) \times S.I. \times K_F \times K_E$.

If one cycle goes from -S.I. to +S.I., then $Sa = S.I. \times K_F \times K_E$.

Where K_E is the correction factor for modulus of elasticity.

B.2.13.6.4 Conclusions

The total damage factor for the containment boundary is less than one. Therefore, the NUHOMS® - MP197TAD TO containment boundary will not fail due to fatigue for 1,000 round trip shipments.

B.2.13.6.5 References

1. American Standard Design Basis for Resistance to Shock and Vibration of Radioactive Material Packages Greater than One Ton in Truck Transport, ANSI, N14.23, May 1980.
2. Shock and Vibration Environments for Large Shipping Containers on Rail Cars and Trucks, NUREG 766510.
3. ASME Boiler and Pressure Vessel Code, Section III, Division 1 and Appendices, 2004 Edition.
4. USNRC Regulatory Guide 7.6, "Design Criteria for the Structural Analysis of Shipping Cask Containment Vessel," Rev. 1, March 1978.

Table B.2.13.6-1 Damage Factor Calculation

Event	Stress Intensity (ksi)	S.I. × K_F (ksi)	S_a (ksi)	Cycles		Damage Factor n / N
				n	N	
Bolt preload	9.9	19.8	10.6	2000	∞	0.000
Leak test	3.6	7.2	3.9	2000	∞	0.000
Pressure fluctuations	2.4	4.8	2.6	2000	∞	0.000
Temperature fluctuations	15.3	30.6	16.4	2000	∞	0.000
Vibration load	1.8	3.6	3.9	-[1]	∞	0.000
Shock load	26.5	53.0	28.4	270,000	700,000	0.386
1 foot drop impact load	27.8	55.6	29.8	1,000	600,000	0.002
					Σ	**0.388**

[1] The number of truck vibration cycles is very large and difficult to estimate. However, since N for this load case is ∞, n / N = 0, for a finite number of shipments.

APPENDIX B.2.13.7
TN44B DSC SHELL ASSEMBLY STRUCTURAL EVALUATION

CONTENTS

B.2.13.7.1 Introduction B.2.13.7-1
B.2.13.7.2 DSC Shell Assembly Structural Analysis B.2.13.7-3
B.2.13.7.2.1 Approach B.2.13.7-3
B.2.13.7.2.2 Loading Conditions B.2.13.7-8
B.2.13.7.2.3 Three-Dimensional Finite Element Models B.2.13.7-11
B.2.13.7.2.4 Stress Analysis Results B.2.13.7-12
B.2.13.7.2.5 DSC Shell Assembly Buckling Analysis B.2.13.7-13
B.2.13.7.3 References B.2.13.7-15

LIST OF TABLES

Table B.2.13.7-1 NCT-1: 30g Side Drop + 20 psi Internal Pressure + Thermal (hot) B.2.13.7-16
Table B.2.13.7-2 NCT-2: 30g Side Drop + 15 psi External Pressure + Thermal (cold) B.2.13.7-17
Table B.2.13.7-3 NCT-3: 50g Bottom End Drop + 20 psi Internal Pressure + Thermal (hot) ... B.2.13.7-18
Table B.2.13.7-4 NCT-4: 50g Bottom End Drop + 15 psi External Pressure + Thermal (cold) B.2.13.7-19
Table B.2.13.7-5 NCT-5: 50g Top End Drop + 20 psi Internal Pressure + Thermal (hot) B.2.13.7-20
Table B.2.13.7-6 NCT-6: 50g Top End Drop + 15 psi External Pressure + Thermal (cold) B.2.13.7-21
Table B.2.13.7-7 HAC-7: 75g Side Drop + 20 psi Internal Pressure B.2.13.7-22
Table B.2.13.7-8 HAC-8: 75g Side Drop + 15 psi External Pressure B.2.13.7-23
Table B.2.13.7-9 HAC-9: 90g Bottom End Drop + 20 psi Internal Pressure B.2.13.7-24
Table B.2.13.7-10 HAC-10: 90g Bottom End Drop + 15 psi External Pressure B.2.13.7-25
Table B.2.13.7-11 HAC-11: 90g Top End Drop + 20 psi Internal Pressure B.2.13.7-26
Table B.2.13.7-12 HAC-12: 90g Top End Drop + 15 psi External Pressure B.2.13.7-27
Table B.2.13.7-13 Stress Results for Weld of Outer Top Cover Plate B.2.13.7-28
Table B.2.13.7-14 Stress Results for Weld of Inner Top Cover Plate B.2.13.7-29

LIST OF FIGURES

Figure B.2.13.7-1 TN44B DSC Shell Assembly Top End 180 Degree Analytical Model B.2.13.7-30
Figure B.2.13.7-2 TN44B DSC Shell Assembly Bottom End 180 Degree Analytical Model B.2.13.7-31
Figure B.2.13.7-3 TN44B DSC Shell Assembly Top End 60 Degree Analytical Model B.2.13.7-32
Figure B.2.13.7-4 TN44B DSC Shell Assembly Bottom End 90 Degree Analytical Model B.2.13.7-33
Figure B.2.13.7-5 Top End Model - Stress Intensity Results for 30g Side Drop + 15 psi External Pressure B.2.13.7-34
Figure B.2.13.7-6 Bottom End Model - Stress Intensity Results for 30g Side Drop + 20 psi Internal Pressure B.2.13.7-34
Figure B.2.13.7-7 Top End Model - Stress Intensity Results for 50g Bottom End Drop + 20 psi Internal Pressure B.2.13.7-35
Figure B.2.13.7-8 Bottom End Model - Stress Intensity Results for 50g Bottom End Drop + 20 psi Internal Pressure B.2.13.7-35
Figure B.2.13.7-9 Top End Model - Stress Intensity Results for 50g Top End Drop + 15 psi External Pressure B.2.13.7-36
Figure B.2.13.7-10 Bottom End Model – Stress Intensity Results for 50g Top End Drop + 15 psi External Pressure B.2.13.7-36
Figure B.2.13.7-11 Top End Model - Stress Intensity Results for 75g Side Drop + 15 psi External Pressure B.2.13.7-37
Figure B.2.13.7-12 Bottom End Model - Stress Intensity Results for 75g Side Drop + 15 psi External Pressure B.2.13.7-37
Figure B.2.13.7-13 Top End Model - Stress Intensity Results for 90g Bottom End Drop + 20 psi Internal Pressure B.2.13.7-38
Figure B.2.13.7-14 Bottom End Model - Stress Intensity Results for 90g Bottom End Drop + 20 psi Internal Pressure B.2.13.7-38
Figure B.2.13.7-15 Top End Model - Stress Intensity Results for 90g Top End Drop + 15 psi External Pressure B.2.13.7-39
Figure B.2.13.7-16 Bottom End Model - Stress Intensity Results for 90g Top End Drop + 15 psi External Pressure B.2.13.7-39

APPENDIX B.2.13.7
TN44B DSC SHELL ASSEMBLY STRUCTURAL EVALUATION

NOTE: References in this appendix are shown as [1], [2], etc., and refer to the reference list in Section B.2.13.7.3.

B.2.13.7.1 Introduction

The NUHOMS®-TN44B DSC shell assembly consists of a cylindrical shell, bottom and top cover plates (inner and outer) and bottom and top shield plugs. The DSC shell assembly functions to support a basket assembly and confine associated fuel assemblies that are contained within the DSC shell assembly.

The DSC shell assembly is constructed from SA-240 Type 304 stainless steel and SA-240 Type 316/316L stainless steel (material will be dual certified to meet requirements of both Type 316 and 316L; material properties are based on Type 316). A lifting device, constructed from Type 316N stainless steel, is connected to the top of the DSC shell assembly using SA-540 Grade B23 Class 1 bolts. There are no penetrations through the confinement vessel. The draining and venting systems are covered by the seal welded outer top closure plate and vent port plug. To preclude air in-leakage, the DSC cavity is pressurized above atmospheric pressure with helium.

The TN44B DSC shell assembly component dimensions are as follows:

- Cylindrical Shell — 0.75" thick plate
- Outer Top Cover Plate — 2.50" thick plate
- Inner Top Cover Plate — 2.00" thick plate
- Top Shield Plug — 5.75" thick plate; 2.65" thick over the support ring (recessed at the bottom perimeter to clear the support ring)
- Support Ring — 0.75" thick plate x 3.00" tall
- Inner Bottom Cover Plate — 1.75" thick plate
- Bottom Shield Plug — 2.75" thick plate
- Outer Bottom Cover Plate — 2.00" thick plate
- Lifting Device — ring with z-shaped section, maximum height of 6.00"

The primary confinement boundary consists of the DSC cylindrical shell, the inner top cover plate, the inner bottom cover plate, the siphon vent block, and the siphon/vent port cover plate, and the associated welds.

The welds made during fabrication of the TN44B DSC shell assembly that affect the confinement boundary of the DSC include the weld applied to the inner bottom cover plate and the circumferential and longitudinal seam welds applied to the shell. These welds are inspected (radiographic or ultrasonic inspection, and liquid penetrant inspection) according to the requirements of Subsection NB of the ASME Code [1]. The vent and siphon block weld is also made during fabrication and is liquid penetrant inspected in accordance with Subsection NB of the ASME Code.

The welds applied to the vent and siphon port covers and the inner top cover plate during closure operations define the confinement boundary at the top end of the TN44B DSC. These welds are applied using a multiple-layer technique with multi-level PT in accordance with Subsection NB of the ASME Code and ISG-15 [6].

The basis for the allowable stresses for the confinement boundary is ASME Code Section III, Division I, Subsection NB Article NB-3200 for normal condition loads (Level A) and Appendix F for accident condition loads (Level D).

B.2.13.7.2 DSC Shell Assembly Structural Analysis

B.2.13.7.2.1 Approach

Finite element analyses are performed in order to quantify stresses in the TN44B DSC shell assembly generated by transport loads. The applied loads considered are normal and accident condition top end, bottom end, and side drops, combined with 20 psig internal and 15 psig external pressures and 100 °F and -20 °F (& -40 °F) environmental conditions. Several three-dimensional finite element models are used to evaluate stresses for the normal and accident loads: 180 degree models are used for non-axisymmetric loads such as temperature loads and side drop loads; a 60 degree model is used for analysis of the top end model for end drop; and a 90 degree model is used for analysis of the bottom end model for end drop. Elastic analyses are employed for normal condition load cases and accident condition end drops. For the accident condition side drop load cases, elastic-plastic analyses are performed. Limit analyses are performed where primary stress limits for normal conditions are exceeded.

Material Properties

Material	Temperature (°F)	Stress Properties (ksi)			Elastic Modulus ($x10^3$ ksi) (E)	Average Coefficient of Thermal Expansion ($x10^{-6}$ in./in.-°F)
		Stress Intensity (S_m)	Yield Strength (S_y)	Ultimate Strength (S_u)		
Stainless Steel ASME SA-240 Type 304 SA-182 Type F304	-20	20.0	30.0	75.0	--	--
	70	--	--	--	28.3	8.5
	100	20.0	30.0	75.0	--	8.6
	200	20.0	25.0	71.0	27.5	8.9
	300	20.0	22.4	66.2	27.0	9.2
	400	18.6	20.7	64.0	26.4	9.5
	500	17.5	19.4	63.4	25.9	9.7
	600	16.6	18.4	63.4	25.3	9.8
	650	16.2	18.0	63.4	--	9.9
	700	15.8	17.6	63.4	24.8	10.0
	750	15.5	17.2	63.3	--	10.0
	800	15.2	16.9	62.8	24.1	10.1

Note: Density, $\rho = 0.284$ lbs/in^3; Poisson's Ratio, $\nu = 0.29$

Material	Temperature (°F)	Stress Properties (ksi)			Elastic Modulus ($x10^3$ ksi) (E)	Average Coefficient of Thermal Expansion ($x10^{-6}$ in./in.-°F)
		Stress Intensity (S_m)	Yield Strength (S_y)	Ultimate Strength (S_u)		
Stainless Steel ASME SA-240 Type 316/316L SA-182 Type F316/F316L	-20	20.0	30.0	75.0	--	--
	70	--	--	--	28.3	8.5
	100	20.0	30.0	75.0	--	8.6
	200	20.0	25.9	75.0	27.5	8.9
	300	20.0	23.4	72.9	27.0	9.2
	400	19.3	21.4	71.9	26.4	9.5
	500	18.0	20.0	71.8	25.9	9.7
	600	17.0	18.9	71.8	25.3	9.8
	650	16.6	18.5	71.8	--	9.9
	700	16.3	18.2	71.8	24.8	10.0
	750	16.1	17.9	71.5	--	10.0
	800	15.9	17.7	70.8	24.1	10.1

Note: Density, $\rho = 0.284$ lbs/in^3; Poisson's Ratio, $\nu = 0.29$

Material	Temperature (°F)	Stress Properties (ksi)			Elastic Modulus ($x10^3$ ksi) (E)	Average Coefficient of Thermal Expansion ($x10^{-6}$ in./in.-°F)
		Stress Intensity (S_m)	Yield Strength (S_y)	Ultimate Strength (S_u)		
Stainless Steel ASME SA-240 Type 316N SA-182 Type F316N	-20	23.3	35.0	80.0	--	--
	70	--	--	--	28.3	8.5
	100	23.3	35.0	80.0	--	8.6
	200	23.3	31.0	80.0	27.5	8.9
	300	23.3	28.5	77.0	27.0	9.2
	400	23.3	26.4	75.1	26.4	9.5
	500	22.3	24.7	74.4	25.9	9.7
	600	21.0	23.4	74.3	25.3	9.8
	700	20.0	22.3	74.3	24.8	10.0

Note: Density, $\rho = 0.284$ lbs/in^3; Poisson's Ratio, $\nu = 0.29$

Material	Temperature (°F)	Stress Properties (ksi)			Elastic Modulus ($x10^3$ ksi) (E)	Average Coefficient of Thermal Expansion ($x10^{-6}$ in./in.-°F)
		Stress Intensity (S_m)	Yield Strength (S_y)	Ultimate Strength (S_u)		
Alloy Steel SA-540 Grade B23 Class 1	-20	50.0	150.0	165.0	--	--
	70	--	--	--	27.8	6.4
	100	50.0	150.0	165.0	--	6.5
	200	47.8	144.0	165.0	27.1	6.7
	300	46.2	140.3	165.0	26.7	6.9
	400	44.8	137.9	165.0	26.2	7.1
	500	43.4	136.0	165.0	25.7	7.3
	600	41.4	133.4	165.0	25.1	7.4
	700	--	129.0	158.6	24.6	7.6

Note: Density, $\rho = 0.284$ lbs/in^3; Poisson's Ratio, $\nu = 0.29$

For the accident condition side drop analyses, the following elastic-plastic material properties are used, conservatively taken at 500 °F.

SA-240, Type 316/316L Stainless Steel at 500 °F [3]	
Modulus of Elasticity, E (psi)	25.9×10^6
Yield Strength (psi)	20,000
Tangent Modulus, E_t (psi)	5% of $E = 1.295 \times 10^6$

SA-240, Type 304 Stainless Steel at 500 °F [3]	
Modulus of Elasticity, E (psi)	25.9×10^6
Yield Strength (psi)	19,400
Tangent Modulus, E_t (psi)	5% of $E = 1.295 \times 10^6$

SA-240, Type 316N Stainless Steel at 500 °F [3]	
Modulus of Elasticity, E (psi)	25.9×10^6
Yield Strength (psi)	24,700
Tangent Modulus, E_t (psi)	5% of $E = 1.295 \times 10^6$

Design Criteria

The resulting stresses are compared with the allowable stresses set forth by ASME B&PV Code Subsection NB [1] and Appendix F [2]. The allowable stresses for both normal and accident conditions for materials at 500 °F are summarized in the following table.

Loading Condition	Stress Category	Stress Criteria [1]	Material	Allowable Stress (ksi)
Normal Conditions, Elastic Analysis (Level A)	Membrane Stress, P_m	S_m	SA-240 Type 304	17.5
			SA-240 Type 316/316L	18.0
			SA-240 Type 316N	22.3
	Local P_L & Membrane + Bending Stress, (P_m or P_L) + P_b	1.5 S_m	SA-240 Type 304	26.3
			SA-240 Type 316/316L	27.0
			SA-240 Type 316N	33.5
	Primary + Secondary Stress, (P_m or P_L) + P_b + Q	3 S_m	SA-240 Type 304	52.5
			SA-240 Type 316/316L	54.0
			SA-240 Type 316N	66.9
Accident Conditions, Elastic-Analysis (Level D)	Membrane Stress, P_m	min of (2.4 S_m, 0.7 S_u)	SA-240 Type 304	42.0
			SA-240 Type 316/316L	43.2
			SA-240 Type 316N	52.1
	Local P_L & Membrane + Bending Stress, (P_m or P_L) + P_b	min of (3.6 S_m, 1.0 S_u)	SA-240 Type 304	63.0
			SA-240 Type 316/316L	64.8
			SA-240 Type 316N	74.4
Accident Conditions, Elastic-Plastic Analysis (Level D)	Membrane Stress, P_m	max of 0.7 S_u, S_y + (S_u – S_y) /3	SA-240 Type 304	44.4
			SA-240 Type 316/316L	50.3
			SA-240 Type 316N	52.1
	Local P_L & Membrane + Bending Stress, (P_m or P_L) + P_b	0.9 S_u	SA-240 Type 304	57.1
			SA-240 Type 316/316L	64.6
			SA-240 Type 316N	67.0

Note that the primary stress limits for normal conditions may be exceeded providing the criteria of NB-3228.1 (below) are satisfied.

Limit Analysis Criteria

Subsection NB-3228.1 of Reference [1] provides relaxation of the limits on General Membrane Stress Intensity (NB-3221.1), Local Membrane Stress Intensity (NB-3221.2), and Primary Membrane Plus Primary Bending Stress Intensity (NB-3221.3), if it can be shown by limit analysis that the specified loadings do not exceed two-thirds of the lower bound collapse load. The yield strength to be used in such a determination is 1.5 S_m.

For the limit side drop analyses, the following elastic-perfectly plastic material properties are used, taken at 500 °F.

SA-240, Type 316/316L Stainless Steel at 500 °F [3]	
Modulus of Elasticity, E (psi)	25.9×10^6
Yield Strength (1.5 S_m) (psi)	27,000
Tangent Modulus, E_t (psi)	0.0

SA-240, Type 304 Stainless Steel at 500 °F [3]	
Modulus of Elasticity, E (psi)	25.9×10^6
Yield Strength (1.5 S_m) (psi)	26,250
Tangent Modulus, E_t (psi)	0.0

SA-240, Type 316N Stainless Steel at 500 °F [3]	
Modulus of Elasticity, E (psi)	25.9×10^6
Yield Strength (1.5 S_m) (psi)	33,450
Tangent Modulus, E_t (psi)	0.0

Weld Criteria

There are two closure welds in the DSC shell assembly design: the weld of the outer top cover plate to the DSC cylindrical shell, and the weld of the inner top cover plate to the DSC cylindrical shell. Both of the closure welds are partial penetration welds. ISG-15 [6] requires that a stress (allowable) reduction factor is used for closure welds to account for weld imperfection or flaws and recommends stress reduction factor of 0.8 based on multi-level PT examination.

The allowable weld stresses for both normal and accident conditions are summarized below.

Allowable Stresses for Partial Penetration Weld of Type 316 Outer Top Cover Plate

Temp. °F	Code Value for Type 316 Base Metal (ksi)			Primary Allowable Stress (ksi)			Primary + Secondary
	S_m	S_y	S_u	Level A $0.8x1.5S_m$	Level D Elastic [1]	Level D E/P [2]	$0.8(3.0S_m)$
500	18.0	20.0	71.8	21.6	51.8	51.7	43.2

Notes:
1. Allowable for Level D elastic analysis is 0.8 times the lesser of $3.6S_m$ or S_u.
2. Allowable for Level D elastic/plastic analysis is 0.8 times $0.9S_u$.

Allowable Stresses for Partial Penetration Weld of Type 304 Inner Top Cover Plate

Temp. °F	Code Value for Type 304 Base Metal (ksi)			Primary Allowable Stress (ksi)			Primary + Secondary
	S_m	S_y	S_u	Level A $0.8x1.5S_m$	Level D Elastic [1]	Level D E/P [2]	$0.8(3.0S_m)$
400	18.6	20.7	64.0	22.3	51.2	46.1	44.6
500	17.5	19.4	63.4	21.0	50.4	45.6	42.0

Notes:
1. Allowable for Level D elastic analysis is 0.8 times the lesser of $3.6S_m$ or S_u.
2. Allowable for Level D elastic/plastic analysis is 0.8 times $0.9S_u$.

B.2.13.7.2.2 Loading Conditions

The load cases considered in this analysis are normal and hypothetical accident condition drops, pressure loads, and temperature distributions (thermal expansion stresses). The normal condition drop loads are combined with internal and external pressure and the 100 °F and -20 °F (and -40 °F) ambient environment thermal loads. The accident condition drop loads are combined with internal and external pressure. The baseline accelerations for NCT and HAC drop conditions are provided in Appendix B.2.13.12. For the quasi-static analyses the baseline g-loads are multiplied by a dynamic load factor calculated in Appendix B.2.13.9. These calculated maximum g-loads are further increased for conservatism in the analyses. The maximum g-loads used are summarized in the following table.

TN44B TAD – DSC Maximum Accelerations

Drop Condition	Appendix B.2.13.12 Baseline Acc. (g)	Appendix B.2.13.9 DSC DLFs	Required DSC Acceleration (g)	DSC Analysis Acceleration (g)
Normal (1') Side Drop	18	1.20	21.6	30
Normal (1') End Drop	32	1.35	43.2	50
Accident (30') Side Drop	59	1.16	68.44	75
Accident (30') End Drop	51	1.57	80.0	90

The following tables summarize both normal and accident condition individual load cases.

TN44B DSC Normal Condition (NCT) Load Cases

Loading	Analysis Type	Service Level	Load	Analysis Method
Hot Environment Thermal Load	Elastic Analysis	A	100 °F Ambient [1]	Finite Element Analysis (3D, 180 deg. model)
Cold Environment Thermal Load	Elastic Analysis	A	-20 °F Ambient [2]	Finite Element Analysis (3D, 180 deg. model)
Internal Pressure	Elastic Analysis	A	20 psi. Internal Pressure	Finite Element Analysis (included in drop analyses)
External Pressure	Elastic Analysis	A	15 psi. External Pressure	Finite Element Analysis (included in drop analyses)
1 Foot Side Drop	Elastic Analysis	A	30*g* Lateral Load	Finite Element Analysis (3D, 180 deg. model)
1 Foot Top End Drop	Elastic Analysis	A	50*g* Axial Load	Finite Element Analysis (3D, 60 deg. model – top end) (3D, 90 deg. model – bottom end)
1 Foot Bottom End Drop	Elastic Analysis	A	50*g* Axial Load	Finite Element Analysis (3D, 60 deg. model – top end) (3D, 90 deg. model – bottom end)

Notes: 1. Thermal stress analyses for the 100 °F condition include both non-shaded and shaded operations.
2. Thermal stress analysesdy for the –20 °F condition also include the –40 °F condition.

TN44B DSC Accident Condition (HAC) Load Cases

Loading	Analysis Type	Service Level	Load	Analysis Method
30 Foot Side Drop	Elastic-Plastic Analysis	D	75*g* Lateral Load	Finite Element Analysis (3D, 180 deg. model)
30 Foot Top End Drop	Elastic Analysis	D	90*g* Axial Load	Finite Element Analysis (3D, 90 deg. model)
30 Foot Bottom End Drop	Elastic Analysis	D	90*g* Axial Load	Finite Element Analysis (3D, 60 deg. model)

The individual loads are combined in the following way.

TN44B DSC Normal Condition (NCT) Load Combinations

Load Case	Individual Loads						
	30g Side Drop	50g Top End Drop	50g Bottom End Drop	20 psi. Internal Pressure	15 psi. External Pressure	Thermal Hot	Thermal Cold
1	X			X		X	
2	X				X		X
3		X		X		X	
4		X			X		X
5			X	X		X	
6			X		X		X

TN44B DSC Accident Condition (HAC) Load Combinations

Load Case	Individual Loads						
	75g Side Drop	90g Top End Drop	90g Bottom End Drop	20 psi. Internal Pressure	15 psi. External Pressure	Thermal Hot	Thermal Cold
7	X			X		X	
8	X				X		X
9		X		X		X	
10		X			X		X
11			X	X		X	
12			X		X		X

B.2.13.7.2.3 Three-Dimensional Finite Element Models

Finite Element Model

Three-dimensional finite element models are constructed to evaluate stresses for the normal and accident loads. A separate set of models is used for analysis of the top-half and bottom-half of the DSC shell assembly. For non-axisymmetric loads such as temperature loads and side drop loads, 180 degree models are used. A 60 degree model is used for analysis of the top end for end drop loading. A 90 degree model is used for analysis of the bottom end for end drop loading. The top end model for bottom end drop loading and the bottom end model for top end drop loading are extended to include the full height of the cylindrical shell. The cylindrical shell, cover plates, shield plugs, lifting device, shield plug support ring, and outer cover plate welds are modeled using ANSYS Solid45 elements.

For the top end models, the lifting device is connected to the outer top cover plate using ANSYS Beam4 elements at the bolt locations. An initial strain is defined for the beam elements to produce a preload of 10 kips at each bolt location. The grapple assembly at the bottom of the DSC shell assembly will be removed prior to transportation in the MP197TAD TO, and therefore, it is excluded from the bottom end models.

Contact between the cover plates and the shield plugs, and between the lifting device and the outer top cover plate are modeled using ANSYS Conta173 and Targe170 elements. The initial gaps between these components are considered to be closed.

For the side drops, gaps between the shield plug and the cylindrical shell are modeled using ANSYS Contac52 elements. Initial gaps are based on the shield plug diameter, the shell inside diameter, and the side drop orientation.

For analyses of side drops, gaps between the DSC shell assembly and the MP197TAD TO cavity are modeled using ANSYS Contac52 elements, and the nodes representing the MP197TAD TO are restrained in all directions. Initial gaps are based on the DSC outside diameter of 66.25", the MP197TAD TO inside diameter of 67", the 0.12" rail thickness, and the side drop orientation. The 30g NCT side drop is assumed to occur centered on the four rails (12° and 38°). For the 75g HAC side drop, two drop conditions are assumed: drop on one rail, and drop on no rails.

Symmetry boundary conditions are defined for all nodes at the symmetry planes. For the extended end drop models, nodes at the end of the cylindrical shell are fully restrained. For the top end drop analyses of the top end model, nodes are axially restrained at the locations of support provided by spacers at the top end of the MP197TAD TO, as shown in Figure B.2.13.7-3. For bottom end drop analyses of the bottom end model, nodes are axially restrained at locations of support provided by the bottom end of the MP197TAD TO with consideration of the recessed ram closure plate, as shown in Figure B.2.13.7-4.

Geometry plots of the finite element analytical models are given in Figures B.2.13.7-1 through B.2.13.7-4.

Loading Conditions

Accelerations are defined in the appropriate direction for each of the drop conditions. For the side drops, a basket/fuel linear weight of 420 lbs/in is considered based on a conservative basket + fuel weight of 74,130 lbs and a basket length of 176.5 inches. This weight is applied along the full length of the DSC shell assembly cavity. The total applied load is consistent with the total conservative weight of the basket and fuel. The load near the end plates (away from the active fuel region) is conservative. This basket/fuel linear weight is multiplied with the applied acceleration value (30g, 75g) to match the correct load for the side drop analyses. The basket/fuel inertial load is applied as a uniform pressure load on the inner surface of the shell over an arc length of 90 degrees (i.e., 45 degrees for the symmetric model).

For top end drop analyses of the top end model, a conservative basket + fuel weight of 73,170 lbs is uniformly distributed over the inside surface of the top shield plug. For bottom end drop analysis of the bottom end model, a conservative basket + fuel weight of 73,170 lbs is uniformly distributed over the area of the inner bottom cover plate. The distributed pressures loads are multiplied by the appropriate acceleration value (50g, 90g) associated with the analyzed drop. The inertial and internal pressure effects of the opposite-half of the DSC assembly are considered through the application of pressure loading on the edge of the shell at the modeled end of the shell (i.e., mid-height).

Internal and external pressures are applied to the appropriate surfaces of the cylindrical shell and cover plates. For each drop configuration, three pressure conditions are considered: 20 psi internal pressure, 15 psi external pressure, and no pressure. Temperature distributions associated with the thermal loads summarized in Section B.2.13.7.2.2 are analyzed using the 180 degree models. The thermal analyses are based on the temperature-dependent material properties tabulated in Section B.2.13.7.2.1.

B.2.13.7.2.4 Stress Analysis Results

The maximum stress intensities in the DSC shell assembly are extracted from the ANSYS results, for all twelve load combinations. Analysis results are postprocessed to obtain linearized stress distributions across sections taken through the thickness of the DSC shell assembly components. This separates the stresses into membrane and membrane + bending components for the evaluation to ASME allowable stresses. These stresses are compared to the normal and accident condition code allowable stress intensities. Tables B.2.13.7-1 through B.2.13.7-12 summarize the maximum calculated and allowable stress intensities in the TN44B DSC shell assembly for normal and accident conditions respectively. Figures B.2.13.7-5 through B.2.13.7-16 are stress contour plots for the controlling load combinations.

As noted in Table B.2.13.7-1 and Table B.2.13.7-2, the Service Level A allowable stresses for some of the DSC shell assembly components are exceeded for the NCT side drop condition. Limit analyses per NB-3228.1 were performed to a load beyond 45g to demonstrate that the 30g loading does not exceed two-thirds of the lower bound collapse load. Elastic-perfectly plastic material properties were specified, with a yield point of $1.5S_m$, and large deflection effects were

included in the analyses. Converged solutions were obtained to 75g (2.5 times the stress analysis acceleration) for both the top-end model and the bottom-end model. The resulting strains in the DSC shell assembly are small, where the maximum total strain at a 30g load step of the limit analysis is 0.32% and occurs in the cylindrical shell.

Closure weld membrane stresses are classified as local membrane stresses in consideration of the discontinuity of the DSC shell assembly at the location of the weld. The 3/4" partial penetration groove weld of the outer top cover plate to the cylindrical shell is modeled with solid elements. For NCT (Level A) loading, linearized stresses are determined in the same manner as for the DSC shell assembly components. For HAC (Level D) loading, the outer top cover plate welded connection is modeled as pinned (secondary stress evaluation is not required for Level D loading). For the pinned condition, nodal forces at the locations of the welds are postprocessed, and the weld stress at each node is calculated as shown below.

The 3/16" partial penetration groove weld of the inner top cover plate to the cylindrical shell is modeled as a pinned connection. Nodal forces at the locations of the welds are postprocessed, and the weld stress at each node is calculated as follows:

$$f_w = F_{resultant} / (L_{tributary})(T_{weld})$$

where

$F_{resultant}$ = maximum resultant nodal force, kips
$L_{tributary}$ = tributary length associated with the node, in.
T_{weld} = weld throat dimension,
0.75 in. (outer top cover plate weld), or
0.1875 in. (inner top cover plate weld)

During welding, the cover plates come into contact with the shell. The calculation of $F_{resultant}$ excludes any radial compressive forces because the components will bear the compressive forces. For Level D side drop loading, weld locations in the immediate vicinity of and directly above the rails are excluded from the weld force tabulations. Near the rail, the cover plates bear directly against the DSC cylindrical shell such that local distortions in the welded connections would allow the load to be carried in bearing between the cover plates and the DSC cylindrical shell. Bearing is not required to be evaluated for the Level D drop conditions.

Table B.2.13.7-13 and Table B.2.13.7-14 summarize the calculated and allowable stresses for the closure welds.

B.2.13.7.2.5 DSC Shell Assembly Buckling Analysis

Stability for the end drops is demonstrated by running a bottom end drop of the top end model and a top end drop of the bottom end model (each with the shell length extended to the full length of the DSC) beyond 200 g. Nonlinear material properties are used at a uniform temperature of 500 °F with a plastic tangent modulus conservatively taken at 1% of the elastic modulus, for stresses beyond the yield strength of the material. Large deflection effects were

included in the analyses. The table below summarizes the buckling loads for the end drop conditions.

End Drop Buckling Loads

Load Combination	Loads	Buckling Load (g)
HAC-9	Bottom End Drop + 20 psi Internal	167.8
HAC-10	Bottom End Drop + 15 psi External	167.7
HAC-11	Top End Drop + 20 psi Internal	$\geq$ 200
HAC-12	Top End Drop + 15 psi External	$\geq$ 200

B.2.13.7.3 References

1. American Society of Mechanical Engineers, ASME Boiler and Pressure Vessel Code, Section III, Subsection NB, 2004 Edition.

2. American Society of Mechanical Engineers, ASME Boiler and Pressure Vessel Code, Section III, Appendix F, 2004 Edition.

3. American Society of Mechanical Engineers, ASME Boiler and Pressure Vessel Code, Section II, Part D, 2004 Edition.

4. ANSYS Computer Code and User's Manuals, Release 10.0.

5. *Manual of Steel Construction*, Ninth Edition, American Institute of Steel Construction, Inc., 1989.

6. Interim Staff Guidance, ISG-15, Rev.0, "Materials Evaluation," U.S. Nuclear Regulatory Commission.

Table B.2.13.7-1
NCT-1: 30g Side Drop + 20 psi Internal Pressure + Thermal (hot)

(ASME Service Level A)

DSC Component	Material	Stress Category	Stress [1] Intensity (ksi)	Allowable [2] Stress (ksi)
Cylindrical Shell	Type 316/316L	P_m	37.57	18.0 [3]
		$P_L + P_b$	39.53	27.0 [3]
		$P_L + P_b + Q$	45.91	54.0
Outer Top Cover Plate	Type 316/316L	P_m	15.83	18.0
		$P_L + P_b$	23.44	27.0
		$P_L + P_b + Q$	30.26	54.0
Inner Top Cover Plate	Type 304	P_m	15.38	17.5
		$P_L + P_b$	25.50	26.3
		$P_L + P_b + Q$	26.20	52.5
Top Shield Plug	Type 304	P_m	15.26	17.5
		$P_L + P_b$	26.14	26.3 [3]
		$P_L + P_b + Q$	26.89	52.5
Support Ring	Type 304	P_m	19.28	17.5 [3]
		$P_L + P_b$	22.53	26.3
		$P_L + P_b + Q$	24.80	52.5
Outer Bottom Cover Plate	Type 316/316L	P_m	14.91	18.0
		$P_L + P_b$	18.60	27.0
		$P_L + P_b + Q$	19.80	54.0
Bottom Shield Plug	Type 304	P_m	7.03	17.5
		$P_L + P_b$	10.62	26.3
		$P_L + P_b + Q$	11.41	52.5
Inner Bottom Cover Plate	Type 304	P_m	18.86	17.5 [3]
		$P_L + P_b$	24.23	26.3
		$P_L + P_b + Q$	28.35	52.5

Notes:
1. All stresses are based on elastic analysis.
2. Allowable stresses are conservatively based on material properties at 500 °F for all components.
3. Allowable stresses are exceeded or are nearly exceeded. The primary stresses listed for these components occur at the locations of the MP197TAD TO rails or at the junction of the cover plates and the cylindrical shell. Stresses away from these locations are significantly lower and are within the primary stress allowables. Limit analyses per NB-3228.1 were performed beyond 45g to demonstrate that 30g loading does not exceed 2/3 of the lower bound collapse load.

Table B.2.13.7-2
NCT-2: 30g Side Drop + 15 psi External Pressure + Thermal (cold)

(ASME Service Level A)

DSC Component	Material	Stress Category	Stress [1] Intensity (ksi)	Allowable [2] Stress (ksi)
Cylindrical Shell	Type 316/316L	P_m	36.99	18.0 [3]
		$P_L + P_b$	39.19	27.0 [3]
		$P_L + P_b + Q$	45.84	54.0
Outer Top Cover Plate	Type 316/316L	P_m	15.59	18.0
		$P_L + P_b$	23.80	27.0
		$P_L + P_b + Q$	30.63	54.0
Inner Top Cover Plate	Type 304	P_m	15.70	17.5
		$P_L + P_b$	25.09	26.3
		$P_L + P_b + Q$	25.79	52.5
Top Shield Plug	Type 304	P_m	14.87	17.5
		$P_L + P_b$	26.14	26.3 [3]
		$P_L + P_b + Q$	26.89	52.5
Support Ring	Type 304	P_m	18.44	17.5 [3]
		$P_L + P_b$	21.62	26.3
		$P_L + P_b + Q$	23.90	52.5
Outer Bottom Cover Plate	Type 316/316L	P_m	14.63	18.0
		$P_L + P_b$	18.72	27.0
		$P_L + P_b + Q$	19.92	54.0
Bottom Shield Plug	Type 304	P_m	6.24	17.5
		$P_L + P_b$	10.26	26.3
		$P_L + P_b + Q$	11.05	52.5
Inner Bottom Cover Plate	Type 304	P_m	19.28	17.5 [3]
		$P_L + P_b$	26.24	26.3 [3]
		$P_L + P_b + Q$	30.36	52.5

Notes:
1. All stresses are based on elastic analysis.
2. Allowable stresses are conservatively based on material properties at 500 °F for all components.
3. Allowable stresses are exceeded or are nearly exceeded. The primary stresses listed for these components occur at the locations of the MP197TAD TO rails or at the junction of the cover plates and the cylindrical shell. Stresses away from these locations are significantly lower and are within the primary stress allowables. Limit analyses per NB-3228.1 were performed beyond 45g to demonstrate that 30g loading does not exceed 2/3 of the lower bound collapse load.

Table B.2.13.7-3
NCT-3: 50g Bottom End Drop + 20 psi Internal Pressure + Thermal (hot)

(ASME Service Level A)

DSC Component	Material	Stress Category	Stress[1] Intensity (ksi)	Allowable[2] Stress (ksi)
Cylindrical Shell	Type 316/316L	P_m	6.95	18.0
		$P_L + P_b$	9.56	27.0
		$P_L + P_b + Q$	14.36	54.0
Outer Top Cover Plate	Type 316/316L	P_m	2.59	18.0
		$P_L + P_b$	4.54	27.0
		$P_L + P_b + Q$	11.36	54.0
Inner Top Cover Plate	Type 304	P_m	1.07	17.5
		$P_L + P_b$	2.07	26.3
		$P_L + P_b + Q$	2.77	52.5
Top Shield Plug	Type 304	P_m	1.63	17.5
		$P_L + P_b$	4.98	26.3
		$P_L + P_b + Q$	5.73	52.5
Support Ring	Type 304	P_m	3.13	17.5
		$P_L + P_b$	5.45	26.3
		$P_L + P_b + Q$	7.73	52.5
Outer Bottom Cover Plate	Type 316/316L	P_m	8.70	18.0
		$P_L + P_b$	12.37	27.0
		$P_L + P_b + Q$	13.57	54.0
Bottom Shield Plug	Type 304	P_m	2.93	17.5
		$P_L + P_b$	8.28	26.3
		$P_L + P_b + Q$	9.07	52.5
Inner Bottom Cover Plate	Type 304	P_m	3.90	17.5
		$P_L + P_b$	8.44	26.3
		$P_L + P_b + Q$	12.56	52.5

Notes:
1. All stresses are based on elastic analysis.
2. Allowable stresses are conservatively based on material properties at 500 °F for all components.

Table B.2.13.7-4
NCT-4: 50g Bottom End Drop + 15 psi External Pressure + Thermal (cold)

(ASME Service Level A)

DSC Component	Material	Stress Category	Stress [1] Intensity (ksi)	Allowable [2] Stress (ksi)
Cylindrical Shell	Type 316/316L	P_m	7.31	18.0
		$P_L + P_b$	9.14	27.0
		$P_L + P_b + Q$	14.52	54.0
Outer Top Cover Plate	Type 316/316L	P_m	2.75	18.0
		$P_L + P_b$	4.82	27.0
		$P_L + P_b + Q$	11.65	54.0
Inner Top Cover Plate	Type 304	P_m	1.26	17.5
		$P_L + P_b$	2.38	26.3
		$P_L + P_b + Q$	3.08	52.5
Top Shield Plug	Type 304	P_m	1.77	17.5
		$P_L + P_b$	5.47	26.3
		$P_L + P_b + Q$	6.22	52.5
Support Ring	Type 304	P_m	2.82	17.5
		$P_L + P_b$	5.58	26.3
		$P_L + P_b + Q$	7.86	52.5
Outer Bottom Cover Plate	Type 316/316L	P_m	8.56	18.0
		$P_L + P_b$	12.17	27.0
		$P_L + P_b + Q$	13.37	54.0
Bottom Shield Plug	Type 304	P_m	3.03	17.5
		$P_L + P_b$	8.14	26.3
		$P_L + P_b + Q$	8.94	52.5
Inner Bottom Cover Plate	Type 304	P_m	4.18	17.5
		$P_L + P_b$	8.28	26.3
		$P_L + P_b + Q$	12.40	52.5

Notes:
1. All stresses are based on elastic analysis.
2. Allowable stresses are conservatively based on material properties at 500 °F for all components.

Table B.2.13.7-5
NCT-5: 50g Top End Drop + 20 psi Internal Pressure + Thermal (hot)

(ASME Service Level A)

DSC Component	Material	Stress Category	Stress[1] Intensity (ksi)	Allowable[2] Stress (ksi)
Cylindrical Shell	Type 316/316L	P_m	8.13	18.0
		$P_L + P_b$	16.72	27.0
		$P_L + P_b + Q$	23.65	54.0
Outer Top Cover Plate	Type 316/316L	P_m	6.56	18.0
		$P_L + P_b$	8.24	27.0
		$P_L + P_b + Q$	15.07	54.0
Inner Top Cover Plate	Type 304	P_m	2.89	17.5
		$P_L + P_b$	4.19	26.3
		$P_L + P_b + Q$	4.90	52.5
Top Shield Plug	Type 304	P_m	2.52	17.5
		$P_L + P_b$	2.86	26.3
		$P_L + P_b + Q$	3.61	52.5
Support Ring	Type 304	P_m	3.50	17.5
		$P_L + P_b$	4.50	26.3
		$P_L + P_b + Q$	6.78	52.5
Outer Bottom Cover Plate	Type 316/316L	P_m	3.47	18.0
		$P_L + P_b$	6.80	27.0
		$P_L + P_b + Q$	8.00	54.0
Bottom Shield Plug	Type 304	P_m	0.45	17.5
		$P_L + P_b$	6.96	26.3
		$P_L + P_b + Q$	7.75	52.5
Inner Bottom Cover Plate	Type 304	P_m	1.56	17.5
		$P_L + P_b$	6.66	26.3
		$P_L + P_b + Q$	10.78	52.5

Notes:
1. All stresses are based on elastic analysis.
2. Allowable stresses are conservatively based on material properties at 500 °F for all components.

Table B.2.13.7-6
NCT-6: 50g Top End Drop + 15 psi External Pressure + Thermal (cold)

(ASME Service Level A)

DSC Component	Material	Stress Category	Stress [1] Intensity (ksi)	Allowable [2] Stress (ksi)
Cylindrical Shell	Type 316/316L	P_m	9.64	18.0
		$P_L + P_b$	18.92	27.0
		$P_L + P_b + Q$	25.85	54.0
Outer Top Cover Plate	Type 316/316L	P_m	6.47	18.0
		$P_L + P_b$	8.11	27.0
		$P_L + P_b + Q$	14.94	54.0
Inner Top Cover Plate	Type 304	P_m	2.82	17.5
		$P_L + P_b$	4.11	26.3
		$P_L + P_b + Q$	4.81	52.5
Top Shield Plug	Type 304	P_m	2.62	17.5
		$P_L + P_b$	2.88	26.3
		$P_L + P_b + Q$	3.63	52.5
Support Ring	Type 304	P_m	3.31	17.5
		$P_L + P_b$	4.72	26.3
		$P_L + P_b + Q$	7.00	52.5
Outer Bottom Cover Plate	Type 316/316L	P_m	4.05	18.0
		$P_L + P_b$	8.15	27.0
		$P_L + P_b + Q$	9.35	54.0
Bottom Shield Plug	Type 304	P_m	0.56	17.5
		$P_L + P_b$	8.25	26.3
		$P_L + P_b + Q$	9.04	52.5
Inner Bottom Cover Plate	Type 304	P_m	1.87	17.5
		$P_L + P_b$	7.32	26.3
		$P_L + P_b + Q$	11.44	52.5

Notes:
1. All stresses are based on elastic analysis.
2. Allowable stresses are conservatively based on material properties at 500 °F for all components.

Table B.2.13.7-7
HAC-7: 75g Side Drop + 20 psi Internal Pressure

(ASME Service Level D)

DSC Component	Material	Stress Category	Stress [1] Intensity (ksi)	Allowable [2] Stress (ksi)
Cylindrical Shell	Type 316/316L	P_m	46.71	50.3
		$P_L + P_b$	55.96	64.6
Outer Top Cover Plate	Type 316/316L	P_m	49.91	50.3
		$P_L + P_b$	55.17	64.6
Inner Top Cover Plate	Type 304	P_m	24.62	44.4
		$P_L + P_b$	55.17	57.1
Top Shield Plug	Type 304	P_m	33.56	44.4
		$P_L + P_b$	43.80	57.1
Support Ring	Type 304	P_m	24.53	44.4
		$P_L + P_b$	32.32	57.1
Outer Bottom Cover Plate	Type 316/316L	P_m	46.24	50.3
		$P_L + P_b$	58.49	64.6
Bottom Shield Plug	Type 304	P_m	19.77	44.4
		$P_L + P_b$	26.84	57.1
Inner Bottom Cover Plate	Type 304	P_L [3]	51.74 [3]	57.1
		$P_L + P_b$	52.82	57.1

Notes:
1. All stresses are based on plastic analysis.
2. Allowable stresses are conservatively based on material properties at 500 °F for all components.
3. The controlling local membrane stress (NB-3213.10) is listed. General membrane stress at locations beyond a distance of $(r\,t)^{1/2}$ from the edge above the rail are well within the allowable membrane stress of 44.4 ksi

Table B.2.13.7-8
HAC-8: 75g Side Drop + 15 psi External Pressure

(ASME Service Level D)

DSC Component	Material	Stress Category	Stress[1] Intensity (ksi)	Allowable[2] Stress (ksi)
Cylindrical Shell	Type 316/316L	P_m	46.71	50.3
		$P_L + P_b$	56.12	64.6
Outer Top Cover Plate	Type 316/316L	P_m	49.91	50.3
		$P_L + P_b$	55.33	64.6
Inner Top Cover Plate	Type 304	P_m	24.62	44.4
		$P_L + P_b$	55.29	57.1
Top Shield Plug	Type 304	P_m	33.31	44.4
		$P_L + P_b$	43.45	57.1
Support Ring	Type 304	P_m	24.49	44.4
		$P_L + P_b$	32.32	57.1
Outer Bottom Cover Plate	Type 316/316L	P_m	46.45	50.3
		$P_L + P_b$	58.73	64.6
Bottom Shield Plug	Type 304	P_m	19.77	44.4
		$P_L + P_b$	25.96	57.1
Inner Bottom Cover Plate	Type 304	P_L[3]	51.78[3]	57.1
		$P_L + P_b$	52.85	57.1

Notes:
1. All stresses are based on plastic analysis.
2. Allowable stresses are conservatively based on material properties at 500 °F for all components.
3. The controlling local membrane stress (NB-3213.10) is listed. General membrane stress at locations beyond a distance of $(r\,t)^{1/2}$ from the edge above the rail are well within the allowable membrane stress of 44.4 ksi.

Table B.2.13.7-9
HAC-9: 90g Bottom End Drop + 20 psi Internal Pressure

(ASME Service Level D)

DSC Component	Material	Stress Category	Stress [1] Intensity (ksi)	Allowable [2] Stress (ksi)
Cylindrical Shell	Type 316/316L	P_m	12.50	43.2
		$P_L + P_b$	16.86	64.8
Outer Top Cover Plate	Type 316/316L	P_m	3.23	43.2
		$P_L + P_b$	6.50	64.8
Inner Top Cover Plate	Type 304	P_m	1.25	42.0
		$P_L + P_b$	3.45	63.0
Top Shield Plug	Type 304	P_m	3.08	42.0
		$P_L + P_b$	9.20	63.0
Support Ring	Type 304	P_m	5.42	42.0
		$P_L + P_b$	9.91	63.0
Outer Bottom Cover Plate	Type 316/316L	P_m	15.58	43.2
		$P_L + P_b$	22.13	64.8
Bottom Shield Plug	Type 304	P_m	5.04	42.0
		$P_L + P_b$	14.79	63.0
Inner Bottom Cover Plate	Type 304	P_m	7.06	42.0
		$P_L + P_b$	15.02	63.0

Notes:
1. All stresses are based on elastic analysis.
2. Allowable stresses are conservatively based on material properties at 500 °F for all components.

Table B.2.13.7-10
HAC-10: 90g Bottom End Drop + 15 psi External Pressure

(ASME Service Level D)

DSC Component	Material	Stress Category	Stress [1] Intensity (ksi)	Allowable [2] Stress (ksi)
Cylindrical Shell	Type 316/316L	P_m	12.83	43.2
		$P_L + P_b$	16.44	64.8
Outer Top Cover Plate	Type 316/316L	P_m	3.39	43.2
		$P_L + P_b$	6.79	64.8
Inner Top Cover Plate	Type 304	P_m	1.40	42.0
		$P_L + P_b$	3.60	63.0
Top Shield Plug	Type 304	P_m	3.22	42.0
		$P_L + P_b$	9.71	63.0
Support Ring	Type 304	P_m	5.11	42.0
		$P_L + P_b$	9.98	63.0
Outer Bottom Cover Plate	Type 316/316L	P_m	15.44	43.2
		$P_L + P_b$	21.93	64.8
Bottom Shield Plug	Type 304	P_m	5.14	42.0
		$P_L + P_b$	14.66	63.0
Inner Bottom Cover Plate	Type 304	P_m	7.34	42.0
		$P_L + P_b$	14.86	63.0

Notes:
1. All stresses are based on elastic analysis.
2. Allowable stresses are conservatively based on material properties at 500 °F for all components.

Table B.2.13.7-11
HAC-11: 90g Top End Drop + 20 psi Internal Pressure

(ASME Service Level D)

DSC Component	Material	Stress Category	Stress [1] Intensity (ksi)	Allowable [2] Stress (ksi)
Cylindrical Shell	Type 316/316L	P_m	9.42	43.2
		$P_L + P_b$	29.03	64.8
Outer Top Cover Plate	Type 316/316L	P_m	11.71	43.2
		$P_L + P_b$	14.71	64.8
Inner Top Cover Plate	Type 304	P_m	5.15	42.0
		$P_L + P_b$	7.49	63.0
Top Shield Plug	Type 304	P_m	4.58	42.0
		$P_L + P_b$	5.09	63.0
Support Ring	Type 304	P_m	6.03	42.0
		$P_L + P_b$	8.02	63.0
Outer Bottom Cover Plate	Type 316/316L	P_m	3.80	43.2
		$P_L + P_b$	11.11	64.8
Bottom Shield Plug	Type 304	P_m	0.96	42.0
		$P_L + P_b$	13.95	63.0
Inner Bottom Cover Plate	Type 304	P_m	2.71	42.0
		$P_L + P_b$	12.42	63.0

Notes:
1. All stresses are based on elastic analysis.
2. Allowable stresses are conservatively based on material properties at 500 °F for all components.

Table B.2.13.7-12
HAC-12: 90g Top End Drop + 15 psi External Pressure

(ASME Service Level D)

DSC Component	Material	Stress Category	Stress [1] Intensity (ksi)	Allowable [2] Stress (ksi)
Cylindrical Shell	Type 316/316L	P_m	9.72	43.2
		$P_L + P_b$	31.17	64.8
Outer Top Cover Plate	Type 316/316L	P_m	11.62	43.2
		$P_L + P_b$	14.58	64.8
Inner Top Cover Plate	Type 304	P_m	5.08	42.0
		$P_L + P_b$	7.40	63.0
Top Shield Plug	Type 304	P_m	4.68	42.0
		$P_L + P_b$	5.12	63.0
Support Ring	Type 304	P_m	5.90	42.0
		$P_L + P_b$	8.30	63.0
Outer Bottom Cover Plate	Type 316/316L	P_m	4.18	43.2
		$P_L + P_b$	12.23	64.8
Bottom Shield Plug	Type 304	P_m	1.11	42.0
		$P_L + P_b$	15.39	63.0
Inner Bottom Cover Plate	Type 304	P_m	2.91	42.0
		$P_L + P_b$	12.82	63.0

Notes:
1. All stresses are based on elastic analysis.
2. Allowable stresses are conservatively based on material properties at 500 °F for all components.

Table B.2.13.7-13
Stress Results for Weld of Outer Top Cover Plate

Load Combination	Service Level	Stress Category	Loads	Weld [1,2] Stress (ksi)	Allowable [3] Stress (ksi)
NCT-1	A	P_L	30g SD + $P_{I(20\ psi)}$	21.11	21.6
		P_L+P_b	30g SD + $P_{I(20\ psi)}$	27.77	21.6 [4]
		P_L+P_b+Q	30g SD + $P_{I(20\ psi)}$ + $TH_{(hot)}$	28.64	43.2
NCT-2	A	P_L	30g SD + $P_{E(15\ psi)}$	19.31	21.6
		P_L+P_b	30g SD + $P_{E(15\ psi)}$	26.51	21.6 [4]
		P_L+P_b+Q	30g SD + $P_{E(15\ psi)}$ + $TH_{(cold)}$	27.38	43.2
NCT-3	A	P_L	50g BED + $P_{I(20\ psi)}$	3.60	21.6
		P_L+P_b	50g BED + $P_{I(20\ psi)}$	5.00	21.6
		P_L+P_b+Q	50g BED + $P_{I(20\ psi)}$ + $TH_{(hot)}$	5.88	43.2
NCT-4	A	P_L	50g BED + $P_{E(15\ psi)}$	3.99	21.6
		P_L+P_b	50g BED + $P_{E(15\ psi)}$	5.55	21.6
		P_L+P_b+Q	50g BED + $P_{E(15\ psi)}$ + $TH_{(cold)}$	6.42	43.2
NCT-5	A	P_L	50g TED + $P_{I(20\ psi)}$	1.50	21.6
		P_L+P_b	50g TED + $P_{I(20\ psi)}$	2.34	21.6
		P_L+P_b+Q	50g TED + $P_{I(20\ psi)}$ + $TH_{(hot)}$	3.21	43.2
NCT-6	A	P_L	50g TED + $P_{E(15\ psi)}$	1.60	21.6
		P_L+P_b	50g TED + $P_{E(15\ psi)}$	2.43	21.6
		P_L+P_b+Q	50g TED + $P_{E(15\ psi)}$ + $TH_{(cold)}$	3.31	43.2
HAC-7	D	P_L	75g SD + $P_{I(20\ psi)}$	8.11	51.7
HAC-8	D	P_L	75g SD + $P_{E(15\ psi)}$	8.07	51.7
HAC-9	D	P_L	90g BED + $P_{I(20\ psi)}$	0.84	51.8
HAC-10	D	P_L	90g BED + $P_{E(15\ psi)}$	0.87	51.8
HAC-11	D	P_L	90g TED + $P_{I(20\ psi)}$	2.07	51.8
HAC-12	D	P_L	90g TED + $P_{E(15\ psi)}$	2.10	51.8

Notes:

1. Stresses are based on plastic analysis for Load Combinations HAC-7 and HAC-8. For all other load combinations, stresses are based on elastic analysis.
2. For the NCT loads, linearized stresses are summarized for the fully-modeled weld. For the HAC loads, the weld is modeled as pinned and the stresses are based on nodal forces, a weld thickness of 0.75 in, and nodal tributary lengths.
3. Allowable stresses are conservatively based on material properties at 500 °F for all load combinations.
4. The bending stress in this weld is conservatively evaluated as a primary stress. Per Note 1 to Table NB-3217-1, this bending stress can be considered as a secondary stress, which would result in a lower stress ratio. Furthermore, a limit analysis per NB-3228.1 was performed to a load beyond 45g to demonstrate that 30g loading does not exceed 2/3 of the lower bound collapse load. The primary stresses listed occur at the locations of the MP197TAD TO rails. Stresses away from these locations are significantly lower and are within the primary stress allowables.

Table B.2.13.7-14
Stress Results for Weld of Inner Top Cover Plate

Load Combination	Service Level	Stress Category	Loads	Weld [1,2] Stress (ksi)	Allowable [3] Stress (ksi)
NCT-1	A	P_L	30g SD + $P_{I(20\ psi)}$	21.54	22.3
		P_L+P_b+Q	30g SD + $P_{I(20\ psi)}$ + $TH_{(hot)}$	22.46	44.6
NCT-2	A	P_L	30g SD + $P_{E(15\ psi)}$	20.92	22.3
		P_L+P_b+Q	30g SD + $P_{E(15\ psi)}$ + $TH_{(cold)}$	21.85	44.6
NCT-3	A	P_L	50g BED + $P_{I(20\ psi)}$	4.27	21.0
		P_L+P_b+Q	50g BED + $P_{I(20\ psi)}$ + $TH_{(hot)}$	5.19	42.0
NCT-4	A	P_L	50g BED + $P_{E(15\ psi)}$	4.51	21.0
		P_L+P_b+Q	50g BED + $P_{E(15\ psi)}$ + $TH_{(cold)}$	5.43	42.0
NCT-5	A	P_L	50g TED + $P_{I(20\ psi)}$	0.90	21.0
		P_L+P_b+Q	50g TED + $P_{I(20\ psi)}$ + $TH_{(hot)}$	1.82	42.0
NCT-6	A	P_L	50g TED + $P_{E(15\ psi)}$	0.45	21.0
		P_L+P_b+Q	50g TED + $P_{E(15\ psi)}$ + $TH_{(cold)}$	1.37	42.0
HAC-7	D	P_L	75g SD + $P_{I(20\ psi)}$	32.79	45.6
HAC-8	D	P_L	75g SD + $P_{E(15\ psi)}$	32.61	45.6
HAC-9	D	P_L	90g BED + $P_{I(20\ psi)}$	3.97	50.4
HAC-10	D	P_L	90g BED + $P_{E(15\ psi)}$	4.08	50.4
HAC-11	D	P_L	90g TED + $P_{I(20\ psi)}$	1.42	50.4
HAC-12	D	P_L	90g TED + $P_{E(15\ psi)}$	1.04	50.4

Notes:

1. Stresses are based on plastic analysis for Load Combinations HAC-7 and HAC-8. For all other load combinations, stresses are based on elastic analysis.
2. Stresses are based on nodal forces, a weld thickness of 3/16 in, and nodal tributary lengths.
3. Allowable stresses are conservatively based on material properties at 500 °F for all load combinations except NCT-1 and NCT-2, for which allowable stresses are based on material properties at 400 °F (bounding for weld location).

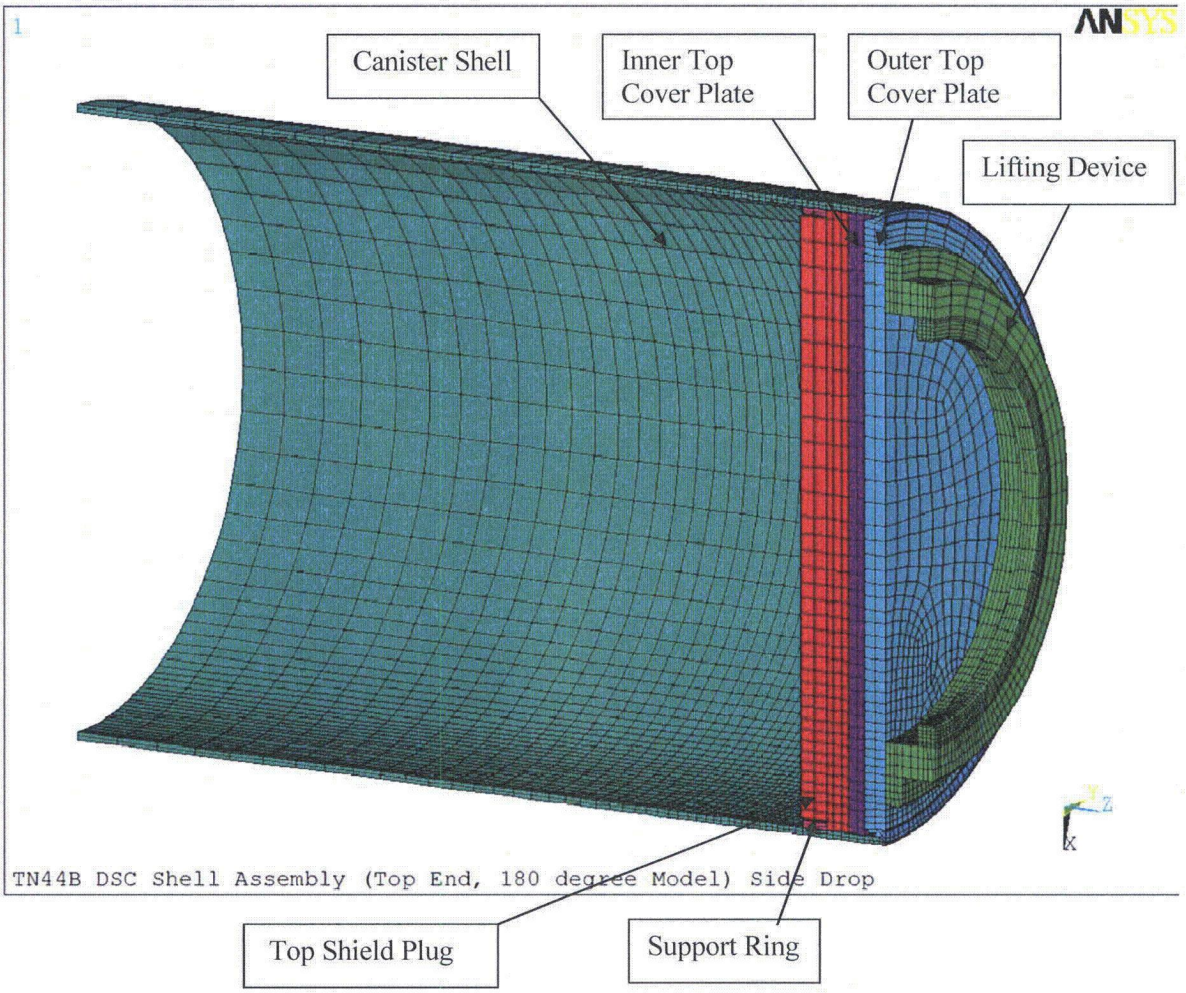

Figure B.2.13.7-1
TN44B DSC Shell Assembly Top End 180 Degree Analytical Model

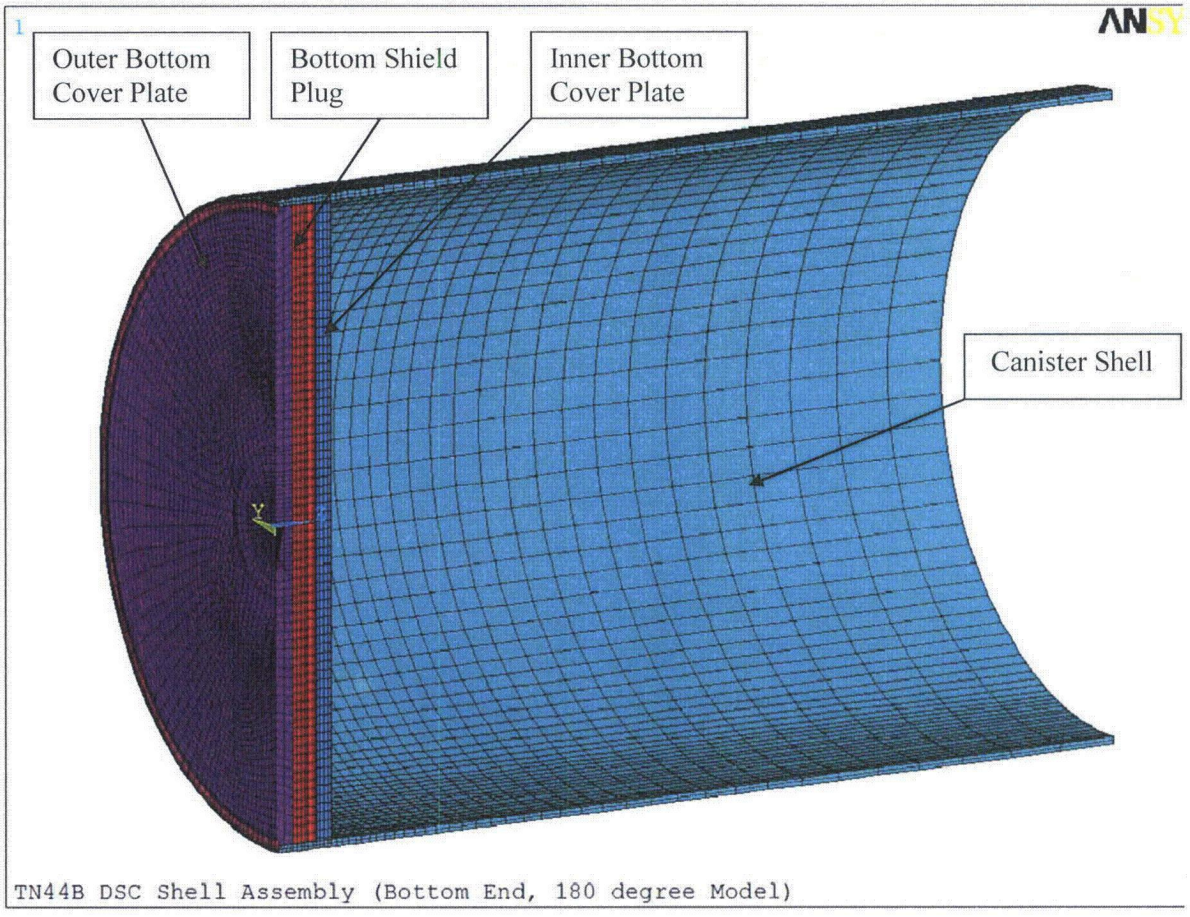

Figure B.2.13.7-2
TN44B DSC Shell Assembly Bottom End 180 Degree Analytical Model

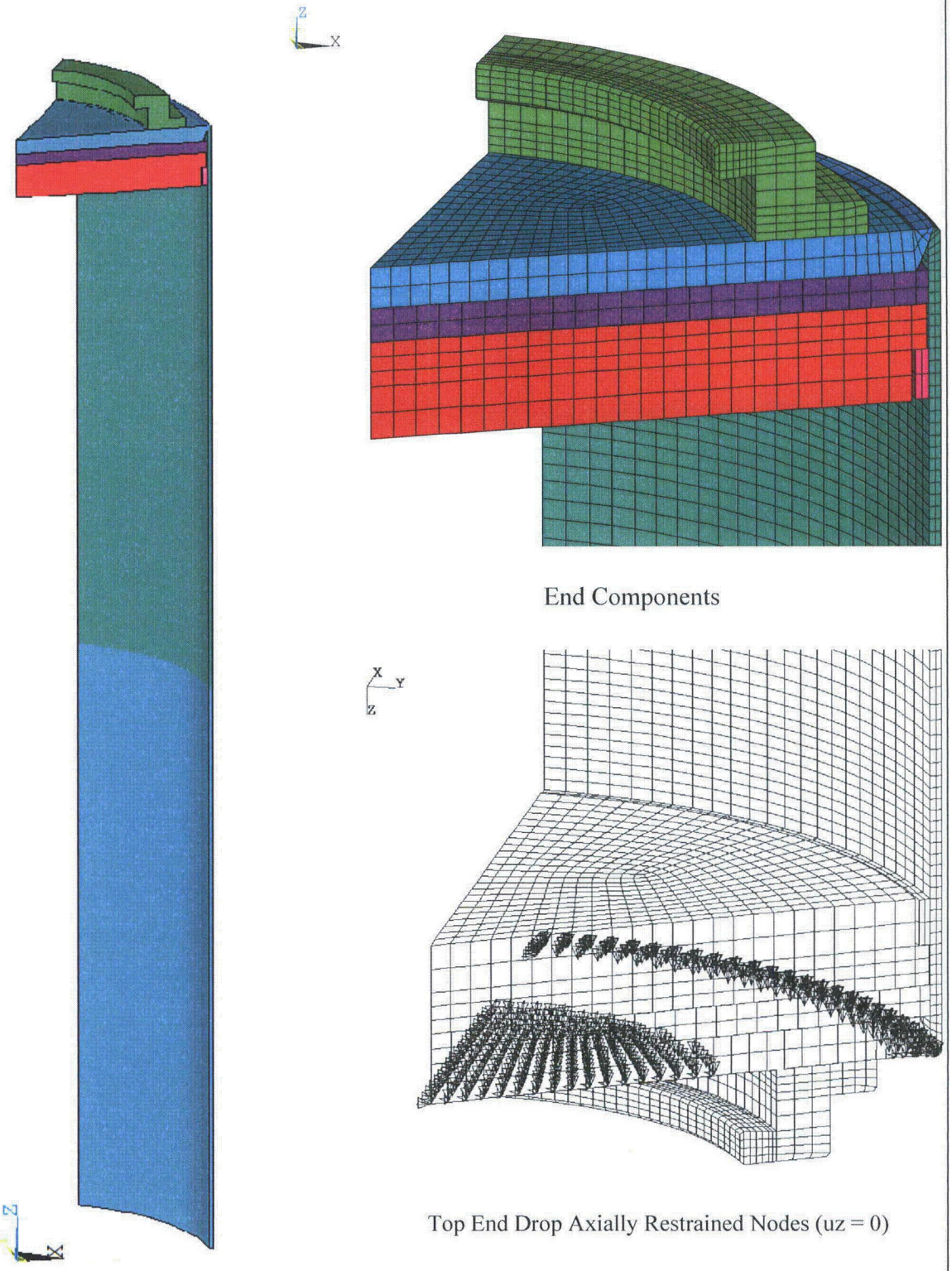

Figure B.2.13.7-3
TN44B DSC Shell Assembly Top End 60 Degree Analytical Model

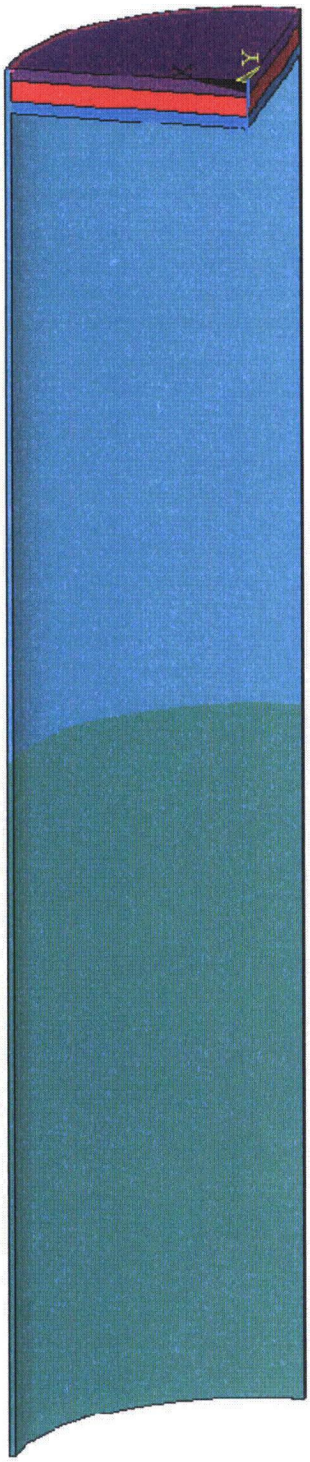

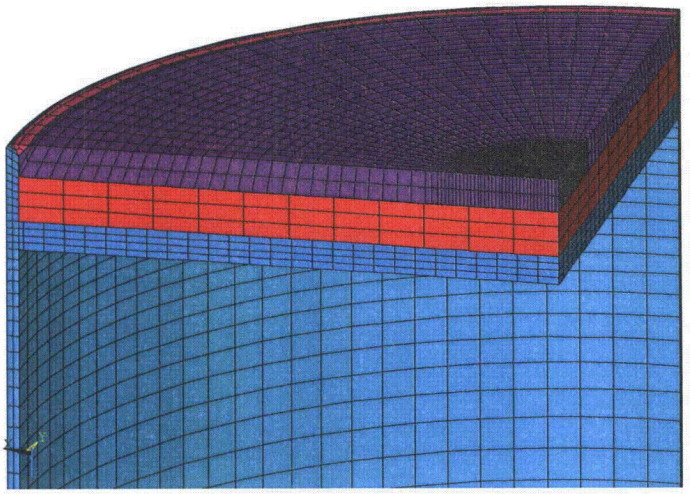

End Components

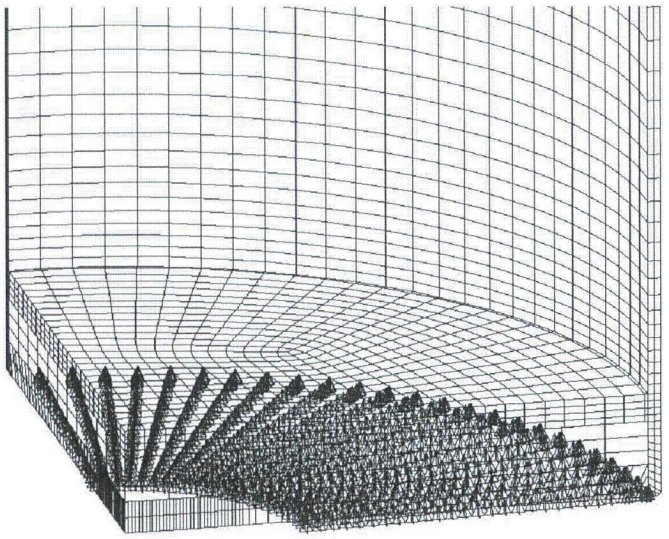

Bottom End Drop Axially Restrained Nodes (uz = 0)

Figure B.2.13.7-4
TN44B DSC Shell Assembly Bottom End 90 Degree Analytical Model

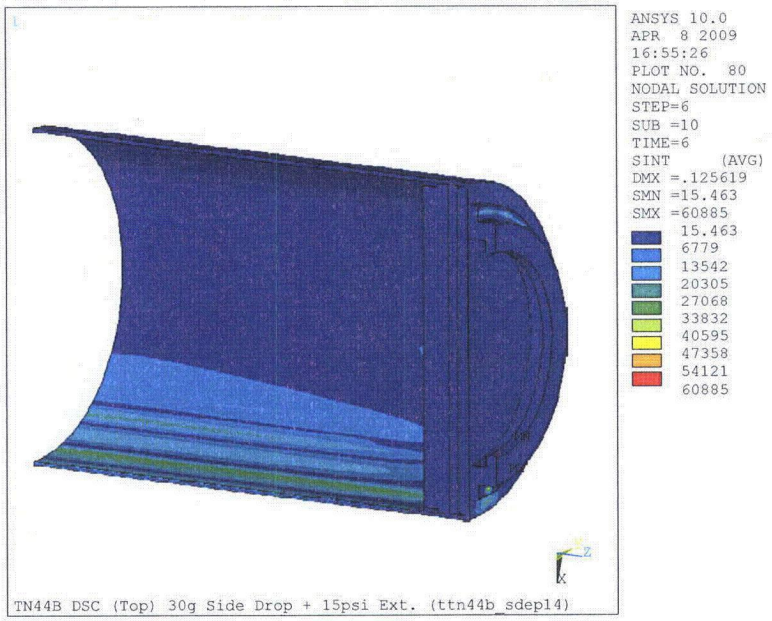

Figure B.2.13.7-5
Top End Model - Stress Intensity Results for 30g Side Drop + 15 psi External Pressure

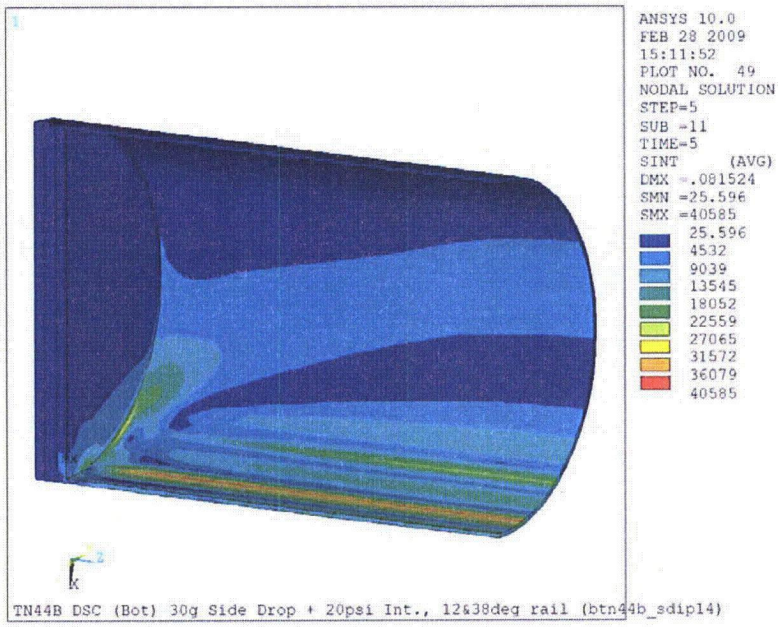

Figure B.2.13.7-6
Bottom End Model - Stress Intensity Results for 30g Side Drop + 20 psi Internal Pressure

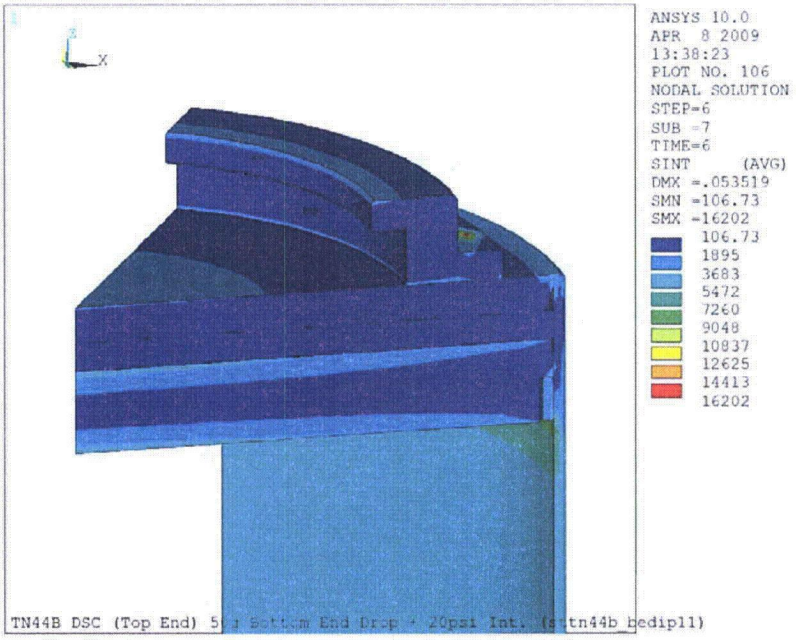

Figure B.2.13.7-7
Top End Model - Stress Intensity Results for 50g Bottom End Drop + 20 psi Internal Pressure

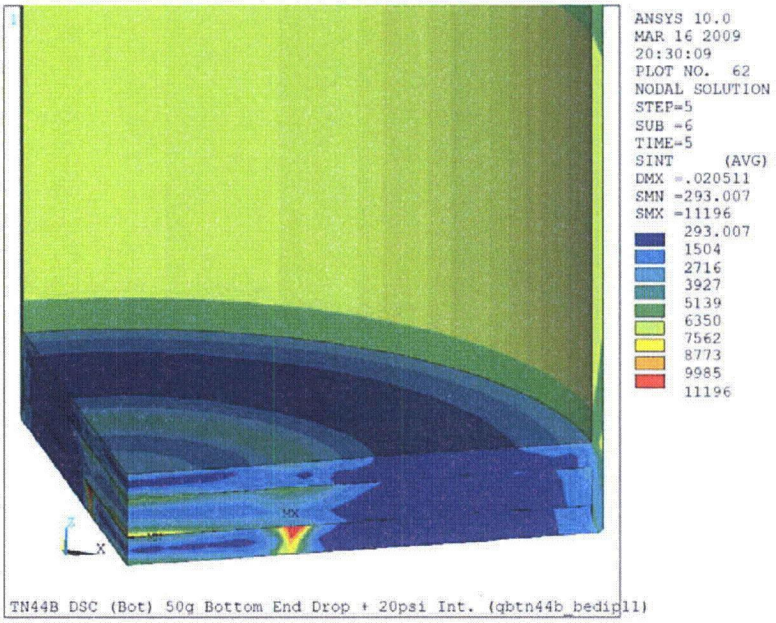

Figure B.2.13.7-8
Bottom End Model - Stress Intensity Results for 50g Bottom End Drop + 20 psi Internal Pressure

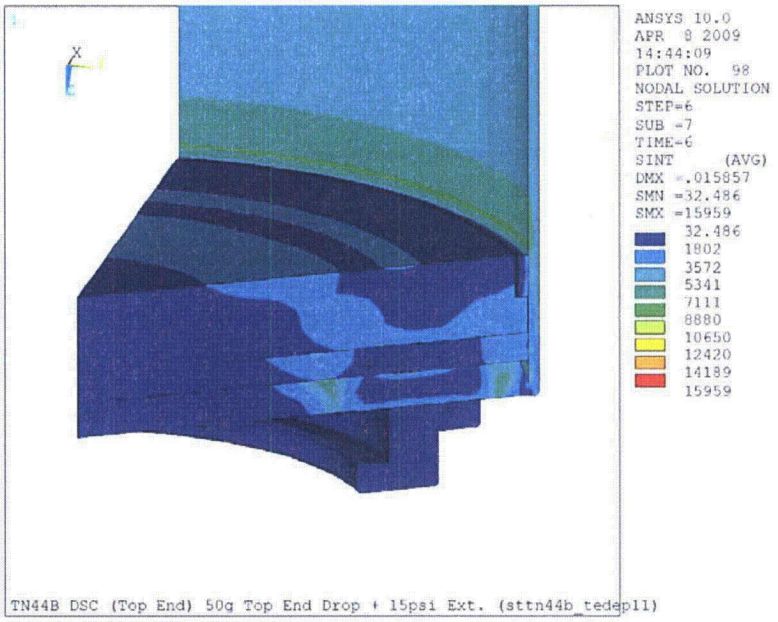

Figure B.2.13.7-9
Top End Model - Stress Intensity Results for 50g Top End Drop + 15 psi External Pressure

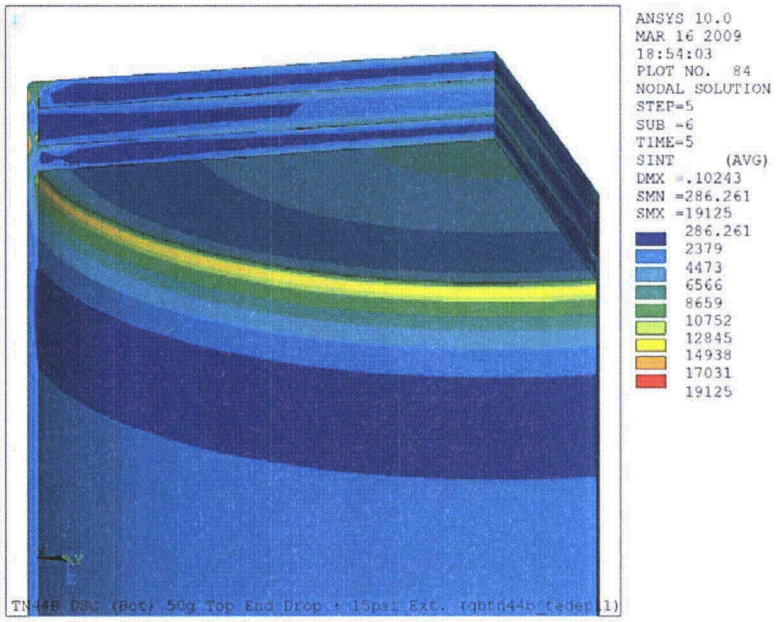

Figure B.2.13.7-10
Bottom End Model – Stress Intensity Results for 50g Top End Drop + 15 psi External Pressure

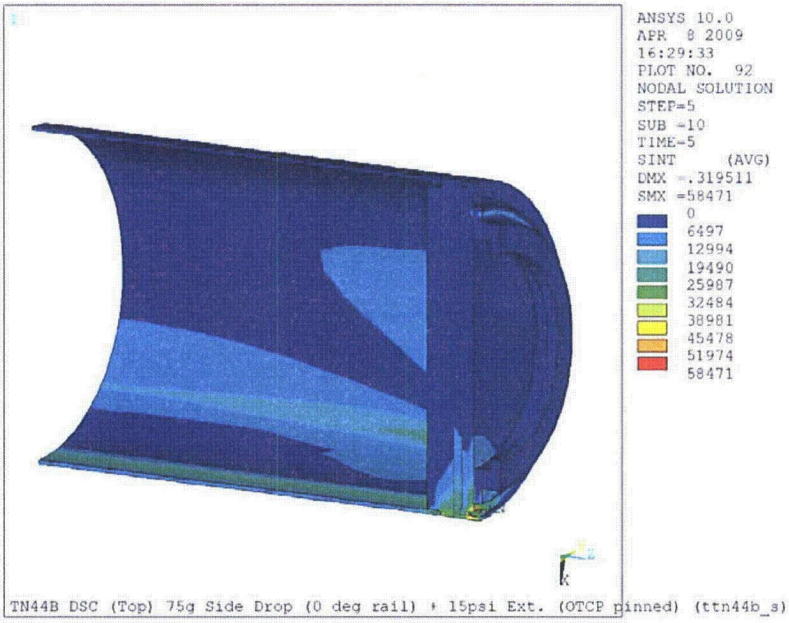

Figure B.2.13.7-11
Top End Model - Stress Intensity Results for 75g Side Drop + 15 psi External Pressure

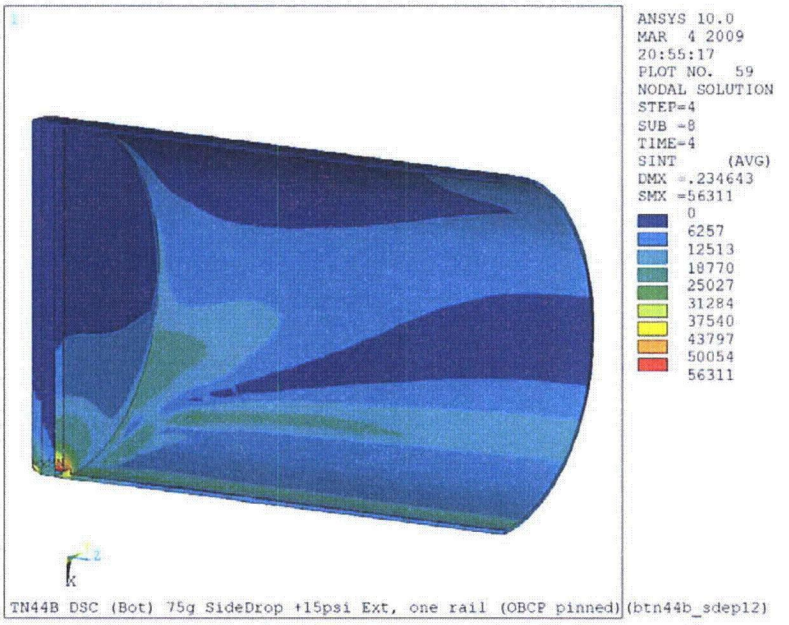

Figure B.2.13.7-12
Bottom End Model - Stress Intensity Results for 75g Side Drop + 15 psi External Pressure

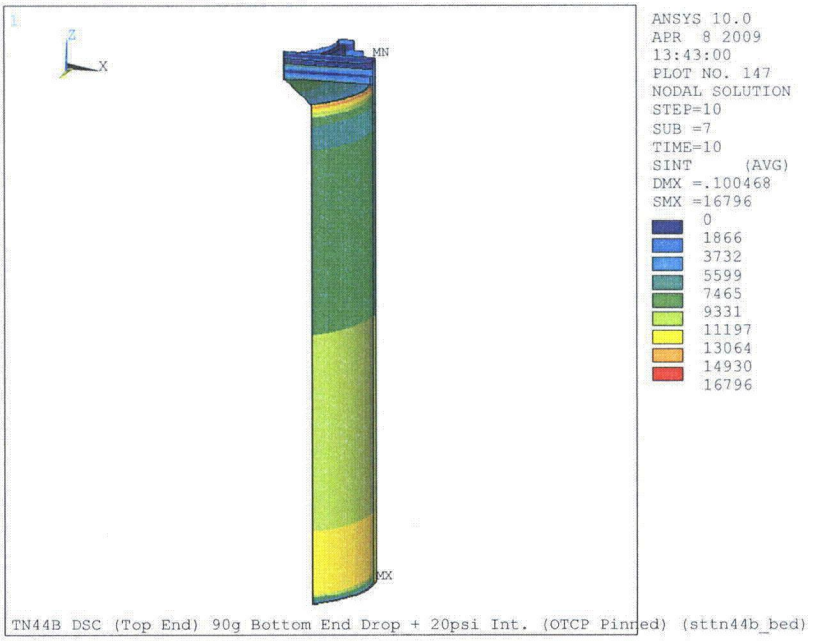

Figure B.2.13.7-13
Top End Model - Stress Intensity Results for 90g Bottom End Drop + 20 psi Internal Pressure

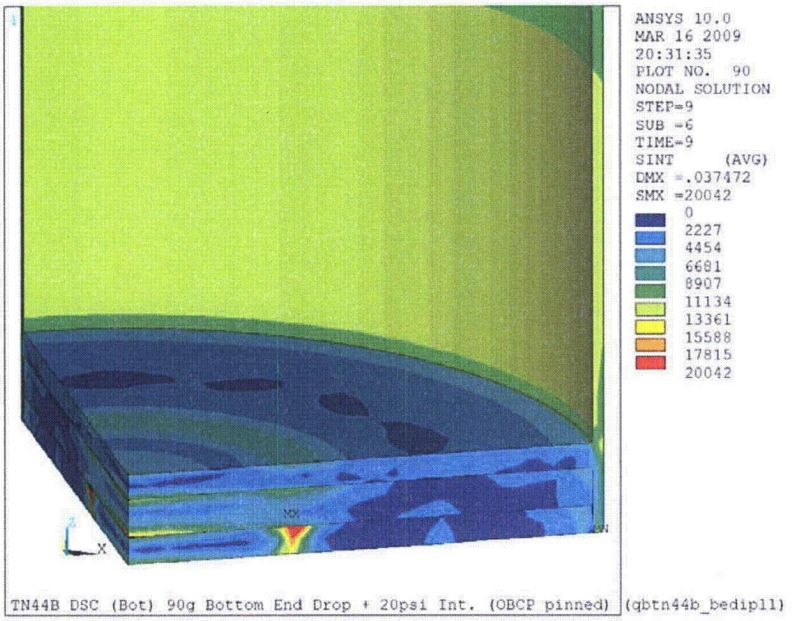

Figure B.2.13.7-14
Bottom End Model - Stress Intensity Results for 90g Bottom End Drop + 20 psi Internal Pressure

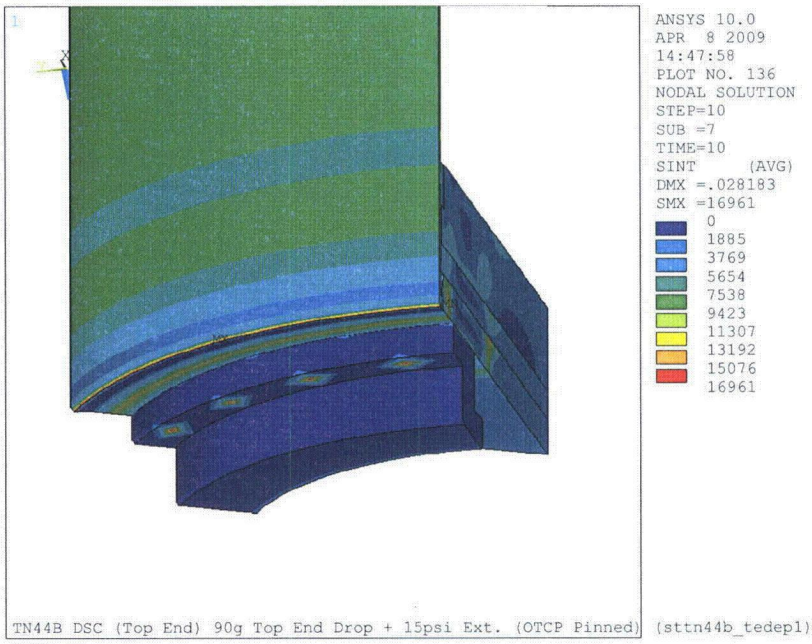

Figure B.2.13.7-15
Top End Model - Stress Intensity Results for 90g Top End Drop + 15 psi External Pressure

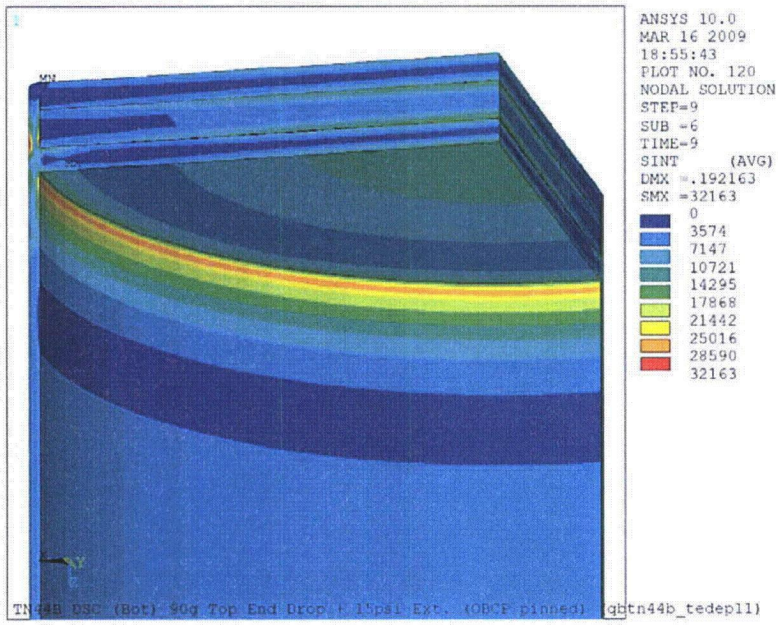

Figure B.2.13.7-16
Bottom End Model - Stress Intensity Results for 90g Top End Drop + 15 psi External Pressure

APPENDIX B.2.13.8
TN44B BASKET ASSEMBLY STRUCTURAL EVALUATION

CONTENTS

B.2.13.8.1 Introduction B.2.13.8-1
B.2.13.8.2 Basket Assembly Structural Analysis B.2.13.8-2
B.2.13.8.2.1 Approach B.2.13.8-2
B.2.13.8.2.2 Loading Conditions B.2.13.8-3
B.2.13.8.2.3 Basket Assembly Stress Analysis B.2.13.8-4
B.2.13.8.2.4 Fuel Basket Assembly Buckling Analysis B.2.13.8-10
B.2.13.8.2.5 Basket Deformations for Effect of Criticality Analyses B.2.13.8-10
B.2.13.8.3 References B.2.13.8-12

LIST OF TABLES

Table B.2.13.8-1 Materials Properties – SA-240/SA-479 304 & SA-182 F304 ..... B.2.13.8-13
Table B.2.13.8-2 Analysis Properties for Aluminum Transition Rails [12] B.2.13.8-14
Table B.2.13.8-3 Materials Properties – SA-240 Type 316/316L & SA-182 F316/316L B.2.13.8-15
Table B.2.13.8-4 Basket Plate and R45 Support Rail Allowable Stress Values B.2.13.8-16
Table B.2.13.8-5 Basket Assembly Normal Condition Loads B.2.13.8-17
Table B.2.13.8-6 Basket Assembly Accident Condition Loads B.2.13.8-18
Table B.2.13.8-7 20g Side Drop + Thermal (hot) B.2.13.8-19
Table B.2.13.8-8 20g Side Drop + Thermal (hot) B.2.13.8-20
Table B.2.13.8-9 Thermal Stress Analysis Results (hot) B.2.13.8-21
Table B.2.13.8-10 75g, 180 Deg. Side Drop on Rails B.2.13.8-22
Table B.2.13.8-11 75g, 180 Deg. Side Drop on Rails B.2.13.8-23
Table B.2.13.8-12 75g, Envelope of Side Drop away from Rails B.2.13.8-24
Table B.2.13.8-13 75g, Envelope of Side Drop away from Rails B.2.13.8-25
Table B.2.13.8-14 TN44B Basket Assembly HAC Buckling Load Summary B.2.13.8-26

LIST OF FIGURES

Figure B.2.13.8-1 TN44B Basket Assembly Model (Excluding Contact and Soft Spring Elements for Clarity) B.2.13.8-27
Figure B.2.13.8-2 TN44B Basket Assembly Model SS Fuel Compartments B.2.13.8-28
Figure B.2.13.8-3 TN44B Basket Assembly Model SS Wrappers B.2.13.8-29
Figure B.2.13.8-4 TN44B Basket Assembly Model Borated SS Steel Plates B.2.13.8-30
Figure B.2.13.8-5 TN44B Basket Assembly R45 SS Transition Rails B.2.13.8-31
Figure B.2.13.8-6 TN44B Basket Assembly R90 Solid Aluminum Transition Rails B.2.13.8-32
Figure B.2.13.8-7 TN44B SS DSC Shell B.2.13.8-33
Figure B.2.13.8-8 TN44B Basket Assembly Thermal Stress Analysis Model B.2.13.8-34
Figure B.2.13.8-9 TN44B Basket Assembly Temperature Profile for Thermal Stress Analysis B.2.13.8-35
Figure B.2.13.8-10 TN44B Basket Assembly Accident Drop Orientations (degrees) B.2.13.8-36

APPENDIX B.2.13.8
TN44B BASKET ASSEMBLY STRUCTURAL EVALUATION

NOTE: References in this appendix are shown as [1], [2], etc., and refer to the reference list in Section B.2.13.8.3.

B.2.13.8.1 Introduction

The NUHOMS®-TN44B DSC consists of a fuel basket assembly and a DSC shell assembly (shell, DSC shell assembly inner bottom and top cover plates and shield plugs). The confinement vessel for the TN44B DSC consists of a shell which is a welded, stainless steel cylinder with a stainless steel bottom closure assembly, and a stainless steel top closure assembly. The DSC shell assembly is analyzed in Appendix B.2.13.7 and the basket assembly is analyzed in this Appendix.

The TN44B basket assembly is a welded assembly of stainless steel boxes and is designed to accommodate 44 BWR fuel assemblies. The basket assembly structure consists of an assembly of stainless steel tubes (fuel compartments), separated by poison plates and aluminum plates, and surrounded by larger stainless steel boxes and basket assembly support rails. The basket assembly contains 44 compartments for proper spacing and support of the fuel assemblies.

The basket assembly structure is open at each end and therefore, longitudinal fuel assembly loads are applied directly to the inside surface of the DSC shell assembly and not to the basket assembly structure. The fuel assemblies are laterally supported in the stainless steel structural boxes. The basket assembly is laterally supported by the basket transition rails and the DSC shell.

The basket assembly is keyed to the DSC at 180° and therefore, it's orientation with respect to the DSC always remains fixed. Under normal transport conditions, the DSC rests on two 3" wide transport support rails attached to the inside of the MP197TAD TO at 168° and 192°. Two additional 3" wide transport support rails are provided at 142° and 218°.

The basket assembly includes:

Four (4) 3 by 3 large boxes (nine compartment assembly); Each box consists of 9 stainless steel fuel compartments (3/16 in. thick.) separated by poison plates (7/16 in. thick.) and aluminum plates (3/16 in. thick.), and wrapped in a 0.105 in. thick stainless plate. Each large box also includes one 7/16 in. thick aluminum plate at one of its four sides and three poison plates (7/16 in thick) at each of the other three sides.

Four (4) 1 by 2 boxes (two compartment assembly); each box consists of 2 stainless steel fuel compartments (3/16 in. thick.) separated by poison plates (7/16 in. thick.) and aluminum plates (1/2 in. and 5/8 in.), and wrapped in a 0.105 in. thick stainless plate.

Eight (8) R45 stainless steel rails; the R45 rails are fabricated from 0.25 in. thick, SA-240, type 304 stainless steel.

Four (4) R90 solid aluminum rails; the R90 rails are fabricated from Type 6061 aluminum.

Between and on the outside of the four (4) 3 by 3 large boxes, and adjacent to the inside plates of the R45 rails, are aluminum thermal plates (1/2 in. thick).

The poison plates and aluminum plates provide the heat conduction path from the fuel assemblies to the DSC cavity wall, and also provide the necessary criticality control. The nominal open dimension of each fuel compartment cell is 6.25 in. x 6.25 in. which provides clearance around the fuel assemblies. The overall basket assembly length (176.5 in., +0.75, -0.00) is less than the DSC cavity length to allow for thermal expansion, tolerances and access to the top of the fuel assemblies.

Stainless steel and aluminum rails are oriented parallel to the axis of the DSC and attached to the periphery of the basket assembly to establish and maintain basket assembly orientation and to support the basket assembly.

Stainless steel plate inserts are placed between the stainless steel tubes and between the outer wrappers at the top and bottom of the basket assembly. These plate inserts are fillet welded to the stainless steel tubes and wrappers to prevent the poison/aluminum plates from sliding in the axial direction during initial handling (before loaded with spent fuel). Once the spent fuel is loaded and enclosed in the DSC, the inner surface of the ends of the DSC maintain the position of the basket assembly poison/aluminum plates.

B.2.13.8.2 Basket Assembly Structural Analysis

B.2.13.8.2.1 Approach

The basket assembly is evaluated for normal and accident condition impact and thermal loads. The basket assembly stress analyses are performed using a finite element method for the side drop and thermal load cases. Analytical hand calculation methods are used for the end drop load cases. Buckling analyses of the basket assembly plates when subjected to lateral impact loads are evaluated using a finite element model and ANSYS guidelines to determine the buckling load. A summary of the basket assembly load cases is provided in Section B.2.13.8.2.2. Stress and buckling analyses results are provided in Sections B.2.13.8.2.3 and B.2.13.8.2.4, respectively. For the normal side drop, not every location meets the applicable stress limits. Therefore, a limit analysis is performed to demonstrate structural stability of the basket assembly for the normal side drop.

Material Properties

The mechanical properties of structural materials used for the stainless steel basket assembly and R45 transition rail plates are shown in Table B.2.13.8-1 as a function of temperature. Similarly, properties for the aluminum R90 transition rails and the stainless steel DSC are shown in Table B.2.13.8-2 and Table B.2.13.8-3, respectively. Unless otherwise noted, the indicated references for materials properties refer to the ASME Code [3]. Borated steel properties used in the analyses are a function of the Type 304 steel properties and are analyzed at 10% and 100% of the strength of the Type 304 steel.

Design Criteria

For normal conditions, the basis for the basket assembly allowable stress is the ASME Code, Section III, Subsection NG [1]. The primary membrane stress intensity and membrane plus bending stress intensities are limited to S_m (S_m is the code allowable stress intensity) and 1.5 S_m, respectively, at any location in the basket assembly for Level A (Normal Service) load combinations.

The ASME Code provides a $3S_m$ limit on primary plus secondary stress intensity for Level A conditions. The $3S_m$ limit is specified to prevent ratcheting of a structure under cyclic loading and to provide controlled linear strain cycling in the structure so that a valid fatigue analysis can be performed.

For accident conditions, stresses are evaluated as short duration Level D conditions as per ASME B&PV Code, Section III, Appendix F [2]. When evaluating the results from the non-linear elastic-plastic analyses, the general primary membrane stress intensity, P_m, shall not exceed the greater of $0.7S_u$ or $S_y + 1/3\ (S_u - S_y)$ and the maximum membrane plus bending stress intensity at any location (P_l or $P_m + P_b$) shall not exceed $0.9\ S_u$. The average shear stress is limited to $0.42\ S_u$.

The allowable stresses (stress intensities) used for both normal and accident conditions are summarized in Table B.2.13.8-4 for the stainless steel components of the basket assembly. Stress limits for the borated steel plates are taken as the same as Type 304 steel for borated steel with strength properties at 100% of those for Type 304. For borated steel with strength properties assumed to be only 10% of those for Type 304 steel, stresses are not evaluated (included for effect only).

The solid aluminum transition rails perform their function by remaining in place. Therefore, for normal and accident condition drop loads (i.e. postulated drops), the rail bodies support the fuel compartment tube structure such that stresses and displacements in the compartment tube structure are acceptable. Since the solid aluminum rails are entrapped between the fuel compartment tube structure and the DSC shell assembly, no additional checks of the aluminum are required for drop loadings. Qualification of the fuel grid demonstrates that the rails perform their intended function.

For evaluation of normal conditions, in accordance with NG-3222 and Note 9 of Figure NG-3221-1, the Limit Analysis provisions of NG-3228 may be used in lieu of satisfying primary stress limits.

B.2.13.8.2.2 Loading Conditions

The basket structure is analyzed for 0°, 30°, 45° and 180° azimuth side drops. Due to the basket structure symmetry, these orientations of side drops are considered to envelop all other possible drop orientations. Tables B.2.13.8-5 and -6 list the normal and accident loading conditions.

A fuel assembly weight of 705 lb. is used in the analyses. A uniform fuel weight distribution is assumed over the active fuel length (144 in.) of the basket. The weight of the unmodelled

aluminum is accounted for by increasing the material density of the adjacent stainless steel plates. The stiffness of the un-modeled aluminum is conservatively neglected in the analyses.

The load resulting from the fuel assembly weight is applied as pressure on the fuel compartment plates of the basket. For the 0° and 180° orientation, the pressure acts only on the horizontal plates. For the 30° and 45° orientation, the pressure was divided into components that act on both horizontal and vertical plates of the basket. The pressures for all orientations are calculated below for 1g accelerations.

- At 0° and 180° degrees; Pressure, p = Fuel assembly wt. / (Panel span x Panel length)
  = 705 lb / (6.25" x 144") = 0.7833 psi
- At 30°; p_v on horizontal plates = p Cos 30^o = 0.7833 x 0.866 = 0.6783 psi
  p_h on vertical plates = p Sin 30^o = 0.7833 x 0.5 = 0.3917 psi
- At 45°; p_v on horizontal plates = p Sin 45^o = 0.7833 x 0.7071 = 0.5539 psi
  p_h on vertical plates = p Cos 45^o = 0.7833 x 0.7071 = 0.5539 psi

For all loadings, the above pressure values are multiplied by the g-load used.

The baseline accelerations for NCT and HAC drop conditions are provided in Appendix B.2.13.12. For the quasi-static static analyses the baseline g-loads are multiplied by a dynamic load factor calculated in Appendix B.2.13.9. These calculated maximum g-loads are further increased for conservatism in the analyses. The maximum g-loads used are summarized in the following table:

TN44B Basket Assembly Maximum Accelerations

Drop Condition	Appendix B.2.13.12 Baseline Acc. (g)	Appendix B.2.13.9 DLFs	Required Acceleration (g)	Analysis Acceleration (g)
Normal 1' Side Drop	18	1.05	18.9	20
Normal 1' End Drop	32	1.06	33.92	40
Accident 30' Side Drop	59	1.03	60.77	75
Accident 30' End Drop	51	1.19	60.69	75

Each normal condition side drop load case is combined with the bounding hot environment thermal load case. The thermal load case evaluated is for a bounding temperature distribution to maximize thermal stresses (see Section B.2.13.8.2.3(D)) due to thermal conditions described in Appendix B.3.

B.2.13.8.2.3 Basket Assembly Stress Analysis

A. Finite Element Model Description

A three-dimensional ANSYS [4] finite element model of the basket assembly, rails and DSC shell is constructed using SHELL43 elements. The overall finite element model of the basket assembly, rails and DSC shell is shown in Figure B.2.13.8-1. Contact elements and soft springs (used for analysis convergence problems only) are not shown for clarity. Analyses are performed where the borated steel material properties used are 10% and 100% of those for Type 304 steel. The weight of the aluminum plates is accounted for by increasing the densities of the adjacent basket assembly plates. Because of the large number of plates in the basket assembly and length of the basket assembly, certain modeling approximations are necessary. Because the rails provide continuous support along the entire length of the basket assembly during a side drop, only a 1 inch long slice of the basket assembly, rail and DSC shell is modeled. At the two cut faces of the model, symmetry boundary conditions are applied (UZ = ROTX = ROTY = 0). The fuel compartment tubes, the stainless steel wrappers, the borated steel plates, the basket assembly rails, and the DSC shell are explicitly included in the model and are shown individually in Figures B.2.13.8-2 through B.2.13.8-7.

The connections between the stainless steel fuel compartments (with intermediate aluminum poison plates) and the outer stainless steel wraps, and between the outer wraps and the stainless steel rails, are primarily made with ANSYS CONTAC52 contact elements (without friction) at every interface. Initial gaps are set to zero so plates will bend together, as appropriate, when loaded together in the normal direction. Using contact elements also allows the elements to separate, as needed, when the loading or internal moments are such that separation may indeed occur. For convergence purposes, soft springs (5 to 10 lb/in) are modeled between adjacent plates, but only near the ends and corners of the plates (not across plate span lengths).

The DSC shell assembly is resting on four sliding rails inside the MP197TAD TO (0.12" thick continuous pad) at approximately 12^{o} and 38^{o} on either side of DSC shell assembly. The basket assembly and DSC shell are analyzed for multiple side drop scenarios. Gaps between the basket assembly periphery and DSC shell, and between the DSC shell and the MP197TAD TO, are modeled using ANSYS CONTAC52 elements. Initial gaps are based on a basket assembly outside diameter of 64.25", a DSC shell inside diameter of 64.75", a DSC shell outside diameter of 66.25", a MP197TAD TO inside diameter of 67", and the side drop orientation.

Contact Element Nonlinearities

Contact elements (CONTAC52) are used to model the actual surface clearance between the basket assembly transition rails and the inside surface of the DSC shell as well as between the outer surface of the DSC shell and the inside surface of the MP197TAD TO. The gap elements also introduce nonlinearities into the model, because the reaction force generated by the gap elements depends on their status (open or closed). The gap element spring constant, K_n, is calculated in the following way.

$$K_n = f E h \quad [4]$$

Where f is a factor usually between 0.01 and 100, E is the material modulus of elasticity (24.8×10^6 psi), and h is a typical "target length" parameter (square root of element contact area).

For a typical element size, where the tributary element contact area is based on approximately 0.5 in. by 0.5 in., the typical "target length" = $(0.5 \times 0.5)^{0.5} = 0.5$ in. Therefore,

$$K_n = 24.8\times10^6 \times 0.5 \times f = 1.24\times10^5 \text{ to } 1.24\times10^9 \text{ lb./in.}$$

In view of the large range in spring constant values, various spring constants were evaluated and used. Some adjustments in initial values were needed to achieve convergence. The range of values ultimately used is from 1E6 lb./in. to 1E8 lb./in. and fall within the range identified above.

B. Normal Condition Side Drop Stress Analysis

A nonlinear stress analysis of the basket assembly structure is conducted in order to compute the elastic stresses for the 180° drop orientation. For the normal 1 ft. drop, other orientations of drops are not possible without developing an accident scenario. Drops away from the rails cannot occur for the normal 1 ft. drop scenario and therefore, are covered by the accident drop conditions. The nonlinearity of analysis is due to the gaps in the model. The load resulting from the fuel assembly weight is applied as pressure load on the fuel compartment plates. At the 180° drop orientation, the pressure acts only on the horizontal plates. The inertia load due to the basket assembly plates, basket assembly support rails and DSC shell dead weight is simulated using the density and appropriate acceleration. The weights of the aluminum plates are included by increasing the adjacent basket assembly plate densities. Analyses are performed where borated steel properties used in the analyses are a function of the Type 304 steel properties, where values for 10% and 100% of the strength of the Type 304 steel are used. A maximum load of 20g is applied in each analysis. The automatic time stepping program option AUTOTS is activated. This option lets the program decide the actual size of the load-substep for a converged solution. The program stops at the load substep when it fails to result in a converged solution. In all side drop runs, ANSYS gave converged solutions up to the 20g applied load.

The maximum nodal basket assembly stress intensities for the two bounding normal drop analyses are listed in Table B.2.13.8-7 (Borated Steel @ 100% of Type 304) and Table B.2.13.8-8 (Borated Steel @ 10% of Type 304). For shell elements, the linearized middle fiber stresses are classified as membrane stresses (P_m) and the linearized top and bottom fiber stresses are classified as membrane plus bending stresses ($P_m + P_b$). Since stresses exceed the normal allowable stress values, a limit analysis per NB-3228.1 was performed at 45g to demonstrate that 20g loading does not exceed 2/3 of the lower bound collapse load. For all cases, the 45g load analyses ran to completion with no indication of collapse or significant strains.

The maximum primary stress intensities associated with the 20g analyses are combined with the maximum thermal stresses calculated in Subsection D of this section and compared with the code allowable stresses (also shown in Table B.2.13.8-7).

C. Normal Condition End Drop Stress Analysis

During an end drop, the fuel assemblies and fuel compartment are forced against the end of the DSC shell assembly. It is important to note that, for any vertical or near vertical loading, the fuel assemblies react directly against the bottom or top end of the DSC shell assembly and not

through the basket assembly structure as in lateral loading. It is the dead weight of the basket assembly only that causes axial compressive stress during an end drop. Axial compressive stresses are conservatively computed assuming that all of the basket assembly weight will be taken by the fuel compartments, stainless steel outer wrappers and stainless steel R45 transition rails only. A conservative basket assembly weight of 42,150 lb. (actual weight is less than 42,000 lb) is used in end drop stress calculations with a normal end drop acceleration of 40g.

Compressive Stress in the Fuel Compartment Tubes, Outer Wrappers, and R45 Basket Assembly Rails

$\sigma_{Axial\text{-}40g} = 75 (W_{basket}) / A_S$

$W_{basket} = 42.15$ kips (conservative compared to actual weight)

Section Area, $A_S = 1000 (W_{LB\text{-}basket} - W_{BS\_plates} - W_{Al\_plates} - W_{Al\_rails}) / (L_{basket}\ \rho)$

$W_{LB\_basket} = 41.00$ kips (lower bound basket weight, conservative for A_S)

$W_{BS\_plates} = 16.57$ kips

$W_{Al\_plates} = 4.99$ kips

$W_{Al\_rails} = 1.71$ kips

$L_{basket} = 176.5$ in

$\rho = 0.29$ lb/in^3

$A_S = 1000 (41.00 - 16.57 - 4.99 - 1.71) / (176.5 (0.29))$

$= 346.0$ in^2

Therefore,

$\sigma_{Axial\text{-}40g} = 40 (42.15) / 346.00$

$= 4.87$ ksi < 15.8 ksi (allowable membrane stress)

D. Thermal Stress Analysis

A conservative thermal stress analysis of the basket assembly is performed based on the thermal heat transfer analysis results. A conservative radial and axial gradient temperature profile is imposed on the basket assembly to bound the effects of the actual thermal gradients. A model similar to the 20g side drop analysis model is used except that the model is extended to a length of approximately one-half the length of the basket assembly. The thermal stress analysis model is shown in Figure B.2.13.8-8. A temperature plot on a one-quarter cross-section of the basket assembly model is shown in Figure B.2.13.8-9.

The DSC shell and MP197TAD TO boundaries (and associated gap/contact elements) are removed because they do not contribute to the solution and significantly increase the solution time. Although, the basket insert plate welds are not credited in the analyses for the basket, local failure at these welds cannot be guaranteed and the imposed restraint at these locations increase the thermal stresses at the center of the basket assembly where the maximum side drop and

thermal stresses coexist. Therefore, a bounding thermal case is evaluated, where the insert plate welds restrain the internal thermal growth of the basket assembly. A summary of the resulting thermal stresses are shown in Table B.2.13.8-9.

E. Summary of Normal Condition Basket Assembly Stress Analysis

Tables B.2.13.8-7 and B.2.13.8-8 summarize the normal condition basket assembly stress analysis results and allowable stresses for the combination of normal side drop and thermal loads. The allowable stress values for the basket assembly components are taken at 700 °F. The basis for the allowable stress values are provided in Note 2 of the stress summary tables. Since stresses exceed the normal allowable stress values, limit analyses per NG-3228.2 were performed at 45g to demonstrate that 20g loading does not exceed 2/3 of the lower bound collapse load. The value of yield for these analyses was taken to be 1.5 S_m for the stainless steel components, and S_y for the R90 solid aluminum transition rails. For all cases, the 45g load analyses ran to completion with no indication of collapse or significant strains.

F. Accident Condition Side Drop Stress Analysis and Results

Loading Conditions

The basket assembly is analyzed for two types of side drops using the ANSYS finite element model described in Section B.2.13.8.2.3A. First, the DSC is assumed to drop away from the MP197TAD TO sliding rails. Under this condition, 45°, 60°, and 90° orientation side drops are considered, because they bound all possible orientations. Second, the DSC is assumed to drop directly on the MP197TAD TO sliding rails at 180° orientation. The lateral load orientation angle is defined in Figure B.2.13.8-10. The load resulting from the fuel assembly weight was applied as a pressure load on the fuel compartment plates. For the 90° and 180° orientations, the pressure was applied only on the horizontal plates, while in other orientations; it was divided into components acting on both the horizontal and vertical plates.

The inertia load due to the basket assembly, rails, and DSC shell dead weight is model by using the appropriate material densities and by applying the appropriate acceleration. As discussed in the section of this Appendix for the normal 1 ft. drop, unmodeled aluminum is accounted for by increasing the adjacent basket assembly plate densities.

Material Properties

The basket assembly fuel compartments and R45 transition rails are constructed from SA-240, Type 304 stainless steel. The R90 transition rails are constructed from ASME aluminum Type 6061. The DSC shell is constructed from SA-240 Type 316/316L stainless steel. A bilinear stress-strain relationship is used to simulate the correct nonlinear material behavior for the short term during dynamic loading from the 30 foot side drop impact. The following elastic and inelastic material properties are used in the analyses:

SA-240, 304 Stainless Steel at 700 °F [3]*	
Modulus of Elasticity, E (psi)	24.8×10^6
Yield Strength (psi)	17,600
Tangent Modulus, E_t (psi)	5% of $E = 1.24 \times 10^6$

* For the borated stainless steel plates, 2 cases are analyzed: one with 100% of these values and one with 10% of these values.

ASME Aluminum Type 6061 at 600 °F [12]	
Modulus of Elasticity, E (psi)	6.8×10^6
Yield Strength (psi)	4,200
Tangent Modulus, E_t (psi)	1% of $E = 68 \times 10^4$

SA-240, 316/316L Stainless Steel at 500 °F [3]	
Modulus of Elasticity, E (psi)	25.9×10^6
Yield Strength (psi)	20,000
Tangent Modulus, E_t (psi)	5% of $E = 1.295 \times 10^6$

The material properties used in the analyses are based on basket assembly plate components at 700°F, R90 solid aluminum transition rails at 600°F, and the DSC shell at 500°F.

Analysis and Results

A nonlinear stress analysis of the fuel basket assembly is conducted to compute the stresses for the 45°, 60°, 90°, and 180° drop orientations. A maximum load of 150g was applied in each analysis. The automatic time stepping program option "Autots" was activated. This option lets the program decide the actual size of the load-substep for a converged solution. Displacements, stresses and forces for each converged substep load were written on ANSYS result files. The program stops at the load substep when it fails to result in a converged solution. In all side drop cases the program gave converged solutions beyond a 75g load. Results were extracted at the 75g load step. Maximum nodal stress intensities in the basket assembly and rails and comparisons to allowable stress values are summarized in Table B.2.13.8-10 through Table B.2.13.8-13. The results show that all stresses are less than the allowable stress values.

G. Accident Condition End Drop Stress Analysis

During an end drop, the fuel assemblies and fuel compartment are forced against the end of the DSC shell assembly. It is important to note that, for any vertical or near vertical loading, the fuel assemblies react directly against the bottom or top end of the DSC shell assembly and not through the basket assembly structure as in lateral loading. It is the dead weight of the basket assembly only that causes axial compressive stress during an end drop. Axial compressive stresses are conservatively computed assuming that all of the basket assembly weight will be taken by the fuel compartments and outer wrappers only. A conservative basket assembly weight of 42,150 lb. (actual weight is less than 42,000 lb) is used in end drop stress calculations with an accident end drop acceleration of 75g.

Compressive Stress in the Fuel Compartment Tubes, Wrappers

$\sigma_{Axial\text{-}75g} = 75 (W_{basket}) / A_S$

W_{basket} = 42.15 kips (conservative compared to actual weight)

$A_S = 346.0 \text{ in}^2$ (from before)

Therefore,

$\sigma_{Axial\text{-}75g} = 75 (42.15) / 346.00$

$= 9.14 \text{ ksi} < 44{,}380 \text{ psi}$ (allowable membrane stress)

B.2.13.8.2.4 Fuel Basket Assembly Buckling Analysis

A. Basket Fuel Compartment Plate and R45 Transition Rail Buckling Analyses

Basket assembly stability, which includes a buckling evaluation of the basket fuel compartment plates and R45 transition rails at the most highly loaded locations for the most challenging drop orientation is determined in this subsection. Fuel compartment stability and R45 transition rail stability is demonstrated by performing a buckling evaluation using an ANSYS finite element analysis approach, including ANSYS guidelines for a buckling analysis.

Basket Assembly Stability Demonstration Using Finite Element Analysis

The same models and analyses performed in Section B.2.13.8.2.3 are used to evaluate the basket plate and R45 transition rail stability when the lateral inertial loading is applied at various angles relative to the plates. Analyses are performed for the same drop orientations described in Section B.2.13.8.2.3 and shown in Figure B.2.13.8-10.

ANSYS Finite Element Analysis Results

For each orientation, the analysis is solved with increasingly higher loading until convergence can no longer be obtained from the FEA model. The limiting buckling results are summarized in Table B.2.13.8-14.

B. Summary of Basket Assembly Buckling Analysis

Table B.2.13.8-14 shows that the limiting drop is a drop away from the rails at an orientation of 45 degrees for cases where the borated steel is at 100% of the strength of the stainless steel. For cases where the borated steel is at 10% of the strength of the stainless steel, the limiting drop is on the rails.

The results of the basket assembly buckling analysis indicate the allowable buckling *g* loads for the TN44 B basket assembly are higher than the applied 75g side drop impact load. Therefore, the basket assembly and rails are structurally adequate with respect to buckling.

B.2.13.8.2.5 Basket Deformations for Effect on Criticality Analyses

To evaluate the effect of basket deformation on the criticality analysis in Chapter B.6, it is necessary to know the relative total deformations of the basket. For this purpose, the maximum relative deflections in the critical fuel compartments during HAC side drops are calculated. The maximum relative deflections of all the fuel compartments are shown below:

Condition	Drop Orientation	Maximum Absolute Relative Displacement (in)[1]	
		Δ_{UX}	Δ_{UY}
Accident Side Drops with 10% Borated Steel	180° on Cask Rails	0.002864	0.039552
	0° away from Cask Rails	0.001234	0.033990
	30° away from Cask Rails	0.015502	0.024395
	45° away from Cask Rails	0.024879	0.020486
Accident Side Drops with 100% Borated Steel	180° on Cask Rails	0.000818	0.013631
	0° away from Cask Rails	0.000000	0.013846
	30° away from Cask Rails	0.007922	0.012859
	45° away from Cask Rails	0.012016	0.011677

Notes:

1. For displacements that indicate fuel compartments have moved closer together. Obtained from results for the 75g load step.

The criticality analyses (Section B.6.3.4.2) assume that the worst location for all of the fuel assemblies in the TN44B basket are when they are all positioned closest to each other relative to the center of the basket; thus any deformation which will cause the fuel assemblies to move further apart is covered by the criticality analysis. Therefore, for the TN44B basket, the relative deformation of the basket is calculated for the fuel compartments which will cause the fuel to move closer together. The maximum relative deformation (elastic plus plastic) of the fuel compartments which will cause the fuel assemblies to move closer together is less than 0.04 in.

The criticality evaluation documented in Chapter B.6, Section B.6.3.4.2 utilizes a minimum compartment size that results in fuel assemblies moving closer to each other by 0.05 in. Therefore, the bounding displacements determined herein are covered by the criticality analysis.

B.2.13.8.3 References

1. American Society of Mechanical Engineers, ASME Boiler and Pressure Vessel Code, Section III, Subsection NG and Appendix F, 2004 Edition.

2. American Society of Mechanical Engineers, ASME Boiler and Pressure Vessel Code, Section III, Appendix F, 2004 Edition.

3. American Society of Mechanical Engineers, ASME Boiler and Pressure Vessel Code, Section II, Part D, 2004 Edition.

4. ANSYS Engineering Analysis System, User's Manual for ANSYS Rev. 10.0.

5. Not used.

6. Not used.

7. Not used.

8. Not used.

9. Baumeister & Marks, *Standard Handbook for Mechanical Engineers*, 7th Edition.

10. American Society of Mechanical Engineers, ASME Boiler and Pressure Vessel Code, Section III, Subsection NB, 2004 Edition.

11. Not used.

12. Kaufman, J.G., ed., "Properties of Aluminum Alloys: Tensile, Creep, and Fatigue Data and High and Low Temperatures", The Aluminum Association (Washington, D.C.) and ASM International (Metals Park, Ohio), 1999.

Table B.2.13.8-1
Materials Properties – SA-240/SA-479 304 & SA-182 F304

Temp (°F)	E (10^3 ksi)	S_m (ksi)	S_y (ksi)	S_u (ksi)	α_{INST} (10^{-6} °F^{-1})	α_{AVG} (10^{-6} °F^{-1})	ρ (lb/in^3)
-20		20.0	30.0	75.0			
70	28.3				8.5	8.5	
100		20.0	30.0	75.0	8.7	8.6	
150			26.7		9.0	8.8	
200	27.5	20.0	25.0	71.0	9.3	8.9	
250			23.6		9.6	9.1	
300	27.0	20.0	22.4	66.2	9.8	9.2	
350					10.0	9.4	
400	26.4	18.6	20.7	64.0	10.2	9.5	
450					10.3	9.6	
500	25.9	17.5	19.4	63.4	10.5	9.7	0.290
550					10.6	9.8	
600	25.3	16.6	18.4	63.4	10.6	9.8	
650		16.2	18.0	63.4	10.7	9.9	
700	24.8	15.8	17.6	63.4	10.8	10.0	
750		15.5	17.2	63.3	10.8	10.0	
800	24.1	15.2	16.9	62.8	10.9	10.1	
850			16.5	62.0	11.0	10.2	
900	23.5		16.2	60.8	11.2	10.2	
950			15.9	59.3	11.3	10.3	
1000	22.8		15.5	57.4	11.4	10.3	
SA-240 304	Table TM-1 pg 696 group G	Table 2A pg 316 line 3	Table Y-1 pg 566 line 27	Table U pg 458 line 23	Table TE-1 pg 669 group 3		AISC
SA-479 304	Table TM-1 pg 696 group G	Table 2A pg 316 line 17	Table Y-1 pg 570 line 3	Table U pg 458 line 40			
SA-182 F304	Table TM-1 pg 696 group G	Table 2A pg 312 line 31	Table Y-1 pg 566 line 10	Table U[1] 458 line 17			

Note:
1. All forgings shall have rough thickness ≤ 5.00" or minimum tensile strength (S_u) shall be 75.0 ksi.

Table B.2.13.8-2
Analysis Properties for Aluminum Transition Rails [12]

6061-O Aluminum (Annealed)

Temperature (°F)	S_u, 6061-O (ksi)	S_y, 6061-O (ksi)	E (ksi)
75	18.0	8.0	9,900
212	18.0	8.0	9,500
300	15.0	8.0	9,100
350	12.0	8.0	8,900
400	10.0	7.5	8,600
450	8.5	6.0	8,300
500	7.0	5.5	7,900
600	5.0	4.2	6,800
700	3.6	3.0	5,500
800	2.8	2.2	--
900	2.2	1.6	--
1000	1.6	1.2	--

Table B.2.13.8-3
Materials Properties – SA-240 Type 316/316L & SA-182 F316/316L

Temp (°F)	E (10^3 ksi)	S_m (ksi)	S_y (ksi)	S_u (ksi)	α_{INST} (10^{-6} °F^{-1})	α_{AVG} (10^{-6} °F^{-1})	ρ (lb/in^3)
-20		20.0	30.0	75.0			0.285
70	28.3				8.5	8.5	
100		20.0	30.0	75.0	8.7	8.6	
150					9.0	8.8	
200	27.6	20.0	25.9	75.0	9.3	8.9	
250					9.6	9.1	
300	27.0	20.0	23.4	72.9	9.8	9.2	
350					10.0	9.4	
400	26.4	19.3	21.4	71.9	10.2	9.5	
450					10.3	9.6	
500	25.9	18.0	20.0	71.8	10.5	9.7	
550					10.6	9.8	
600	25.3	17.0	18.9	71.8	10.6	9.8	
650		16.6	18.5	71.8	10.7	9.9	
700	24.8	16.3	18.2	71.8	10.8	10.0	
750		16.1	17.9	71.5	10.8	10.0	
800	24.1	15.9	17.7	70.8	10.9	10.1	
850							
900							
950							
1000							
SA-240 316[1]	Table TM-1 Page 696 Group G	Table 2A Page 304 Line 13	Table Y-1 Page 558 Line 5	Table U Page 453.1 Line 7	Table TE-1 Group 3 Page 669		AISC
SA-182 F316[1]	Table TM-1 Page 696 Group G	Table 2A Page 304 Line 11	Table Y-1 Page 558 Line 2	Table U Page 453.1 Line 4			

Note:
1. Material will be dual certified to meet requirements of both Type 316 and 316L. Material properties based on Type 316.

Table B.2.13.8-4
Basket Plate and R45 Support Rail Allowable Stress Values

Loading Condition	Stress Category	Stress Criteria [1]	Basket Plate Allowable Stress At 700 °F (ksi.)	Support Rail Allowable Stress At 700 °F (ksi.)
Normal Conditions, Elastic Analysis(1)	Membrane Stress, P_m	S_m	15.08	15.8
	Membrane + Bending Stress, $P_m + P_b$	1.5 S_m	23.70	23.7
	Average Shear Stress	0.6 S_m	9.48	9.48
	Primary + Secondary Stress, $P_m + P_b + Q$	3 S_m	47.40	47.4
Accident Conditions, Elastic-Plastic Analysis	Membrane Stress, P_m	0.7 S_u	44.40	44.4
	Membrane + Bending Stress, $P_m + P_b$	0.9 S_u	57.10	57.1
	Average Shear Stress	0.42 S_u	26.63	26.63

Note:
1. In accordance with NG-3222 and Note 9 of Figure NG-3221-1, the Limit Analysis provisions of NG-3228 may be used.

Table B.2.13.8-5
Basket Assembly Normal Condition Loads

Loading	Basket Orientation	Service Level	Load	Analysis Method
Thermal Load	Horizontal	A	100 °F Ambient	Finite Element Analysis
1 Foot Side Drop	Horizontal	A	20g Lateral Load	Finite Element Analysis
1 Foot End Drop	Vertical	A	40*g* Axial Load	Analytical Hand Calculation

Table B.2.13.8-6
Basket Assembly Accident Condition Loads

Loading	Basket Orientation	Service Level	Load	Analysis Method
30 Foot Side Drop	Horizontal	D	75*g* Lateral Load	Finite Element Analysis
30 Foot End Drop	Vertical	D	75*g* Axial Load	Analytical Hand Calculation

Table B.2.13.8-7
20g Side Drop + Thermal (hot)

(Borated Steel @ 100% of Type 304)

Basket Component	Material	Stress Category	Stress (ksi) [1]	
			Calculated	Allowable[2]
Fuel Compartments	ASME SA-240 Type 304	Primary Membrane	2.83	15.8
		Membrane + Bending	18.43	23.7
		Primary + Secondary	31.42	47.4
SS Wrappers (1 x 2 boxes)	ASME SA-240 Type 304	Primary Membrane	3.65	15.8
		Membrane + Bending	34.27[4]	23.7
		Primary + Secondary	47.72[5]	49.8
SS Wrappers (3 x 3 boxes)	ASME SA-240 Type 304	Primary Membrane	3.19	15.8
		Membrane + Bending	23.49	23.7
		Primary + Secondary	49.31[5]	49.8
Borated SS Plates	ASTM A887 Type 304B4	Primary Membrane	1.57	15.8
		Membrane + Bending	12.69	23.7
		Primary + Secondary	29.37	47.4
R45 SS Transition Rails	ASME SA-240 Type 304	Primary Membrane	5.46	15.8
		Membrane + Bending	23.38	23.7
		Primary + Secondary	38.56	47.4
DSC Shell[6]	Type 316/316L	Primary Membrane	4.34	N/A
		Membrane + Bending	36.05	N/A
		Primary + Secondary	36.05	N/A

Notes:
1. All stresses are stress intensities and are based on elastic analysis.
2. Allowable stresses are conservatively based on basket plate components and SS transition rails at 700°F, and the DSC shell at 500°F, unless noted otherwise.
3. Drop is on MP197TAD TO rails located at +/-12 degrees and +/-38 degrees from the reference angle of 180 degrees.
4. Stress exceeds allowable. Therefore, Limit Analyses are performed per ASME NG-3228.2 at 45g to demonstrate that 20g loading does not exceed 2/3 of the lower bound collapse load.
5. Maximum combined stresses occur at locations where the temperature is less than 600 °F. Therefore, the allowable is based on 600 °F.
6. DSC shell stresses are the result of basket assembly stress analysis at the axial center of the DSC shell assembly, do not include pressure and/or thermal stresses, and are evaluated in Appendix B.2.13.7.

Table B.2.13.8-8
20g Side Drop + Thermal (hot)
(Borated Steel @ 10% of Type 304)

Basket Component	Material	Stress Category	Stress (ksi) [1]	
			Calculated	Allowable[2]
Fuel Compartments	ASME SA-240 Type 304	Primary Membrane	3.21	15.8
		Membrane + Bending	13.88	23.7
		Primary + Secondary	26.87	47.4
SS Wrappers (1 x 2 boxes)	ASME SA-240 Type 304	Primary Membrane	2.91	15.8
		Membrane + Bending	28.01[4]	23.7
		Primary + Secondary	47.72[5]	49.8
SS Wrappers (3 x 3 boxes)	ASME SA-240 Type 304	Primary Membrane	2.91	15.8
		Membrane + Bending	28.01[4]	23.7
		Primary + Secondary	49.31[5]	49.8
R45 SS Transition Rails	ASME SA-240 Type 304	Primary Membrane	5.76	15.8
		Membrane + Bending	22.77	23.7
		Primary + Secondary	37.95	47.4
DSC Shell[6]	Type 316/316L	Primary Membrane	3.92	N/A
		Membrane + Bending	36.49	N/A
		Primary + Secondary	36.49	N/A

Notes:
1. All stresses are stress intensities and are based on elastic analysis. Borated stainless steel plate stresses are not shown because minimal credit is taken for the strength of the borated stainless steel and are modeled for effect only.
2. Allowable stresses are conservatively based on basket plate components and SS transition rails at 700°F, and the DSC shell at 500°F, unless noted otherwise.
3. Drop is on MP197TAD TO rails located at +/-12 degrees and +/-38 degrees from the reference angle of 180 degrees.
4. Stress exceeds allowable. Therefore, Limit Load Analyses are performed per ASME NG-3228.2 at 45g to demonstrate that 20g loading does not exceed 2/3 of the lower bound collapse load.
5. Maximum combined stresses occur at locations where the temperature is less than 600 °F. Therefore, the allowable is based on 600 °F. Stresses are conservatively based on 100% borated steel strength.
6. DSC shell stresses are the result of basket assembly stress analysis at the axial center of the DSC shell assembly, do not include pressure and/or thermal stresses, and are evaluated in Appendix B.2.13.7.

Table B.2.13.8-9
Thermal Stress Analysis Results (hot)
(Borated Steel @ 100% of Type 304)

Basket Component	Material	Stress Category	Stress (ksi) [1]
Fuel Compartments	ASME SA-240 Type 304	Q	12.99
SS Wrappers (1 x 2 boxes)	ASME SA-240 Type 304	Q	13.45
SS Wrappers (3 x 3 boxes)	ASME SA-240 Type 304	Q	25.82
Borated SS Plates	ASTM A887 Type 304B4	Q	16.68
R45 SS Transition Rails	ASME SA-240 Type 304	Q	15.18

Notes:
1. All stresses are stress intensities and are based on elastic analysis. Stresses for the case where borated steel is 10% strength are not limiting.

Table B.2.13.8-10
75g, 180 Deg. Side Drop on Rails

(Borated Steel @ 100% of Type 304)

Basket Component	Material	Stress Category	Stress (ksi) [1]	
			Calculated	Allowable[2]
Fuel Compartments	ASME SA-240 Type 304	Primary Membrane	12.83	44.40
		Membrane + Bending	21.77	57.10
SS Wrappers	ASME SA-240 Type 304	Primary Membrane	8.51	44.40
		Membrane + Bending	26.07	57.10
Borated SS Plates	ASTM A887 Type 304B4	Primary Membrane	6.54	44.40
		Membrane + Bending	25.10	57.10
R45 SS Transition Rails	ASME SA-240 Type 304	Primary Membrane	19.15	44.40
		Membrane + Bending	26.08	57.10
DSC Shell	Type 316/316L	Primary Membrane	5.55	50.3
		Membrane + Bending	32.19	64.6

Notes:
1. All stresses are stress intensities and are based on elastic-plastic analysis.
2. Allowable stresses are conservatively based on basket plate components and SS transition rails at 700°F, and the DSC shell at 500°F, unless noted otherwise.

Table B.2.13.8-11
75g, 180 Deg. Side Drop on Rails

(Borated Steel @ 10% of Type 304)

Basket Component	Material	Stress Category	Stress (ksi) [1]	
			Calculated	Allowable[2]
Fuel Compartments	ASME SA-240 Type 304	Primary Membrane	17.76	44.40
		Membrane + Bending	25.02	57.10
SS Wrappers	ASME SA-240 Type 304	Primary Membrane	8.43	44.40
		Membrane + Bending	28.45	57.10
R45 SS Transition Rails	ASME SA-240 Type 304	Primary Membrane	21.39	44.40
		Membrane + Bending	38.08	57.10
DSC Shell	Type 316/316L	Primary Membrane	5.79	50.30
		Membrane + Bending	29.73	64.60

Notes:
1. All stresses are stress intensities and are based on elastic-plastic analysis. Borated stainless plate stresses are not shown because minimal credit is taken for the strength of the borated stainless steel and are modeled for effect only.
2. Allowable stresses are conservatively based on basket plate components and SS transition rails at 700°F, and the DSC shell at 500°F, unless noted otherwise.

Table B.2.13.8-12
75g, Envelope of Side Drop away from Rails
(Borated Steel @ 100% of Type 304)

Basket Component[3]	Material	Stress Category	Stress (ksi) [1]	
			Calculated	Allowable[2]
Fuel Compartments	ASME SA-240 Type 304	Primary Membrane	11.78	44.40
		Membrane + Bending	27.47	57.10
SS Wrappers	ASME SA-240 Type 304	Primary Membrane	9.67	44.40
		Membrane + Bending	29.70	57.10
Borated SS Plates	ASTM A887 Type 304B4	Primary Membrane	4.68	44.40
		Membrane + Bending	19.84	57.10
R45 SS Transition Rails	ASME SA-240 Type 304	Primary Membrane	21.45	44.40
		Membrane + Bending	33.68	57.10
DSC Shell	Type 316/316L	Primary Membrane	2.60	50.30
		Membrane + Bending	24.59	64.60

Notes:
1. All stresses are stress intensities and are based on elastic-plastic analysis.
2. Allowable stresses are conservatively based on basket plate components and SS transition rails at 700°F, and the DSC shell at 500°F, unless noted otherwise.
3. Drop is away from MP197TAD TO rails. Results envelope the 45 deg., 60 deg., and 90 deg. drop orientations.

Table B.2.13.8-13
75g, Envelope of Side Drop away from Rails
(Borated Steel @ 10% of Type 304)

Basket Component[3]	Material	Stress Category	Stress (ksi) [1]	
			Calculated	Allowable[2]
Fuel Compartments	ASME SA-240 Type 304	Primary Membrane	12.98	44.40
		Membrane + Bending	28.06	57.10
SS Wrappers	ASME SA-240 Type 304	Primary Membrane	11.58	44.40
		Membrane + Bending	30.51	57.10
R45 SS Transition Rails	ASME SA-240 Type 304	Primary Membrane	21.84	44.40
		Membrane + Bending	35.79	57.10
DSC Shell	Type 316/316L	Primary Membrane	2.59	50.30
		Membrane + Bending	24.62	64.60

Notes:
1. All stresses are stress intensities and are based on elastic-plastic analysis. Borated stainless steel plate stresses are not shown because minimal credit is taken for the strength of the borated stainless steel and are modeled for effect only.
2. Allowable stresses are conservatively based on basket plate components and SS transition rails at 700°F, and the DSC shell at 500°F, unless noted otherwise.
3. Drop is away from MP197TAD TO rails. Results envelope the 45 deg., 60 deg., and 90 deg. drop orientations.

Table B.2.13.8-14
TN44B Basket Assembly HAC Buckling Load Summary

Drop Direction	Borated Steel @ XX% of Type 304	Buckling Load[1] (g)
180-deg. Drop[2]	100	149.7
45-deg. Drop	100	115.0
60-deg. Drop	100	132.5
90-deg. Drop	100	139.6
180-deg. Drop[2]	10	85.1
45-deg. Drop	10	90.8
60-deg. Drop	10	88.7
90-deg. Drop	10	88.5

Notes:
1. HAC g-load associated with last converged load step.
2. Drop is on MP197TAD TO rails located at +/-12 degrees from the reference angle of 180 degrees.

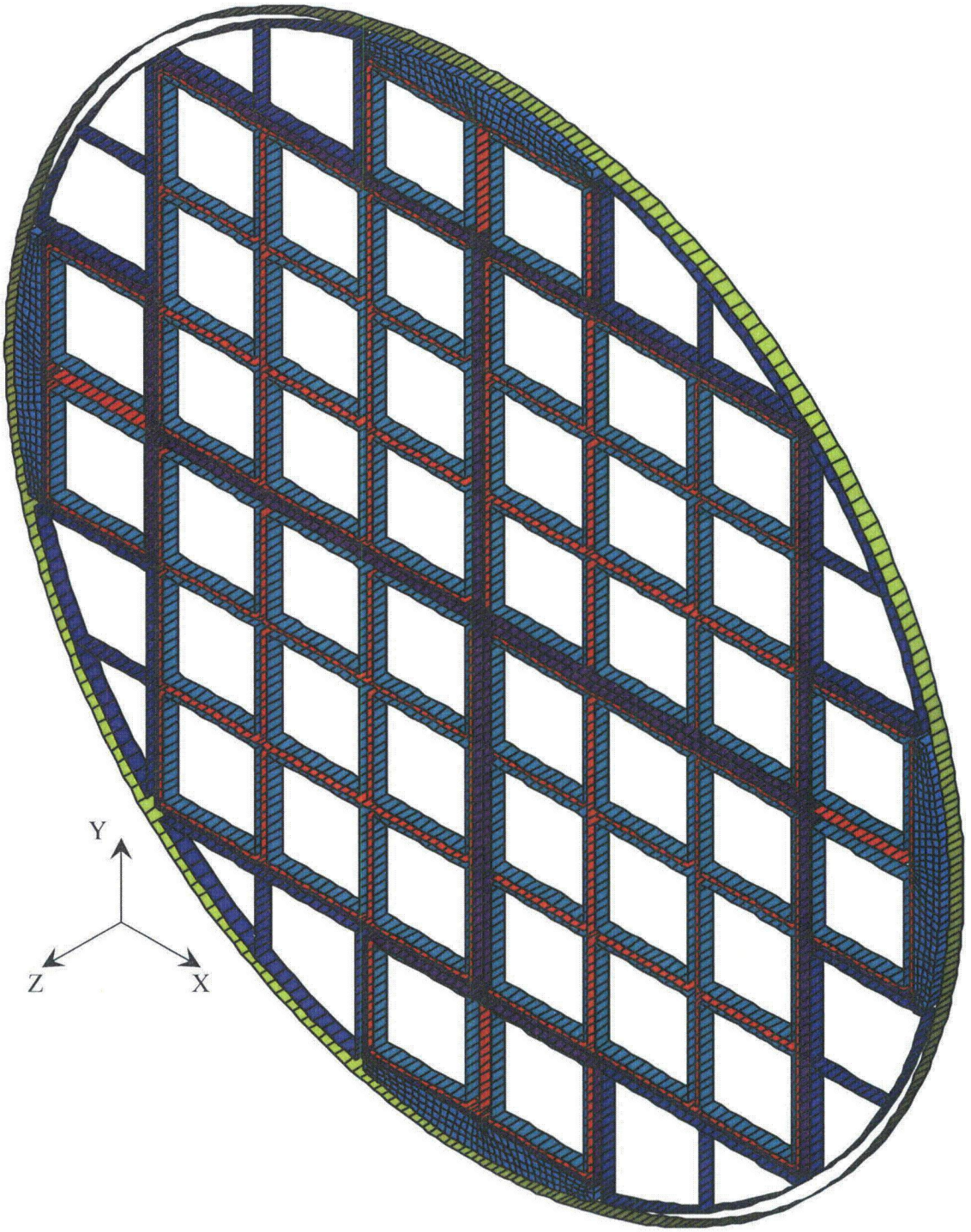

Figure B.2.13.8-1
TN44B Basket Assembly Model
(Excluding Contact and Soft Spring Elements for Clarity)

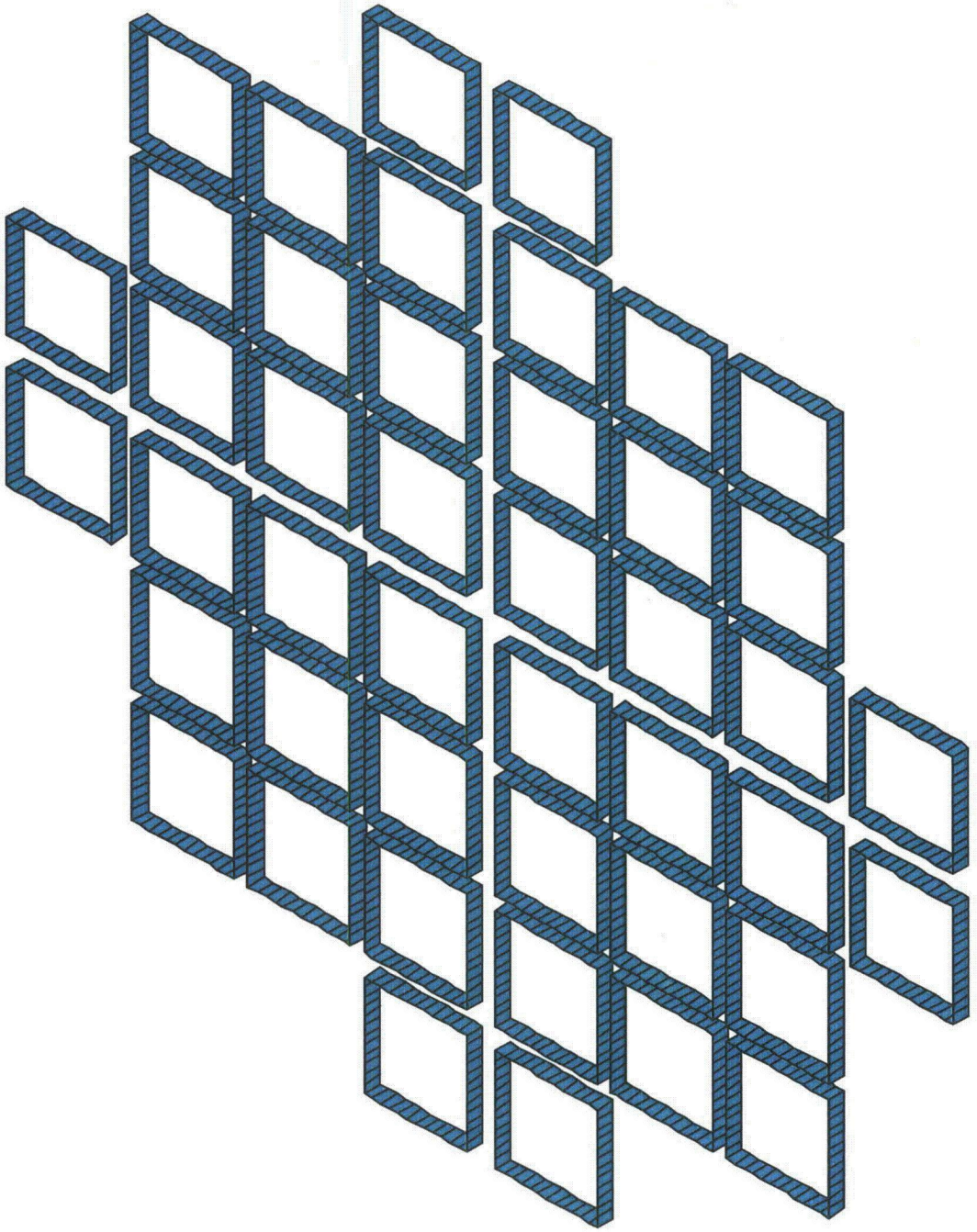

Figure B.2.13.8-2
TN44B Basket Assembly Model SS Fuel Compartments

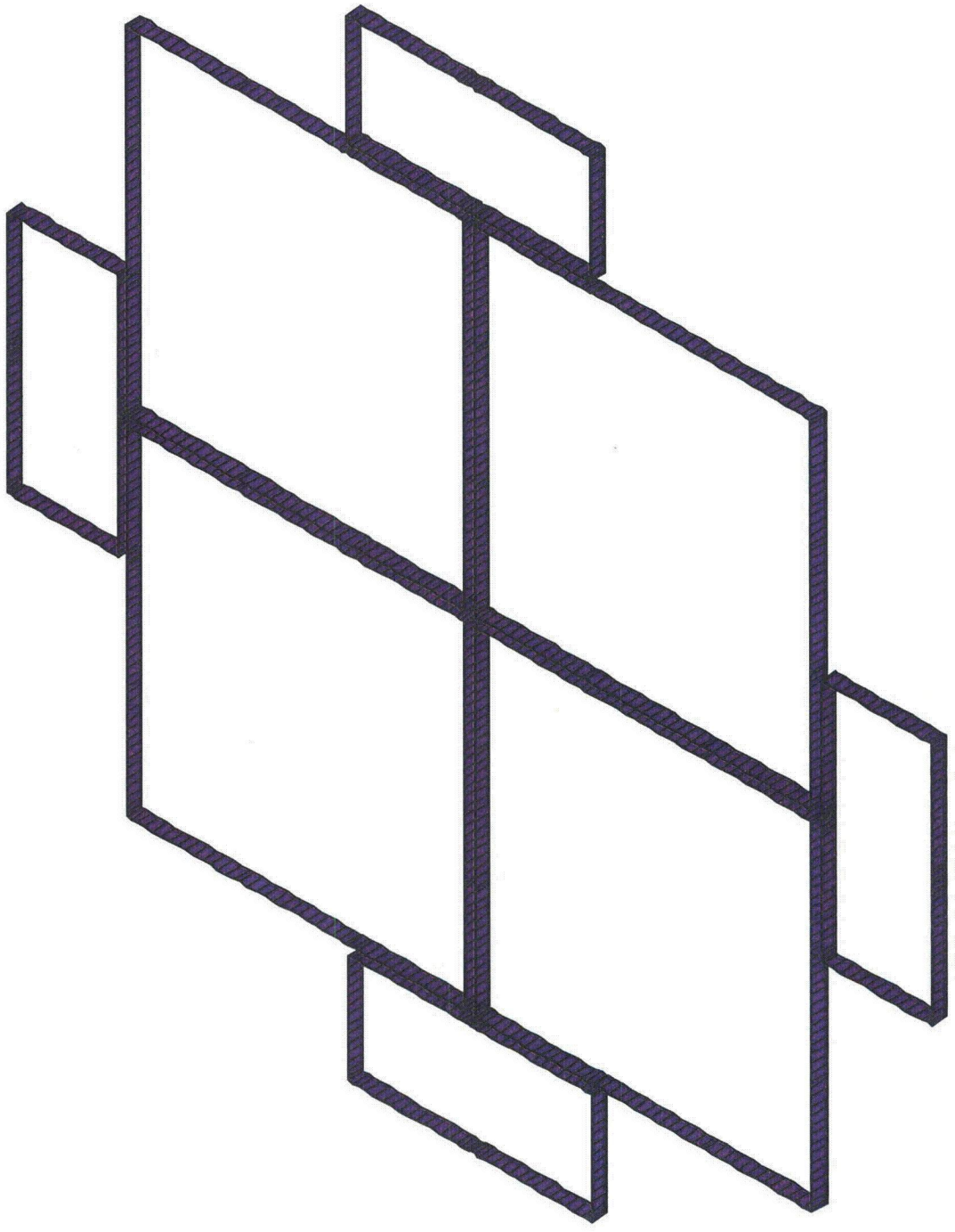

Figure B.2.13.8-3
TN44B Basket Assembly Model SS Wrappers

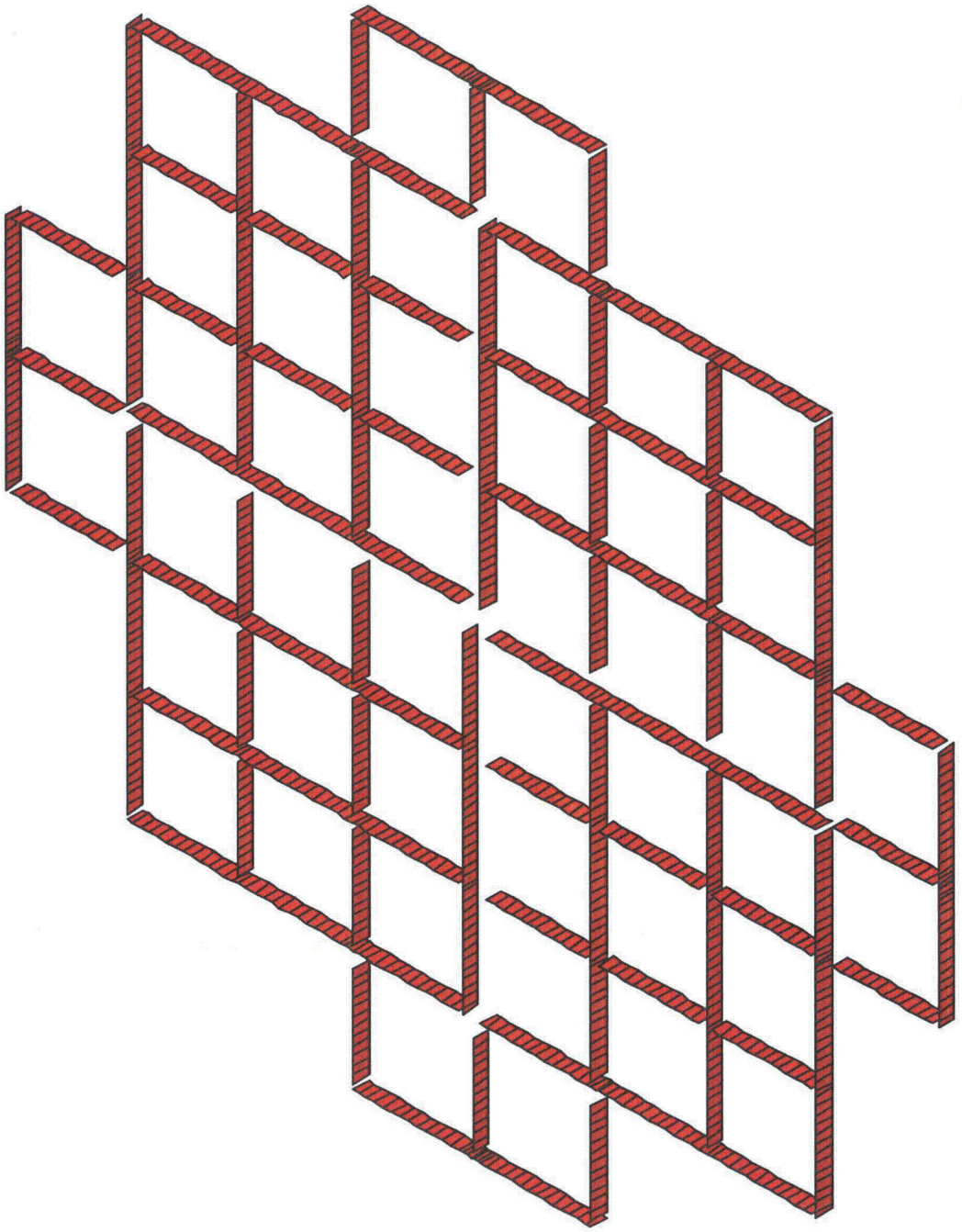

Figure B.2.13.8-4
TN44B Basket Assembly Model Borated SS Steel Plates

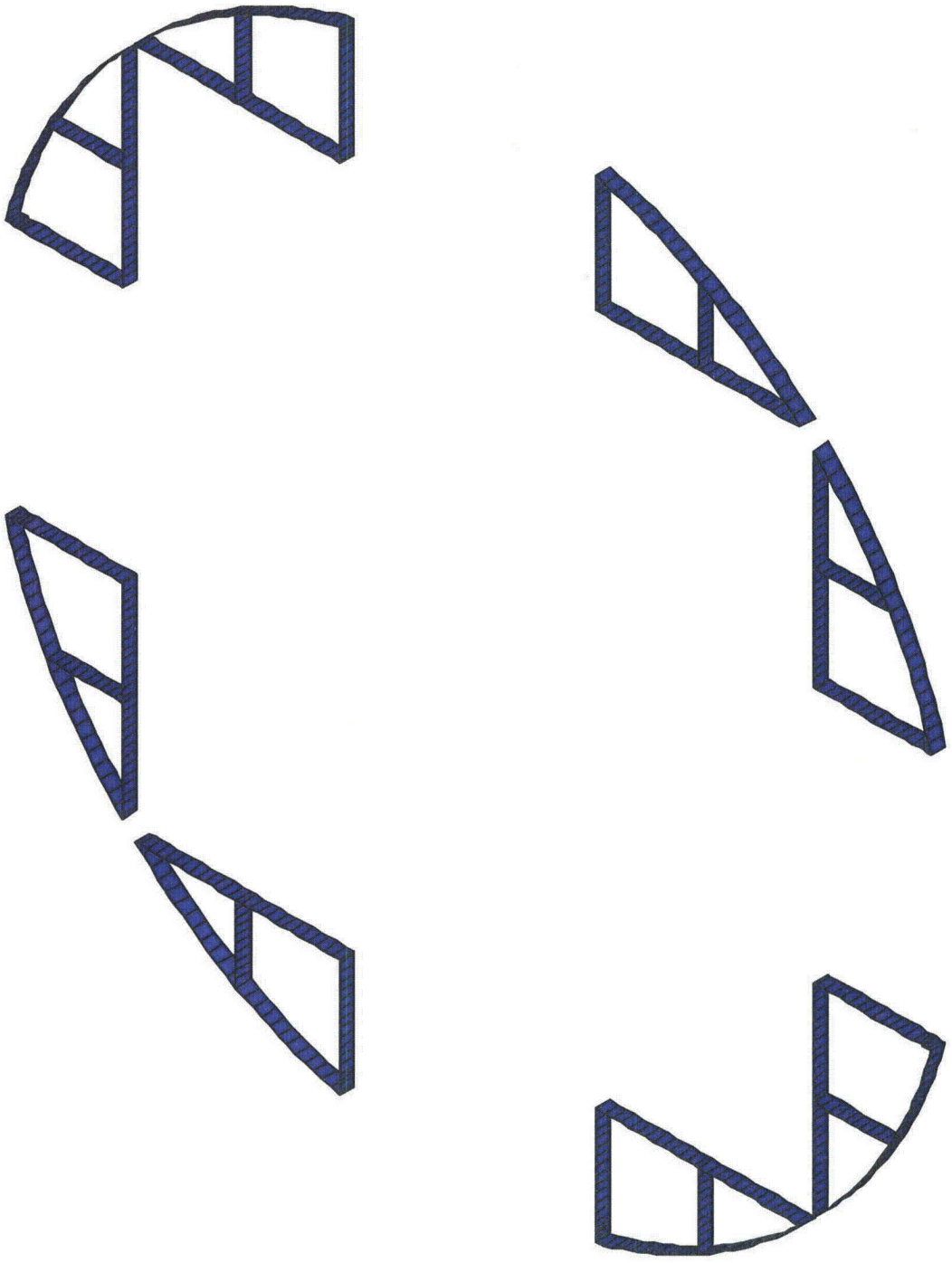

Figure B.2.13.8-5
TN44B Basket Assembly R45 SS Transition Rails

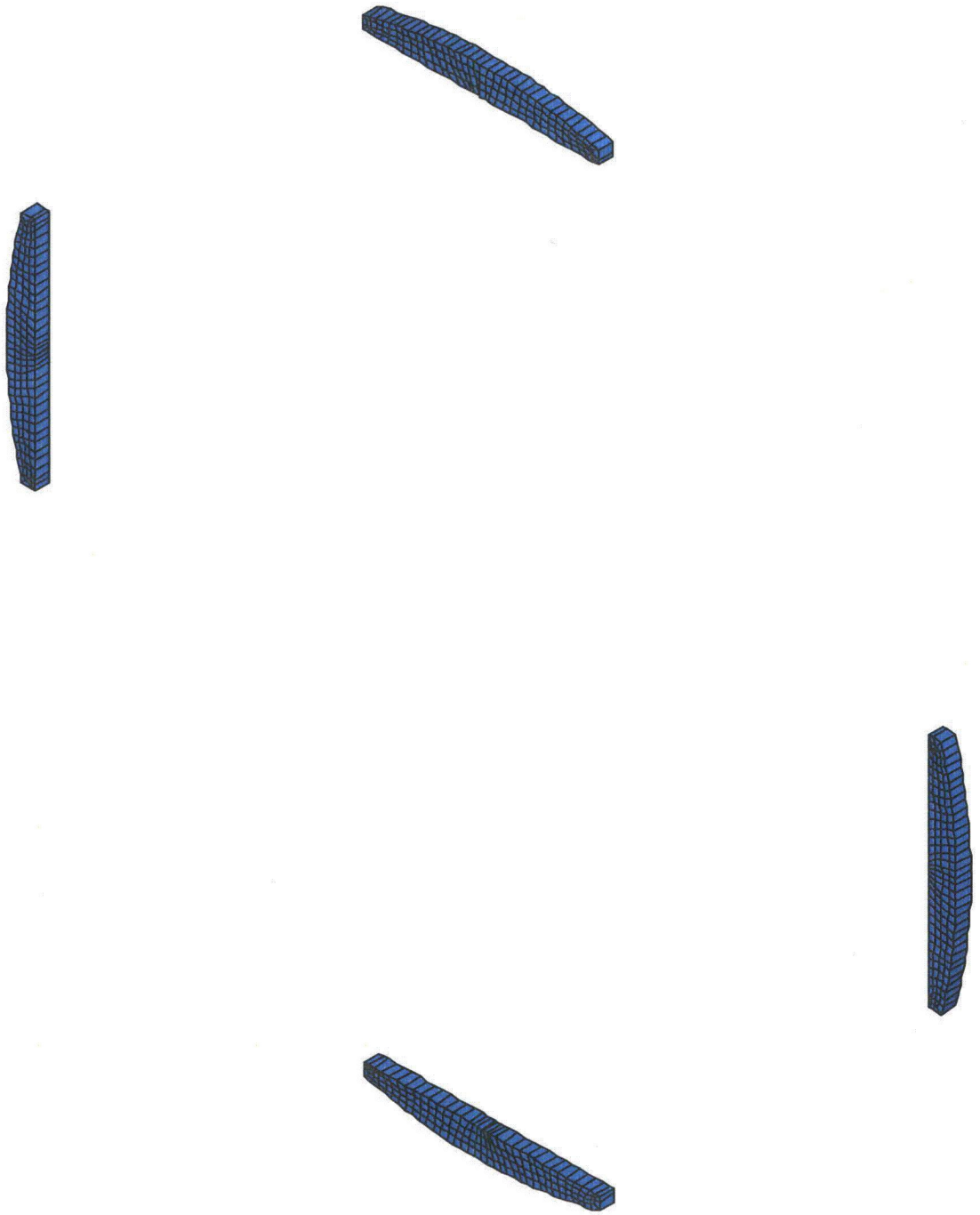

Figure B.2.13.8-6
TN44B Basket Assembly R90 Solid Aluminum Transition Rails

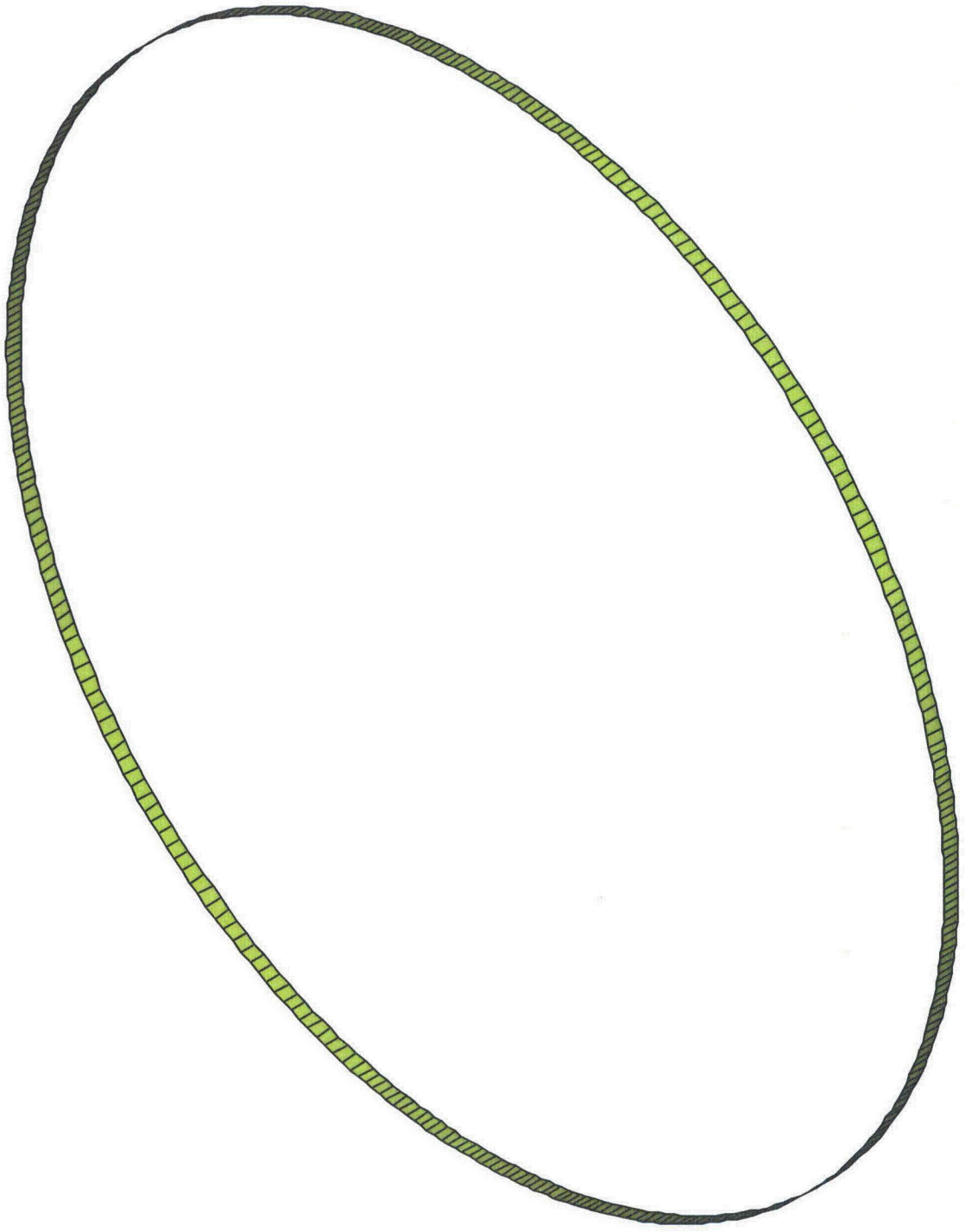

Figure B.2.13.8-7
TN44B SS DSC Shell

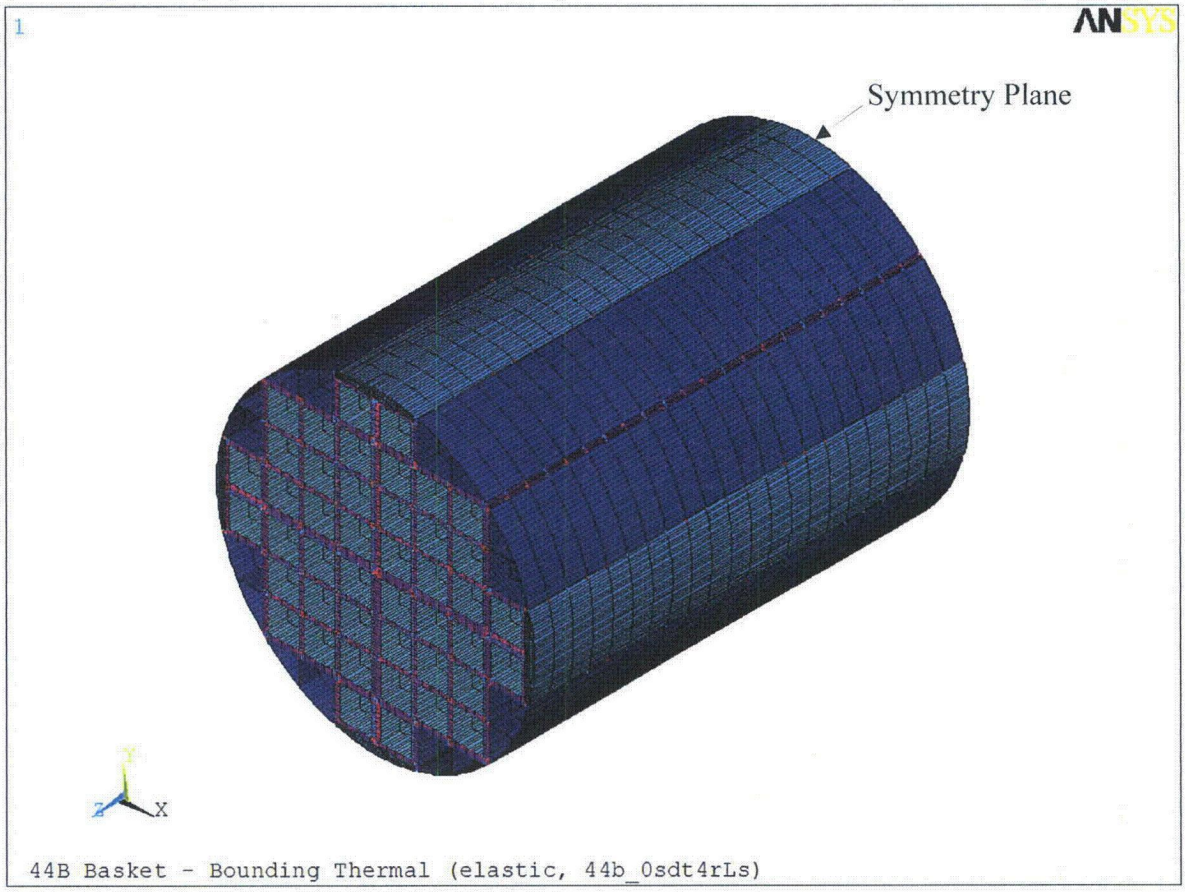

Figure B.2.13.8-8
TN44B Basket Assembly Thermal Stress Analysis Model

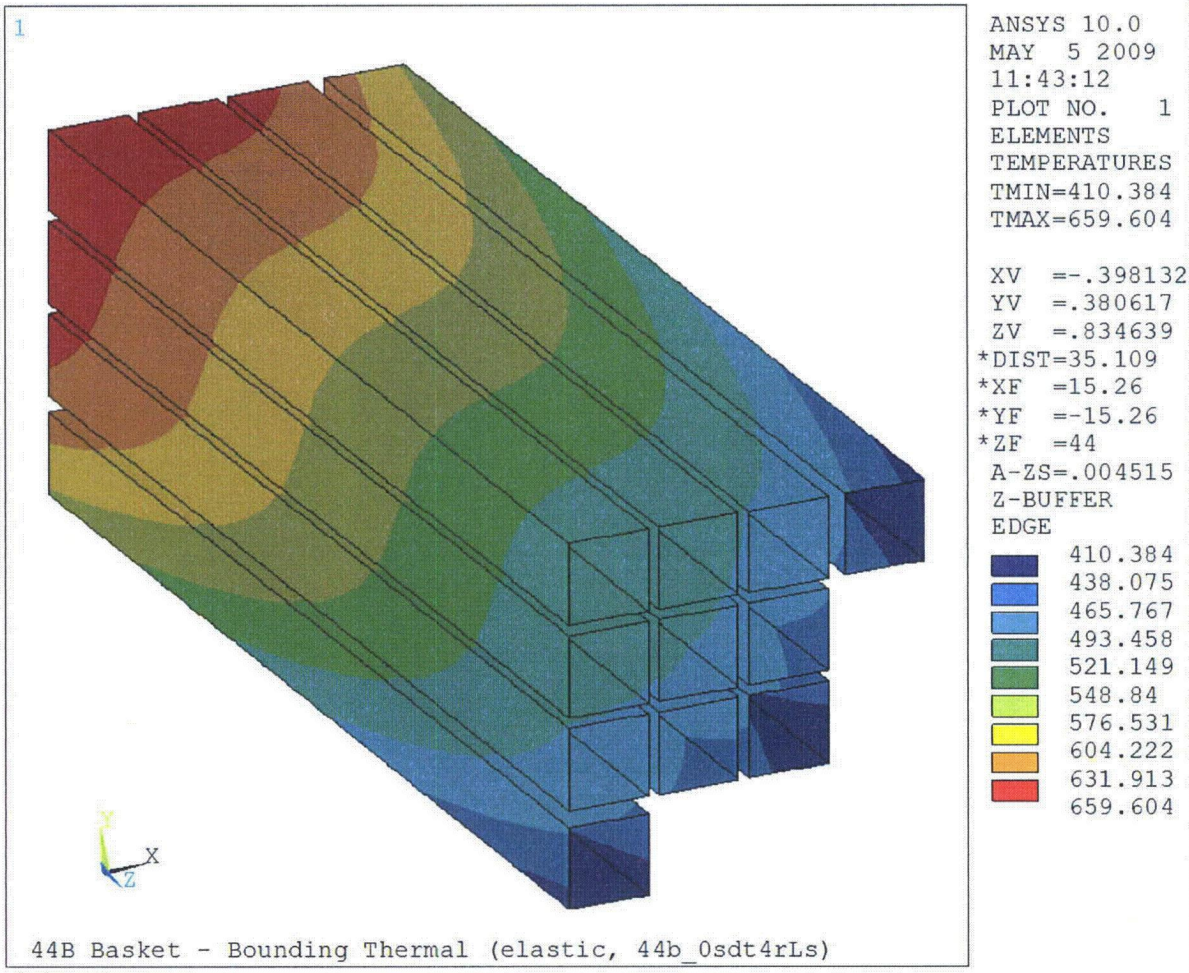

Figure B.2.13.8-9
TN44B Basket Assembly Temperature Profile for Thermal Stress Analysis
(Quarter Cross-Section View)

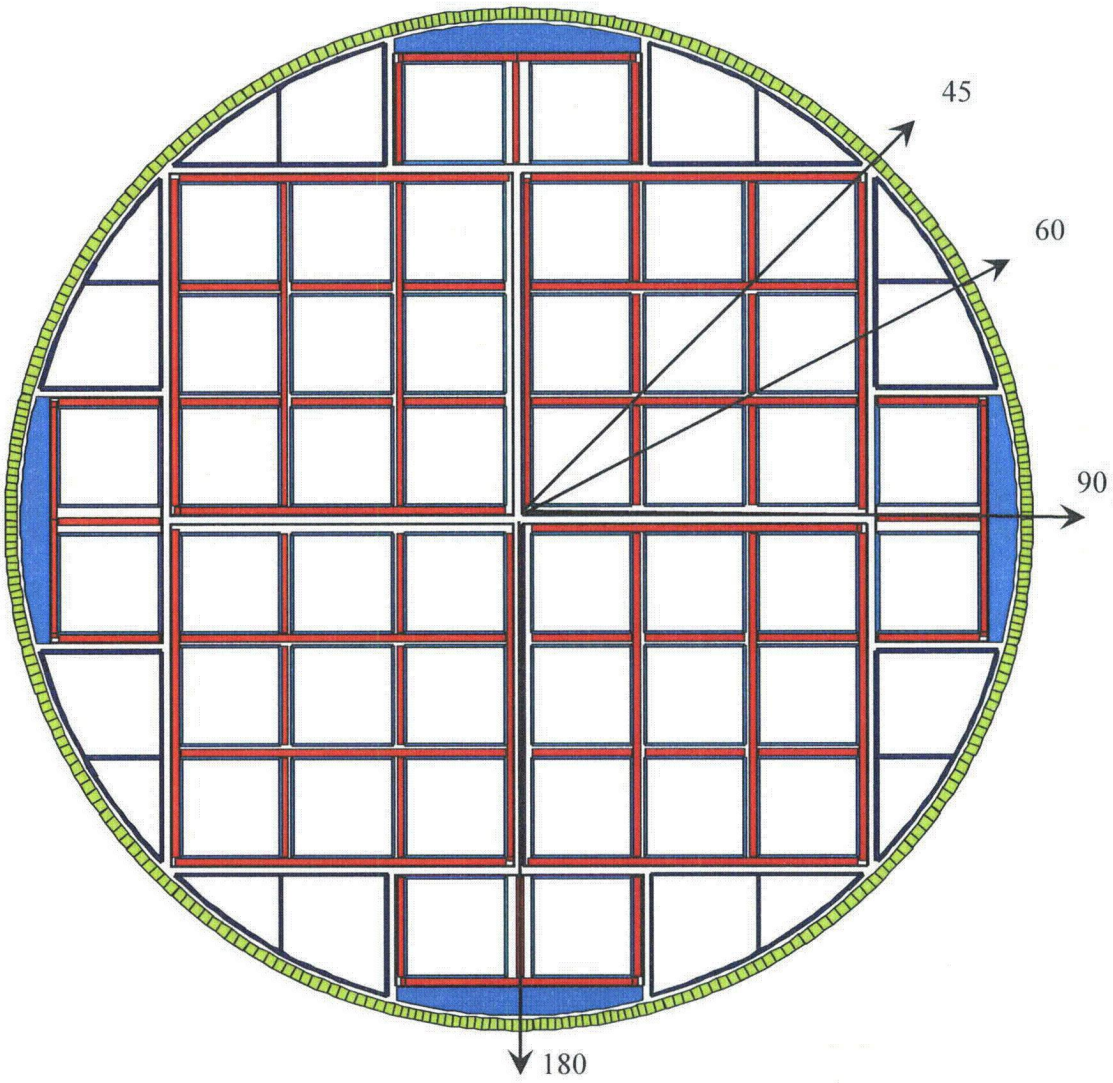

Figure B.2.13.8-10
TN44B Basket Assembly Accident Drop Orientations (degrees)

APPENDIX B.2.13.9
MP197TAD TO DYNAMIC LOAD FACTOR DETERMINATION

CONTENTS

B.2.13.9.1 Introduction B.2.13.9-1
B.2.13.9.2 Natural Frequencies During End Drop B.2.13.9-3
B.2.13.9.3 Natural Frequencies during Side Drop B.2.13.9-5
B.2.13.9.4 Dynamic Load Factor Calculations B.2.13.9-7
B.2.13.9.5 References B.2.13.9-8

LIST OF TABLES

Table B.2.13.9-1 Lowest Natural Frequencies of the TN44B Basket During End Drop B.2.13.9-9
Table B.2.13.9-2 Lowest Natural Frequencies of the TN44B DSC Shell During Side Drop B.2.13.9-9
Table B.2.13.9-3 Lowest Natural Frequencies of Bounding BWR Fuel Claddings During Side Drop B.2.13.9-10
Table B.2.13.9-4 MP197TAD TO - Dynamic Load Factor Results Summary B.2.13.9-10
Table B.2.13.9-5 BWR Fuel Cladding Dynamic Load Factor Results Summary B.2.13.9-10

LIST OF FIGURES

Figure B.2.13.9-1 Modal Analysis Model of TN44B Basket to Determine Limiting Fuel Compartment Span B.2.13.9-11
Figure B.2.13.9-2 Modal Analysis of TN44B Basket to Determine Limiting Fuel Compartment Span B.2.13.9-12
Figure B.2.13.9-3 Conservative Modal Analysis Model of TN44B Basket Limiting Fuel Compartment Span B.2.13.9-13
Figure B.2.13.9-4 Conservative Modal Analysis of TN44B Basket Limiting Fuel Compartment Span B.2.13.9-14
Figure B.2.13.9-5 Bounding BWR 10x10 Fuel Cladding First Mode Shape B.2.13.9-15
Figure B.2.13.9-6 Finite Element Model for DLF Calculation B.2.13.9-16
Figure B.2.13.9-7 MP197TAD TO Transport Cask DLF Curves B.2.13.9-17

APPENDIX B.2.13.9
MP197TAD TO DYNAMIC LOAD FACTOR DETERMINATION

NOTE: References in this appendix are shown as [1], [2], etc., and refer to the reference list in Section B.2.13.9.5.

B.2.13.9.1 Introduction

The purpose of the analysis presented in this appendix is to determine the dynamic load factors (DLF) for the MP197TAD TO internals. The DLFs account for accelerations associated with the relative displacements between the MP197TAD TO and the TN44B DSC shell assembly, basket assembly, and fuel assemblies during the cask drop events.

The DLFs are calculated using a spring-mass finite element model [1]. Acceleration time-histories from the cask side and end drops, documented in Appendix B.2.13.12, are applied to the spring-mass model and the DLFs are calculated based on the $u_{max\ dynamic}$ / $u_{max\ static}$ ratios of displacements.

Three components of the MP197TAD TO transport package internals with the longest and, therefore, most significant natural frequencies are the DSC, basket (with fuel assemblies), and the fuel assemblies. The DLFs for each component are calculated separately.

Four load cases are evaluated in this analysis; normal and accident cases due to longitudinal loading (end drop), and normal and accident loading due to transverse loading (side drop).

During an end drop of the DSC shell assembly, the limiting fundamental natural frequency is based on displacement at the inner bottom cover plate for a top end drop. During an end drop of the basket assembly, the fundamental natural frequency is taken to be that of a simply-supported beam without axial constraint, under longitudinal vibration, where the mass of the fuel assemblies is not lumped with the basket. Longitudinal DLFs are not applicable to the fuel assemblies because the analyses used for the qualification of the fuel assemblies under axial drop conditions do not use DLFs.

During a side drop, the fundamental natural frequency of the DSC shell is taken to be that of a cylinder in a radial-axial mode and simply-supported without axial constraint. For transverse vibration due to a basket side drop, the masses of the fuel assemblies are included and modal analyses are conducted using ANSYS [1]. For the side drop of the fuel assemblies, modal analyses are also conducted using ANSYS [1].

Notation

The notation used in this analysis is taken from Blevins [2], and is as follows.

- E, Modulus of Elasticity, (psi).
- f_i, f_{ij}, Fundamental natural frequency, (Hz.).
- I, Moment of inertia of the beam, (in.^{4}).

- L, Length of beam or cylindrical shell, (in.).
- m, Mass per unit length of the beam, (lbm.in.$^{-1}$).
- μ, Mass density, (lbm.in.$^{-3}$).
- v, Poisson's ratio.
- R, Outer radius of the cylindrical shell, (in.).

B.2.13.9.2 Natural Frequencies During End Drop

DSC Shell Assembly

For a DSC end drop, the lowest frequency of the DSC system is that associated with bending of the inner bottom cover plate under a top end drop. The lower bound of the fundamental frequency of the DSC's inner bottom cover plate is calculated using the equation from Reference [2].

Natural Frequency, $f = \frac{1}{2\pi}\left(\frac{g}{\Delta}\right)^{1/2}$, where, g = 386.4 in/sec^2

$\Delta_2 = \Delta_p - \Delta_1$, maximum deflection at center of inner bottom cover plate relative to the DSC walls.

Δ_p = deflection under a 1g top end down analysis at the center of the inner bottom cover plate, in. (from the same model and analysis described in Appendix B.2.13.7).

= 0.00190959 in.

Δ_1 = deflection under a 1g top end down analysis on the DSC cylinder at the elevation of the inner cover plate, in. (from the same model and analysis described in Appendix B.2.13.7).

= 0.000506404 in.

Δ_2 = 0.00190959 – 0.000506404 = 0.001403186 in.

Then f_2 = 83.5 Hz, $\omega_2 = 2 \pi f_2 = (k_2 / M_2)^{1/2}$

Where k_2 and M_2 are as defined in Table 6-2 (Frame 2) of Reference [2] and are associated with the inner bottom cover plate.

Therefore, $k_2 / M_2 = (2 \pi f_2)^2$ = 2.75254 E5 rad^2 / sec^2

The effect of the axial flexibility of the DSC walls on lowering the frequency of the inner bottom cover plate is considered.

Using the same formula shown above, a lower bound axial frequency of the DSC wall is calculated for a Δ_1 = 0.000506404 in.:

f_1 = 139.0 Hz, $\omega_1 = 2 \pi f_1 = (k_1 / M_1)^{1/2}$

Where k_1 and M_1 are as defined in Table 6-2 (Frame 2) of Reference [2] and are associated with the DSC shell.

Therefore, $k_1 / M_1 = (2 \pi f_1)^2$ = 7.62765 E5 rad^2 / sec^2

The ratio of the DSC mass that is effective in the DSC axial mode to the inner cover plate mass (M_1 / M_2) is approximately 8.

Therefore, $k_2 / M_1 = k_2 / M_2 \times M_2 / M_1 = 1/8 \times k_2 / M_2 = 3.4407$ E4 rad^2 / sec^2

The effect of this axial flexibility of the DSC walls on the frequency of the inner bottom cover plate is determined by use of the following equation, for the two degree of freedom system consisting of the inner bottom cover plate sprung off of the single degree of freedom representation of the DSC cylinder, from Reference [2]:

$$f = 1/(2^{3/2}\pi) \times (k_1/M_1 + k_2/M_1 + k_2/M_2 - ((k_1/M_1 + k_2/M_1 + k_2/M_2)^2 - 4\, k_1k_2/M_1M_2))^{1/2})^{1/2}$$

For a ratio of the DSC mass that is effective in the DSC axial mode to the inner cover plate mass of 8, the lowest frequency of the two degree of freedom system is calculated to be:

$f = 80.8$ Hz

Basket

The fundamental natural frequency of a simply-supported basket structure under axial vibration simplifies to that of a uniform beam axially free at both ends. The fundamental natural frequency of a uniform beam free at both ends, under longitudinal vibration is as follows [2]:

$$f_1 = \frac{\lambda_1}{2\pi L}\left(\frac{E}{\mu}\right)^{1/2}$$

Where,
$\lambda_1 = \pi$
E = Young's modulus @ 700°F, psi (24.8E+06 psi)
L = Minimum length of the basket in inches (176.5 in.)
μ = Average mass density ($lbm\text{-}in^{-3}$)

The total bounding weight and volume of the assembly of basket components (exclusive of fuel assemblies) used for the calculation are 42,149 lbs (greater than actual) and 184,883 in^3 (less than actual), respectively; resulting in an upper bound average mass density of 0.000590 $lbm\text{-}in.^{-3}$. Calculated parameter values and the lower bound frequency are shown in Table B.2.13.9-1. The lower bound (end drop) natural frequency of the basket assembly is calculated to be 580.8 Hz.

B.2.13.9.3 Natural Frequencies during Side Drop

DSC Shell

The fundamental natural frequency of the DSC shell radial-axial mode is determined assuming the cylindrical shell is simply-supported without axial constraint. The natural frequency of the cylindrical shell radial-axial mode is given by the following ([2], p. 305, Table 12-2, Frame 5).

$$f_{ij} = \frac{\lambda_{ij}}{2\pi R}\left(\frac{E}{\mu(1-\nu^2)}\right)^{1/2}$$

Where,
E = Young's modulus @ 500°F, psi (2.59E+07 psi)
R = Average shell radius, in. (32.75 in.)
ν = Poisson's ratio (0.3)
μ = Mass density, (lbm.in.$^{-3}$) (0.00075 lbm.in.$^{-3}$)

$$\lambda_{ij} = \frac{\left\{(1-\nu^2)(j\pi R/L)^4 + (h^2/12R^2)\left[i^2+(j\pi R/L)^2\right]^4\right\}^{1/2}}{(j\pi R/L)^2 + i^2}$$

Where,
L = Cavity length, in (179.38 in.)
h = thickness, in (0.75 in.)

Calculated parameter values and the lower bound frequency are shown in Table B.2.13.9-2. The (side drop) natural frequency of the DSC shell is calculated to be 66.5 Hz.

Basket Assembly

The fundamental natural frequency of the basket assembly during side drops is calculated via ANSYS finite element analysis. The finite element model from Appendix B.2.13.8 is used as the basis for the modal analyses.

Material properties are conservatively based on a basket temperature of 700 °F and a periphery rail temperature of 700 °F for the stainless steel rails and 600 °F for the aluminum rails. Weight densities are changed to mass densities ($\rho_m = \rho_w /386.4$). The Appendix B.2.13.8 basket model applied the fuel assembly load as a pressure load, which is not appropriate for a modal analysis. For the modal analyses, the fuel assemblies are represented by masses and are applied to the basket panels using ANSYS MASS21 elements.

The finite element model from Appendix B.2.13.8 is used as the basis for the performance of a general modal analysis, which is then used to identify the span associated with the limiting (lowest) frequency. The gap (contact) elements, including boundary gaps between the DSC and the cask nodes, of the full basket model of Appendix B.2.13.8 are replaced with rigid springs (a

modal analysis cannot have nonlinear elements). As discussed in Appendix B.2.13.8, the cask nodes are restrained in all directions. This effectively supports the basket at the rails' periphery for the general modal analysis. The model is shown in Figure B.2.13.9-1. This assumption results in the prediction of natural frequencies of the basket plates including fuel assembly inertia mass. A plot of the modal analysis results for the lowest frequency is shown in Figure B.2.13.9-2.

Based on the results of this general modal analysis, the limiting fuel compartment span (with adjacent plates) is conservatively modeled using simply-supported spans and pinned boundary conditions as shown in Figure B.2.13.9-3. Credit is taken for only 1 fuel compartment plate per fuel assembly and 10% of the borated steel strength, which gives a lower bound frequency of 147.9 Hz as shown in Figure B.2.13.9-4.

Fuel Rod Cladding

ANSYS modal analyses are performed to determine the lateral natural frequencies of a single fuel rod cladding for differenct fuel types. The weight of the fuel pellets is included in the equivalent density of the fuel cladding No changes are made to the ANSYS model described in Appendix B.2.13.11 and modal analyses are performed to determine the lowest natural frequencies.

The natural frequencies for the fuel cladding are summarized in Table B.2.13.9-3 and the lowest frequency for the bounding fuel cladding is shown in Figure B.2.13.9-5.

B.2.13.9.4 Dynamic Load Factor Calculations

ANSYS transient dynamic analyses are performed using finite element models consisting of a damped spring oscillator, COMBIN14, and a structural mass, MASS21, element to calculate DLFs for 1' and 30' end and side drops. The finite element model is shown in Figure B.2.13.9-6. The acceleration time histories of the 1' and 30' end and side drops are applied to the mass element and the DLF is calculated:

$$DLF = u_{max\ dynamic} / u_{max\ static}$$

Where,
$u_{max\ static}$ – calculated by max g load x mass / stiffness
$u_{max\ dynamic}$ – calculated by ANSYS

Unit mass is assumed for all analyses, and the stiffness and damping (7% damping is used) are calculated based on the desired frequency of the spring using the following equations:

$$k = m(2\pi f)^2$$

Where,
m – mass
f – desired frequency

$$c = 2\zeta\sqrt{(km)}$$

where,
ζ – damping ratio
k – stiffness
m – mass

DLFs are calculated for each drop condition for a frequency range from 5 to 200 Hz and are shown in Figure B.2.13.9-7. The DLFs for the TN44B DSC shell assembly and basket assembly are summarized in Table B.2.13.9-4. Fuel cladding DLFs are summarized in Table B.2.13.9-5.

B.2.13.9.5 References

1. ANSYS Computer Code and User's Manual, Release 10.

2. Blevens, Robert D., "Formulas for Natural Frequency and Mode Shape," Krieger Publishing Company, Florida, 1984.

Table B.2.13.9-1
Lowest Natural Frequencies of the TN44B Basket During End Drop

Parameter Description	Value[1]
Length of Basket (in.)	176.5
Weight of Steel + Aluminum (lbs.)	42,149
Volume of Steel + Aluminum (in^3)	184,883
Average Weight Density (lbs/in^3)	0.22798
Average Mass Density ($lbm. / in^3$)	0.0000590
Young's Modulus @700 °F (psi)	2.48E+07
Frequency of Basket (End Drop), f_1, Hz	580.7972

Notes: (1) Values are equal to or conservative with respect to actual values.

Table B.2.13.9-2
Lowest Natural Frequencies of the TN44B DSC Shell During Side Drop

Parameter Description	Value
ν - Poisson's ratio	0.3
i for fundamental mode i =3	3
j for fundamental mode j =1	1
μ - Mass Density ($lbm\ in^{-3}$)	0.00075
E - Young's Modulus @ 500F (psi)	2.59E+07
h – thickness (in)	0.75
R - Average Shell Radius (in)	32.75
L - Cavity Length (in)	179.38
$\lambda_{ij}=\lambda_{31}$	0.0703
Radial-Axial Lowest Frequency	66.483

Table B.2.13.9-3
Lowest Natural Frequencies of Bounding BWR Fuel Claddings During Side Drop

BWR Fuel Assembly	7x7	8x8	9x9	10x10
Lowest Natural Frequency (Hz)	42.12	35.38	31.67	30.62

Table B.2.13.9-4
MP197TAD TO - Dynamic Load Factor Results Summary

Loading Condition / Component	Max. DLF
1' (normal) end drop / basket	1.06
1' (normal) end drop / DSC shell	1.35
30' (accident) end drop / basket	1.19
30' (accident) end drop / DSC shell	1.57
1' (normal) side drop / basket	1.05
1' (normal) side drop / DSC shell	1.20
30' (accident) side drop / basket	1.03
30' (accident) side drop / DSC shell	1.16

Table B.2.13.9-5
BWR Fuel Cladding Dynamic Load Factor Results Summary

Drop	DLF
1 ft fuel side drop	1.57
30 ft fuel side drop	1.50

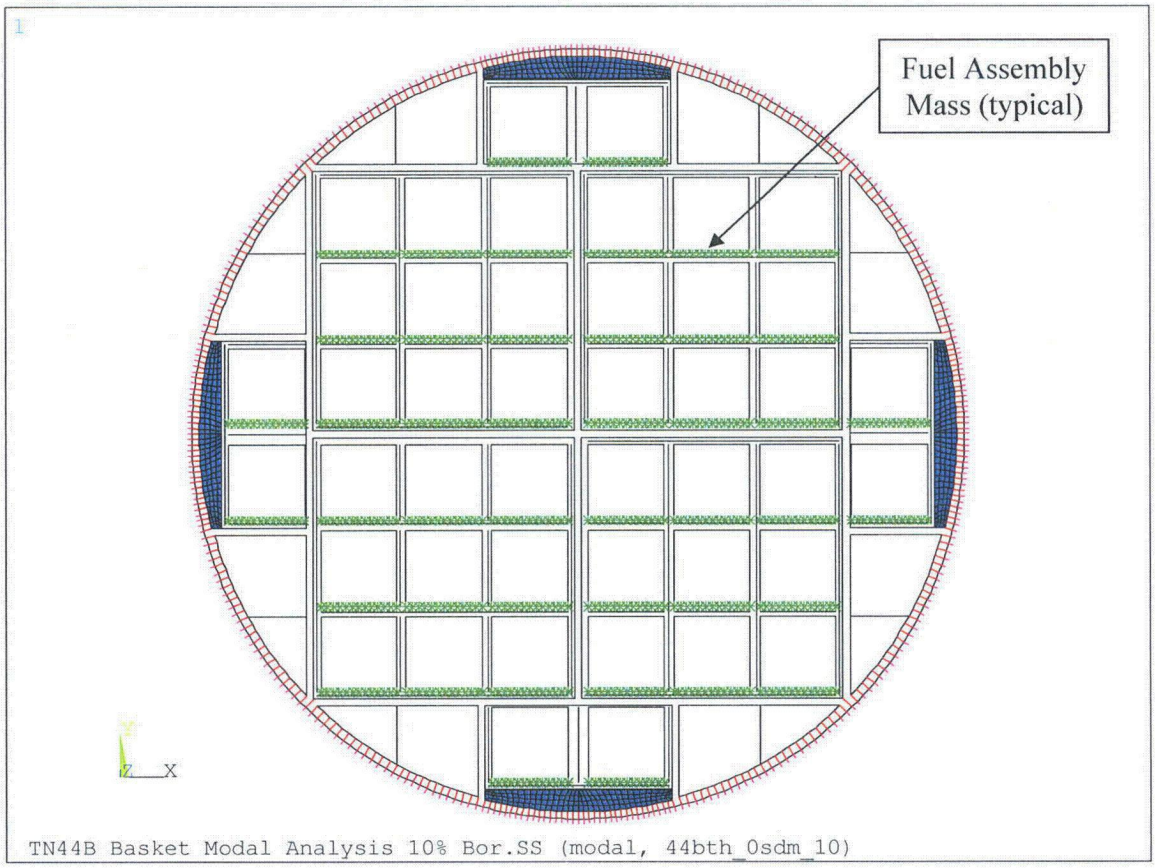

Figure B.2.13.9-1
Modal Analysis Model of TN44B Basket to Determine Limiting Fuel Compartment Span
(springs between plates not shown for clarity)

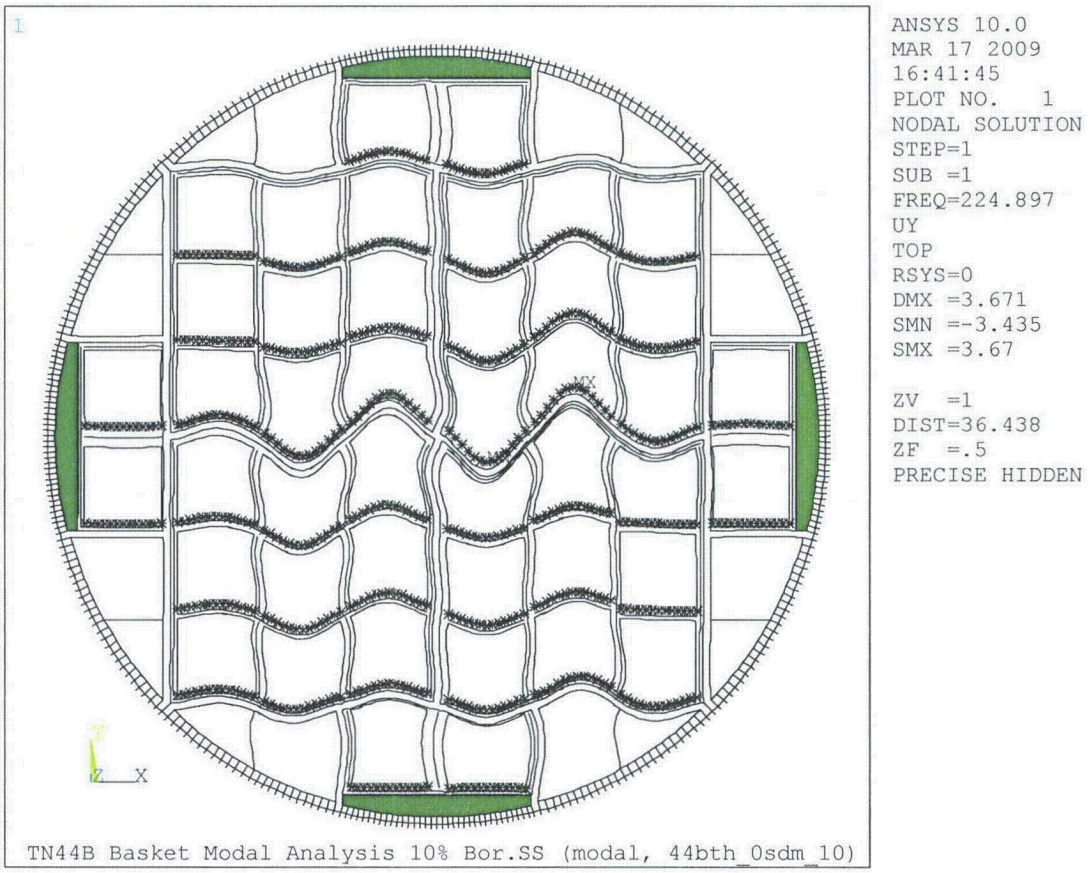

Figure B.2.13.9-2
Modal Analysis of TN44B Basket to Determine Limiting Fuel Compartment Span

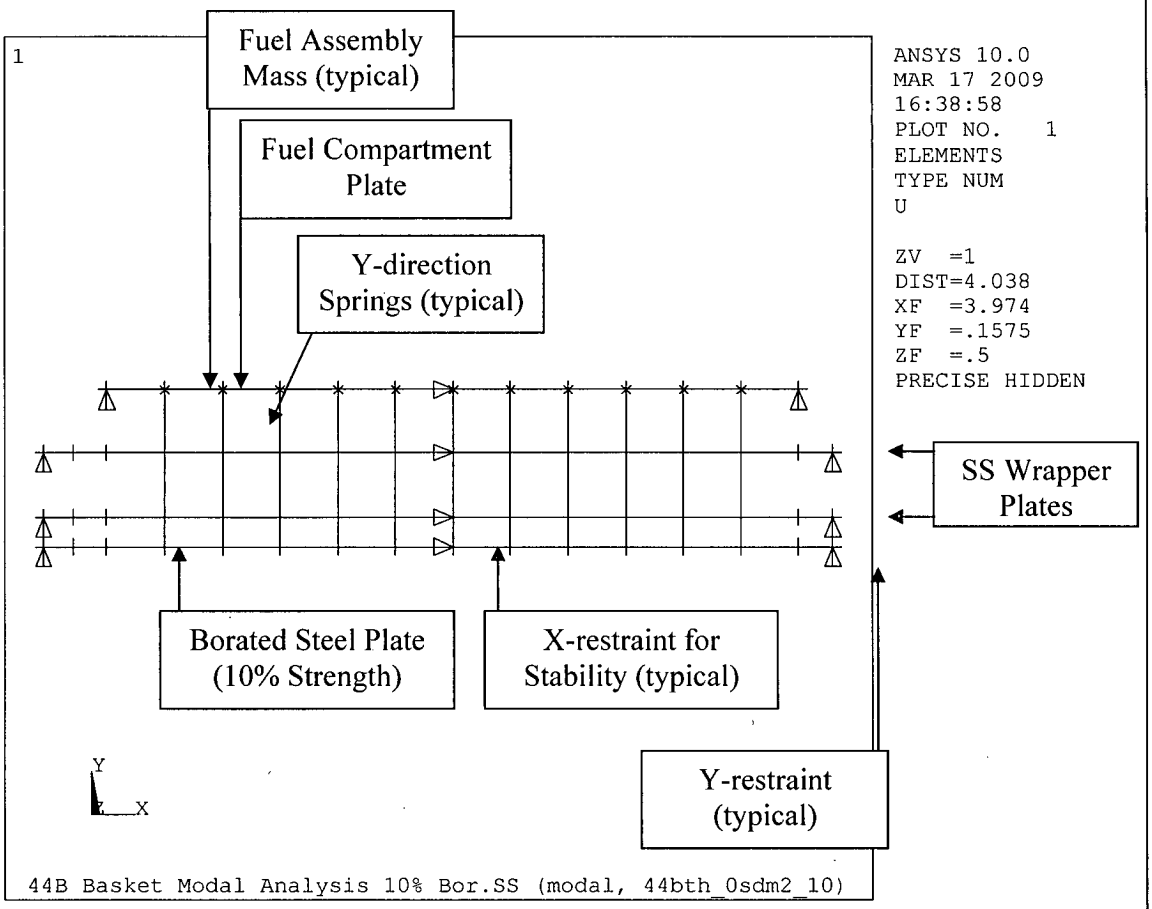

Figure B.2.13.9-3
Conservative Modal Analysis Model of TN44B Basket Limiting Fuel Compartment Span

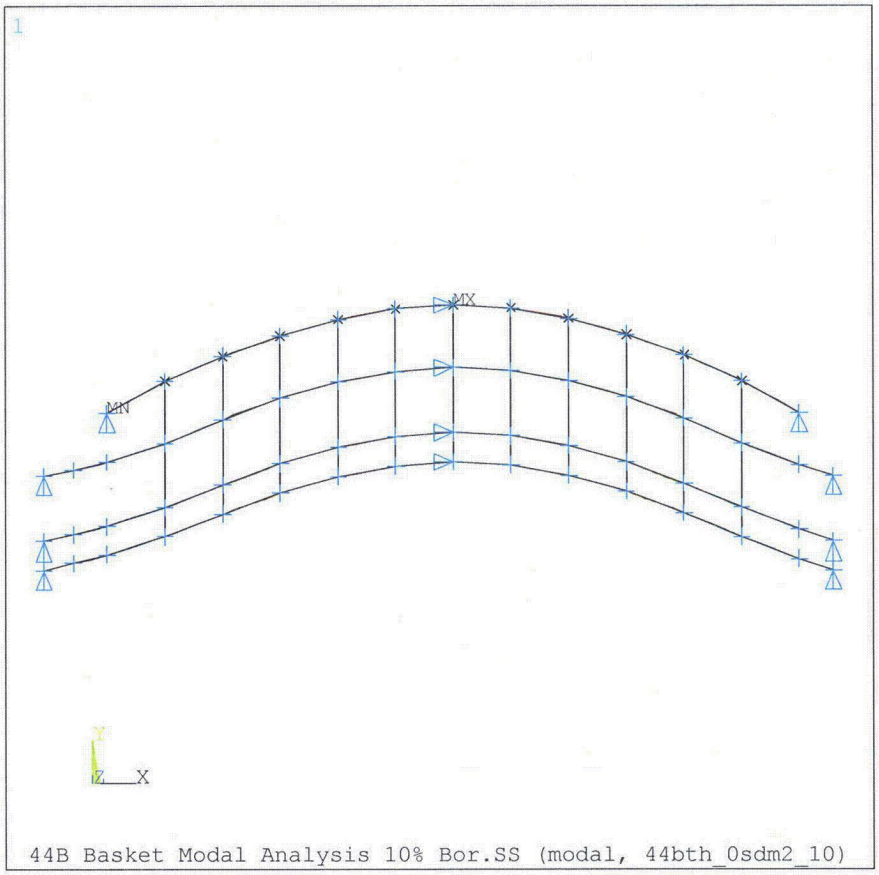

Figure B.2.13.9-4
Conservative Modal Analysis of TN44B Basket Limiting Fuel Compartment Span

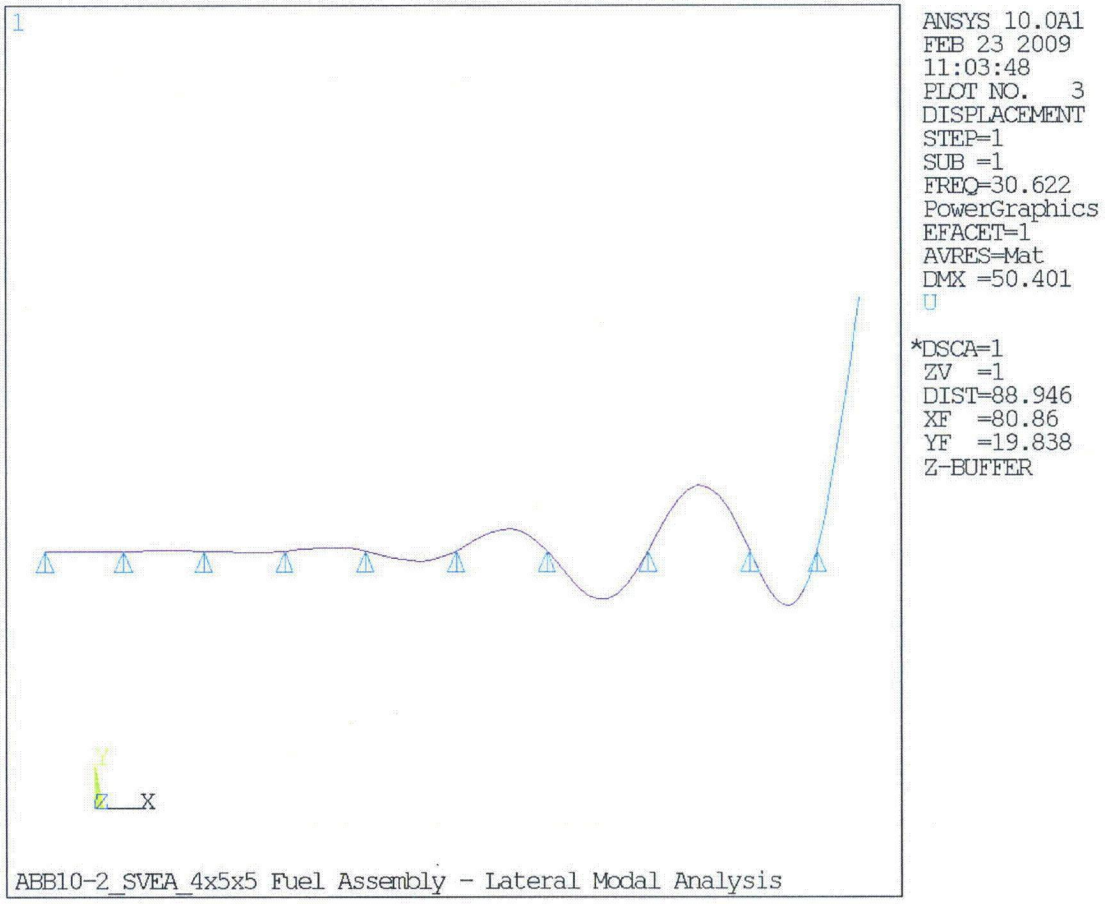

Figure B.2.13.9-5
Bounding BWR 10x10 Fuel Cladding First Mode Shape

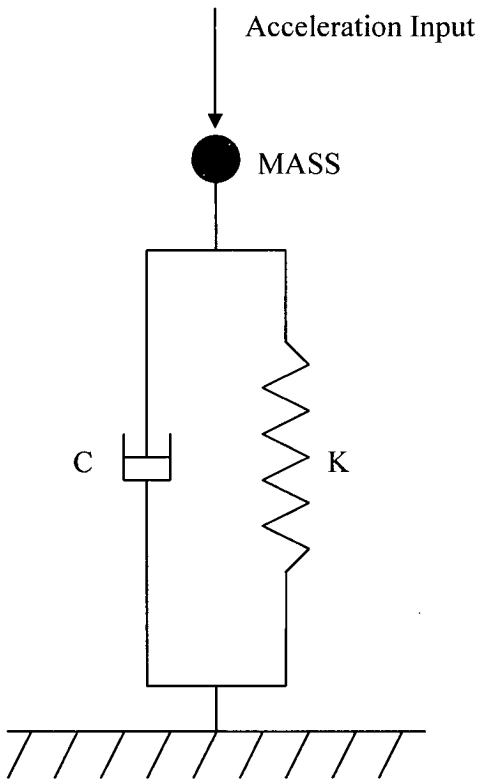

Figure B.2.13.9-6
Finite Element Model for DLF Calculation

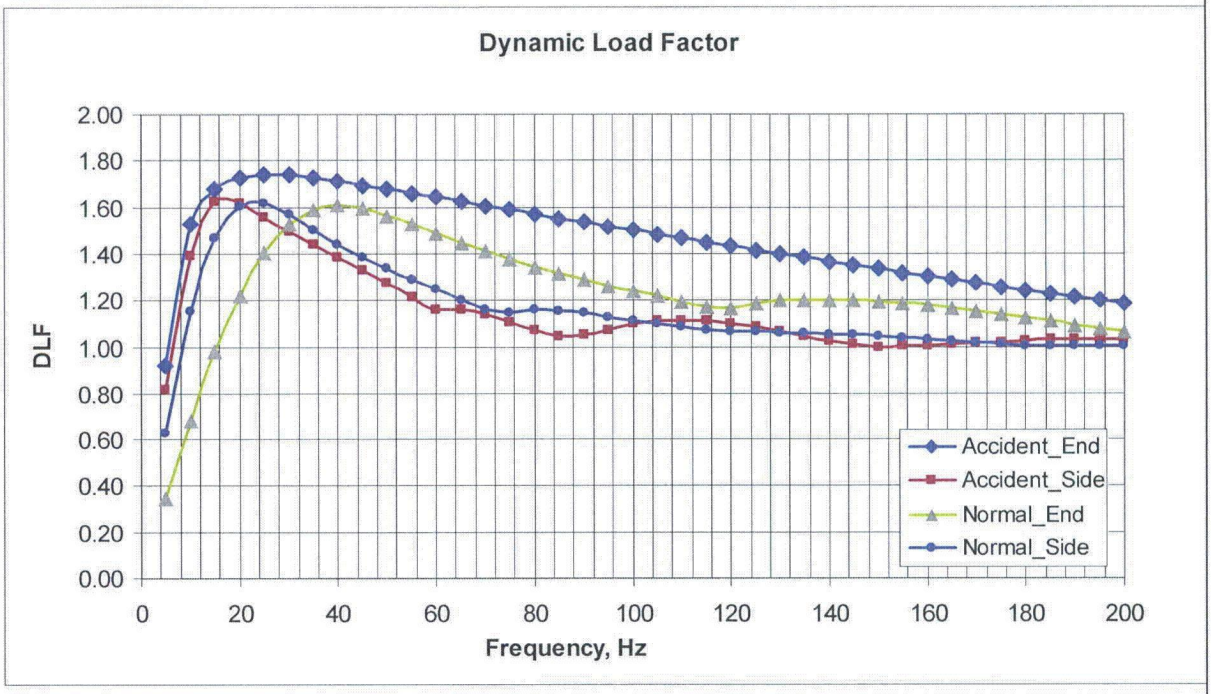

Figure B.2.13.9-7
MP197TAD TO Transport Cask DLF Curves

Appendix B.2.13.10
MP197TAD TO Thermal Expansion Evaluation

CONTENTS

B.2.13.10.1 Purpose B.2.13.10-1
B.2.13.10.2 Radial Thermal Expansion B.2.13.10-2
B.2.13.10.3 Axial Thermal Expansion B.2.13.10-4
B.2.13.10.4 Results and Conclusions B.2.13.10-6
B.2.13.10.5 Reference B.2.13.10-7

Appendix B.2.13.10
MP197TAD TO Thermal Expansion Evaluation

NOTE: References in this appendix are shown as [1], [2], etc., and refer to the reference list in Section A.2.13.10.5.

B.2.13.10.1 Purpose

In this appendix, the thermal expansion of the components of the MP197TAD TO is evaluated. The thermal loads considered are the 100°F, -20°F and -40°F ambient normal condition of transport (NCT), temperature distributions computed in Chapter B.3.

The thermal analysis of the TN44B DSC for NCT is described in Chapter B.3. This analysis is performed to determine the MP197TAD TO components temperatures for the NCT with maximum solar heating, maximum decay heat from the DSC contents for 100°F ambient and with only the maximum decay heat from the DSC contents for -20°F and -40°F ambient temperatures. The results of the thermal analysis are used to evaluate the effects of axial and radial thermal expansion in the MP197TAD TO components

Volumetric average temperatures of the TN44B DSC shell and MP197TAD TO inner shell are obtained using ANSYS [1] from Chapter B.3. The results are listed in the following table. The average volumetric temperatures for DSC shell and inner shell from the hottest cross section of the DSC are used in computing the radial hot gaps. Axial hot gaps are computed using the average volumetric temperature computed over the full length of the DSC shell and inner shell.

Summary of Average Component Temperature for NCT Thermal Analysis

Ambient Temperature	Average Calculated Temperatures for Radial Gap (°F)		Average Calculated Temperatures for Axial Gap (°F)	
	DSC shell	Inner Shell	DSC shell	Inner Shell
-40°F	283	212	261	196
-20°F	297	229	276	213
100°F	384	325	363	308

To verify that adequate clearance exists between the TN44B DSC and MP197TAD TO cavity for free thermal expansion, the thermal expansions between various components are calculated.

The following table lists the coefficients of thermal expansion used in this section.

Thermal Expansion Coefficients (10^{-6} in/in/°F)

T (°F)	SA-240 Type 304/304N	SA-240 Type 316/316L	Aluminum (Al6063)
70	8.5	8.5	12.1
100	8.6	8.6	12.4
150	8.8	8.8	12.7
200	8.9	8.9	13.0
250	9.1	9.1	13.1
300	9.2	9.2	13.3
350	9.4	9.4	13.4
400	9.5	9.5	13.6
450	9.6	9.6	13.8
500	9.7	9.7	13.9
550	9.8	9.8	14.1
600	9.8	9.8	14.2
650	9.9	9.9	
700	10	10.0	
750	10	10.0	
800	10.1	10.1	
850	10.2	10.2	
900	10.2	10.2	
950	10.3	10.3	
1000	10.3	10.3	

The following table presents the dimensions used in this calculation:

Dimensions used in Calculating Thermal Expansion (in.)

DSC	Heat Load, kW	$OD_{Canister,Cold}$	$L_{Canister,Cold}$	$L_{CAN,Lift,Cold}$	$ID_{Shell,TO,Cold}$	$L_{Cavity,TO,Cold}$
TN44B	22	66.25	196.25	6.25	67	206

B.2.13.10.2 Radial Thermal Expansion

The maximum outside diameter of the TN44B DSC when exposed to the hot environment is:

$$OD_{Canister,Hot} = OD_{Canister,Cold}[1+\alpha_{CAN}(T_{avg,CAN,Shell} - T_{ref})]$$

where:

- $OD_{Canister,Hot}$ = Hot outer diameter of TN44B DSC, *in*
- $OD_{Canister,Cold}$ = Cold outer diameter of TN44B DSC, *in*
- α_{CAN} = Thermal expansion coefficient of TN44B DSC shell material, 10^{-6} in./in./°F
- $T_{avg,CAN,Shell}$ = Volumetric average temperature of TN44B DSC shell, ^{o}F
- T_{ref} = Reference temperature = 70°F

The maximum outside diameter of TN44B DSC is calculated in the table below.

Maximum Outside Diameter of Hot TN44B DSC (in.)

Ambient Temperature	$OD_{Canister,Cold}$	$T_{avg,CAN,Shell}$	α_{CAN}	$OD_{Canister,Hot}$
°F	in.	°F	$°F^{-1}$	in.
-40°F	66.25	283	9.17E-06	66.379
-20°F		297	9.19E-06	66.388
100°F		384	9.47E-06	66.447

The minimum hot inside diameter of the MP197TAD TO inner shell is:

$$ID_{Shell,TO,Hot} = ID_{Shell,TO,Cold}[1+\alpha_{Shell,TO}(T_{avg,Shell,TO} - T_{ref})]$$

where:

- $ID_{Shell,TO,Hot}$ = Hot inner diameter of MP197TAD TO inner shell, *in*
- $ID_{Shell,TO,Cold}$ = Cold inner diameter of MP197TAD TO inner shell, *in*
- $\alpha_{Shell,TO}$ = Thermal expansion coefficient of MP197TAD TO inner shell material, 10^{-6} in./in./°F
- $T_{avg,Shell,TO}$ = Volumetric average temperature of MP197TAD TO inner shell, $°F$
- T_{ref} = Reference temperature = 70°F

The minimum inside diameter of the MP197TAD TO inner shell is calculated in the table below.

Minimum Inner Diameter of Hot MP197TAD TO inner shell (in.)

Ambient Temperature	$ID_{Shell,TO,Cold}$	$T_{avg,Shell,TO}$	$\alpha_{Shell,TO}$	$ID_{Shell,TO,Hot}$
°F	in.	°F	$°F^{-1}$	in.
-40°F	67.00	212	8.95E-06	67.085
-20°F		229	9.02E-06	67.096
100°F		325	9.30E-06	67.159

The resulting hot diametrical gaps between the TN44B DSC and the MP197TAD TO inner liner are calculated as follows and are presented in the table below.

$$\Delta_{HOT\_GAP,Dia} = ID_{Shell,TO,Hot} - OD_{Canister,Hot}$$

Diametrical Hot Gap (in.)

Ambient Temperature (°F)	Hot Diametrical Gap, $\Delta_{HOT\_GAP,Dia}$
-40°F	0.706
-20°F	0.708
100°F	0.712

Adequate clearance has been provided between the outside diameter of the TN44B DSC and the inner diameter of the MP197TAD TO inner liner to permit free thermal expansion.

B.2.13.10.3 Axial Thermal Expansion

Free movement of the TN44B canister in the axial direction is restricted by the use of canister lifting device spacers attached to the inner surface of the TAD TO lid. These spacers have a height of 6.25" and are made of Aluminum 6063. A canister lifting device is attached to the top of the TN44B canister. The TN44B canister lifting device has a height of 6.00" and is made of ASTM A182 Type F316N or ASTM A240 Type 316N.

To bound the expansion between the TN44B canister and the TAD TO inner cavity in the axial direction, the average temperature of the TAD-TO canister lifting device spacer with a height of 6.25" is considered equal to the average temperature of the canister shell.

Thermal expansion of the TN44B DSC and the TN44B DSC Lifting Device spacer in the axial direction when exposed to the hot environment is:

$$L_{Canister,Hot} = L_{Canister,Cold}[1+\alpha_{CAN}(T_{avg,CAN,Shell} - T_{ref})]$$

$$L_{CAN,Lift,Hot} = L_{CAN,Lift,Cold}[1+\alpha_{CAN,Lift}(T_{avg,CAN,Lift} - T_{ref})]$$

where:

- $L_{Canister,Hot}$ = Maximum hot length of the TN44B DSC, *in*
- $L_{Canister,Cold}$ = Maximum cold length of the TN44B DSC, *in*
- $L_{CAN,Lift,Cold}$ = Length of the TN44B DSC lifting device spacer, *in*
- $L_{CAN,Lift,Hot}$ = Hot Length of the TN44B DSC lifting device spacer, *in*
- α_{CAN} = Thermal expansion coefficient of TN44B DSC shell material, 10^{-6} in./in./°F
- $\alpha_{CAN,Lift}$ = Thermal expansion coeff. of TN44B DSC lifting device spacer, 10^{-6} in./in./°F
- $T_{avg,CAN,Lift}$ = Volumetric average temperature of TN44B DSC lifting device spacer, ^{o}F
- $T_{avg,Shell,TO}$ = Volumetric average temperature of MP197TAD TO inner shell, ^{o}F
- T_{ref} = Reference temperature = 70°F

The maximum length of each TN44B DSC and TN44B DSC Lifting Device spacer is calculated as noted above and is presented in the table below.

Maximum Length of Hot TN44B DSC and TN44B DSC Lifting Device

Ambient Temperature	$T_{avg,DSC}$	α_{CAN}	$L_{Cansiter,Hot}$	$\alpha_{CAN,Lift}$	$L_{CAN,Lift,Hot}$
°F	°F	$°F^{-1}$	in.	$°F^{-1}$	in.
-40°F	261	9.12E-06	196.592	1.31E-05	6.266
-20°F	276	9.15E-06	196.620	1.32E-05	6.267
100°F	363	9.43E-06	196.792	1.35E-05	6.275

The length of the MP197TAD TO cavity, $L_{Cavity,TO,Cold}$ at room temperature is 206 in. The length of the MP197TAD TO cavity when exposed to the hot environment is:

$$L_{Cavity,TO,Hot} = L_{Cavity,TO,Cold}[1+\alpha_{Shell,TO}(T_{avg,Shell,TO} - T_{ref})]$$

where:

- $L_{Cavity,TO,Hot}$ = Hot MP197TAD TO cavity length, *in*
- $L_{Cavity,TO,Cold}$ = Cold MP197TAD TO cavity length, *in*
- $\alpha_{Shell,TO}$ = Thermal expansion coefficient of MP197TAD TO inner shell material, 10^{-6} in./in./°F
- $T_{avg,Shell,TO}$ = Volumetric average temperature of MP197TAD TO inner shell, ^{o}F
- T_{ref} = Reference temperature = 70°F

The minimum length of the hot MP197TAD TO cavity is calculated in the table below.

Minimum Length of Hot MP197TAD TO Cavity

Ambient Temperature	$T_{avg,Shell,TO}$	$\alpha_{Shell,TO}$	$L_{Shell,TO,Hot}$
°F	°F	$°F^{-1}$	in.
-40°F	196	8.89E-06	206.231
-20°F	213	8.95E-06	206.264
100°F	308	9.23E-06	206.453

The resulting hot axial gap between the TN44B DSC (and TN44B DSC Lifting Device) and the MP197TAD TO cavity is calculated as follows and is listed in the table below.

$$\Delta_{HOT\_GAP,AXIAL} = L_{Cavity,TO,Hot} - (L_{Canister,Hot} + L_{CAN,Lift,Hot})$$

Axial Hot Gap

Ambient Temperature	Axial Hot Gap, $\Delta_{HOT\_GAP,AXIAL}$
°F	in.
-40°F	3.373
-20°F	3.377
100°F	3.386

Adequate clearance has been provided between the TN44B DSC and the MP197TAD TO cavity length to permit free thermal expansion.

B.2.13.10.4 Results and Conclusions

Based on the results of the above analyses, there is adequate clearance between the various components of the TN44B DSC and MP197TAD TO to allow free thermal expansion. Consequently, no significant stress will develop in the NUHOMS® MP197TAD TO due to thermal expansion. The following table summarizes the thermal expansion calculation results from the above analyses.

Thermal Expansion of MP197TAD TO Components

Ambient Temperature	Hot Diametrical Gap	Hot Axial Gap
°F	in	in
-40°F	0.706	3.373
-20°F	0.708	3.377
100°F	0.712	3.386

B.2.13.10.5 Reference

1. ANSYS Computer Code and User's Manual, Release 8.1 and 10.0.

Appendix B.2.13.12
MP197TAD TO Impact Limiter Analysis Using LS-DYNA

CONTENTS

B.2.13.12.1 Introduction B.2.13.12-1
B.2.13.12.2 NUHOMS®-MP197 Transport Package 1/3 Scale Impact Limiter Drop Testing B.2.13.12-1
B.2.13.12.3 MP197 1/3 Scale LS-DYNA Benchmark Analysis B.2.13.12-2
B.2.13.12.4 1/3 Scale Impact Limiter Benchmark Analysis Results B.2.13.12-6
B.2.13.12.5 MP197TAD TO Transport Package LS-DYNA Impact Analysis B.2.13.12-8
B.2.13.12.6 Analysis Results B.2.13.12-13
B.2.13.12.7 Additional Analysis Results for Slap Down Drop Analyses B.2.13.12-13
B.2.13.12.8 Sensitivity Studies of MP197TAD TO Impact Limiter Analysis B.2.13.12-13
B.2.13.12.9 Baseline g Loads for Structural Evaluations B.2.13.12-14
B.2.13.12.10 Impact Limiter Bolt Evaluation B.2.13.12-15
B.2.13.12.11 References B.2.13.12-23

LIST OF TABLES

Table B.2.13.12-1 Effective Plastic Strain vs. Scale Factor for Concrete Material B.2.13.12-24
Table B.2.13.12-2 Tabulated Pressures vs. Volumetric Strain for Concrete Material B.2.13.12-24
Table B.2.13.12-3 Wood Segment Material Properties at Room Temperature B.2.13.12-25
Table B.2.13.12-4 Wood Segment Material Properties at - 20 °F Temperature B.2.13.12-25
Table B.2.13.12-5 Pressure vs. Volumetric Strain for Wood Properties at Room Temperature B.2.13.12-26
Table B.2.13.12-6 Pressure vs. Volumetric Strain for Wood Properties at -20 °F B.2.13.12-27
Table B.2.13.12-7 Peak Nodal Accelerations, Wood Crush Depths, and Impact Duration Comparisons B.2.13.12-28
Table B.2.13.12-8 Summary of the Full Scale Impact Limiter Analysis Results B.2.13.12-29
Table B.2.13.12-9 Calculation of Total Moment B.2.13.12-30
Table B.2.13.12-10 Summary of Stresses (ksi) B.2.13.12-31

LIST OF FIGURES

Figure B.2.13.12-1 1/3 Scale Impact Limiter Finite Element Model Overview B.2.13.12-32
Figure B.2.13.12-2 1/3 Scale Impact Limiter Finite Element Model for Side Drop B.2.13.12-33
Figure B.2.13.12-3 1/3 Scale Impact Limiter Finite Element Model for End Drop B.2.13.12-34
Figure B.2.13.12-4 1/3 Scale Impact Limiter Finite Element Model for 20° Slap Down Drop B.2.13.12-35
Figure B.2.13.12-5 Plot of Maximum Deformation for 1/3 Scale Side Drop B.2.13.12-36
Figure B.2.13.12-6 Plot of Maximum Deformation for 1/3 Scale End Drop (-20°F) B.2.13.12-37
Figure B.2.13.12-7 Plot of Maximum Deformation for 1/3 Scale 20° Slap Down Drop (First Impact) B.2.13.12-38
Figure B.2.13.12-8 Plot of Maximum Deformation for 1/3 Scale 20° Slap Down Drop (Second Impact) B.2.13.12-39
Figure B.2.13.12-9 1/3 Scale Side Drop Acceleration Time History (From LS-DYNA) B.2.13.12-40
Figure B.2.13.12-10 1/3 Scale Side Drop Acceleration Time History, Accelerometer 1 ..... B.2.13.12-41
Figure B.2.13.12-11 1/3 Scale Side Drop Acceleration Time History, Accelerometer 10 ..... B.2.13.12-42

Figure B.2.13.12-12 1/3 Scale End Drop (-20°F) Acceleration Time History (From LS-DYNA) B.2.13.12-43
Figure B.2.13.12-13 1/3 Scale End Drop (-20°F) Acceleration Time History, Accelerometer 11 ..... B.2.13.12-44
Figure B.2.13.12-14 1/3 Scale End Drop (-20°F) Acceleration Time History, Accelerometer 7 ..... B.2.13.12-45
Figure B.2.13.12-15 1/3 Scale 20° Slap Down Drop Acceleration Time History - First Impact (From LS-DYNA) B.2.13.12-46
Figure B.2.13.12-16 1/3 Scale 20° Slap Down Drop Acceleration Time History - Second Impact (From LS-DYNA) B.2.13.12-47
Figure B.2.13.12-17 1/3 Scale 20° Slap Down Drop Acceleration Time History, Accelerometer 10 (First Impact) B.2.13.12-48
Figure B.2.13.12-18 1/3 Scale 20° Slap Down Drop Acceleration Time History, Accelerometer 1 (Second Impact) B.2.13.12-49
Figure B.2.13.12-19 MP197TAD TO Impact Limiter Finite Element Model Overview B.2.13.12-50
Figure B.2.13.12-20 MP197TAD TO Impact Limiter Finite Element Model for End Drop Orientation B.2.13.12-51
Figure B.2.13.12-21 MP197TAD TO Impact Limiter Finite Element Model for Side Drop Orientation B.2.13.12-52
Figure B.2.13.12-22 MP197TAD TO Impact Limiter Finite Element Model for CG Over Corner Orientation B.2.13.12-53
Figure B.2.13.12-23 MP197TAD TO Impact Limiter Finite Element Model for 20° Slap Down Orientation B.2.13.12-54
Figure B.2.13.12-24 MP197TAD TO Impact Limiter Finite Element Model for 15° Slap Down Orientation B.2.13.12-55
Figure B.2.13.12-25 MP197TAD TO Impact Limiter Finite Element Model for 10° Slap Down Orientation B.2.13.12-56
Figure B.2.13.12-26 Regions of Nodes Averaged for Time History B.2.13.12-57
Figure B.2.13.12-27 MP197TAD TO 30' End Drop Acceleration Time History (Room Temperature) B.2.13.12-58
Figure B.2.13.12-28 MP197TAD TO 30' End Drop Acceleration Time History (-20°F) B.2.13.12-59
Figure B.2.13.12-29 MP197TAD TO 30' Side Drop Acceleration Time History B.2.13.12-60
Figure B.2.13.12-30 MP197TAD TO 30' CG Over Corner Drop Acceleration Time History B.2.13.12-61
Figure B.2.13.12-31 MP197TAD TO 30' 20° Slap Down Drop Acceleration Time History (First Impact) B.2.13.12-62
Figure B.2.13.12-32 MP197TAD TO 30' 20° Slap Down Drop Acceleration Time History (Second Impact) B.2.13.12-63
Figure B.2.13.12-33 MP197TAD TO 30' 15° Slap Down Drop Acceleration Time History (First Impact) B.2.13.12-64
Figure B.2.13.12-34 MP197TAD TO 30' 15° Slap Down Drop Acceleration Time History (Second Impact) B.2.13.12-65
Figure B.2.13.12-35 MP197TAD TO 30' 10° Slap Down Drop Acceleration Time History (First Impact) B.2.13.12-66
Figure B.2.13.12-36 MP197TAD TO 30' 10° Slap Down Drop Acceleration Time History (Second Impact) B.2.13.12-67
Figure B.2.13.12-37 MP197TAD TO 1 Foot Normal Condition End Drop Acceleration Time History B.2.13.12-68
Figure B.2.13.12-38 MP197TAD TO 1 Foot Normal Condition Side Drop Acceleration Time History B.2.13.12-69
Figure B.2.13.12-39 Plot of Maximum Deformation for MP197TAD TO 30' End Drop B.2.13.12-70

Figure B.2.13.12-40 Plot of Maximum Deformation for MP197TAD TO 30' End Drop (-20 °F) B.2.13.12-71
Figure B.2.13.12-41 Plot of Maximum Deformation for MP197TAD TO 30' Side Drop B.2.13.12-72
Figure B.2.13.12-42 Plot of Maximum Deformation for MP197TAD TO 30' CG Over Corner Drop B.2.13.12-73
Figure B.2.13.12-43 Plot of Maximum Deformation for MP197TAD TO 30' 20° Slap Down Drop (First Impact) B.2.13.12-74
Figure B.2.13.12-44 Plot of Maximum Deformation for MP197TAD TO 30' 20° Slap Down Drop (Second Impact) B.2.13.12-75
Figure B.2.13.12-45 Plot of Maximum Deformation for MP197TAD TO 30' 15° Slap Down Drop (First Impact) B.2.13.12-76
Figure B.2.13.12-46 Plot of Maximum Deformation for MP197TAD TO 30' 15° Slap Down Drop (Second Impact) B.2.13.12-77
Figure B.2.13.12-47 Plot of Maximum Deformation for MP197TAD TO 30' 10° Slap Down Drop (First Impact) B.2.13.12-78
Figure B.2.13.12-48 Plot of Maximum Deformation for MP197TAD TO 30' 10° Slap Down Drop (Second Impact) B.2.13.12-79
Figure B.2.13.12-49 Plot of Maximum Deformation for MP197TAD TO 1 Foot Normal Condition End Drop B.2.13.12-80
Figure B.2.13.12-50 Plot of Maximum Deformation for MP197TAD TO 1 Foot Normal Condition Side Drop B.2.13.12-81
Figure B.2.13.12-51 Locations of Nodes Used to Compute Rotational Acceleration for MP197TAD TO B.2.13.12-82
Figure B.2.13.12-52 Vertical Acceleration Along Cask During First and Second Impact for 20° Slap Down Drop (Used to Compute Rotational Acceleration) B.2.13.12-83
Figure B.2.13.12-53 Vertical Acceleration Along Cask During First And Second Impact for 15° Slap Down Drop (Used to Compute Rotational Acceleration) B.2.13.12-84
Figure B.2.13.12-54 Vertical Acceleration Along Cask During First And Second Impact for 10° Slap Down Drop (Used to Compute Rotational Acceleration) B.2.13.12-85
Figure B.2.13.12-55 Bolt Forces Around Top and Bottom Impact Limiters for MP197TAD TO 20° Slap Down Drop B.2.13.12-86
Figure B.2.13.12-56 Bolt Forces Around Top and Bottom Impact Limiters for MP197TAD TO 15° Slap Down Drop B.2.13.12-87
Figure B.2.13.12-57 Bolt Forces Around Top and Bottom Impact Limiters for MP197TAD TO 10° Slap Down Drop B.2.13.12-88
Figure B.2.13.12-58 Cask Rigid Body Resultant Acceleration for MP197TAD TO 20° Slap Down Drop B.2.13.12-89
Figure B.2.13.12-59 Cask Rigid Body Resultant Acceleration for MP197TAD TO 15° Slap Down Drop B.2.13.12-90
Figure B.2.13.12-60 Cask Rigid Body Resultant Acceleration for MP197TAD TO 10° Slap Down Drop B.2.13.12-91
Figure B.2.13.12-61 Free Body Diagram of Top Impact Limiter during Shallow Angle Slap Down Drop B.2.13.12-92

Appendix B.2.13.12
MP197TAD TO Impact Limiter Analysis Using LS-DYNA

NOTE: References in this appendix are shown as [1], [2], etc., and refer to the reference list in Section B.2.13.12.11.

B.2.13.12.1 Introduction

The results of the 1/3 scale drop tests of the impact limiters previously performed for the NUHOMS®-MP197 transport package [1] are used to benchmark the analysis model and methodology for the NUHOMS®-MP197HB impact limiters. For this purpose, a 1/3 scale model of the NUHOMS®-MP197 in the tested configuration is developed and analyzed using the LS-DYNA [2] computer program, and the analysis results are compared to the 1/3 scale NUHOMS®-MP197 drop test results as described in Appendix A.2.10.9 of the NUHOMS®-MP197 SAR. The benchmarked model, methodology, and material properties are then used to develop the full scale MP197TAD TO LS-DYNA model as described in Section B.2.13.12.5.

B.2.13.12.2 NUHOMS®-MP197 Transport Package 1/3 Scale Impact Limiter Drop Testing

A series of drop tests have been previously performed on a one-third scale mockup of the MP197 transport package equipped with impact limiters. The test program details and test results are described in Appendix 2.10.9 of the NUHOMS®-MP197 SAR. The tests were performed to evaluate impact limiter performance for the 30 foot free drop hypothetical accident conditions. The cask was dropped in three different orientations, including a 90° end drop, 0° side drop and a 20° slap down. The 90° end drop orientation was performed with the impact limiters chilled to -20 °F in order to analyze the effects of low temperature on impact limiter performance.

For purposes of carrying out the testing program, four 1/3 scale impact limiters were constructed and tested. These are identified as impact limiter numbers 1, 2, 3, and 4 in the table below. The various drop test orientations were performed in the sequence shown in the following table.

Test Number	Drop Orientation	Drop Height	Impact Limiter Number	Location of Impact Limiter in Cask
1	0° Side Drop	30 Feet	1	Top
			2	Bottom
2	20° Slap Down	30 Feet	3	Top (2^{nd} Impact)
			2	Bottom (1^{st} Impact)
3	90° End Drop	30 Feet	3	Top
			4	Bottom (Impact End, -20°F)

B.2.13.12.3 MP197 1/3 Scale LS-DYNA Benchmark Analysis

This section describes the series of analysis used to benchmark the impact limiter analysis methodology against the results of the 1/3 scale impact limiter drop testing program documented in Appendix 2.10.9 of this SAR. For this purpose a finite element model of the 1/3 scale MP197 cask mockup equipped with impact limiters is developed using the LS-DYNA computer program [2]. The LS-DYNA finite element model is analyzed for the same three hypothetical accident conditions as those in the test program, as summarized in Section B.2.13.12.2: 30' end drop (-20 °F), 30' side drop (room temperature), and 30' 20° slap down (room temperature). The finite element analysis results are compared to the actual drop test results documented in Appendix 2.10.9 of this SAR, to benchmark the adequacy of the finite element model.

A. Description of Finite Element Model

The finite element analysis model is a representation of the surrogate 1/3 scale MP197 cask used for the actual drop tests with an impact limiter installed on each end of the cask. The impact limiter model incorporates the individual balsa or redwood sections that make up the impact limiter and the stainless steel cover shell. The impact limiter incorporates a thermal shield consisting of an aluminum plate interfacing with the cask and aluminum spacer blocks that create a thermal gap with the cask lid at each end. The finite element model includes the aluminum spacer blocks. The aluminum plate itself is not modeled as it would have negligible contribution to the structural performance of the cask. Additional features such as the impact limiter attachment bolts and alignment tubes are also included in the LS-DYNA model. The impact surface, which consists of a steel plate over a thick concrete pad is also included in the model.

The impact limiter wood sections, the concrete pad and steel plate are modeled in LS-DYNA using fully integrated S/R 8-node solid elements. The cask model and aluminum thermal spacer blocks are modeled with fully integrated quadratic 8 node elements. The impact limiter shell is modeled with fully integrated shell elements.

The impact limiter attachment bolts and associated inner and outer bolt tubes are modeled as a combination of spring elements and beam elements. The outer alignment tubes and inner welded bolt tubes are modeled as beam elements with the proper dimensions. The inner bolt tube is welded to the stainless steel impact limiter shell. The section of bolt extending from the bolt boss to the impact limiter shell is modeled as a beam section. The beam is fixed to the bolt boss on one end. The other end is fixed to the impact limiter shell in a way that approximates the bolt penetrating the shell. For the end drop condition, this end of the beam is coupled to the shell in the X and Y directions. For the side drop and slap-down conditions, this end of the beam is coupled to the shell in the Y and Z directions. The remaining section of bolt is modeled as a non-linear spring. The spring has a tensile stiffness and a negligibly small compression stiffness. This is done in order to model the bolt slipping through the tube during compression. The small compression spring rate prevents instabilities within LS-DYNA. Bolts located on the axis of symmetry are modeled with modified dimensions that have half the moment of inertia and half the cross sectional area.

Only one-half of the cask, impact limiters, steel plate and concrete are modeled, as the entire arrangement is reasonably symmetric about the x-y plane. The distribution of the thermal shield spacer blocks is not symmetric to the plane of symmetry. However, the slight asymmetry is negligible since the effect of the blocks is still captured.

The three analyzed drop accident conditions are as follows:

1. 30' end drop (-20°F)
2. 30' side drop (room temperature)
3. 30' 20° slap down (room temperature)

Drop models have consistent room temperature wood properties except the chilled end drop which has modified wood properties to simulate a -20°F environment. The slap down scenario has the cask initially rotated 20° from the horizontal side drop position and includes an impact limiter at both ends.

The finite element model and different drop orientations can be seen in Figure B.2.13.12-1 through Figure B.2.13.12-4.

B. Cask Model and Steel Plate Material

The cask model and steel impact plate are modeled as A36 steel with the following properties:

$E = 27.7\times10^6$ psi
$v = 0.3$
$S_y = 30.0$ ksi
Tangent Modulus, $E_T = 2\%\ E = 5.540\times10^5$ psi

C. Impact Limiter Shell Material

The impact limiter shell is modeled as SA-240 Type 304 stainless steel with the following properties:

$E = 28.3\times10^6$ psi
$v = 0.3$
$S_y = 30.0$ ksi
Tangent Modulus, $E = 1.0X10^5$ psi
Strain Failure, $\varepsilon = 0.3$
Mass density, $\rho_{eff} = 9.405\times10^{-4}$ lb sec^2/in^4

The density of the impact limiter shell is adjusted to account for the weight of those components not included in the model, such as the lifting lugs. The measured weight of the actual 1/3 scale cask mockup with both impact limiters installed is 9,750 lbs.

D. Concrete Material

The concrete is modeled using material law 16 in LS-DYNA, which was developed specifically for granular type materials. Material constants are implemented into Material Model 16, Mode II.B in LS-DYNA. The material modeled represents 4,200 psi compressive strength concrete. A summary of the input used in the analysis is as follows:

Yield stress versus pressure relationships used:

$$\sigma_{\max} = a_0 + \frac{P}{a_1 + a_2 P}$$

$$\sigma_{failed} = a_{0f} + \frac{P}{a_{1f} + a_2 P}$$

$\rho = 2.09675 \times 10^{-4}$ lb. sec.^{2} / in.^{4}
$v = 0.22$
$a_0 = 1606$
$a_1 = 0.418$
$a_2 = 8.35 \times 10^{-5}$
$b_1 = 0$
$a_{0f} = 0.0$ psi.
$a_{1f} = 0.385$

The above yield stress versus pressure curves are used to describe either a hardening or softening behavior of the concrete material, as follows:

$$\sigma_{yield} = \sigma_{failed} + \eta(\sigma_{\max} - \sigma_{failed})$$

The scale factor η as a function of plastic strain is tabulated in Table B.2.13.12-1.

The maximum principal stress tensile failure cutoff is set at 870 psi. Strain rate effects are neglected in the analysis.

The pressure-volume behavior of the concrete is modeled with the pressure versus volumetric strain relationship shown in Table B.2.13.12-2 using the equation of state feature (EOS_Tabulated_Compaction) in LS-DYNA.

An unloading bulk modulus of 700,000 psi is assumed to be constant at any volumetric strain.

One percent reinforcement is assumed in the concrete pad to account for the pad reinforcement. The material properties used for the reinforcing bar are as follows.

$E = 30 \times 10^6$ psi.
$v = 0.3$

S_y = 30,000 psi.
Tangent Modulus, $E_T = 30 \times 10^4$ psi.

E. Impact Limiter Wood Segment Material

The impact limiter wood is modeled using the Mat_Modified_Honeycomb material model in LS-DYNA (material type 126), which models crushable materials with anisotropic behavior. References [4] and [5] document the use of *Mat _Honeycomb* material model in LS-DYNA to model wood in a similar application. Since the crush strength of wood is not isotropic, separate material properties are used in directions parallel and perpendicular to the wood grain. Strain rate effects are neglected in the analysis. Table B.2.13.12-3 summarizes the wood segment material properties [3]. Table B.2.13.12-4 summarizes the wood segment material properties increased by 20% [3] for the -20° F temperature condition. All redwood and balsa materials have a strain failure of 0.4, which is conservatively high.

The pressure versus volumetric strain relationship defines the crush strength of the wood segments. Table B.2.13.12-5 shows the pressure versus strain curves for redwood and balsa parallel and perpendicular to the wood grain for the average room temperature wood properties [3]. Table B.2.13.12-6 shows the same for the 20% increased wood properties for the -20° F ambient condition. The pressure strain curve is assumed to be initially linear with a slope of the modulus of elasticity E, and then flat up to a locking strain of 0.8 for balsa and 0.6 for redwood.

F. Bolt and Alignment Tube Material

There are 12 bolts that attach each impact limiter to the cask. The following elastic, linearly plastic material properties are used for the bolts in the finite element model.

SA-540 GR. B24 CL. 1
$E = 27.8 \times 10^6$ psi
$v = 0.3$
$S_y = 75.0$ ksi
Tangent Modulus, $E_T = 2\%\ E = 5.56 \times 10^5$ psi

The bolts that attach the impact limiters to the cask are modeled as circular cross section beams. For the side drop and slap down conditions, the bolt tube sections at the symmetry plane are modeled as hollow circular cross section beams with modified dimensions to represent half the area and moment of inertia.

The springs representing the sections of bolts within the impact limiter were given spring rates representing that of the bolt. The length of bolt used for the spring rate calculation is 10". For the side drop and slap down conditions, the springs at the plane of symmetry were given half the spring rate. The springs at the plane of symmetry for the end drop condition were left unchanged as the bolts would be in compression and therefore would have negligible affect on the analysis.

Bolt alignment tubes are modeled as tube beams. The alignment tubes modeled at the plane of symmetry are also full-size as their strength difference is minimal in this analysis. The following elastic, linearly plastic material properties are used for the bolt tubes:

SA-249 Type 304

$E = 28.3 \times 10^6$ psi
$v = 0.3$
$S_y = 30.0$ ksi
Tangent Modulus, $E = 10^5$ psi

G. Boundary Conditions and Initial Conditions

One-half of the cask and impact limiters are modeled with symmetry boundary conditions used to simulate the full structure. The lowest point of the impact limiter shell is initially placed within 0.25" of the steel impact plate to minimize run time. An initial velocity corresponding to the drop height is applied to the model. The initial velocity computed for a 30' drop is 527.45 in/sec.

The automatic surface-to-surface contact definition in LS-DYNA (*Contact_Automatic_Single_Ssurface*) is applied to model for the contact between any two parts of the model. A conservatively low coefficient of friction of 0.25 is applied between all the contact surfaces. The use of a low value for the coefficient of friction is conservative because less energy is absorbed due to friction resulting in greater impact acceleration forces.

An interior contact (Contact_Interior) contact definition is applied to the elements modeling the wood sections to prevent hourglassing due to the high level of deformation. Hourglassing occurs when an element undergoes extreme deformation and inverts to a negative volume.

Non-reflecting boundaries are applied to the bottom and sides of the modeled concrete not aligned with the plane of symmetry (bottom, left side, right side, and back) to prevent artificial stress waves from reflecting.

B.2.13.12.4 1/3 Scale Impact Limiter Benchmark Analysis Results

Table B.2.13.12-7 summarizes the results of the LS-DYNA analysis in terms of peak filtered accelerations, maximum crush depths, and impact durations for the three drop cases analyzed and compare them with similar parameters obtained from the test results. The maximum accelerations from the tests and the LS-DYNA analyses model are divided by three to represent the accelerations of a full scale MP197 cask. Impact durations and crush depths are unchanged (compare 1/3 scale analysis results to1/3 scale test results). Figures B.2.13.12-5 through B.2.13.12-8 show the deformed shapes of the impact limiters for each drop case analyzed.

The acceleration time histories from the LS-DYNA analyses and from the 1/3 scale testing are shown in the figures summarized in the table below:

Drop Test Case	Figures from LS-DYNA Analysis	Figures from 1/3 Scale Testing	
Side Drop	Figure B.2.13.12-9	Figure B.2.13.12-10	Figure B.2.13.12-11
End Drop	Figure B.2.13.12-12	Figure B.2.13.12-13	Figure B.2.13.12-14
20° Slap Down	Figure B.2.13.12-15 (1st Impact)	Figure B.2.13.12-17 (1st Impact)	
	Figure B.2.13.12-16 (2nd Impact)	Figure B.2.13.12-18 (2nd Impact)	

As described in Appendix 2.10.9 of this SAR, accelerometers were used to measure the response deceleration time histories for each test. The accelerometers were placed along the test body at 0°, 90°, 180°, and 270° orientations at approximately the center of gravity location and adjacent to each impact limiter.

The test response acceleration time histories shown in Figures B.2.13.12-10, -11, -13, -14, -17, and -18 are representative of the test case indicated. The peak g load calculated from the LS-DYNA analysis is compared with the measured averaged g loads from all the accelerometers.

The analysis results shown in Table B.2.13.12-7 agree well with the measured results of the impact limiter drop tests. The LS-DYNA accelerations are slightly higher due to the conservatism in analysis. The impact time durations match closely with those of the measured results. Wood crush depths are also similar. Therefore, it can be concluded that the LS-DYNA model and analysis methodology implemented as described in this section accurately predicts the response of the impact limiters during the accidental drop.

B.2.13.12.5 MP197TAD TO Transport Package LS-DYNA Impact Analysis

The benchmarked model and analysis methodology used for the 1/3 scale LS DYNA analysis of the MP197 described in Section B.2.13.12.3 are used to develop a full scale LS-DYNA model of the MP197TAD TO transport cask equipped with impact limiters. The model is used to determine the rigid body acceleration time history and impact limiter crush depths for the following hypothetical drop conditions:

1. 30' End Drop (room temperature)
2. 30' End Drop (-20°F)
3. 30' Side Drop
4. 30' CG Over Corner Drop
5. 30' 20° Slap Down
6. 30' 15° Slap Down
7. 30' 10° Slap Down
8. 1' Normal Condition End Drop
9. 1' Normal Condition Side Drop

Impact limiter attachment bolt forces are also determined for the slap down drop scenarios.

A. Finite Element Model Description

A finite element model of the MP197TAD TO transport cask with impact limiters installed at each end of the cask is developed in order to determine the cask's rigid body acceleration and impact limiter crush depths due to normal conditions of transport and hypothetical accident condition drop scenarios.

Because of the complexity of the analysis, the modeled cask is a simplified version of the actual MP197TAD TO transport cask. The simplified cask model maintains the same geometry as the actual cask in those areas that interface with the impact limiters. However, density and other dimensions are modified so that the modeled cask has the same dynamic characteristics (mass, center of gravity, and mass moments of inertia properties) as the actual MP197TAD TO cask.

The material properties used in the analysis of the MP197TAD TO cask are the same as those used for the 1/3 scale MP197 benchmarking analysis described in Section B.2.13.12.3. The density of the modeled cask and the stainless steel impact limiter shell are modified in order to duplicate the dynamic characteristics of the actual MP197TAD TO cask. The failure strain of the stainless steel shell has been increased from 0.3 to 0.8. This is conservative as it would only increase impact acceleration.

The finite element analysis model includes a representation of the actual MP197TAD TO cask with an impact limiter installed on each end of the cask. The impact limiter section of the model incorporates the individual balsa or redwood sections that make up the impact limiter and the stainless steel cover shell. The aluminum spacer rings of the thermal shield are included in the model. The model includes a concrete block with a steel plate on top to represent the impact

surface. Only ½ of the cask, impact limiters, steel plate and concrete are modeled as the entire arrangement is reasonably symmetric about the x-y plane.

The impact limiter wood sections, cask model, concrete pad and steel plate are modeled in LS-DYNA using fully integrated S/R 8-node solid elements. The aluminum thermal spacer rings are modeled with fully integrated quadratic 8 node elements. The impact limiter shell is modeled with fully integrated shell elements.

Additional features, such as the impact limiter attachment bolts and associated outer alignment and inner welded tubes are modeled as a combination of spring elements and beam elements. The alignment tubes and welded tubes are modeled as beam elements welded to the stainless steel impact limiter shell.

The drop scenarios analyzed include the hypothetical accident condition drop with a drop height of 30 feet and the 1-foot normal condition of transport drop. Wood properties at room temperatures are used for all analysis cases except for the 30 feet end drop for which modified wood properties to simulate a -20°F environment is used. The CG over corner drop is 66.4° from the horizontal side drop position. The slap down cases are 20°, 15°, and 10° from the horizontal side drop position.

Figures B.2.13.12-19 through B.2.13.12-25 show the MP197TAD TO finite element model and the different drop orientations analyzed.

B. Material Properties

The material properties used in this analysis are the same as those used for the 1/3 Scale MP197 Drop Analysis Benchmark. The material properties required to perform the analysis include modulus of elasticity, E, shear modulus, G, Poison's ratio, v, and material density, ρ, for the cask model, impact limiter shell, wood segments, steel plate and concrete.

C. Cask Model and Steel Plate Material

The following elastic, linearly plastic material properties for mild steel (A-36) are used for the steel plate and cask model.

$E = 27.7\times10^6$ psi
$v = 0.3$
$S_y = 30.0$ ksi
Tangent Modulus, $E_T = 2\%\ E = 5.540\times10^5$ psi

D. Cask Model

The cask model has the same mass, center of gravity, and moment of inertia as the actual cask. The critical moment of inertia is about Y-axis which is perpendicular to the plane of symmetry of the model. The moments of inertia about the other two axes do not influence this analysis due to the boundary conditions.

The dimensions and density of the modeled cask are adjusted to have the same mass, center of gravity, and moment of inertia as the actual cask. The geometry of the modeled cask is similar to the actual cask except that the center section has a smaller diameter. The reduced diameter area is offset from the geometric center to affect the center of gravity.

E. Impact Limiter Shell

The following elastic, linearly plastic material properties are used for the impact limiter shell.

Stainless Steel (SA-240 Type 304)

$E = 28.3\times10^6$ psi
$\nu = 0.3$
$S_y = 30.0$ ksi
Tangent Modulus = 10^5 psi
Strain Failure, $\varepsilon = 0.8$, conservatively high for model stability

The density of the impact limiter shell is adjusted to calibrate the weight of the impact limiter model. This is to take into account for the mass of those impact limiter parts not included in the model.

F. Concrete

The concrete material model and properties are identical to those used for the 1/3 scale MP197 model in Section B.2.13.12.3.

G. Impact Limiter Wood Segments

The impact limiter wood is modeled using the Mat_Modified_Honeycomb material model (Material type 126) in LS-DYNA, which models crushable materials with anisotropic behavior such as wood. Since the crush strength of wood is not isotropic, separate material properties are used in directions parallel and perpendicular to the wood grain. Wood crush strengths and density are taken from the MP197 1/3 Scale Benchmark Analysis. The redwood and balsa are modeled with a tensile failure strain of 0.4.

H. Bolt and Alignment Tubes

There are 12 bolts that attach each impact limiter to the cask model. The following elastic, linearly plastic material properties are used for the bolts.

SA-540 GR. B24 CL. 1
$E = 27.8\times10^6$ psi
$\nu = 0.3$
$S_y = 75.0$ ksi
Tangent Modulus, $E_T = 2\%\ E = 5.56\times10^5$ psi

Bolts at the symmetry plane are modeled as hollow circular cross section beams with modified dimensions to represent approximately half the moment of inertia. The cross sectional area of the bolts at the plane of symmetry is conservatively larger than half of the fullsize bolts.

Each bolt has a bolt alignment tube and a welded bolt tube. The following elastic, linearly plastic material properties are used for the bolt tubes:

SA-312 Type 304

$E = 28.3 \times 10^6$ psi
$\nu = 0.3$
$S_y = 30.0$ ksi
Tangent Modulus, $E = 10^5$ psi

Bolt alignment tubes and welded bolt alignment tubes are modeled as tube beams. Tubes at the plane of symmetry were modeled with complete section properties. The difference in strength is negligible

I. Boundary and Initial Conditions

Because of symmetry, one-half of the cask and impact limiters is modeled with symmetry boundary conditions in order to simulate the full structure. The initial velocity is computed by equating potential and kinetic energies. For a 30 foot drop, the initial velocity is 527.5 in/sec. For a 1 foot drop, the initial velocity is 96.3 in/sec.

An automatic surface to surface (contact_automatic_single_surface) contact definition is applied between all parts where contact is feasible. Due to the larger deformations of the impact limiters compared to those of the benchmark analysis, additional contact definitions are applied. An eroding surface to surface (contact_eroding_single_surface) contact definition is applied during cg over corner and side drops. Interior (contact_automatic_general_interior) contact definitions are also applied to the wood parts to prevent elements from inverting and becoming negative volumes due to large deformations and hourglassing. A conservatively low coefficient of friction (static and kinetic) of 0.25 is applied between all contact surfaces.

Non-reflecting boundaries are applied to the bottom and sides of the modeled concrete not aligned with the plane of symmetry (bottom, left side, right side, and back) to prevent artificial stress waves from reflecting. Both dilatation and shear waves are damped.

J. Data Reduction

The following table lists the duration of the analysis for each drop condition. The time step was automatically chosen by the LS-DYNA program based on the minimum model element size.

Drop Condition	Run Duration (sec)
30' End Drop (Room temperature)	0.05
30' End Drop (-20°F)	0.05
30' Side Drop	0.07
30' Slap Down 20°	0.2
30' Slap Down 25°	0.2
30' Slap Down 10°	0.2
30' CG Over Corner Drop	0.1
1' Normal Condition End Drop	0.05
1' Normal Condition Side Drop	0.05

The resulting nodal acceleration time histories are computed by LS-DYNA. The nodal accelerations averaged from the center region of nodes for the end drop and cg over corner. Results are averaged from the top region of nodes for the side drop due to the cg of the cask being biased towards the top of the cask. Slap down results are averaged for both the top and bottom of the cask due to the dual impacts. Figure B.2.13.12-26 shows the regions of nodes averaged.

The time step in the LS-DYNA analysis is 50 μsec. Therefore, by the Nyquist theorem, the frequency content of the nodal acceleration data ranges from zero Hz, up to the following maximum frequency, f_{max}.

$$f_{max} = \frac{1}{2}\frac{1}{50\times10^{-6}\,\text{sec}} = 10\,\text{kHz}$$

The natural frequencies of the MP197TAD TO cask model, which can be excited by an impact event, are significantly lower than 10kHz. These natural modes of the transport cask involve small displacements (and therefore low stresses) at frequencies higher than that of the rigid body motion of the transport cask. These high frequency accelerations mask the true rigid body motion of the transport cask, because both the low frequency rigid body acceleration and the high frequency natural vibration accelerations superimpose. The net acceleration is contained in the raw data computed by LS-DYNA. Therefore, filtering is necessary to remove these high frequency accelerations.

The averaged raw data for each cross section is filtered using a low pass Butterworth filter with different cutoff frequencies depending on the orientation of the model in order to recover the actual rigid body acceleration of the cask model. A 180 Hz cutoff frequency is used for the end drop conditions and the CG over corner drop. A 100 Hz cutoff frequency is used for side drop conditions including the slap down runs. The cutoff frequencies are conservative because they will filter out some but not all of the high vibration modes of the cask model in their respective

locations and drop orientations. Therefore, the response predicted by the filtered results includes more dynamics than simply the rigid body motion of the transport cask.

B.2.13.12.6 Analysis Results

Table B.2.13.12-8 summarizes the results of the LS-DYNA analysis in terms of peak filtered accelerations, impact durations, maximum crush depths, and provides the corresponding time history plot for the drop scenarios analyzed. Impact limiter crush depth is based on the deformation of the cask into the impact limiter in the vertical direction.

Impact durations are visually determined from the acceleration time history plots (Figures B.2.13.12-27 through B.2.13.12-38). Note that the units in Figures B.2.13.12-27 through B.2.13.12-38 are in/sec^2.

Figures B.2.13.12-39 through Figure B.2.13.12-50 show the impact limiter maximum deformation plots.

B.2.13.12.7 Additional Analysis Results for Slap Down Drop Analyses

The peak rotational acceleration is calculated for the slap down conditions based on the cask interface forces and rotational centers. Figure B.2.13.12-51 shows the locations of nodes groups selected to determine acceleration during peak acceleration of the first and second impacts. Figures B.2.13.12-52 through B.2.13.12.-54 show the plot results for the 20°, 15°, and 10° slap down drop cases.

The rotational centers are at 174.43" from the bottom for the first impact and 61.09" from the bottom for the second impact of the slap down 20°. The rotational centers are at 165.24" from the bottom for the first impact and 60.24" from the bottom for the second impact of the slap down 15°.The rotational centers are at 162.80" from the bottom for the first impact and 60.74" from the bottom for the second impact of the slap down 10°.

Axial and shear bolt forces at various positions around the impact limiter are plotted for the slap down 20°, 15° and 10° cases in Figures B.2.13.12-55 through B.2.13.12-57.

Rigid body accelerations for the entire cask model are shown in Figures B.2.13.12-58 through B.2.13.12-60 for the slap down 20°, 15°, and 10° runs.

B.2.13.12.8 Sensitivity Studies of MP197TAD TO Impact Limiter Analysis

This MP197TAD TO cask impact limiter analysis is similar to the MP197HB cask impact limiter analysis [1] in mesh size, bolt modeling, boundary conditions, wood property orientation, friction and overall model geometry. Therefore, the sensitivity studies performed for the MP197HB cask impact limiter analysis to show the adequacy of the model also apply to this MP197TAD TO cask impact limiter analysis.

The four following sensitivity studies were performed for the MP197HB cask impact limiter analysis.
1) Effect of wood element mesh density and effect of bolts on calculated impact load
2) Unyielding impact surface sensitivity
3) Bolt forces with radial perpendicular wood properties
4) Cask model geometry and friction sensitivity

B.2.13.12.9 Baseline g Loads for Structural Evaluations

Based on the LS-DYNA calculated impact accelerations shown in Table B.2.13.12-8, the wood property at -20°F temperature will increase the g load approximately by 11% (48.9/44.1=1.11). Therefore, the g loads resulting from room temperature are conservatively increased by 14% and used as baseline g loads for component structural evaluations. The following table shows the baseline g load to be used for the cask body structural evaluations.

Baseline g Loads for Cask Body Structural Evaluations

Drop Orientation		Peak rigid body deceleration	Factor	Baseline g Loads[(1)]
30' End Drop		44.1 g	1.14	51 g
30' Side Drop		51.6 g	1.14	59 g
30' CG Over Corner Drop		30.2 g (Vertical to ground)	1.14	35 g
30' Slap Down (10°)	1st Impact	Translation (23.0g)	1.14	27 g
		Rotational (α = 131.9 rad/sec^2)	1.14	α =150 rad/sec^2
	2nd Impact	Translation (28.9g)	1.14	33
		Rotational (α = 165.9 rad/sec^2)	1.14	α =189 rad/sec^2
30' Slap Down (15°)	1st Impact	Translation (21.7g)	1.14	25 g
		Rotational (α = 111.4 rad/sec^2)	1.14	α =127 rad/sec^2
	2nd Impact	Translation (27.9g)	1.14	32
		Rotational (α = 176.2 rad/sec^2)	1.14	α =201 rad/sec^2
30' Slap Down (20°)	1st Impact	Translation (23.6g)	1.14	27
		Rotational (α = 105.7 rad/sec^2)	1.14	α = 120 rad/sec^2
	2nd Impact	Translation (26.5g)	1.14	30
		Rotational (α = 175.6 rad/sec^2)	1.14	α = 200 rad/sec^2
1' End Drop		27.6 g	1.14	32
1' Side Drop		15.6 g	1.14	18

B.2.13.12.10 Impact Limiter Bolt Evaluation

The purpose of this section is to determine the stresses in the MP197TAD TO impact limiter attachment bolts and blocks.

The worst loading occurs in the top impact limiters attachment blocks during the second impact of a shallow angle slap–down drop.

Twelve impact limiter attachment bolts take the moment applied during a shallow angle slap–down drop.

One evaluation is made using the maximum tensile force found in Figure B.2.13.12-55 for a bolt during a 20 degree slap down drop, which is equal to 250,000 lb. The maximum tensile force F in a bolt considered in this case will be conservatively taken equal to 114% of that value, or 285,000 lb.

Due to lack of benchmarking of the previous method, another evaluation is made where the tensile force in the bolts is calculated by considering the equilibrium of moments each bolt is submitted to, conservatively assuming that:

1. The lateral force exerted on the impact limiter by the cask comes from the full weight of the cask (270,000 lbs) and is centered in the middle of the impact limiter cavity (at a distance 14.875 in from the bottom of the impact limiter);

2. The g load for the second impact of a 20 degree angle slap down drop is 30g;

3. The friction coefficient μ between the cask and the impact limiter and between the impact limiter and the impact surface is 0.42 [6], based on hard steel against hard steel friction properties.

Since the bottom impact limiter crushes during the first impact, the top impact limiter impacts with a slight angle during the second impact, and its bottom edge crushes first. Therefore, the reaction force on the impact limiter is located close to the bottom edge of the impact limiter. However, to maximize bolt forces, it is conservatively assumed that the reaction force is exerted on the other side of the lateral force exerted by the cask, at a distance from that lateral force equal to 10% of the depth of the impact limiter cavity.

Material mechanical properties for the impact limiter, attachment bolts, attachment bolts blocks and for the cask shell are taken at 350°F. However, material properties used for checking thread engagement length are taken at room temperature.

Nut factor for empirical relation between the applied torque and achieved preload is 0.135 for neolube lubricant.

B.2.13.12.10.1 Stress Calculations

A. Evaluation Based on the Calculated Tensile Force

A.1 Bolt Stress

The 1 ¾ – 5UNC attachment bolts are made of SA–540 Gr. B23, Cl. 1 (see Appendix B.1.4.1), which has an ultimate strength S_u = 165.0 ksi at 350°F [7].

The diameter D of the shank is 1.484 in. Its maximum diameter is 1.75 in (see Appendix B.1.4.1).

The critical tensile area of the attachment bolt is in the bolt shank since the threads are 1 ¾ – 5UNC. The minimum tensile area of the bolt is:

$$A = 0.25 \times \pi \times D^2 = 0.25 \times \pi \times 1.484^2 = 1.730 \text{ in}^2.$$

The tensile stress in the bolts is equal to:

$$\sigma = \frac{F}{A} = \frac{285{,}000}{1.730} = 164.7 \text{ ksi}$$

The allowable tensile stress in the impact limiter attachment bolts for hypothetical accident conditions of transport is taken equal to their ultimate strength, 165 ksi.

A.2 Attachment Bolt Block Analysis

The material used for the impact limiter bolts attachment blocks is SA-240 Type 304 or SA–182 Type F304 (S_u = 65.1 ksi). The material used for the cask body outer shell is SA–240 Type 304 (S_u = 65.1 ksi).

Each block (dimensions 6.81 × 8.00) is welded to the cask body with an all–around e = 0.75 in groove weld.

The allowable primary plus bending stress for the impact limiter bolts attachment blocks is taken to be the ultimate strength.

The allowable shear stress in the welds between the top flange of the cask and the attachment blocks is taken equal to 0.42 × S_u = 27.3 ksi, using the lowest ultimate strength value of the two.

The weld area of a single attachment bolt block is:

$$A_{weld} = L_1 \times L_2 - (L_1 - 2 \times e) \times (L_2 - 2 \times e)$$

Where L_1 and L_2 are the dimensions of the block (L_1 = 6.81 in and L_2 = 8.00 in), and e is the size of the weld (see above).

$$A_{weld} = 6.81 \times 8.00 - (6.81 - 2 \times 0.75) \times (8.00 - 2 \times 0.75) = 19.96 \text{ in}^2$$

The weld moment of inertia is:

$$I_{weld} = \frac{L_1 \times L_2^3 - (L_1 - 2\times e)\times (L_2 - 2\times e)^3}{12} = \frac{6.81\times 8.00^3 - 5.81\times 7.00^3}{12} = 124.5\ \text{in}^4$$

The maximum moment applied to the block weld is:

$$M_{weld} = F \times \frac{D_1 - D_2}{2}$$

Where D_1 is the bolt circle diameter, 83.00 in and D_2 the outer diameter of the cask, 79.00 in.

$$M_{weld} = 285{,}000 \times \frac{83.00 - 79.00}{2} = 570{,}000\ \text{in.lb}$$

The bending stress in the block weld is:

$$\sigma_b = \frac{M_{weld} \times {}^{L_2}\!/_{2}}{I_{weld}} = \frac{570{,}000 \times {}^{8}\!/_{2}}{169.0} = 13.5\ \text{ksi}$$

The shear stress in the block weld is:

$$\tau = \frac{F}{A_{weld}} = \frac{285{,}000}{19.96} = 14.3\ \text{ksi}$$

The stress intensity in the block weld is:

$$S.I. = \sqrt{\sigma_b^2 + 4\tau^2} = \sqrt{13.5^2 + 4\times 14.3^2} = 31.6\ \text{ksi}$$

B. Evaluation Based on Moments Equilibrium

B.1 Bolt Force

The lateral force exerted by the cask on the top impact limiter is equal to:
$R = W \times g = 270{,}000 \times 30 = 8{,}100{,}000$ lb

Where W is the weight of the cask and g is the g–load assumed for the second impact.

Figure B.2.13.12-61 shows the free body diagram of top impact limiter during slap down drop.

The location of the reaction force on the impact limiter when the second impact occurs is:

$$x_3 = x_1 + \frac{d}{10} = \frac{d}{2} + \frac{d}{10} = \frac{6\times d}{10} = 17.85\ \text{in}$$

Where d is the depth of the cavity in the impact limiter.

The crush depth of the top impact limiter is approximately 10.30 in. (see Table B.2.13.12-8). Therefore:

$$x_2 = \frac{O.D._{IL} - D_2}{2} - [Crush\ Depth] = \frac{125.00 - 79.00}{2} - 10.30 = 12.70\ \text{in}$$

Where $O.D._{IL}$ is the outer diameter of the impact limiter.

The moment applied to the impact limiter is (the associated force acts to pull the impact limiter away from the cask when the moment is clockwise):

$$M = (x_3 - x_1) \times R = (17.85 - 14.875) \times 8{,}100{,}000 = 2.41 \times 10^7\ \text{in.lb}\ \text{(clockwise)}.$$

There is also an additional frictional force that acts to pull the impact limiter away from the cask. The magnitude of this force is equal to:

$$F_f = \mu \times R = 0.42 \times 10{,}727{,}500 = 4.51 \times 10^6\ \text{lb}$$

The resulting moment due to friction is:

$$M_f = F_f \times x_2 = 3.40 \times 10^6 \times 12.70 = 4.32 \times 10^7\ \text{in.lb}\ \text{(clockwise)}$$

The total prying moment is:

$$M_{tot} = M_f + M = 4.32 \times 10^7 + 2.41 \times 10^7 = 6.73 \times 10^7\ \text{in.lb}\ \text{(clockwise)}$$

Assume that only the impact limiter bolts hold the impact limiters in place, and that the impact limiter tends to pivot around the edge of the cask. The force distribution among the bolts will be linearly proportional to their distance from the pivot point. The angular location α is measured from 0°, which corresponds to the upper vertical orientation.
The vertical distance is equal to:

$$V.D. = \frac{I.L._{DBC} \times \cos(\alpha) + O.D._{Cask}}{2}$$

Where $I.L._{DBC}$ is the bolt circle diameter for the impact limiters (83.00 in).

Negative vertical distances correspond to bolts that are below the crush line of the impact limiter. These bolts are conservatively considered to be ineffective and do not carry any of the prying load.

The bolts farthest away from the target surface (bolts 1 and 12) are assumed to carry the maximum tensile force F_{max}. All other bolts are assumed to carry a tensile force linearly proportional to their distance from the target surface. Therefore, each bolt carries the prying moment listed in Table B.2.13.12-9.

The tensile force f_i and moment m_i for bolt i of moment arm x_i are:

$$f_i = \frac{x_i}{\max(x_i)} F_{max} \quad \text{and} \quad m_i = \frac{x_i^2}{\max(x_i)} F_{max}$$

We can equate this total moment with M_{tot} calculated above and solve for F_{max}.

$$365.09 \text{ x } F_{max} = M_{tot} = 6.73 \text{ x } 10^7 \text{ in.lb.}$$

Therefore, F_{max} = 184,347 lb.

B.2 Bolt Stress

The tensile stress in the bolts is equal to:

$$\sigma = \frac{184{,}347}{1.730} = 106.6 \text{ ksi}$$

B.3 Attachment Bolt Block Analysis

The maximum moment applied to the block weld is:

$$M_{weld} = 184{,}347 \times \frac{83.00 - 79.00}{2} = 368{,}694 \text{ in.lb}$$

The bending stress in the block weld is:

$$\sigma_b = \frac{M_{weld} \times c}{I_{weld}} = \frac{368{,}694 \times 8/2}{124.5} = 11.8 \text{ ksi}$$

The shear stress in the block weld is:

$$\tau = \frac{F_{max}}{A_{weld}} = \frac{184{,}347}{13.81} = 13.3 \text{ ksi}$$

The stress intensity in the block weld is:

$$S.I. = \sqrt{\sigma_b^2 + 4\tau^2} = \sqrt{11.8^2 + 4 \times 13.3^2} = 29.1 \text{ksi}$$

B.2.13.12.10.2 Minimum Engagement Length for Attachment Bolt and Block

The minimum engagement length L_e for the bolt and block is ([8], p. 1490):

$$L_e = \frac{2A_t}{3.146 \times K_{n\max}\left[\frac{1}{2} + .57735n(E_{s\min} - K_{n\max})\right]}$$

For a 1 ¾ –5UNC 2A bolt:

A_t = tensile stress area = 1.90 in^2;

n = number of threads per inch = 5;

K_{nmax} = maximum minor diameter of internal threads = 1.568 in ([8], p. 1728);

E_{smin} = minimum pitch diameter of external threads = 1.6085 in ([8], p. 1728).

Substituting the values given above gives:

$$L_e = \frac{2 \times 1.90}{3.146 \times 1.568 \times \left[\frac{1}{2} + .57735 \times 5 \times (1.6085 - 1.568)\right]} = 1.249 \text{ in}$$

The required engagement length Q is ([8], p. 1491):

$$Q = J \times L_e$$

Where J is equal to ([8], p. 1490):

$$J = \frac{A_s \times S_{u(bolt)}}{A_n \times S_{u(block)}}$$

Where A_s and A_n are ([8], p. 1491):

$$\begin{cases} A_s = 3.1416nL_eK_{n\max}\left[\frac{1}{2n} + .57735(E_{s\min} - K_{n\max})\right] \\ A_n = 3.1416nL_eD_{s\min}\left[\frac{1}{2n} + .57735(D_{s\min} - E_{n\max})\right] \end{cases}$$

For a 1 ¾ –5UNC 2A bolt:

D_{smin} = minimum major diameter of external threads = 1.7268 in ([8], p. 1728);

E_{nmax} = maximum pitch diameter of internal threads = 1.6317 in ([8], p. 1728).

Therefore:

$$A_s = 3.1416 \times 5 \times 1.249 \times 1.568 \times \left[\frac{1}{2 \times 5} + .57735 \times (1.6085 - 1.568)\right] = 3.80 \text{ in}^2$$

$$A_n = 3.1416 \times 5 \times 1.249 \times 1.7268 \times \left[\frac{1}{2 \times 5} + .57735 \times (1.7268 - 1.6317)\right] = 5.25 \text{ in}^2$$

So:

$$J = \frac{3.80 \times 165.0}{5.25 \times 65.1} = 1.83$$

The required engagement length is therefore:

$$Q = 1.83 \times 1.249 = 2.29 \text{ in}$$

The threaded length is 3.50 in, which is greater than 2.29 in.

B.2.13.12.10.3 Bolt Torque

A bolt tensile stress σ_t of 15,000 psi is assumed.

$$F_a = \sigma_t \times A_t = 15{,}000 \times 1.90 = 28{,}500 \text{ lb}$$

Where A_t is the bolt tensile stress area.

$$Q = K \times D_b \times F_a = 0.135 \times 1.75 \times 28{,}500 = 6{,}733 \text{ in.lb} = 561 \text{ ft.lb}$$

Where F_a is the bolt force, Q is the applied torque, K is the nut factor, and D_b the nominal bolt diameter at the threads.

A bolt torque of 550 to 575 ft.lb is specified.

For a bolt torque of 550 ft.lb:

$$F_a = \frac{Q}{K \times D_b} = \frac{550 \times 12}{0.135 \times 1.75} = 27{,}937 \text{ lb}$$

For a bolt torque of 575 ft.lb:

$$F_a = \frac{Q}{K \times D_b} = \frac{575 \times 12}{0.135 \times 1.75} = 29{,}206 \text{ lb}$$

Therefore, the maximum tensile stress in the bolt is:

$$\sigma = \frac{F_a}{A} = \frac{29{,}206}{1.730} = 16.9\,\text{ksi}$$

This is less than the yield stress of the bolts, 139.1 ksi.

B.2.13.12.10.4 Conclusions

The stresses are summarized in Table B.2.13.12-10. All of the stresses calculated for the impact limiter bolts, attachment bolt blocks, and lifting lugs are less than the allowable stresses regardless of the method used. Therefore, the MP197TAD TO impact limiter attachments are structurally adequate.

The required engagement length is 2.29 in, which is less than the threaded length of 3.50 in.

B.2.13.12.11 References

1. Application for Revision 3 to Certificate of Compliance No. 9302 for the Model No. NUHOMS®-MP197 Packaging, April 14, 2009, USNRC Docket No. 71-9302.
2. LS-DYNA Keyword User's Manual, Volumes 1 & 2, Version 9.71s, Rev. 7600.398 August 17, 2006, Livermore Software Technology Corporation.
3. Wood Handbook: Wood as an Engineering Material, Forest Products Laboratory, General Technical Report, FPL-GTR-113, United States Department of Agriculture.
4. Karl Klein, Johannes Will, and Thomas Seider, "Numerical Simulation of Wood Filled Impact Limiter with LS-DYNA," November 10-12, 2004, International Congress Center Dresden, Germany.
5. Alexander A. Ryabov, Vladimir I. Romanov, Sergey S. Kukanov, and Sergey G. Skurikhin, "Numerical Simulation of Dynamic Deformation of Air Transport Package PAT-2 in Accident Impacts," 9th International LS-DYNA Users Conference.
6. Standard Handbook for Mechanical Engineers, Baumeister & Marks, 7th Edition, McGraw-Hill, 1967.
7. ASME Boiler and Pressure Vessel Code, Section II, Materials Specifications, Parts A, B, C, and D, 2004 with 2006 addenda.
8. Machinery Handbook, 26th Edition, Industrial Press, 2000.

Table B.2.13.12-1
Effective Plastic Strain vs. Scale Factor for Concrete Material

Effective Plastic Strain	Scale Factor, η
0	0
0.00094	0.289
0.00296	0.465
0.00837	0.629
0.01317	0.774
0.0234	0.893
0.04034	1.0
1.0	1.0

Table B.2.13.12-2
Tabulated Pressures vs. Volumetric Strain for Concrete Material

Volumetric Strain, ε	Pressure (psi)
0	0
-0.006	4,600
-0.0075	5,400
-0.01	6,200
-0.012	6,600
-0.02	7,800
-0.038	10,000
-0.06	12,600
-0.0755	15,000
-0.097	18,700

Table B.2.13.12-3
Wood Segment Material Properties at Room Temperature

	Redwood	Balsa
Density, ρ	3.445×10-5 lbm/in^3 (23 lb/ft^3)	1.647×10-5 lbm/in^3 (11 lb/ft^3)
Shear Modulus, G parallel to grain	13,266 psi	2,205 psi
Shear Modulus, G perpendicular to grain	92,862 psi	16,317 psi
Elastic Modulus parallel to grain	1,210,000 psi	441,000 psi
Elastic Modulus perpendicular to grain	107,334 psi	6,615 psi
Tensile Strain Failure*	0.4	0.4

*Tensile strain failures are conservatively high.

Table B.2.13.12-4
Wood Segment Material Properties at - 20 °F Temperature

	Redwood	Balsa
Density, ρ	3.445×10-5 lbm/in^3 (23 lb/ft^3)	1.647×10-5 lbm/in^3 (11 lb/ft^3)
Shear Modulus, G parallel to grain	15,919 psi	2,646 psi
Shear Modulus, G perpendicular to grain	111,434 psi	19,580 psi
Elastic Modulus parallel to grain	1,447,000 psi	529,000 psi
Elastic Modulus perpendicular to grain	128,800 psi	7,938 psi
Tensile Strain Failure*	0.4	0.4

*Tensile strain failures are conservatively high.

Table B.2.13.12-5
Pressure vs. Volumetric Strain for Wood Properties at Room Temperature

Redwood Parallel to Grain	
Volumetric Strain (ΔV/V)	**Pressure (psi)**
0.000	0
0.0043 (Yield)	5175
0.6 (Lock)	5200

Redwood Perpendicular to Grain	
Volumetric Strain (ΔV/V)	**Pressure (psi)**
0.000	0
0.0059 (Yield)	630
0.6 (Lock)	640

Balsa Parallel to Grain	
Volumetric Strain (ΔV/V)	**Pressure (psi)**
0.000	0
0.0036 (Yield)	1610
0.8 (Lock)	1650

Balsa Perpendicular to Grain	
Volumetric Strain (ΔV/V)	**Pressure (psi)**
0.000	0
0.049 (Yield)	324
0.8 (Lock)	330

Table B.2.13.12-6
Pressure vs. Volumetric Strain for Wood Properties at -20 °F

Redwood Parallel to Grain	
Volumetric Strain (ΔV/V)	**Pressure (psi)**
0.000	0
0.0043 (Yield)	6210
0.6 (Lock)	6300

Redwood Perpendicular to Grain	
Volumetric Strain (ΔV/V)	**Pressure (psi)**
0.000	0
0.0059 (Yield)	756
0.6 (Lock)	770

Balsa Parallel to Grain	
Volumetric Strain (ΔV/V)	**Pressure (psi)**
0.000	0
0.0036 (Yield)	1928
0.8 (Lock)	1950

Balsa Perpendicular to Grain	
Volumetric Strain (ΔV/V)	**Pressure (psi)**
0.000	0
0.049 (Yield)	389
0.8 (Lock)	400

Table B.2.13.12-7
Peak Nodal Accelerations, Wood Crush Depths, and Impact Duration Comparisons
(1/3 Scale Test Results vs. 1/3 Scale LS-DYNA Analysis)

		Test Results	**LS-DYNA Model**
End Drop (-20°F)	Acceleration	65g	65.1g
	Impact Duration	0.010 sec.	0.012 sec.
	Wood Crush Depth	2.5"	2.8"
Side Drop	Acceleration	61g	65.6g
	Impact Duration	0.012 sec.	0.013 sec.
	Wood Crush Depth	2.69"-2.75"	2.7"-2.9"
20° Slap Down 1st Impact	Acceleration at Center of Cask	17g	20.8g
	Acceleration at Bottom of Cask	36g	40.1g
	Impact Duration	0.016 sec.	0.018 sec.
	Wood Crush Depth Bottom Limiter	4.92"	4.9"
20° Slap Down 2nd Impact	Acceleration at Center of Cask	32g	36.3g
	Acceleration at Top of Cask	73g	72.2g
	Impact Duration	0.009 sec.	0.010 sec.
	Wood Crush Depth Upper Limiter	2.42"(1)	2.8"

NOTE:
(1) Re-examination of the MP197 test results: It shows that the crush depth is 2.42" instead of 4.72" as specified in Appendix 2.10.9 of the MP197 main SAR[1].

Table B.2.13.12-8
Summary of the Full Scale Impact Limiter Analysis Results

Drop Scenario			Peak Acceleration (g)	Impact Duration (sec)	Impact Limiter Crush Depth (in)	Time History Figure Number
30' End Drop (Room Temp)			44.1	0.045	9.2	B.2.13.12-27
30' End Drop (-20°F)			48.9	0.043	8.4	B.2.13.12-28
30' Side Drop			51.6	0.05	9.7	B.2.13.12-29
30' Slap Down 20°	1st Impact	Vertical Acceleration	42.3	0.055	13.7	B.2.13.12-31
		Rigid Body	Translational 23.6			B.2.13.12-58
			Rotation α = 105.7			
	2nd Impact	Vertical Acceleration	63.3	0.045	10.3	B.2.13.12-32
		Rigid Body	Translational 26.5			B.2.13.12-58
			Rotation α = 175.6			
30' Slap Down 15°	1st Impact	Vertical Acceleration	41.6	0.05	12.5	B.2.13.12-33
		Rigid Body	Translational 21.7			B.2.13.12-59
			Rotation α = 111.4			
	2nd Impact	Vertical Acceleration	64.2	0.04	11.7	B.2.13.12-34
		Rigid Body	Translational 27.9			B.2.13.12-59
			Rotation α = 176.2			
30' Slap Down 10°	1st Impact	Vertical Acceleration	47.4	0.045	11.2	B.2.13.12-35
		Rigid Body	Translational 23.0			B.2.13.12-60
			Rotation α = 131.9			
	2nd Impact	Vertical Acceleration	63.1	0.04	12.1	B.2.13.12-36
		Rigid Body	Translational 28.9			B.2.13.12-60
			Rotation α = 165.9			
30' CG Over Corner			30.2	0.09	27.1	B.2.13.12-30
1' Normal Condition End Drop			27.6	0.02	0.8	B.2.13.12-37
1' Normal Condition Side Drop			15.6	0.04	0.7	B.2.13.12-38

Table B.2.13.12-9
Calculation of Total Moment

	Angular location	**Vertical distance (in)**	**Moment arm (in)**	**Moment ($/F_{max}$)**
Bolt #1	15°	79.59	79.59	79.59
Bolt #2	45°	68.84	68.84	59.55
Bolt #3	75°	50.24	50.24	31.72
Bolt #4	105°	28.76	28.76	10.39
Bolt #5	135°	10.16	10.16	1.30
Bolt #6	165°	-0.59	0.00	0.00
Bolt #7	195°	-0.59	0.00	0.00
Bolt #8	225°	10.16	10.16	1.30
Bolt #9	255°	28.76	28.76	10.39
Bolt #10	285°	50.24	50.24	31.72
Bolt #11	315°	68.84	68.84	59.55
Bolt #12	345°	79.59	79.59	79.59
			Total	**365.09**

Table B.2.13.12-10
Summary of Stresses (ksi)

Component		Calculated (Base on Tensile Force)	Calculated (Base on Moments)	Allowable
Impact Limiter Attachment Bolts		164.7	106.6	165.0
Attachment Block Welds	Shear	14.3	13.3	27.3
	Stress Intensity	31.6	29.1	65.1

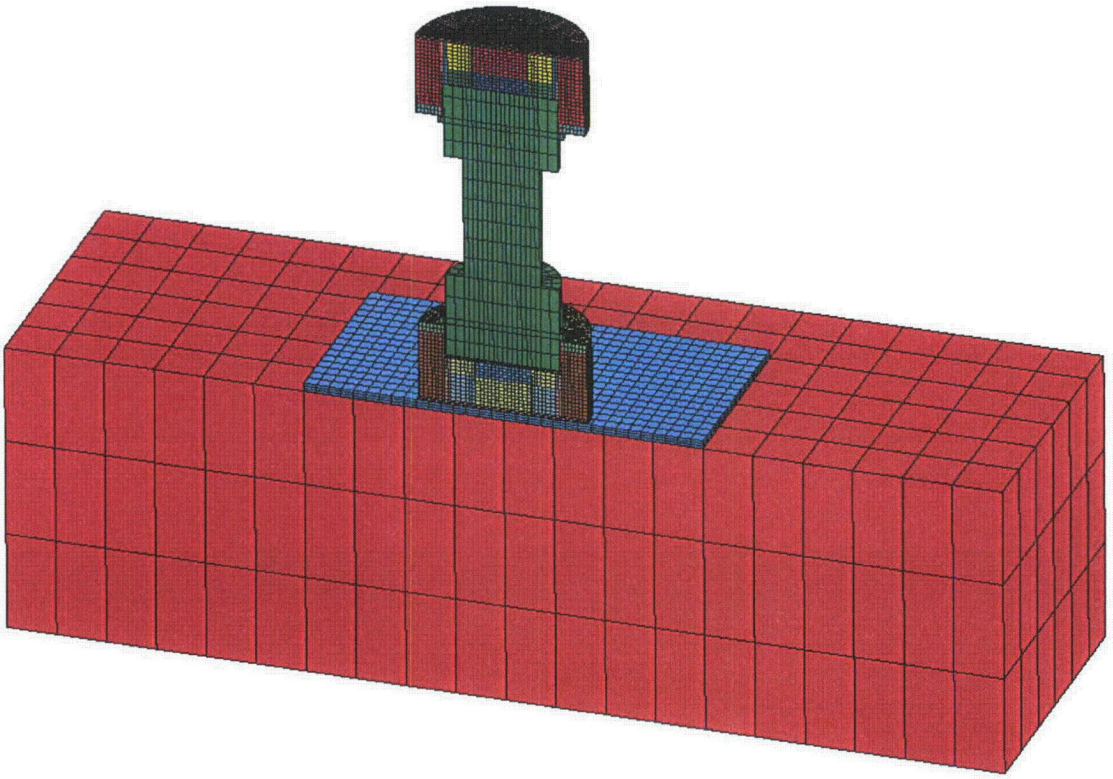

Figure B.2.13.12-1
1/3 Scale Impact Limiter Finite Element Model Overview

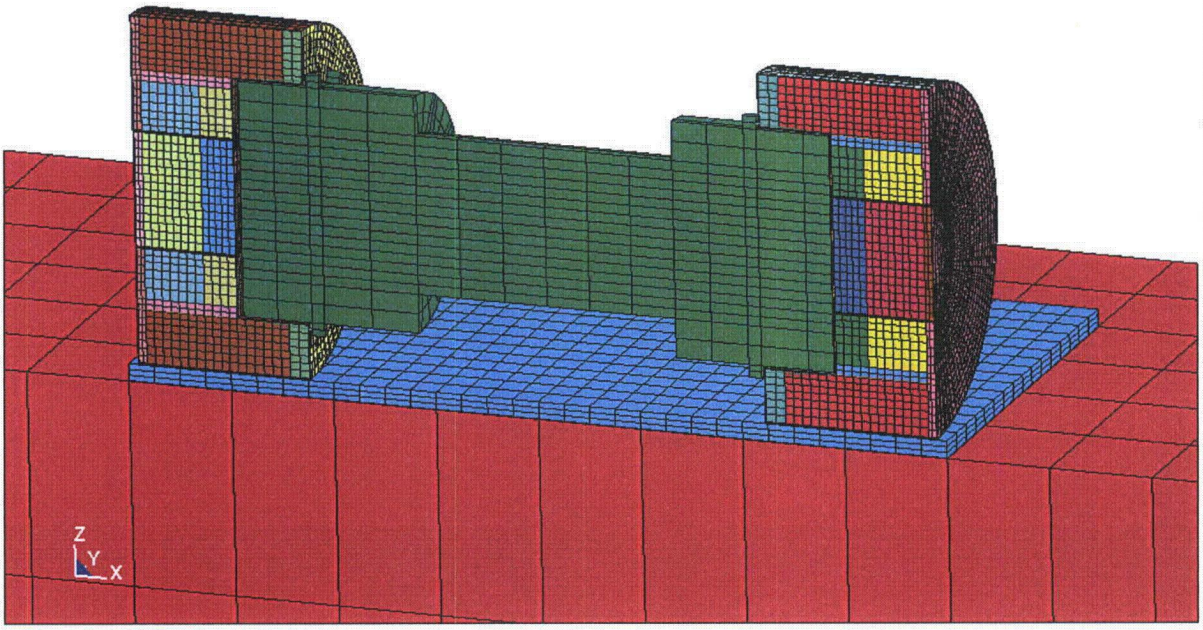

Figure B.2.13.12-2
1/3 Scale Impact Limiter Finite Element Model for Side Drop

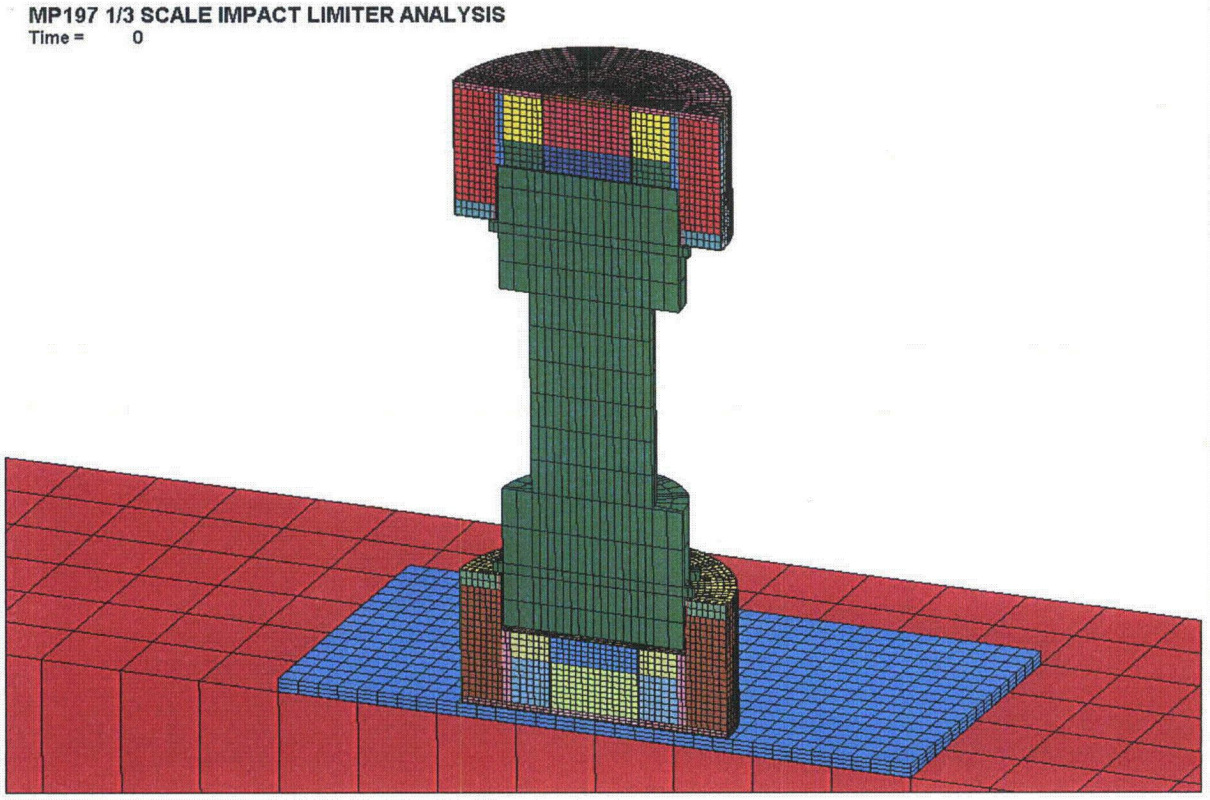

Figure B.2.13.12-3
1/3 Scale Impact Limiter Finite Element Model for End Drop

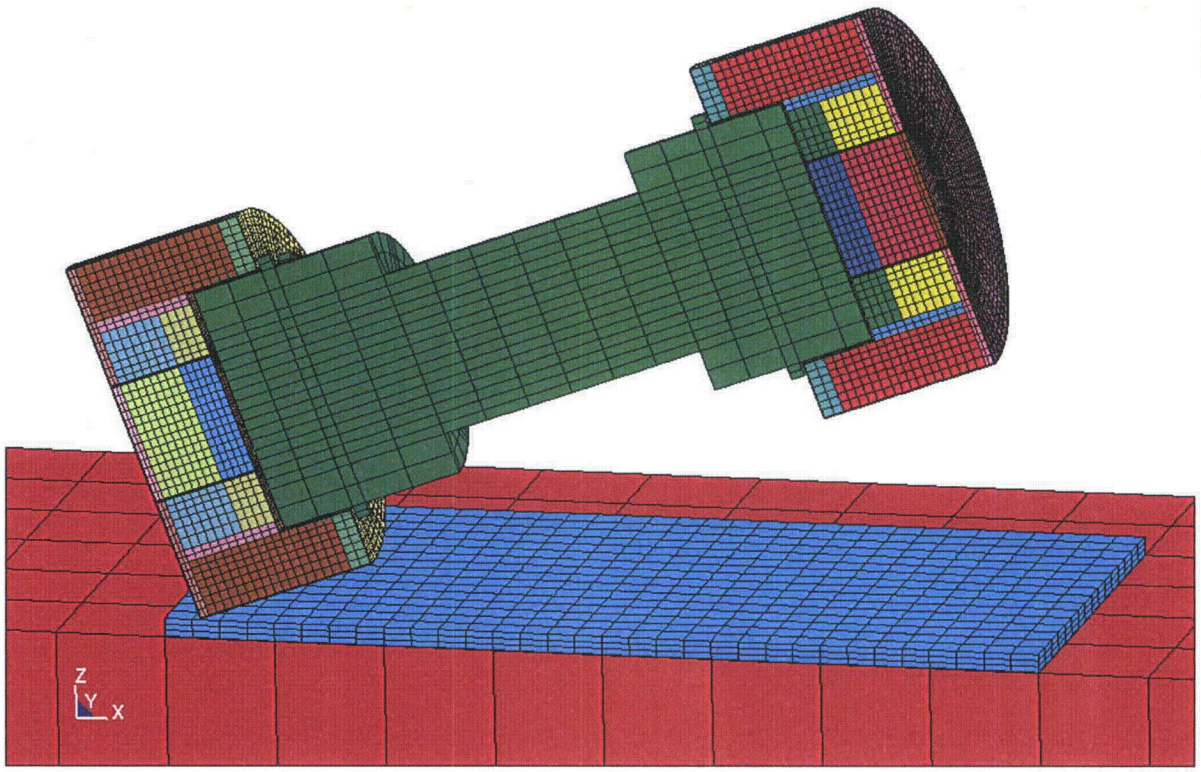

Figure B.2.13.12-4
1/3 Scale Impact Limiter Finite Element Model for 20° Slap Down Drop

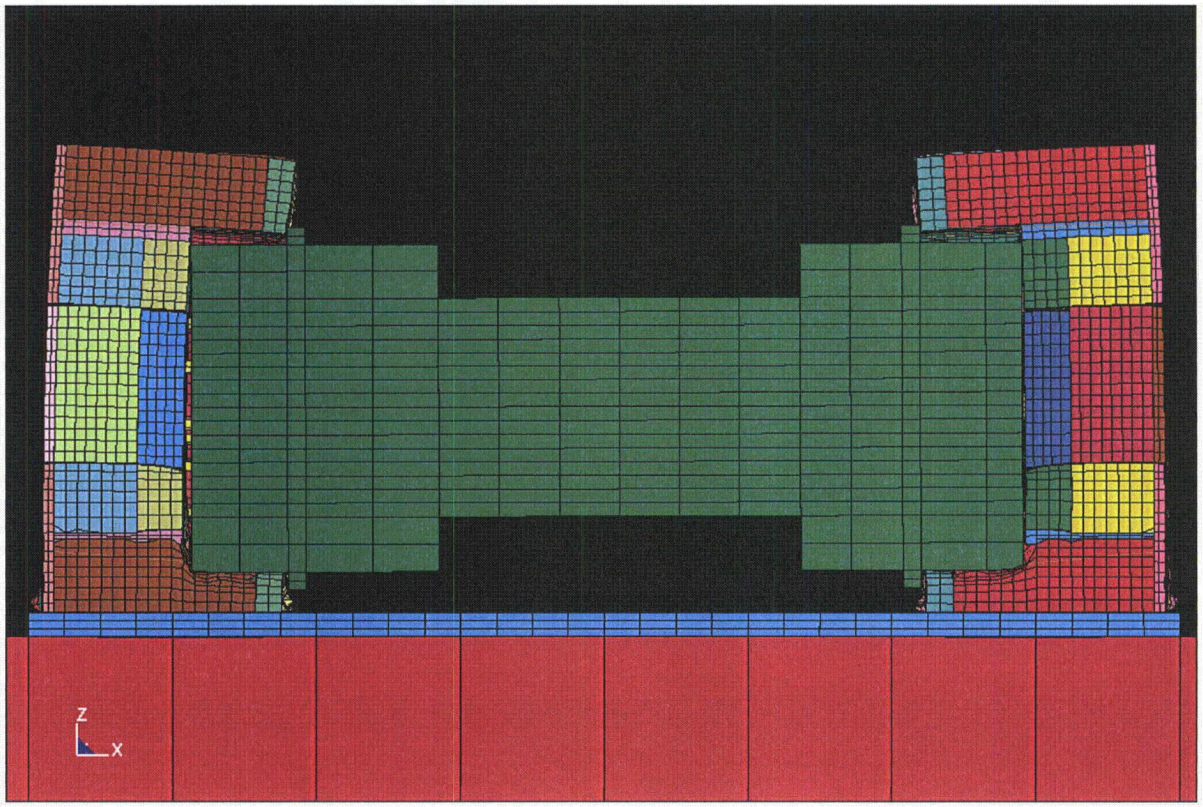

Figure B.2.13.12-5
Plot of Maximum Deformation for 1/3 Scale Side Drop

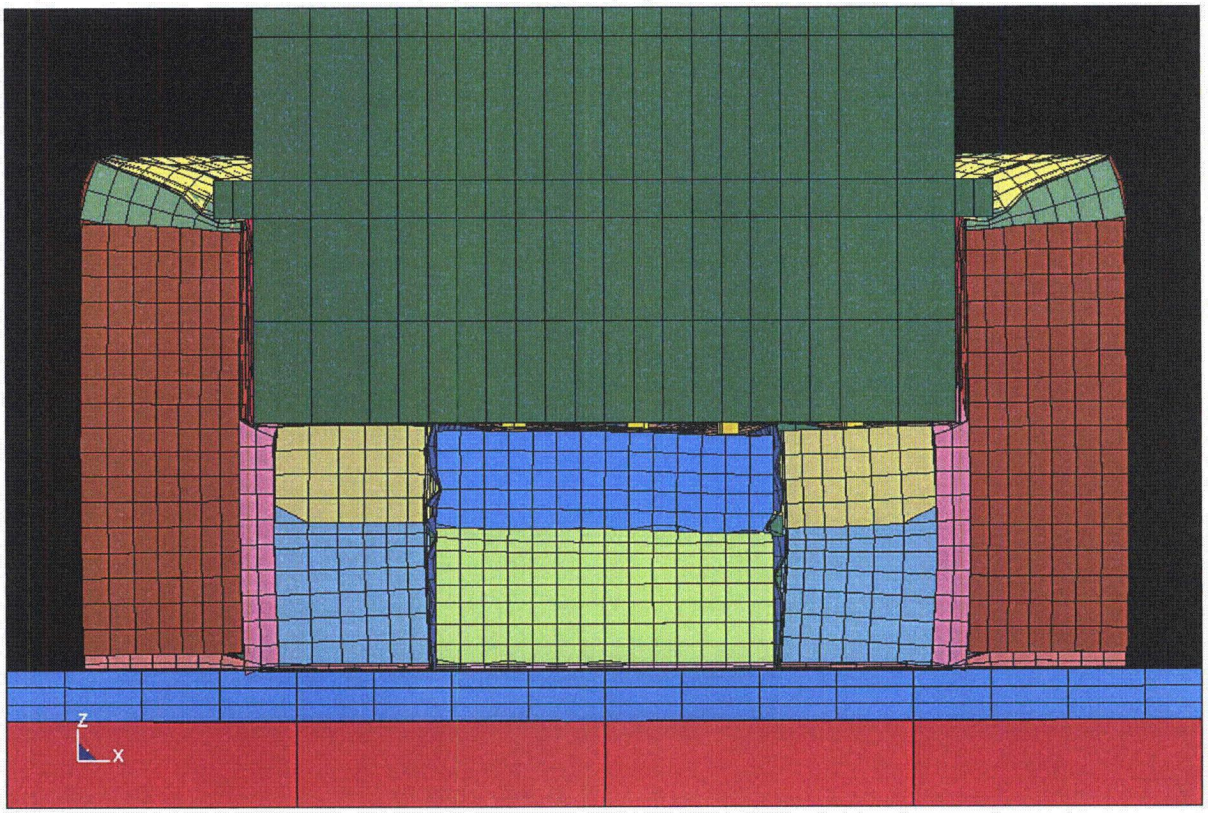

Figure B.2.13.12-6
Plot of Maximum Deformation for 1/3 Scale End Drop (-20°F)

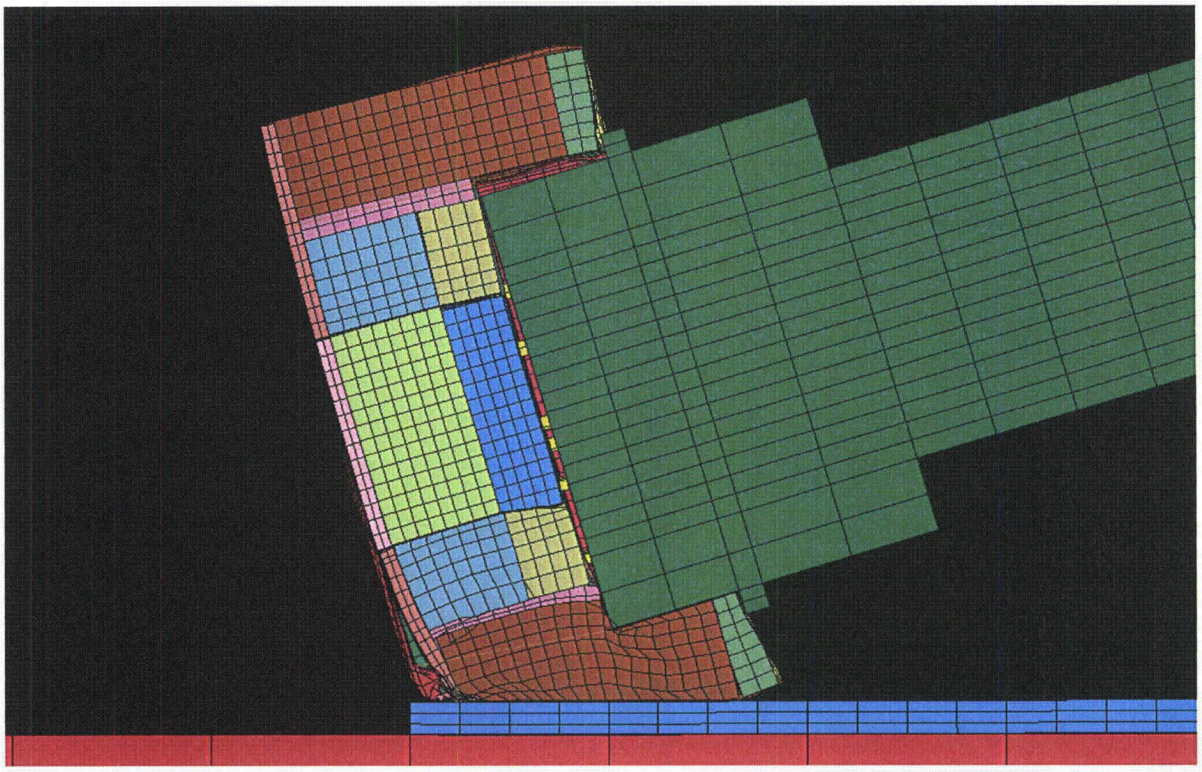

Figure B.2.13.12-7
Plot of Maximum Deformation for 1/3 Scale 20° Slap Down Drop (First Impact)

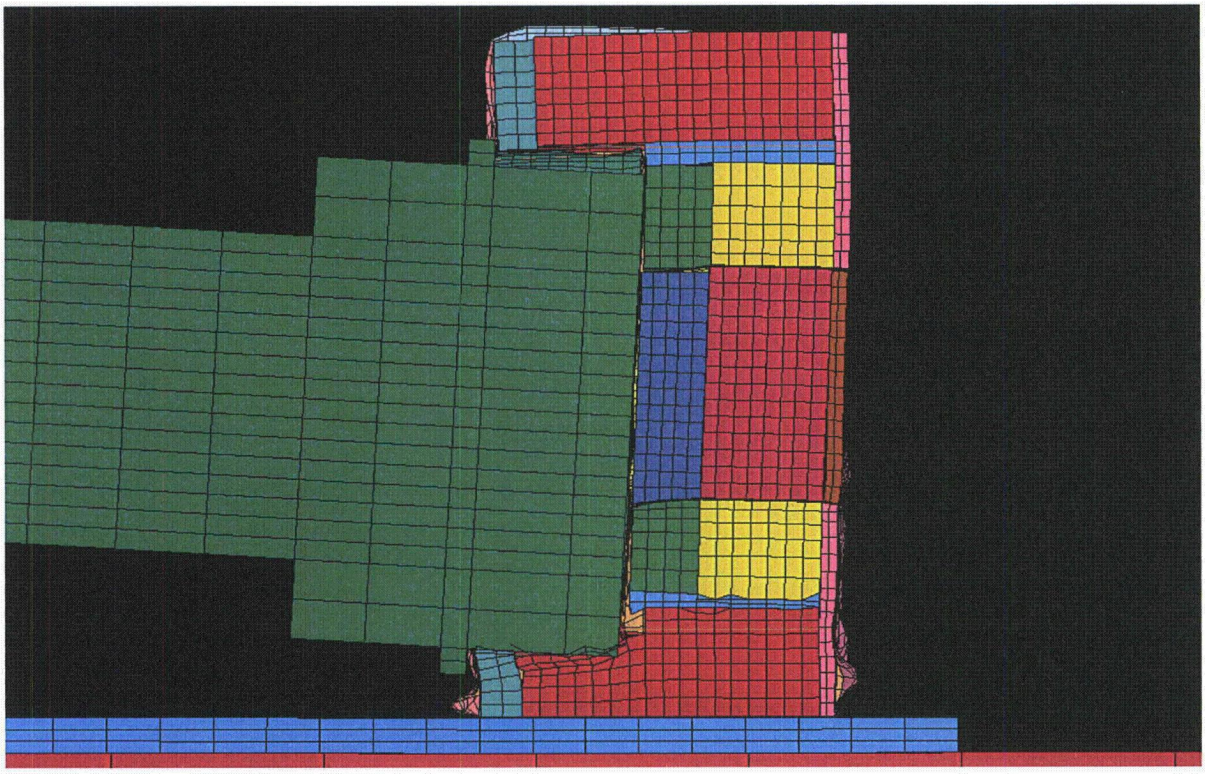

Figure B.2.13.12-8
Plot of Maximum Deformation for 1/3 Scale 20° Slap Down Drop (Second Impact)

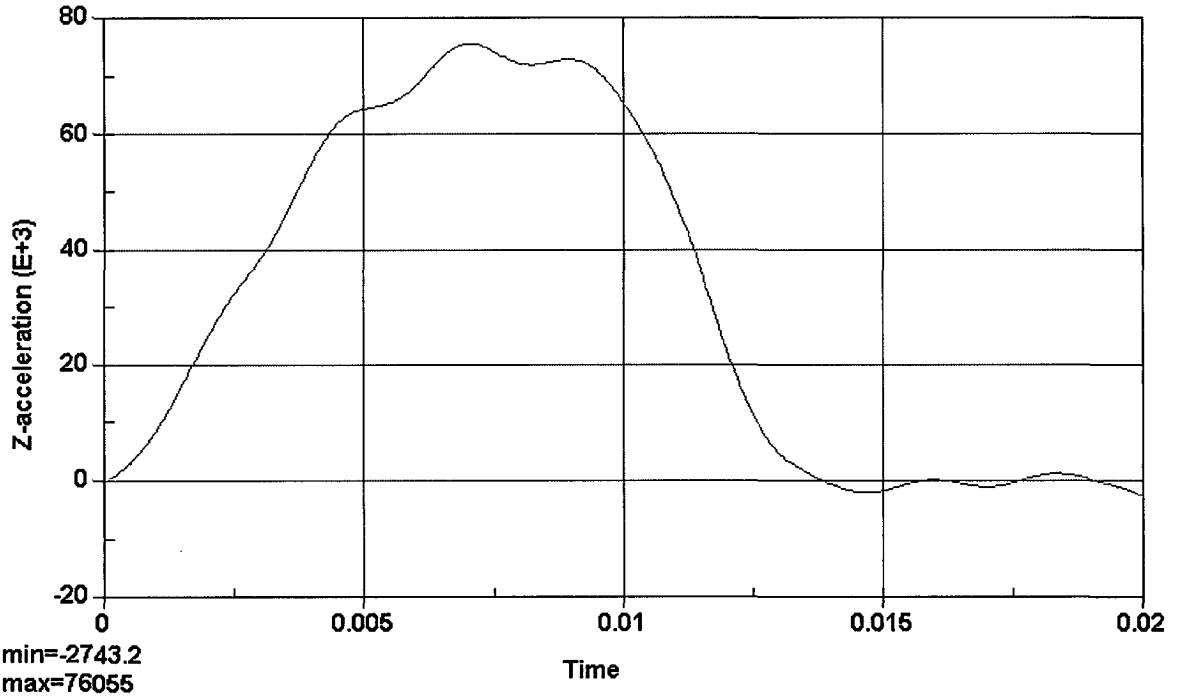

Note: The acceleration unit is in/sec^2 and unit for time is sec.

Figure B.2.13.12-9
1/3 Scale Side Drop Acceleration Time History (From LS-DYNA)

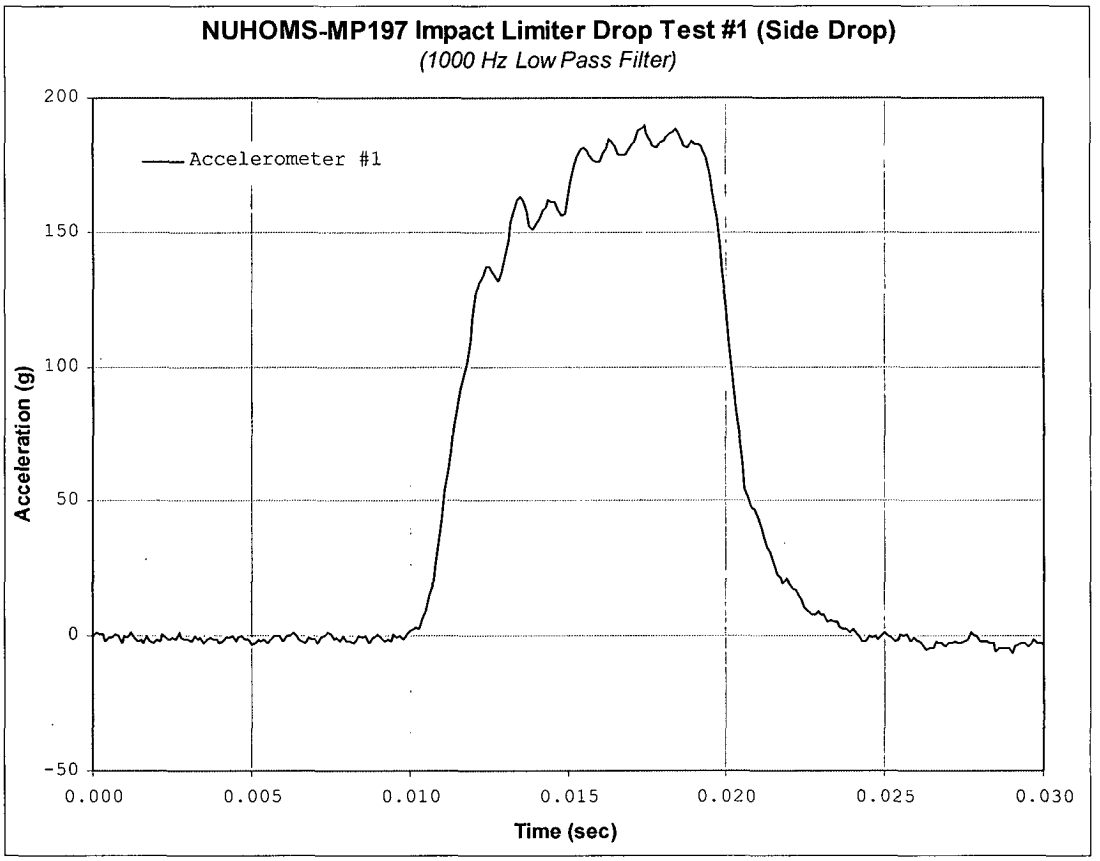

Figure B.2.13.12-10
1/3 Scale Side Drop Acceleration Time History, Accelerometer 1

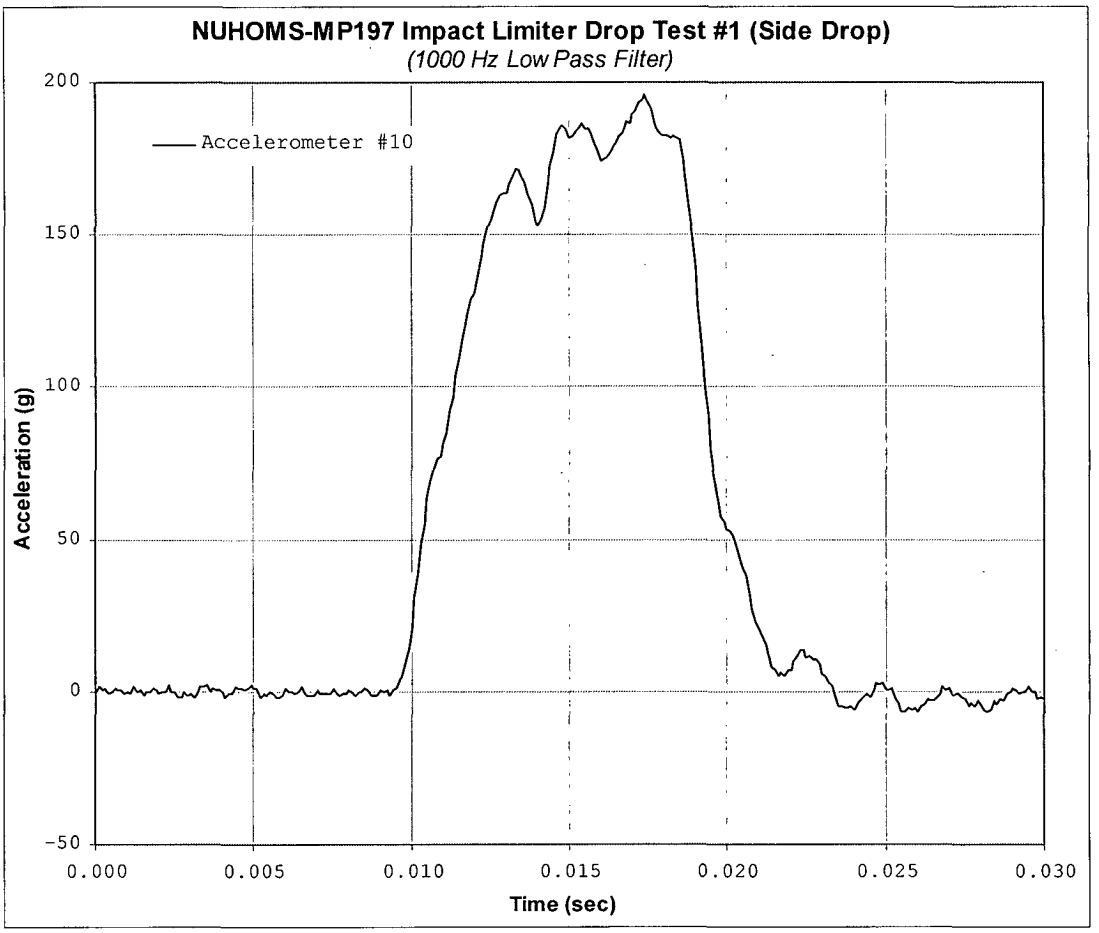

Figure B.2.13.12-11
1/3 Scale Side Drop Acceleration Time History, Accelerometer 10